R-07-47

Thermal properties

Site descriptive modelling Forsmark – stage 2.2

Pär-Erik Back, John Wrafter, Jan Sundberg
Geo Innova AB

Lars Rosén, Sweco Viak AB

September 2007

Svensk Kärnbränslehantering AB
Swedish Nuclear Fuel
and Waste Management Co
Box 5864
SE-102 40 Stockholm Sweden
Tel 08-459 84 00
+46 8 459 84 00
Fax 08-661 57 19
+46 8 661 57 19

ISSN 1402-3091
SKB Rapport R-07-47

Thermal properties

Site descriptive modelling
Forsmark – stage 2.2

Pär-Erik Back, John Wrafter, Jan Sundberg
Geo Innova AB

Lars Rosén, Sweco Viak AB

September 2007

Preface

This report presents the thermal site descriptive model for the Forsmark area, modelling stage 2.2. The thermal modelling work presented in this report relies heavily on the new methodology described in the strategy report for thermal modelling during site investigations, version 2.0 /Back and Sundberg 2007/.

In addition to the authors, the following persons have participated in the project: Märta Ländell (temperature, heat capacity and temperature dependence), Nils Kellgren (stochastic geologic simulation) and Tommy Norberg (transformation and statistical analysis of stochastic geologic simulations).

Summary

This report presents the thermal site descriptive model for the Forsmark area, modelling stage 2.2. The thermal modelling is based on the methodology outlined in Figure A. The methodology is applied separately for each rock domain. Starting at the upper part of Figure A the simulation scale (1) is defined as one of the first steps in the methodology. This scale determines how lithological data (2) should be prepared and if a change of support (5) (change of scale) is required for the thermal data (4). The lithological data acquired from boreholes and mapping of the rock surface need to be reclassified into thermal rock classes, TRCs (3). The main reason is to simplify the simulations.

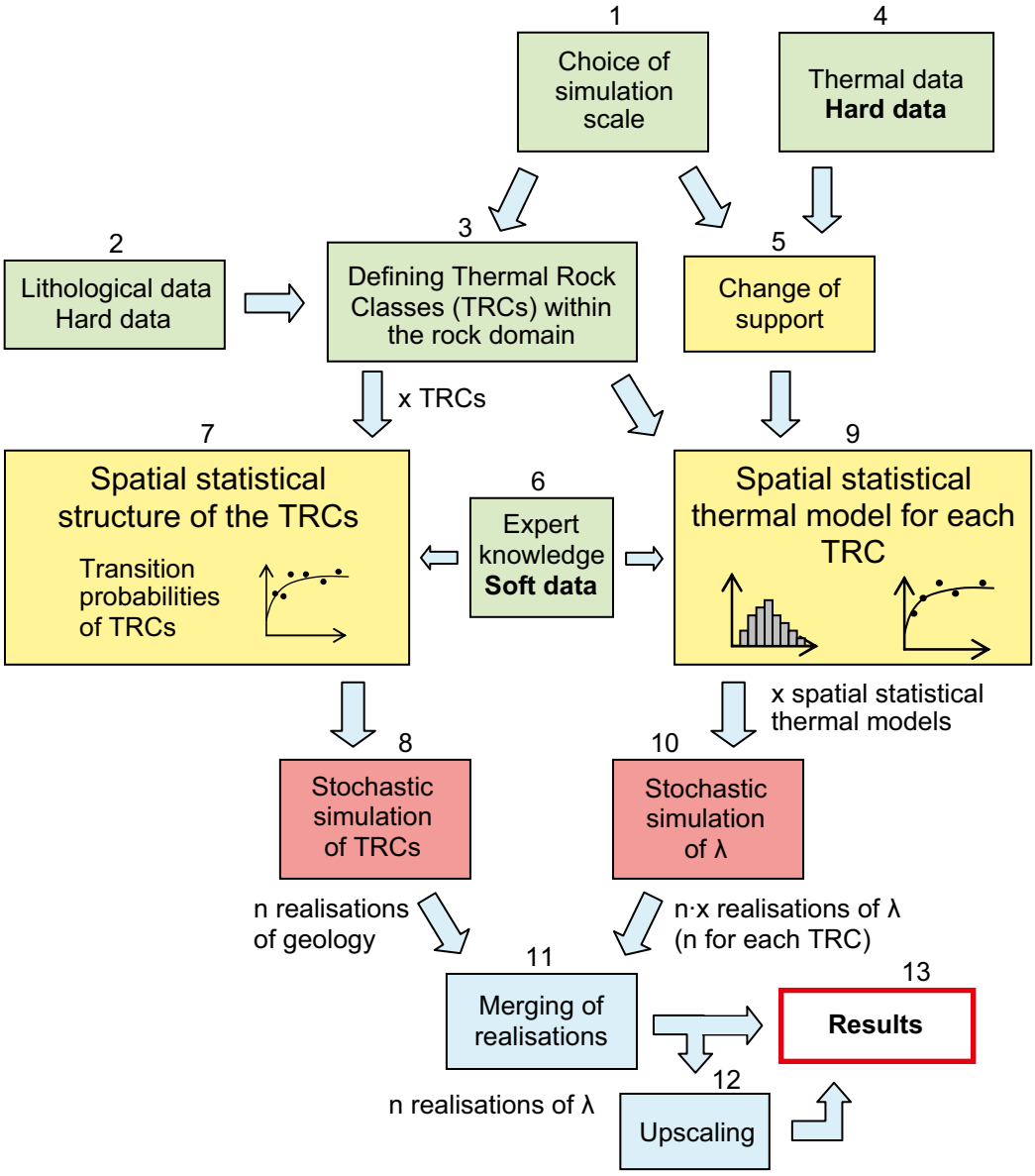

Figure A. *Schematic description of the approach for thermal modelling of a rock domain (λ represents thermal conductivity).*

The lithological data are used to construct models of the transition between different TRCs, thus describing the spatial statistical structure of each TRC (7). The result is a set of transition probability models that are used in the simulation of TRCs (8). The intermediate result of this first stochastic simulation is a number of realisations of the geology, each one equally probable. Based on the thermal data, a spatial statistical thermal model is constructed for each TRC (9). It consists of a statistical distribution and a variogram for each TRC. These are used in the stochastic simulation of thermal conductivity (10) and the result is a number of equally probable realisations of thermal conductivity for the domain.

In the next step, the realisations of TRCs (lithology) and thermal conductivity are merged (11), i.e. each realisation of geology is filled with simulated thermal conductivity values. The result is a set of realisations of thermal conductivity that considers both the difference in thermal properties between different TRCs, and the variability within each TRC. If the result is desired in a scale different from the simulation scale, i.e. the canister scale, upscaling of the realisations can be performed (12). The result (13) is a set of equally probable realisations of thermal properties.

The presented methodology was applied to rock domain RFM029 and RFM045. The main results are sets of realisations of thermal properties that can be used for further processing, most importantly for statistical analysis and numerical temperature simulations for the design of repository layout (distances between deposition holes). The main conclusions of the thermal modelling are:

- The choice of scale has a profound influence on the distribution of thermal conductivity values. The variance decreases and the lower tail percentiles increase significantly as the scale of observation increases from 1 m to 5 m. Best estimates of the 0.1 percentile of thermal conductivity are:
  - Domain RFM029: 2.30 W/(m·K) for the 1 m scale and 2.87 W/(m·K) for the 5 m scale.
  - Domain RFM045: 2.25 W/(m·K) for the 1 m scale and 2.33 W/(m·K) for the 5 m scale.
- The discretisation error of amphibolite is believed to be the largest uncertainty for the 1 m scale for domain RFM029. This error results in conservative estimates (believed to be too low) of the lower percentiles. For other cases, the uncertainties associated with the spatial structure of TRCs (lithology) and the spatial statistical thermal models of each TRC are believed to be the most important ones.
- Low-conductive rocks, mainly amphibolite and the tonalitic varieties of granodiorite to tonalite are decisive for the lower tail of the thermal conductivity distribution of a domain. The shape of the tail is therefore mainly determined by how these rock types are modelled. One of the most important uncertainties for the result for domain RFM045 is how amphibolite was modelled. Based on relatively limited data, the typical lengths of amphibolite rock bodies are modelled as being significantly longer than in domain RFM029. This may have resulted in a too heavy lower tail of the distribution of thermal conductivity for domain RFM045.

In conclusion, the resulting thermal models are judged to represent the modelled rock domains, but may overemphasise the importance of the low-conductive amphibolite.

Contents

1 Introduction

1.1 Background

1.1.1 Overview

The Swedish Nuclear Fuel and Waste Management Company (SKB) is undertaking site characterisation at two different locations, the Forsmark and Simpevarp/Laxemar areas, with the objective of siting a geological repository for spent nuclear fuel. The investigations are conducted in campaigns, data freezes. After each data freeze, the site data are analysed and site descriptive modelling is carried out. A site descriptive model (SDM) is a synthesis of geology, rock mechanics, thermal properties, hydrogeology, hydrogeochemistry and a surface system description.

So far, three versions of a site descriptive model have been completed in the Forsmark area. Version 0 /SKB 2002/ established the state of knowledge prior to the site investigation. Version 1.1 /SKB 2004/ was completed during 2004 and version 1.2 in June 2005 /SKB 2005a/. Version 1.2 of the SDM concluded the initial site investigation work (ISI). It formed the basis for a preliminary repository layout (layout D1), a preliminary safety evaluation (PSE) of the Forsmark site /SKB 2005b/ and a safety assessment (SR-Can) of repository layout D1 at Forsmark /SKB 2006a/.

The complete site investigation (CSI) work comprises three stages, concluding with a final multi-disciplinary SDM for Forsmark, SDM-Site, during modelling stage 2.3. An important component of all three stages is to address and continuously try to resolve uncertainties of importance for repository engineering and safety assessment. Model stage 2.1 /SKB 2006b/ included an assessment of data contained in data freeze 2.1 with the primary aim of providing feedback for the completion of the site investigation work. The most comprehensive thermal modelling efforts within the CSI are performed within model stage 2.2. The results of the thermal modelling in model stage 2.2 for the Forsmark site are compiled in this report. Stage 2.3 will address any unresolved issues of importance through further analysis, and will be documented in a separate report. However, additional data is not expected. The findings from both the 2.2 modelling stage and the supplementary 2.3 analyses will be summarised in the final multi-disciplinary SDM Forsmark.

1.1.2 Thermal properties

The “global” temperature field around a repository mainly depends on the time-dependent generated heat, boundary conditions, initial temperature conditions and mean values of large-scale thermal transport properties. The thermal processes at this scale are quite slow and insensitive to local variations in the thermal properties. The demands for high accuracy in the thermal property distribution are lower compared to the local scale.

The local temperature field around a canister is of primary concern for the design of a repository. The current design criterion is specified as the maximum temperature allowed in the bentonite buffer outside the canisters /SKB 2006a/. To fulfil the temperature requirement, a low rock thermal conductivity leads to larger distances between canisters than in the case of a high thermal conductivity.

The sensitivity in canister temperature to changes in the thermal properties is highest for the area closest to the canister. It is therefore of special interest to analyse if there is a spatial variation in the thermal properties in the rock mass at the canister scale that will influence the canister temperature.

In order to analyse the scale at which variations of thermal conductivity is significant for the temperature on the canister, a preliminary numerical study based on rock thermal conductivity distribution has been made /Sundberg et al. 2005b/. They found that the spatial variability started

to have an influence on the canister temperature at a scale as small as 1 m and that the influence increased approximately linearly up to 10 m. Consequently, the maximum canister temperature is influenced by thermal conductivities for a range of scales. The characteristic scale would be in the order of 2–5 m, which is logical considering the dimensions of the canister and the dominating role of the contribution of the local canister to its own temperature.

The term "thermal properties" involves thermal conductivity, thermal diffusivity, heat capacity, temperature and the coefficient of thermal expansion.

Thermal conductivity λ [W/(m·K)] is defined as a materials ability to transport thermal energy. Thermal conductivity is the most important transport property. Thermal diffusivity κ [m^2/s] is a measure of a materials ability to level out temperature differences. Heat capacity C [$J/(m^3 \cdot K)$] is defined as a materials capacity to store heat. These properties are related to each other as follows:

$\kappa = \lambda / C$

Due to the relation, it is only necessary to discuss two of these three properties. In this report the interest is concentrated on thermal conductivity and heat capacity. The temperature dependence for these properties is also of interest due to the temperature increase in a repository. Anisotropy in thermal conductivity influences the temperature field in a repository and is therefore also of interest to determine.

The temperature is of primary interest in order to determine the temperature at repository depth, the starting temperature for the heat increase in a repository. The coefficient of thermal expansion describes the expansion of rock versus the increase in temperature. However, there has been no focus on this property in the current report.

A table summarising the thermal properties and parameters that should be predicted/described by the thermal model is provided in /Back and Sundberg 2007/, including the acceptable uncertainty for the various parameters.

1.2 Scope and objectives

The main objective of the thermal modelling stage 2.2 for Forsmark is to provide an adequate spatial statistical description of the rock mass thermal conductivity and its uncertainties for the needs of repository design and safety assessment.

This report synthesizes the thermal investigations at the Forsmark site. The report reviews the thermal data used and describes the statistical evaluation of this data. The temperature at repository depth is determined directly from data. Stochastic modelling produces a set of 3D realisations, which are used to describe the spatial distribution of thermal conductivity. From the different stochastic realisations, the low percentiles of thermal conductivity are determined, and the scale dependence of thermal conductivity is evaluated. These are two criteria of importance for repository design. The lower tail of the thermal conductivity distribution is of central importance to the decision of canister spacing and must therefore be properly described. In forthcoming work, the thermal realisations will be used as input to numerical temperature modelling of a repository.

The data employed to support the findings presented in this model originate from the Forsmark 2.2 data freeze. The rock domain model, produced as part of the geological modelling in stage 2.2 /Stephens et al. 2007/, forms the geometric framework for modelling of thermal properties. The methodology employed for thermal modelling in stage 2.2 has been fundamentally revised compared to previous model versions, and has been documented in a separate strategy report /Back and Sundberg 2007/. The modelling involves stochastic simulation based on both the spatial statistical structure of lithologies and the spatial distribution of thermal conductivities. By merging the realisations of the lithological and thermal simulations, a distribution of thermal properties is produced that takes into account the spatial variability within and between different rock types.

The data used for thermal modelling are considered to be representative for the volume of rock that may host the final repository. The thermal properties of two rock domains, RFM029 and RFM045 within the target volume at Forsmark, are modelled. Results are presented for different scales. Anisotropy of thermal conductivity of the rock mass resulting from foliation is evaluated from analysis of measurements in different directions. Anisotropy of thermal conductivity caused by the orientation of subordinate rock bodies is evaluated directly from the modelling results. The impact of alteration on thermal properties is investigated. The remaining uncertainties in understanding the thermal properties are outlined.

1.3 Setting

The rock volume for which thermal properties have been investigated in modelling stage 2.2 is defined by the target volume within the local model volume as defined in /Stephens et al. 2007/. The target volume includes the rock volume identified as suitable for the excavation of the repository /SKB 2005c/. The target area is located within a tectonic lens, which developed more than 1,850 million years ago and was affected by variable degrees of ductile deformation. Inside the lens, the geology is dominated by a metagranite, whereas the geology outside the lens is more heterogeneous and shows a higher degree of ductile deformation relative to that observed inside the tectonic lens. The target area is dominated by a medium-grained granite to granodiorite, whereas locally aplitic granite is abundant. Important subordinate rock types are fine to medium-grained granodiorite and tonalite, amphibolite and pegmatite /SKB 2006b/. For illustration of the surface geology, see Figure 1-1.

Two rock domains have been defined within the target volume, domain RFM029 and RFM045 /Stephens et al. 2007/. The dominant rock type in domain RFM029 is the medium-grained granite to granodiorite, whereas domain RFM045 is dominated by the aplitic granite, which is commonly albitized, a critical feature that forms the basis for the separation of these two domains /Stephens et al. 2007/.

1.4 This report

1.4.1 Structure of this report

The thermal modelling work presented in this report relies heavily on the methodology described in the strategy report for thermal modelling during site investigations, version 2.0 /Back and Sundberg 2007/. This represents a major departure from the modelling approach employed in model stages 1.2 and 2.1. Integration of geological information critical to thermal modelling was performed through close cooperation with the geology team.

Chapter 2 presents an overview of the previous thermal modelling work, and briefly describes the geological model stage 2.2, which forms the foundation for the thermal modelling. Chapter 3 summarises the primary thermal and geophysical logging data that where available for model stage 2.2. Preliminary statistical analyses of these data are also covered in Chapter 3. Chapter 4 begins with a presentation of the conceptual model and is followed by a comprehensive description of the strategy employed for the thermal modelling.

The first part of Chapter 5 lists the main assumptions of the thermal modelling. This is followed by a description of aspects of the geology and the geological model that are relevant to thermal modelling. The last two sections of Chapter 5 address the spatial statistical models and simulation of both geology (lithology) and thermal conductivity. Chapter 6 presents and evaluates the results of the thermal modelling at rock domain level. The final part of this chapter addresses the uncertainties inherent in the thermal model. Chapter 7 summarises the conclusions of the thermal modelling work.

The report contains a number of appendices that are linked to various modelling steps in Chapters 5 and 6.

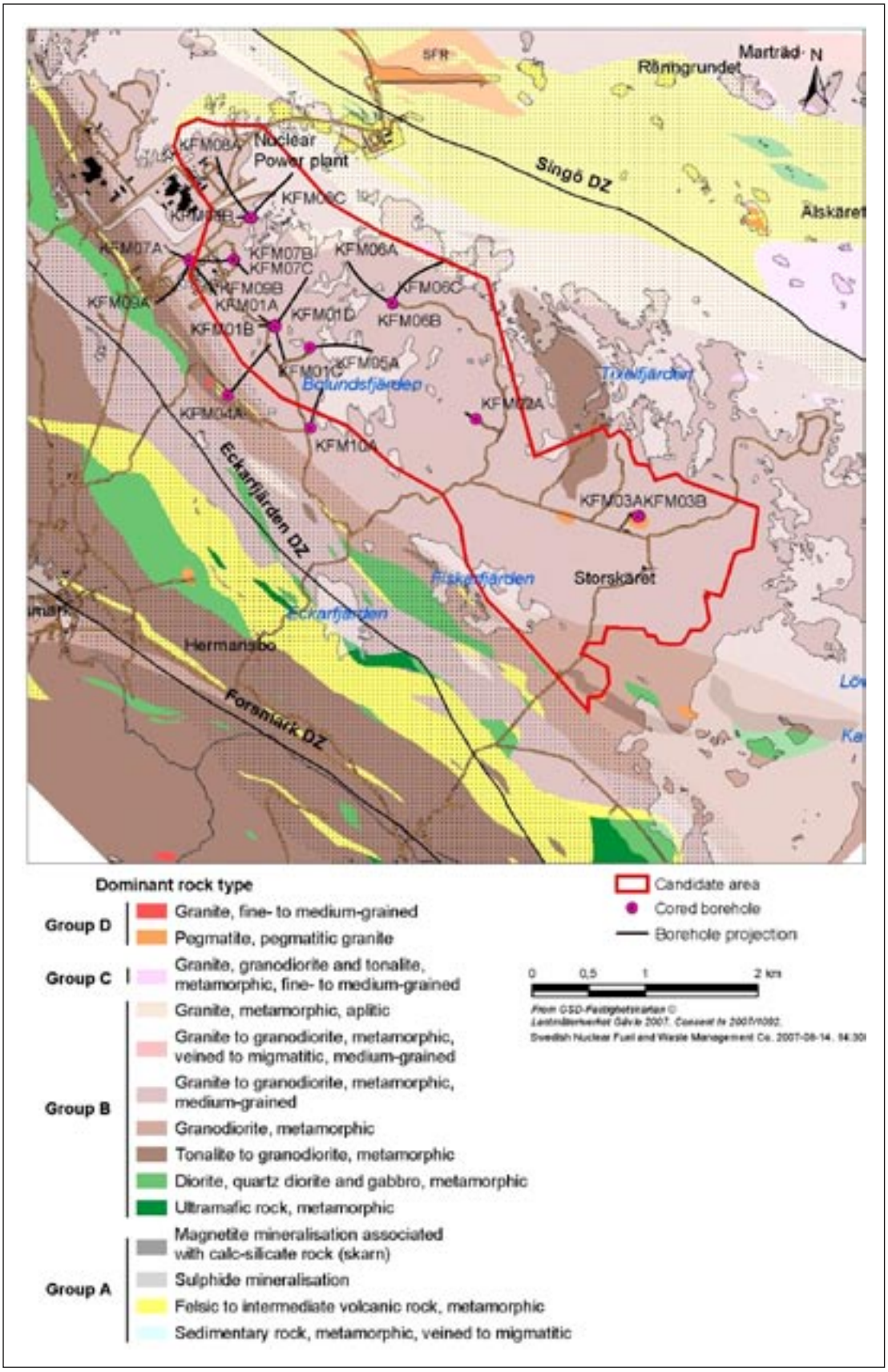

Figure 1-1. *Geology of the Forsmark area and location of boreholes referred to in this report. The major groups of rocks are distinguished on the basis of their relative age, Group A being the oldest and Group D the youngest.*

Figure 1-2. *Local model area in Forsmark.*

1.4.2 Terminology

Definitions of terms important in the thermal modelling work and used in this report are defined below.

Rock type. Each rock type identified in the mapping of bedrock and drill cores has been assigned a name by SKB. Each rock name has an associated name code. Subsequently in the description of the thermal properties, rock types will generally be identified and described by their rock code, as well as by their name. Table 1-1 lists the name codes for the rock types referred to in this report.

Table 1-1. Translation between rock codes and names of different rock types.

Rock code	Rock name
101057	Granite to granodiorite, metamorphic, medium grained
101056	Granodiorite, metamorphic
101054	Tonalite to granodiorite, metamorphic
101051	Granodiorite to tonalite, metamorphic, fine- to medium-grained
101061	Pegmatite, pegmatitic granite
103076	Felsic to intermediate volcanic rock, metamorphic
101058	Granite, metamorphic, aplitic
111058	Granite, fine- to medium-grained
101033	Diorite, quartz diorite and gabbro, metamorphic
101004	Ultramafic rock, metamorphic
102017	Amphibolite

Rock domain. A rock domain in Forsmark refers to a rock volume having rock units that show similar composition, grain size, degree of homogeneity, and degree and style of ductile deformation /Stephens et al. 2007/. Rock domains are used in 3D geometric modelling work. A rock unit is the smallest undivided volume in a 3D geological model /Munier et al. 2003/.

Deformation zone. A deformation zone refers to an essentially 2D structure, along which there is a concentration of ductile and/or brittle deformation /Munier et al. 2003/. A complete list of deformation zones identified in single-hole interpretations are given in /Stephens et al. 2007/.

Thermal rock class (TRC). A thermal rock class comprises one or more rock types having similar thermal properties. Geological properties such as composition, mode of occurrence and age are also considered when classifying thermal rock classes.

Anisotropy. Two types of geological phenomena are believed to result in anisotropy of thermal conductivity within the rock mass at Forsmark. These are (1) anisotropy due to foliation/lineation, and (2) anisotropy due to the preferred orientation of subordinate rock bodies. See Section 4.1.3 for a fuller discussion of anisotropy.

Target volume. The target volume as defined in /Stephen et al. 2007/ includes the rock volume identified as suitable for hosting a final repository. It defines the boundaries of the volume for which thermal modelling has been carried out during stage 2.2. This volume comprises part of rock domain RFM029, as well as domain RFM045.

A glossary of geostatistical terms used in the report is provided in /Back and Sundberg 2007/.

2 Previous model versions and input from geology

2.1 Previous model versions

Thermal modelling work performed as part of stages 1.2 and 2.1 are reported in /Sundberg et al. 2005a/ and /SKB 2006b/. Based on modelling performed as part of model version 1.2 /Sundberg et al. 2005a/, thermal properties were reported for two rock domains, namely RFM029 and RFM012. Results for domain 29 indicated that the mean thermal conductivity of this domain is 3.55 W/(m·K), with a standard deviation of 0.22 W/(m·K). The lower 2.5 percentile for the 0.7 m scale was estimated at 2.9 W/(m·K).

In stage 2.1, new data, in addition to limited modelling efforts, indicated that the statistics of thermal conductivity for domain RFM029 required revision /SKB 2006b/. It was estimated that the mean thermal conductivity is likely to be slightly lower (by up to 0.1 W/(m·K)) than indicated in model version 1.2. More importantly, the lower 2.5 percentile of thermal conductivity, for 0.8 m scale, was suspected to be considerably lower than reported in version 1.2 (up to 0.3 W/(m·K) lower). These revisions were the result of taking into account the presence of amphibolite, which although volumetrically subordinate, was found to have a much less favourable thermal conductivity. Calculations from mineral compositions indicated a thermal conductivity of about 2.4 W/(m·K), considerably lower than all other common rock types present at the Forsmark site. (Slightly different scales were chosen in stages 1.2 (0.7 m) and 2.1 (0.8 m) to estimate percentiles of thermal conductivity that would err on the conservative side for the 1 m scale. However, no significant differences between these scales are expected.)

It is important to point out that previous model versions were based on a previous version of the geological model. This is particularly relevant for domain RFM045. This domain had not been defined in model stage 1.2, and since little modelling was performed during stage 2.1, there are no previous modelling results available for comparison.

One of the main uncertainties remaining after previous model versions concerns the possible effect of anisotropy of thermal conductivity, caused by both small-scale structures such as foliation/lineation, and preferentially oriented bodies of subordinate rocks, primarily amphibolite. In the current model stage, efforts are made to quantify the anisotropy of thermal properties.

2.2 Geological model overview and input to thermal modelling

The target volume includes the rock volume identified as suitable for hosting a final repository. It defines the boundaries of the volume for which thermal modelling has been carried out during stage 2.2. The rock domain model stage 2.2 (see Figure 2-1) forms the basis for the following discussion concerning the thermal properties of the rock mass within the target volume at Forsmark /Stephens et al. 2007/. A rock domain is a part of the rock mass for which geological properties (lithology, structure, etc) can be considered essentially similar in a statistical sense /Munier et al. 2003/. For this reason, it is appropriate to describe thermal properties, which are intimately related to lithological properties, at rock domain level.

Two rock domains have been identified within the target volume. Domain RFM029 makes up the major part of the target volume and will constitute the bulk of any future repository volume. The much smaller domain RFM045 is also located within the intended repository volume. Thermal properties of domains RFM029 and RFM045 are evaluated within this report.

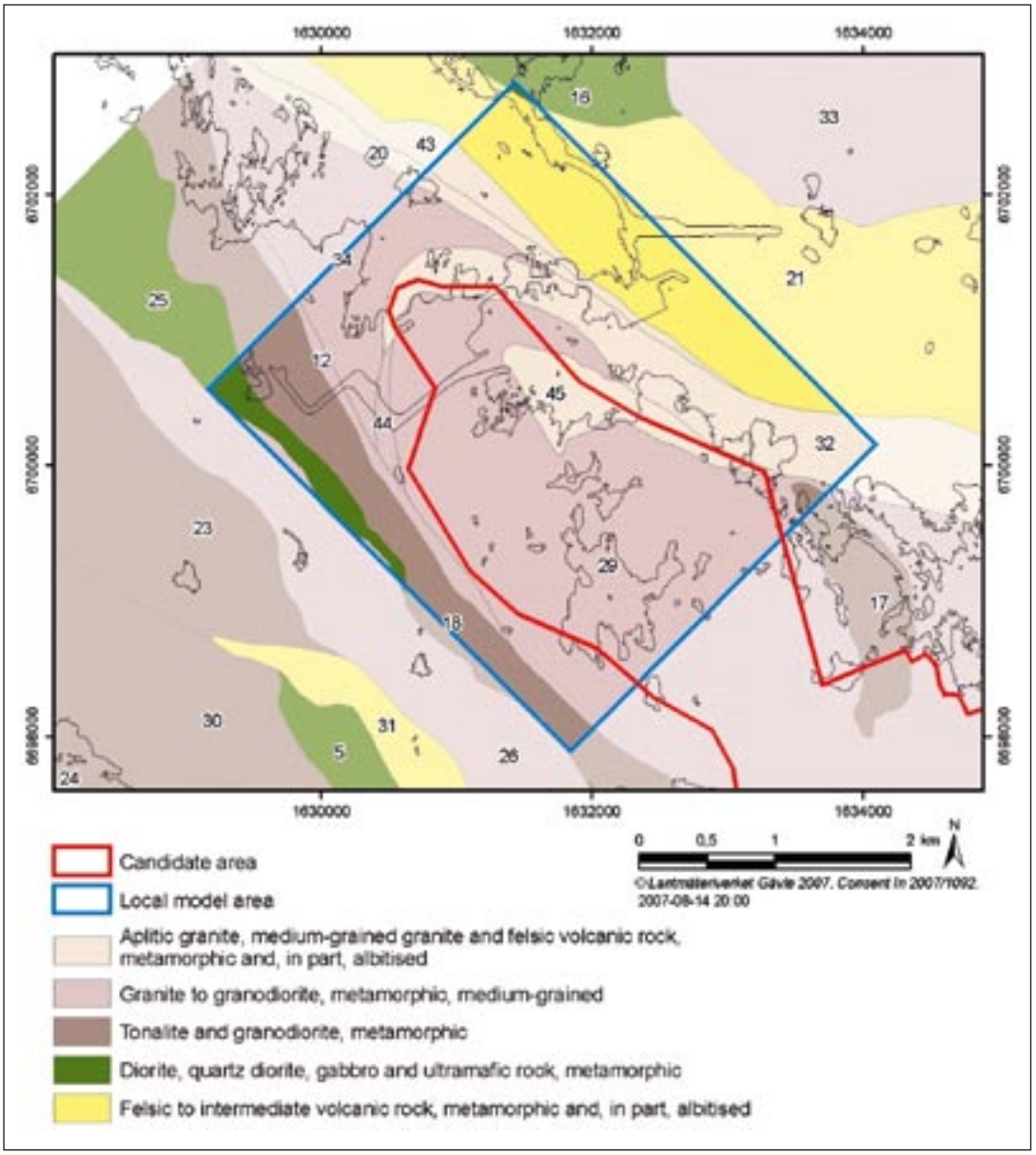

Figure 2-1. *Rock domains in the Forsmark area.*

Both domain 29 and 45 are characterised by quartz-rich granitoids, which are favourable from a thermal properties perspective. The dominating rock type in domain RFM029 is granite to granodiorite (rock code 101057, see Table 1-1). In domain RFM045, the dominant rock type is the generally bleached aplitic granite (101058). The bleaching, caused by Na-K alteration (albitization), is a distinctive feature for this domain. Important subordinate rock types in both domains are pegmatite (101061), granodiorite to tonalite (with subordinate granite), metamorphic, fine to medium grained (101051), and amphibolite (102017). The latter two rocks are somewhat more abundant in domain 45 than in domain 29 /Stephens et al. 2007/. For a more detailed description of the rock type composition in the different domains, see /Stephens et al. 2007/. Numerous deformation zones have been modelled deterministically in the geological model, stage 2.2 / Stephens et al. 2007/. In the thermal modelling work, focus is placed on characterising the properties of the intact rock outside these deformation zones, since deposition holes for canisters in a future repository will be positioned some distance from these zones.

The rocks of domain 29, deformation zones excluded, are generally fresh, with faintly to weakly altered rock making up less than 10% of the volume. As mentioned above, alteration (mainly albitisation) is a common feature of domain 45. Since alteration has resulted in a different, more variable mineral composition, the thermal properties are likely to have been affected.

All rock types have been subjected to some degree of metamorphism and ductile deformation. In general, linear ductile fabrics dominate over planar fabrics, such as foliation, in domains 29 and 45, both of which lie within the Forsmark tectonic lens. These domains are considered to be affected by a lower degree of ductile strain than domains outside the tectonic lens. However, the intensity of tectonic foliation increases towards the marginal parts of domain 29, where it commonly has a NNW strike and is steeply dipping /Stephens et al. 2007/.

The subordinate rock type of most importance for thermal modelling is amphibolite, because of its relatively low thermal conductivity and preferred orientation. The latter may cause anisotropy in thermal properties. The orientation of amphibolite bodies generally follows the orientation of the ductile structures, which means that they are aligned parallel to the limbs and hinge of the major fold structure inside the tectonic lens. Close to the margin of the tectonic lens they strike NNW and are sub-vertical /Stephens et al. 2007/.

Input from geology to the thermal modelling includes:

- A lithological domain classification of each borehole used for geometric modelling of rock domains within the Forsmark area /Stephens et al. 2007/ is used as input to the thermal modelling work.
- Lithological data (rock type and alteration) and deformation zone data /Stephens et al. 2007/ from about 16 cored boreholes have also been used for the purpose of describing and modelling thermal properties.
- The orientation, size and shape of subordinate rock types based on hard data from borehole mapping, in addition to expert judgements by the geological team have been used.
- The nature of ductile deformation within the Forsmark area based on hard data and expert geological judgements.

3 Overview and assessment of investigation data

3.1 Databases

The Forsmark thermal modelling stage 2.2 has used quality-assured primary data acquired prior to the data freeze dated 29 September, 2006. The data used in modelling includes all data available in previous model versions in addition to new data between data freezes 2.1 and 2.2. An overview of all the data available and used in the thermal modelling work conducted during stage 2.2 is compiled in Table 3-1. The main additions to the database between data freezes 2.1 and 2.2 for the purpose of thermal modelling are:

- Laboratory measurement of thermal properties and density for a number of important subordinate rock types, as well as the dominating granite. Some of the samples tested were of altered rock.
- Investigation of anisotropy of thermal properties (caused by foliation within the dominant granite rock) by field measurement close to drill site 7. Laboratory measurements for comparative purposes were also performed.
- Boremap mapping of nine cored boreholes.
- Geophysical borehole logging data (density and temperature) from nine cored boreholes.
- Modal analysis data from both fresh and altered rock.

The primary data are described and evaluated in more detail in the subsequent sections of this chapter.

3.2 Thermal conductivity and diffusivity from measurements

3.2.1 Method

Laboratory measurements of the thermal conductivity and thermal diffusivity on rock samples have been performed using the TPS (Transient Plane Source) method. In the method a thin disc (heat generating/temperature measuring) contained between two pieces of a sample, see description in /Sundberg 2003/. The 79 measurements available in stage 2.1 /SKB 2006b/ are supplemented by 53 new measurements, including samples from boreholes KFM01A (4 samples), KFM01C (10 samples), KFM01D (2 samples), KFM04A (1 sample), KFM05A (5 samples), KFM06A (6 samples), KFM07A (9 samples), and KFM08A (16 samples) /Adl-Zarrabi 2005ab, 2006abc/. The majority of the samples were taken from drill core that was mapped as being unaltered. Four samples of granite to granodiorite (101057) have been affected by oxidation, whereas eight samples of aplitic granite (101058) have been subjected to albitisation.

3.2.2 Results

Summary statistics of thermal conductivity and thermal diffusivity for each rock type are presented in Table 3-2 and Table 3-3, respectively. The main improvements of the database concern the subordinate rock types, granodiorite to tonalite (101051) and amphibolite (102017), pegmatite (101061) and granite (111058). Measurements of these rocks were few or lacking completely in the previous model version. The results of all thermal conductivity measurements are visualised in Figure 3-1.

Table 3-1. Available rock thermal data and their treatment in Forsmark modelling stage 2.2. Report numbers in italics show data available at data freezee 1.2.

Data specification	Reference to data report		Usage in F2.2, analysis/modelling
Data from core-drilled boreholes			
Temperature and density logging	Results	Interpret.	Data used for describing natural temperature variations with depth.
KFM01A	P-03-103	P-04-80	
KFM01B	P-04-145	P-04-80	Estimation of thermal conductivity from density based on relationship between these two parameters.
KFM01C	P-06-123	P-06-152	
KFM01D	P-06-168	P-06-216	
KFM02A	P-04-97	P-04-98	
KFM03A	P-04-97	P-04-98	
KFM04A	P-04-144	P-04-143	Density data also used to study and model spatial correlation in thermal conductivity.
KFM05A	P-04-153	P-04-154	
KFM06A	P-05-17	P-05-51	
KFM06C	P-05-276	P-06-84	
KFM07A	P-05-159	P-05-119	
KFM07B	P-06-22	P-06-126	
KFM07C	P-07-04	P-07-78	
KFM08A	P-05-159	P-05-202	
KFM08C	P-07-05	P-06-258	
KFM09B	P-06-123	P-06-152	
KFM10A	P-07-05	P-06-258	
Boremap mapping			Major and subordinate rock type distribution. Data used for identification of rock type at drill core samples locations and in situ logging. Data used as input to stochastic simulation of lithologies.
KFM01A	P-03-23		
KFM01B	P-04-114		
KFM01C	P-06-133		
KFM01D	P-06-132		
KFM02A	P-03-98		
KFM03A	P-03-116		
KFM04A	P-04-115		
KFM05A	P-04-295		
KFM06A	P-05-101		
KFM06C	P-06-79		
KFM07A	P-05-102		
KFM07B	P-06-80		
KFM07C	P-06-205		
KFM08A	P-05-203		
KFM08B	P-05-203		
KFM08C	P-06-203		
KFM09B	P-06-131		
KFM10A	P-06-204		
Laboratory test of density			Data used for investigation of relationship between density and thermal conductivity
KFM01A	*P-04-166,* P-06-234		
KFM01C	P-06-67, P-06-234		
KFM01D	P-06-234		
KFM02A	P-04-167		
KFM03A	P-04-168		
KFM04A	*P-04-169,* P-06-234		
KFM05A	P-06-234		
KFM06A	*P-05-124,* P-06-234		
KFM07A	P-05-215		
KFM08A	P-05-220		

Data specification	Reference to data report	Usage in F2.2, analysis/modelling
Laboratory test of thermal properties		Estimation of thermal conductivity, thermal diffusivity and specific heat capacity.
KFM01A	*P-04-159,* P-06-233	
KFM01C	P-06-66, P-06-233	
KFM01D	P-06-233	
KFM02A	P-04-161	
KFM03A	P-04-162	
KFM04A	*P-04-199,* P-06-233	
KFM05A	P-06-233	
KFM06A	*P-05-123,* P-06-233	
KFM07A	P-05-214	
KFM08A	P-05-219	
Anisotropy in thermal properties for KFM04A and KFM90B	P-06-285	Estimation of anisotropy in thermal properties.
	P-07-194	
Inter-laboratory comparison of TPS measurements for KFM01A	P-04-186	
Modal analysis		Estimation of thermal conductivity from mineralogical composition of the bedrock. Statistical analysis. Impact of alteration on mineralogy and thermal conductivity.
KFM01A	*P-04-103, P-04-159,* P-06-233, P-06-209	
KFM01A	P-06-209	
KFM02A	*P-04-103, P-04-161,* P-06-209	
KFM03A	P-04-103, P-04-162	
KFM03B	P-04-103	
KFM04A	P-04-199, P-05-156	
KFM05A	*P-05-156,* P-06-233	
KFM06A	*P-05-156,* P-06-233	
KFM07A	P-06-209	
KFM08A	P-06-209	
KFM08B	P-06-209	
Laboratory test of thermal expansion		Estimation of the thermal expansion coefficient.
KFM01A	P-04-163	
KFM02A	P-04-164	
KFM03A	P-04-165	
KFM04A	P-04-198	
KFM05A	P-07-33	
KFM06A	P-07-33	
Large-scale field measurement of thermal properties		Analysis of anisotropy in thermal conductivity
KFM90B,C,D,E,F	/Sundberg et al. 2007b/	
Surface and near-surface data		
Laboratory test of thermal properties		Thermal transport properties for some samples. Comparison with modelled results.
Surface samples	P-03-08	
Modal analysis		Estimation of thermal conductivity from mineralogical composition of the bedrock.
Surface samples	P-03-75, P-04-87, P-05-156	
Small-scale field measurement of thermal properties		Analysis of anisotropy in thermal conductivity
Close to drill site KFM07	/Sundberg et al. 2007b/	
Modelling		
Ductile deformation zones	R-07-15	Density logging data from within deformation zones removed prior to spatial correlation analysis.
Site descriptive model – geology, stage 2.2.	R-07-45	Rock domain model, including analysis of alteration, used as input for thermal modelling.

Table 3-2. Measured thermal conductivity (W/m·K)) of different rock types using the TPS method.

Rock code	Rock name	Sample location	Mean	St. dev.	Max	Min	Number of samples
101057	Granite to granodiorite, metamorphic, medium grained	Boreholes KFM01A, KFM01C KFM01D KFM02A, KFM03A, KFM04A, KFM07A, KFM08A and surface	3.68	0.17	4.01	3.25	74[1]
101056	Granodiorite, metamorphic	Boreholes KFM04A	3.04	0.09	3.20	2.98	5
101054	Tonalite to granodiorite, metamorphic	Borehole KFM03A, and surface	2.73	0.19	2.94	2.45	5
101051	Granodiorite and tonalite, metamorphic, fine- to medium grained	Boreholes KFM01A, KFM01C KFM03A, KFM05A, KFM06A, KFM08A	2.85	0.26	3.39	2.46	12
101058	Granite, metamorphic, aplitic	Borehole KFM06A KFM08A	3.85	0.13	4.06	3.68	12[2]
	Albitised/altered		3.89	0.13	4.06	3.70	8
	Not albitised/altered		3.77	0.12	3.95	3.68	4
101061	Pegmatite, pegmatitic granite	Borehole KFM07A, KFM08A	3.33	0.20	3.50	3.07	4
102017	Amphibolite	Boreholes KFM01A, KFM01C KFM01D, KFM05A, KFM07A, KFM08A	2.33	0.10	2.48	2.21	12
111058	Granite, fine- to medium-grained	Boreholes KFM01C KFM04A, KFM05A, KFM06A	3.47	0.17	3.62	3.22	5
103076	Felsic to intermediate volcanic rock, metamorphic	Boreholes KFM01C KFM08A	2.54		2.99	2.09	2
101033	Diorite, quartz diorite and gabbro, metamorphic	Surface	2.28				1

[1] Includes four altered samples. [2] Both altered and unaltered samples included.

Table 3-3. Measured thermal diffusivity (mm²/s) of different rock types using the TPS method.

Rock code	Rock name	Sample location	Mean	St. dev.	Max	Min	Number of samples
101057	Granite to granodiorite, metamorphic, medium grained	Boreholes KFM01A, KFM01C KFM01D KFM02A, KFM03A, KFM04A, KFM07A, KFM08A and surface	1.71	0.11	2.05	1.47	74[1]
101056	Granodiorite, metamorphic	Boreholes KFM04A	1.35	0.05	1.42	1.29	5
101054	Tonalite to granodiorite, metamorphic	Borehole KFM03A, and surface	1.30	0.13	1.51	1.18	5
101051	Granodiorite and tonalite, metamorphic, fine- to medium grained	Boreholes KFM01A, KFM01C KFM03A, KFM05A, KFM06A, KFM08A	1.30	0.14	1.65	1.14	12
101058	Granite, metamorphic, aplitic	Borehole KFM06A KFM08A	1.86	0.07	1.97	1.68	12[2]
101061	Pegmatite, pegmatitic granite	Borehole KFM07A, KFM08A	1.74	0.11	1.83	1.58	4
102017	Amphibolite	Boreholes KFM01A, KFM01C KFM01D, KFM05A, KFM07A, KFM08A	0.95	0.04	1.03	0.88	12
111058	Granite, fine- to medium-grained	Boreholes KFM01C KFM04A, KFM05A, KFM06A	1.62	0.11	1.72	1.47	5
103076	Felsic to intermediate volcanic rock, metamorphic	Boreholes KFM01C KFM08A	1.13		1.36	0.90	2
101033	Diorite, quartz diorite and gabbro, metamorphic	Surface	0.98				1

[1] Includes four altered samples. [2] Both altered and unaltered samples included.

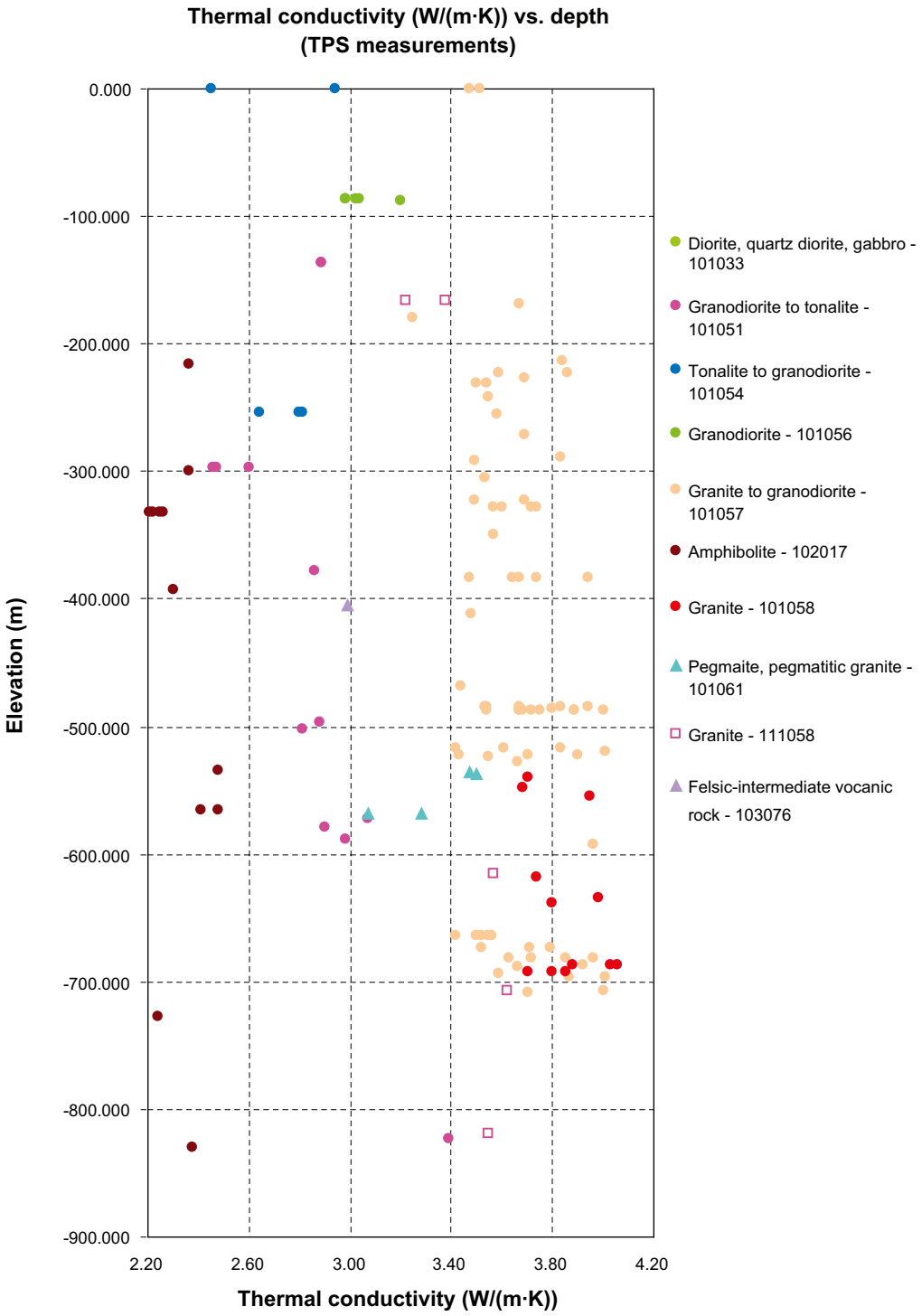

Figure 3-1. *Thermal conductivity versus elevation for different rock types. Samples measured using the TPS method.*

Four of the granite to granodiorite (101057) samples are from sections mapped (boremap) as altered (faint to medium oxidation). Their thermal conductivities range from 3.25 to 4.01 which are the lowest and highest values of the complete data set. The mean is 3.77 which is slightly higher than the mean of the unaltered samples (3.67) but the number of samples is too small to make any definite conclusions regarding the effect of alteration on thermal conductivity.

The samples of rock type 101058 (granite, aplitic) can be divided into two groups according to whether or not they have been affected by alteration (albitization or oxidation) /Petersson et al. 2005a/. Although albitised samples have a higher mean thermal conductivity than non-albitised samples based on TPS measurements, the difference is small (Table 3-2).

The additional new data for the dominant rock, granite to granodiorite (101057), have little effect on the summary statistics (mean and standard deviation) described in stage 2.1. A comparison of data from different boreholes (Table 3-4) and different depths (Figure 3-1) indicates little large scale spatial variation in thermal conductivity.

As regards the dominant rock type (granite to granodiorite, 101057), good spatial coverage has been achieved by the sampling programme, data deriving from several boreholes from north to south, and at varying depths. Many of the samples were taken in groups of approximately 3–5 samples located close to each other. Declustering techniques were applied to evaluate possible bias (see 5.4.2). Data for the other rock types are rather sparse but, at least for those rock types considered to be important, relatively good spatial coverage was achieved by sampling several boreholes.

3.3 Thermal conductivity from mineral composition

3.3.1 Method

The thermal conductivity of rock samples has been calculated by the SCA method (Self Consistent Approximation) using mineral compositions from modal analyses and reference values of the thermal conductivity of different minerals, as described in /Sundberg 1988, Sundberg 2003/.

The following data were available for calculations by the SCA-method.

- Modal analyses from samples (192 in total) included in Forsmark site modelling stage 2.1 /SKB 2006b/.
- A total of 19 new modal analyses:
  - Four samples of granodiorite to tonalite (101051) taken close to samples for measurements of thermal properties /Adl-Zarrabi 2006c/.
  - 15 samples analysed as part of a study investigating the effects of oxidation/alteration on the mineralogy of granites /Sandström and Tullborg 2006/.

For samples where the sum of the volume fraction of minerals diverges slightly from 100%, the proportions of the minerals present were corrected so that they summed to 100%.

Table 3-4. Measured thermal conductivity of granite to granodiorite 101057 using the TPS method. Comparison of samples from boreholes KFM01A, KFM02A, KFM03A, KFM04A, KFM07A and KFM08A.

	KFM01A	KFM02A	KFM03A	KFM04A	KFM07A	KFM08A
No. of samples	27	15	6	10	5	7
Mean	3.71	3.74	3.65	3.61	3.66	3.52
St. dev.	0.17	0.18	0.16	0.16	0.12	0.08

Reference values of thermal conductivity for different minerals have been taken from /Horai 1971, Horai and Baldridge 1972/. In Table 3-5, the thermal conductivities of minerals used in Forsmark modelling stage 2.2 together with the values used in stage 2.1 are presented. The main difference is the change in the value adopted for K-feldspar, which in Forsmark granites has been reported to be dominated by microcline /Petersson et al. 2004a, Sandström and Tullborg 2006/. Thermal conductivity values for different forms of plagioclase are given in the table. Oligoclase is the most common form in the granitoid rocks at Forsmark /Petersson et al. 2005a/. In altered rocks, plagioclase is typically saussuritized, and comprises albite and other alteration products /Sandström and Tullborg 2006/. Slightly higher thermal conductivities were assigned to these forms (see discussion below). The rock type granite (101058) is typically altered

Table 3-5. Summarized thermal conductivities W/(m·K) of minerals used in the current report compared to earlier versions.

Mineral	Forsmark 1.2	Forsmark 2.1	Forsmark 2.2
Actinolite	–	3.45	3.45
Adularia			2.05
Allanite	3.00	3.00	3.00
Amphibole	3.39	–[1]	–[1]
Apatite	1.38	1.38	1.38
Biotite	2.02	2.02	2.02
Calcite	3.59	3.59	3.59
Chlorite	5.15	5.15	5.15
Clay minerals			3.0
Clinopyroxene	3.20	4.36[2]	4.36[2]
Epidote	2.83	2.83	2.83
Hornblende	2.81	2.81	2.81
Alkali feldspar	2.29	2.40	2.49[3]
Magnetite	5.10	5.10	5.10
Muscovite	2.32	2.32	2.32
Olivine	4.57	4.57	4.57
Opaque	3.00	3.00	6.6/8.2[4]
Orthopyroxene	3.20	4.00	4.00[5]
Plagioclase: oligoclase (An_{15})	1.93	1.93	1.93[6]
Plagioclase: albite ($An_{2.5}$)			2.20[7]
Plagioclase: saussuritized			2.22
Prehnite	3.58	3.58	3.58
Pumpellyite			3.0
Quartz	7.69	7.69	7.69
Serpentine	3.53	–	3.53
Talc	–	6.10	6.10
Titanite	2.34	2.34	2.34
Zircon	4.54	4.54	4.54

[1] Where amphibole is quoted in the modal analyses it is assumed to be hornblende /Stephens 2007/.

[2] Mean of values for diopside and augite, two common forms of clinopyroxene.

[3] Value for microcline, the primary K-feldspar /Sandström and Tullborg 2006/.

[4] Mean of values for magnetite and hematite assuming 75% magnetite and 25% hematite in fresh rocks and equal proportions of these minerals in altered rocks /based on Sandström and Tullborg 2006/.

[5] Mean of Fs_0 – Fs_{50}, the most common compositional range of orthopyroxene in mafic plutonic rocks.

[6] From curve based on data from /Horai 1971/ and presented in /Sundberg et al. 2005a/.

[7] From curve based on data from /Horai 1971/.

Yellow: data missing, estimated values.

Red: unknown chemical composition of the mineral.

/Petersson et al. 2005a/. Although the alteration has been described as albitization, the anorthite content of plagioclase in these rocks is 8-16 (mean 12.5) which means a slightly higher thermal conductivity than for fresh samples but not as high as for pure albite. Therefore, plagioclase in these albitised samples has been assigned the same thermal conductivity value as unaltered plagioclase in the calculations. All data have been recalculated using the revised thermal conductivity values.

3.3.2 Results

The results of the SCA calculations based on modal analyses arranged according to rock type are presented in Table 3-6. Apart from some albitized samples of granite (101058) and granite to granodiorite (101057), the data are derived from rocks mapped as fresh in the boremap mapping.

Table 3-7 shows SCA calculations for granite to granodiorite (101057), the dominating rock type, divided according to location (per borehole and surface samples). Similar to that found in the TPS data, the mean and standard deviation of thermal conductivity are similar for all boreholes, although it should be noted that statistical tests were not performed.

As regards the dominant rock type (granite to granodiorite, 101057), good spatial coverage has been achieved by the sampling programme, data deriving from several boreholes from north to south, and at varying depths. The representativness of the SCA data for the different rock types would not be improved by declustering, although it may still be the case for some subordinate rock types that data are concentrated to a restricted part of the target volume. For example, for rock types with codes 101054, 103076 and 111058 (see Table 3-6) most or all of the samples are from the surface, which means that these rock types at depth are not represented. This is not the case for the more important rock types, granite to granodiorite (101057), granodiorite to tonalite (101051), amphibolite (102017) and granite (101058), for which about half of the data are derived from drill core samples.

Table 3-6. Thermal conductivity (W/(m·K)) calculated from mineralogical composition using the SCA method. Apart from some samples of albitized granite (101058), altered samples are not included.

Rock code	Rock name	Arithmetic mean	St. dev.	Max	Min	Number of samples
101057	Granite to granodiorite	3.64	0.27	4.53	2.72	84
101051	Granite, granodiorite and tonalite	3.14	0.24	3.51	2.61	31
101054	Tonalite to granodiorite	3.02	0.36	4.00	2.28	26
101061	Pegmatite, pegmatitic granite	3.57	0.17	3.74	3.32	5
101033	Diorite, quartz diorite and gabbro	2.53	0.22	3.00	2.26	11
101004	Ultramaphic rock	3.89		4.03	3.75	2
101056	Granodiorite	3.14	0.22	3.55	2.83	11
101058	Granite, aplitic[1]	3.80	0.30	4.21	3.47	11
102017	Amphibolite	2.42	0.08	2.52	2.31	4
103076	Felsic to intermediate volcanic rock	3.08	0.39	3.66	2.50	15
111058	Granite	3.51	0.42	4.08	3.06	4

[1] Albitised samples included.

Table 3-7. Calculated (SCA method) thermal conductivity of granite to granodiorite (101057) for samples from individual boreholes and from the surface.

	KFM01A	KFM02A	KFM03A	KFM04A	KFM05A	KFM06A	Surface
Mean	3.77	3.58	3.69	3.52	3.71	3.60	3.56
No. of samples	15	17	11	6	3	1	29
St. dev.	0.32	0.33	0.21	0.20	0.20		0.19

3.3.3 Influence of alteration on thermal conductivity

Mineralogical changes associated with alteration can be expected to influence the thermal properties of the rock. To investigate the effect of alteration on rock thermal conductivities, point counting data of thin sections from a study by /Sandström and Tullborg 2006/ of altered rock and their unaltered equivalents were analysed.

At Forsmark, alteration affects the rock mass both inside and outside the deformation zones, and has been documented in surface samples /Stephens et al. 2003, 2005/ and in borehole samples /Petersson et al. 2004a/. Oxidation is the most common form of alteration. At the mineral scale, the main alteration phenomena are saussuritization of plagioclase, and chloritization of biotite /Petersson et al. 2004a, Petersson et al. 2005a, Sandström and Tullborg 2006/. Another more locally occurring form of alteration is albitization, which mainly affects rock type granite (101058), while less commonly found in granite to granodiorite (101057). This form of alteration has been found mainly in KFM06A and at the surface /Petersson et al. 2005a/. Many of the minerals associated with alteration, e.g. sericite, chlorite, have thermal conductivities that differ from their parent minerals, for example, feldspars, biotite.

Point counting data from the study by /Sandström and Tullborg 2006/ are based on samples from boreholes KFM01A, 02A, 07A, 08A and 08B, and were taken outside deformation zones. In order to calculate the thermal conductivity of these rock samples using the SCA method, it is necessary to estimate the thermal conductivity of saussuritized plagioclase and chloritized biotite, which are the most common alteration products. Typical mineral compositions for these phases were approximated from /Sandström and Tullborg 2006/ and /Sandström 2006/ and are summarised in Table 3-8. The derived thermal conductivity for saussuritized plagioclase is rather insensitive to variations in the proportions of the different alteration minerals since the common components (albite and adularia) have rather similar thermal conductivities, see Table 3-5. For both plagioclase and biotite, the thermal conductivities of the altered phases are higher, much higher in the case of chloritized biotite, than the unaltered mineral.

The mean thermal conductivities for the altered and unaltered samples for granodiorite to tonalite (101051) and granite to granodiorite (101057) are summarised in Table 3-9. The number of altered samples is too low (3 and 6 respectively) to allow any meaningful conclusions regarding the effect of alteration to be based on a simple comparison of mean thermal conductivities. Instead the altered samples may be valuably compared with the unaltered samples analysed as part of the same study /Sandström and Tullborg 2006/ on a thermal conductivity versus quartz

Figure 3-2. *Photos of fresh and altered granite to granodiorite (101057), from /Sandström and Tullborg 2006/.*

Table 3-8. Approximated mineral compositions of altered plagioclase and biotite.

Original mineral phase	Altered mineral name	Alteration mineralogy	Mean TC	TC of original mineral
Plagioclase	Saussuritized plagioclase	Albite (75%), adularia (20%), epidote (2%), sericite (2%) and hematite (1%)	2.22	1.93
Biotite	Chloritized biotite	Chlorite (75%), adularia (10%), prehnite and pumpellyite (10%), titanite (5%)	4.28	2.02

Table 3-9. Calculated (SCA method) thermal conductivity of altered and unaltered varieties of rock types 101051 (granodiorite to tonalite) and 101057 (granite to granodiorite).

Rock code	Alteration	Mean	Number of samples
101051	Oxidised /Sandström and Tullborg 2006/	3.68	3
	Fresh /Sandström and Tullborg 2006/	3.51	1
	Fresh – all	3.14	31
101057	Oxidised /Sandström and Tullborg 2006/	3.93	6
	Fresh /Sandström and Tullborg 2006/	3.97	5
	Fresh – all	3.64	84

content plot. In Figure 3-3 it can be clearly seen that for a given quartz content, the calculated thermal conductivity for altered samples is consistently higher than that for unaltered samples. The difference, about 0.25 W/(m·K), can only be explained by the properties of minerals other than quartz. In fresh rock, non-quartz minerals are dominated by feldspars and biotite, whereas in altered rocks it is these minerals that have been affected by alteration. The effect of increased porosity in altered rocks on thermal conductivity has been estimated to approximately 0.01 W/(m·K), given an average difference in porosity between altered and unaltered specimens of less than 0.2% /Sandström and Tullborg 2006/.

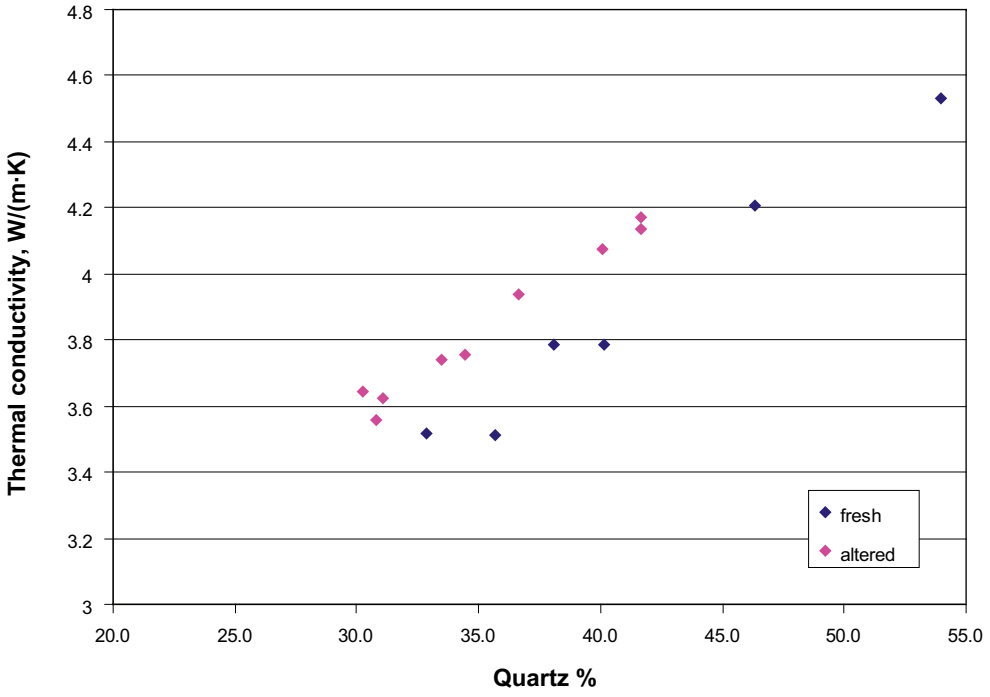

Figure 3-3. *Thermal conductivity versus quartz content for unaltered and altered samples. The altered samples include a sample of granite to granodiorite, rock code 101057, (KFM08B, 91.36 m) judged as fresh from the core sample but shown to be altered under the optical microscope /Sandström and Tullborg 2006/.*

The samples of granite (101058) can be divided into two groups according to whether or not they have been affected by albitization /Petersson et al. 2005a/. Albitization has involved the replacement of K-feldspar by an albite-rich form of plagioclase, and enrichment of quartz relative to unaltered equivalents /Petersson et al. 2005a/. Common to all rocks subjected to albitization is bleaching or whitening. Comparison of albitised and non-albitised varieties in Table 3-10 indicates that the former have higher thermal conductivities than their unaltered equivalents. Laboratory measurements (TPS) of granite (101058) show the same relationship between altered and unaltered samples, although the difference is smaller, see 3.2.2.

The samples for thin section analysis used in SCA calculations summarised in Section 3.3.2 above were generally taken from drill cores sections recorded as fresh in the boremap mapping. It should be noted, however, that thin section analysis indicates that alteration is present even in samples from sections of cores for which no alteration has been recorded in the boremap mapping /Sandström and Tullborg 2006/. This means that the estimations of thermal conductivity for these "fresh" samples may be slightly conservative. Comparison of SCA data with laboratory measured values in Section 3.3.4 indicates that any differences are likely to be small.

3.3.4 Comparison with laboratory measurements

For several of the borehole cores on which samples have been taken for laboratory determination of thermal conductivity (TPS method), sampling for modal analysis and SCA calculations has also been carried out /Sundberg et al. 2005b/. The objective is to compare determinations from the different methods so as to evaluate the accuracy of the SCA calculations. SCA data for samples presented in previous model versions have been recalculated using the revised mineral thermal conductivities, see Table 3-5. For the comparison, the SCA and TPS samples closest to one another in the borehole core have been used. It should be emphasised that the samples are not exactly the same. Therefore, some of the observed differences are probably a result of sampling.

In Table 3-11, new data pairs for granodiorite to tonalite (101051) are presented. The correspondence between measured thermal conductivity (TPS) and calculated thermal conductivity (SCA) is quite good if one sample is excluded. In Table 3-12 and Figure 3-4, TPS and SCA data for

Table 3-10. Calculated (SCA method) thermal conductivity of altered (albitised) and unaltered varieties of granite (101058).

Rock code	Rock name	Alteration	Mean	Number of samples	Comment
101058	Granite, aplitic	unaltered	3.68	7	KFM06A and surface
101058	Granite, aplitic	albitised	3.97	4	KFM06A and surface

Table 3-11. Specification of samples included in the comparison of thermal conductivity (W/(m·K)) calculated from mineral composition (SCA) and measured with TPS method. The samples are of granodiorite to tonalite (101051).

Borehole/sample ID	Rock code	Secup (m) SCA	SCA	Secup (m) TPS	TPS	Diff. (SCA-TPS)/ TPS (%)
KFM01A	101051	838.43	3.35	837.92	3.39	–1.2%
KFM03A	101051	305.87	3.14	305.75	2.47	27.0%
KFM05A	101051	686.94	3.04	686.99	3.07	–1.0%
KFM05A	101051	708.4	3.04	708.26	2.98	2.0%
KFM06A	101051	588.64	3.21	588.50	2.88	11.5%
Mean (excl. sample KFM03A)[1]			3.16		3.08	2.6%
Correlation coefficient, r (excl. sample KFM03A)[1]						0.624

[1] Sample KFM03A (305 m) is omitted from the calculation of the mean as the SCA value is considered to be unrepresentative of this rock type in this borehole section. Three TPS determinations on samples from the same section give thermal conductivity values of c. 2.5 W/(m·K).

several rock types are compared. For granite to granodiorite (101057) a good agreement is found between the means of measured (TPS) and calculated (SCA) values. However, within the interval of thermal conductivities defined by laboratory measurements, there is no clear relationship between TPS and SCA values. This is most likely due to the random errors associated with 1) the point counting method and 2) the sampling method; the comparison is made between proximal, but different samples. Thus, the SCA method is less useful for estimating the conductivity value of individual samples (large random noise). However, together the complete data set for granite to granodiorite (101057) represents the rock type fairly well, although the variance is slightly high. For the other two rock types, tonalite to granodiorite (101054) and granodiorite (101056), there are too few samples on which to base any firm conclusions.

Table 3-12. Comparison of thermal conductivity (W/(m·K)) calculated by different methods for four rock types. SCA values are calculated from mineralogical composition and the TPS values by laboratory measurement. Samples are from boreholes KFM01A, KFM02A, KFM03A and KFM04A, KFM05A, KFM06A and from the outcrops. Mean refers to arithmetic mean.

Method	Granite to granodiorite (101057) 24 samples	Granodiorite to tonalite (101051) 4 samples	Tonalite to granodiorite (101054) 2 samples	Granodiorite (101056) 2 samples
Calculated (SCA) Mean	3.68	3.15	3.00	3.00
Measured (TPS) Mean	3.67	2.96	2.63	3.00
Diff. (SCA-TPS)/TPS	0.3%	2.6%	14.1%	0.1%

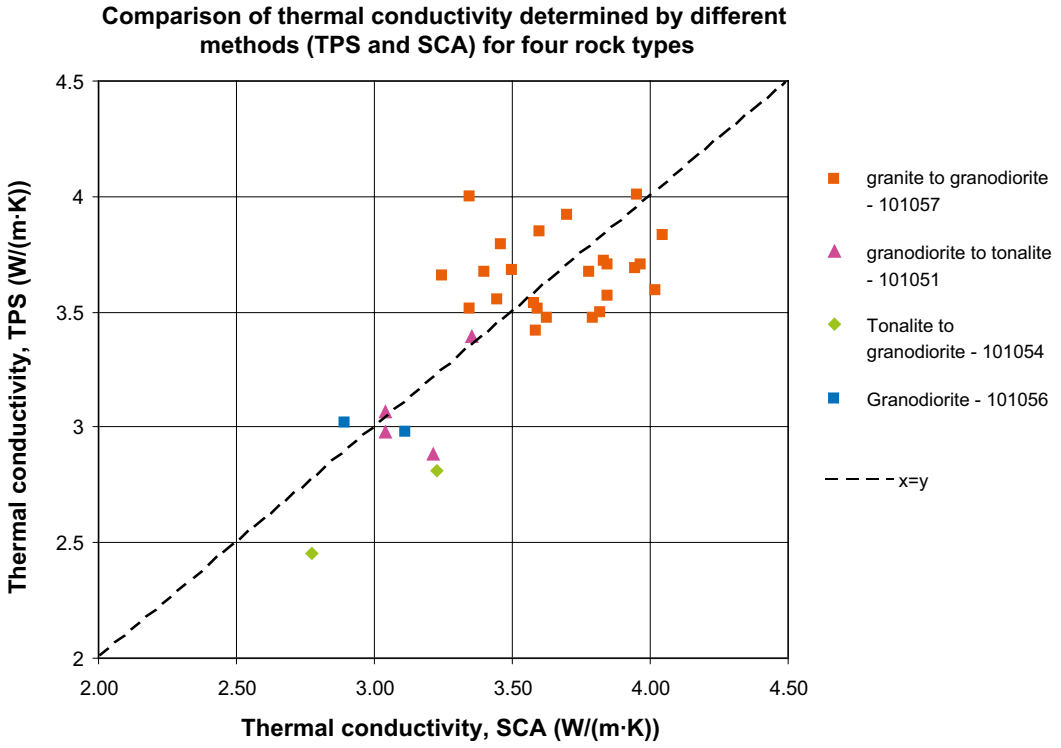

Figure 3-4. *Comparison between thermal conductivity calculated from SCA and measured by the TPS-method for four rock types. The line through the data points represents x = y and is included to aid interpretation. The correlation coefficient (r) for the relationship between the two variables is 0.736. For the comparison, the SCA and TPS samples closest to one another in the borehole core have been used. It should be emphasised that the samples are not exactly the same. Therefore, some of the observed differences are probably a result of sampling. Data from level 305 m in borehole KFM03A is considered erroneous and has been omitted from the diagram.*

Table 3-13 presents a comparison of TPS and SCA data for all rock types. In previous model versions /Sundberg et al. 2005a, SKB 2006/ a significant discrepancy between the mean thermal conductivity determined by the TPS and the SCA methods was found for granodiorite to tonalite (101051). An explanation put forward was that the TPS data (3 samples only) suffered from lack of representativity in a rock type with a large variation in composition. The incorporation of the new TPS data produces a significant reduction in the difference of the means, see Table 3-13. Since the data set, especially the TPS measurements, is still rather small, and may suffer from a lack of representativity, there is no conclusive evidence that indicates that the SCA method overestimates the thermal conductivity for this rock type. The same argument holds for other rock types such as felsic to intermediate volcanic rock (103076) and tonalite to granodiorite (101054), which also display large compositional variations.

3.4 Thermal conductivity from density

3.4.1 Introduction

A relationship between density and measured (TPS) thermal conductivity for Ävrö granite in Laxemar/Simpevarp is well established /Sundberg 2003b, Sundberg et al. 2005a, Wrafter et al. 2006, Sundberg et al. 2007a/, and when applied to borehole density logging data, has been used for modelling of thermal conductivity along continuous sections of boreholes. A corresponding relationship has not previously been observed for any of the rock types within the Forsmark site investigation area. With the availability of additional data, a renewed investigation is warranted. An interesting rock type in this context is granodiorite to tonalite (101051), which displays a wide range of compositions /SKB 2006b/ and densities (based on density logging data from several boreholes).

Establishing relationships between density and thermal conductivity is important since it allows the more reliable use of borehole density data for analysing the spatial correlation structure of thermal properties (see Section 5.4.2).

Table 3-13. Thermal conductivity (W/(m·K)) calculated from the SCA and TPS methods.

Rock code	Rock name	SCA mean	n	TPS mean	n	Comment
101057	Granite to granodiorite	3.64	84	3.67	70	Altered samples excluded
101051	Granite, granodiorite and tonalite	3.14	31	2.85	12	
101054	Tonalite to granodiorite	3.02	26	2.73	5	TPS unrepresentative
101033	Diorite, quartz diorite and gabbro	2.53	11	2.28	1	
101056	Granodiorite	3.14	11	3.04	5	TPS unrepresentative
101058	Granite, aplitic	3.78	12	3.85	12	Albitised samples included
101061	Pegmatite, pegmatitic granite	3.57	5	3.33	4	TPS unrepresentative
102017	Amphibolite	2.42	4	2.33	12	
111058	Granite	3.51	4	3.47	5	
103076	Felsic to intermediate volcanic rock	3.08	15	2.54	2	

3.4.2 Method

The relationship between density and thermal conductivity for all investigated rock types is illustrated in Figure 3-5. For rock types other than granodiorite to tonalite (101051) and amphibolite (102017), no valid relationships are apparent. However, the observed relationship between density and thermal conductivity for all rock types together is consistent with the results of theoretical calculations presented in /Sundberg et al. 2007a/.

A cross plot of thermal conductivity and density for the 12 available samples of granodiorite to tonalite (101051) is shown in Figure 3-6. A second-order equation describes the relationship between these variables rather well (Figure 3-6 and Equation 3-1). Recently acquired data for amphibolite (102017) also display a correlation between density and thermal conductivity, although the range in thermal conductivity is small.

$y = 3.35416E{-}05x^2 - 0.1895611x + 270.3315 \qquad R^2 = 0.93 \qquad$ Equation 3-1

Based on the relationship between density and thermal conductivity established for granodiorite to tonalite (101051) above, density values given by the density loggings of boreholes could be used to deterministically assign a thermal conductivity value to each logged decimetre section of granodiorite to tonalite (101051) within selected borehole intervals. Prior to performing these calculations, each borehole was assessed as regards suitability for determining thermal conductivity from density. Suitable borehole intervals were those that fulfilled the following requirements:

- boreholes within the target volume,
- boreholes for which random noise levels in density logging data are less than 20 kg/m^3,
- borehole sections comprising granodiorite to tonalite (101051) thicker than 2 m. The reason for this is to minimise boundary effects produced by surrounding rock types,
- borehole sections outside identified deformation zones, as reported in the geological model, v. 2.2 /Olofsson et al. 2007/.

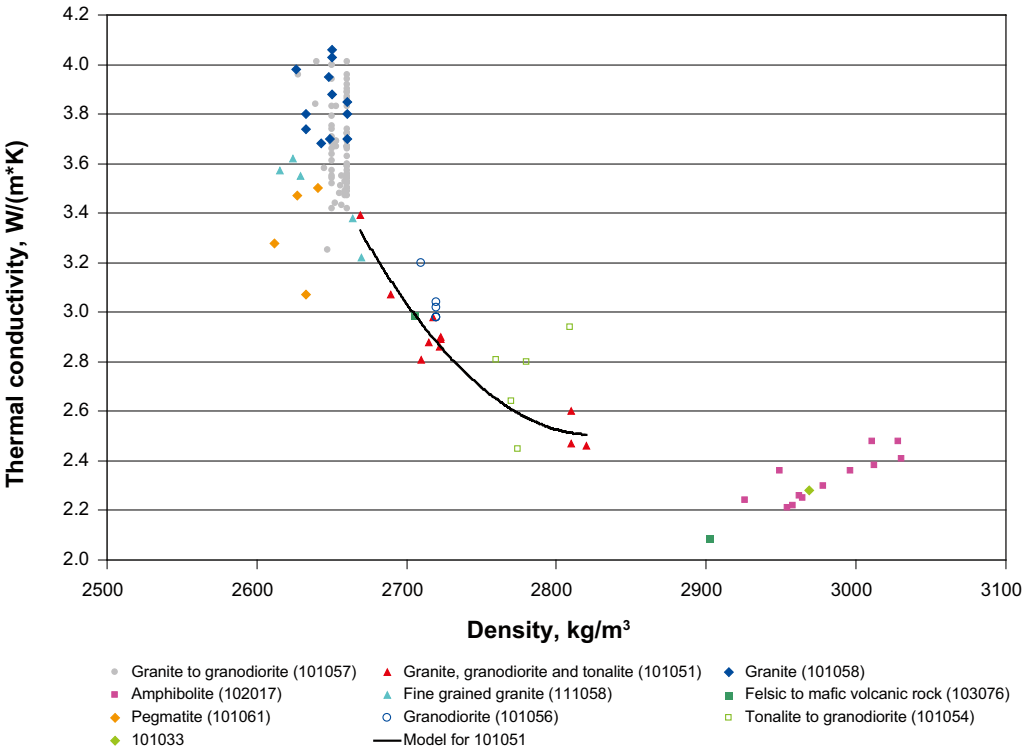

Figure 3-5. *Relationships between density and thermal conductivity for all rock types.*

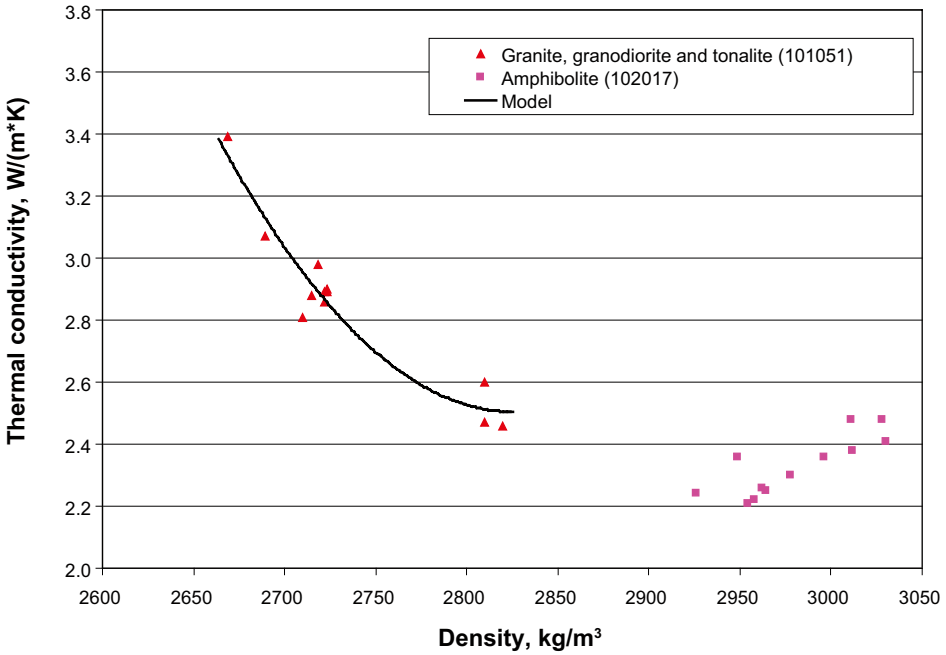

Figure 3-6. *Cross plot of density and thermal conductivity (TPS measurements) for granodiorite to tonalite (101051) and amphibolite (102017). Based on linear regression, Equation 3-1 is the relationship used in this study to describe granodiorite to tonalite (101051). For the purposes of modelling thermal conductivity from density loggings, it is assumed that the established relationship is valid within the density interval 2,625–2,850 kg/m³, although data is not available for the entire interval*

Borehole KFM01D was excluded because of poor calibration between logged density and measured density (Sicada database – activity comment). Based on the above criteria, data from six boreholes were used for the calculations, namely KFM01A, 01B, 04A, 05A, 06A and 08A. Borehole KFM03A lies outside the target volume and the density logging data have very high (53 kg/m³) noise levels /Thunehed 2004/, this borehole could justifiably be excluded from the analysis. However, because of indications from laboratory measurements that granodiorite to tonalite (101051) in this borehole has very low thermal conductivities, analysis of the density loggings in KFM03A was considered justified.

Density logging data for all boreholes were re-sampled, calibrated and filtered /Mattsson and Keisu 2004, 2005, Mattsson et al. 2004, Thunehed and Keisu 2004/. Petrophysical data from KFM01A and KFM02A were used for calibrating the density logs /Petersson et al. 2004a/. Noise levels for the evaluated boreholes, with the exception of KFM03A, vary between 9 and 20 kg/m³, which are above the recommended levels (3–5 kg/m³) for all density logs /Mattsson and Keisu 2004/. The logged data were filtered using a 3-point average filter to reduce the effect of high-frequency measurement noise.

3.4.3 Results for granodiorite to tonalite (101051)

For the purposes of modelling thermal conductivity from density loggings for rock type granodiorite to tonalite (101051), it is assumed that the established relationship, Equation 3-1 is valid within the density interval 2,625–2,850 kg/m³. This range corresponds to the thermal conductivity interval 2.50–3.86 W/(m·K), which for the upper limit is slightly outside the interval of measured data. Many of the high values of thermal conductivity produced are likely to be an effect of the random noise in the density loggings. The lower limit of the model is slightly higher than the minimum valued based on laboratory measurements, which means there is a risk of truncating the lower values of the distribution, and increasing the proportion of values at about 2.5 W/(m·K). Table 3-14 summarises the results of the measurements for each borehole. A comparison of the different boreholes is displayed graphically in Figure 3-7.

Boreholes KFM01A, 01B and 04A are characterised by relatively high thermal conductivities, whereas KFM05A, 06A and 08A are characterised by generally lower conductivities. KFM03A, which lies outside the target volume, has the lowest thermal conductivities, and, despite the uncertainties associated with the data for this borehole, can be considered to be clearly anomalous. Systematic down-borehole (subvertical) trends in thermal conductivity could not be discerned from the data.

Table 3-14. Thermal conductivity of granodiorite to tonalite (101051) determined from density loggings from several boreholes, using the relationship between thermal conductivity and density established in Equation 3-1.

Borehole ID	No. of measurements within density interval 2,625–2,850 kg/m³	% measurements excluded (outside model density interval)	% of borehole comprised of rock type 101051[1]	Thermal conductivity, W/(m·K) – Mean (st.dev.) 0.1 m scale	Thermal conductivity, W/(m·K) – Mean (st.dev.) 1 m scale
KFM01A	749	15	10.8%	3.32 (0.30)	3.29 (0.22)
KFM01B	130	22	6.1%	3.51 (0.24)	3.45 (0.18)
KFM04A	331	17	11.6%	3.29 (0.29)	3.23 (0.20)
KFM05A	47	0	5.0%	2.99 (0.17)	2.98 (0.05)
KFM06A	266	2	6.6%	2.96 (0.25)	2.93 (0.16)
KFM08A	48	2	1.1%	2.98 (0.20)	2.93 (0.04)
KFM03A	246	23	9.9%	2.55 (0.10)	2.57 (0.07)
All boreholes, excl. KFM03A	1,571			3.25 (0.32)	3.20 (0.25)

[1] Based on boremap data with rock types > 1 m borehole length.

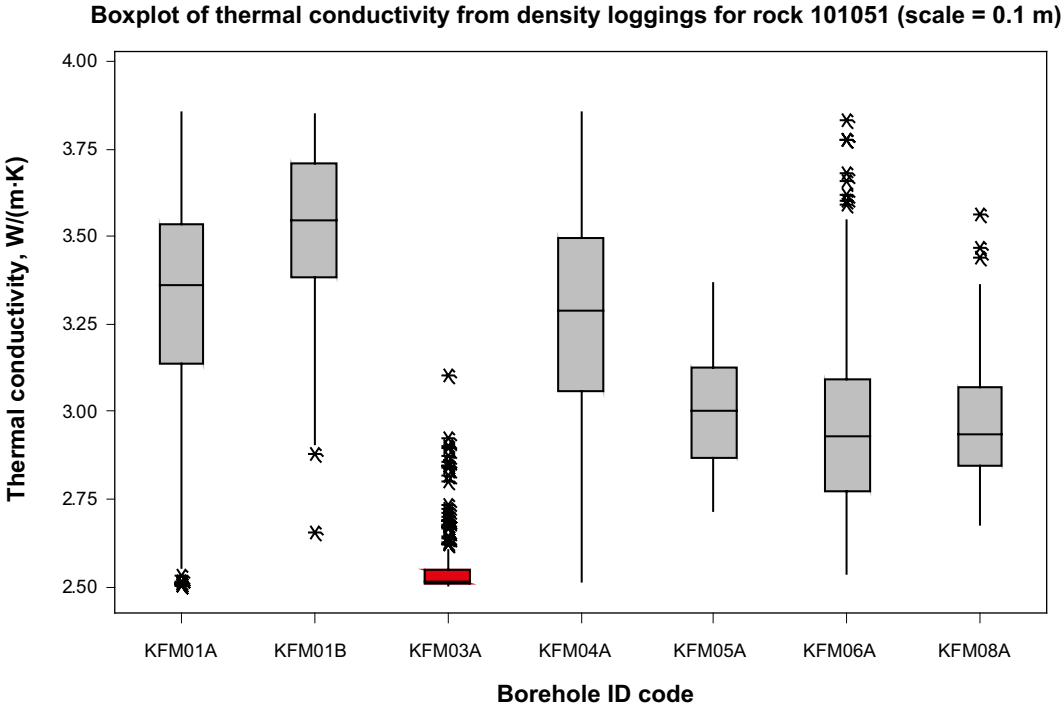

Figure 3-7. *Thermal conductivity of granodiorite to tonalite (101051) estimated from density loggings for individual boreholes. Large uncertainty associated with values for borehole KFM03 (in red).*

The frequency histograms in Figure 3-8 display the distribution of thermal conductivity values for granodiorite to tonalite (101051), calculated from density loggings for all boreholes at two different scales, 0.1 m and 1 m. The 0.1 m scale represents the resolution of the density logging data. Upscaling to 1 m borehole lengths is performed by calculating the geometric mean of the 0.1 m values within each 1 m length; see /Sundberg et al. 2005b/. The main difference between the two scales is the significant reduction in standard deviation with upscaling (Table 3-14). The histogram of conductivities at 1 m scale clearly show that their may be three or more modes present, which in turn indicates the existence of distinct compositional subtypes within this rock type. Given the rock type's wide compositional range (described as granodiorite to tonalite, with subordinate granite /SKB 2006b/), it is not surprising that a correspondingly wide range in thermal conductivities is also displayed.

The proportions of granodiorite to tonalite (101051) in domain 029 and domain 045 are c. 5% and c. 9% respectively, based on an assessment of all available boreholes /Stephens et al. 2007/.

3.4.4 Comparison between measurements and calculations for granodiorite to tonalite (101051)

In order to evaluate how well the model for granodiorite to tonalite (101051) in Equation 3-1 (cf. Figure 3-6) reflects the actual thermal conductivity of this rock type in the borehole, measured samples (TPS) were compared with values estimated from density logging.

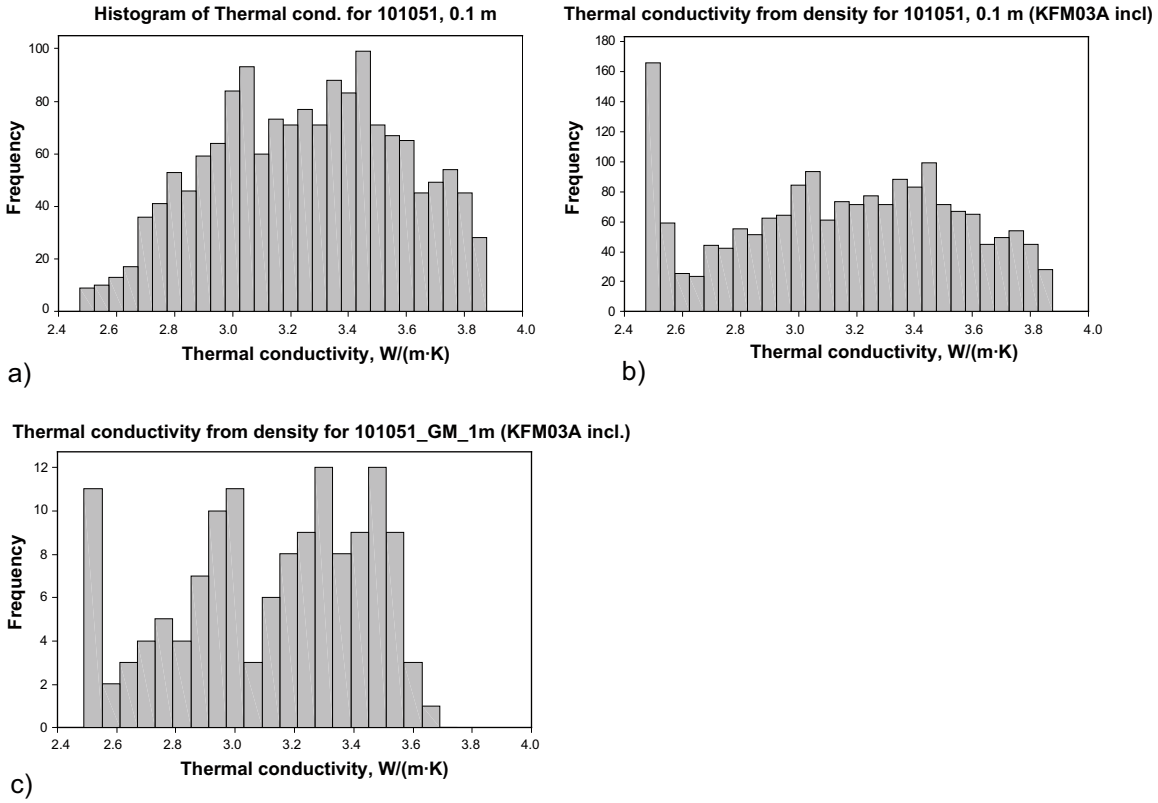

Figure 3-8. *Thermal conductivity of granodiorite to tonalite (101051) calculated from density loggings; a) scale 0.1 m, KFM03A excluded, b) scale 0.1 m, KFM03A included, c) geometric means scale 1 m, KFM03A included. The upscaling to 1 m is performed by applying the geometric mean equation to 1 dm values, see /Sundberg et al. 2005b/.*

Twelve TPS measurements of granodiorite to tonalite from boreholes KFM01A, 04A, 05A, 06A and 08A were compared with calculations of thermal conductivity from density logging for the corresponding sections of the borehole. The results of the comparisons are presented in Table 3-15 and Figure 3-9. The samples from KFM03A are excluded from the calculation of the mean because of the large difference between measured and logged density, which can be explained by the poor quality (large noise) of the density logging data for this borehole /Thunehed 2004/. The comparison indicates that in relation to laboratory measurements, the density loggings overestimate the thermal conductivity by on average 2.3%, which is equivalent to less than 0.1 W/(m·K). Direct density measurements on samples and density loggings from the corresponding borehole interval have also been compared. The mean logged density for the nine sample positions is only slightly lower (about 10 kg/m^3) than the mean measured density of the core samples from the same locations. In terms of thermal conductivity this is equivalent to an overestimation of thermal conductivity by about 0.1 W/(m·K).

In conclusion, the results indicate that density loggings can be used to estimate the thermal conductivity of granodiorite to tonalite (101051) with a rather high degree of certainty along continuous sections of borehole, although there would appear to be a tendency for determinations from density logs to slightly overestimate thermal conductivity.

3.5 Measurement of anisotropy of thermal conductivity due to foliation

All rock types in domains 29 and 45 have been subjected to some degree of ductile deformation, both lineation and foliation. The preferred alignment of mineral grains produced by this deformation may produce anisotropy in thermal transport properties. Anisotropy of thermal properties in the rock mass may impact on the design of a deep repository. For this reason, the directional dependence of thermal properties caused by foliation within deformed granite at the Forsmark site has been investigated in a large scale field experiment, combined with laboratory

Table 3-15. Comparison of thermal conductivity (W/(m·K)) measured by the TPS method and calculated thermal conductivity from density loggings of the same borehole sections for granodiorite to tonalite (101051).

Borehole	Secup	Seclow	Thermal cond. from TPS, W/(m·K)	Thermal cond. from density logging, W/(m·K)	Measured wet density, kg/m^3	Logged density, kg/m^3
KFM03A	305.63	305.69	2.46	*2.54*	2,820	*2,856*
KFM03A	305.69	305.75	2.60	*2.56*	2,810	*2,865*
KFM03A	305.75	305.82	2.47	*2.57*	2,810	*2,871*
KFM01A	837.92	838.00	3.39	3.61	2,669	2,644
KFM01C	184.13	184.22	2.89	No density data	2,722	No data
KFM01C	184.22	184.28	2.89	No density data	2,723	No data
KFM05A	686.99	687.13	3.07	3.25	2,689	2,677
KFM05A	695.56	695.70	2.90	3.03	2,723	2,701
KFM05A	708.26	708.40	2.98	2.85	2,718	2,724
KFM06A	588.50	588.64	2.88	2.77	2,715	2,737
KFM06A	594.73	594.88	2.81	3.00	2,710	2,705
KFM08A	460.19	460.26	2.86	2.87	2,722	2,721
Mean (excl. KFM03)			2.98	3.05	2,710	2,701
Mean difference% – (density log.–meas.) /meas.				2.34%		–0.20%

Values in italics have large uncertainty.

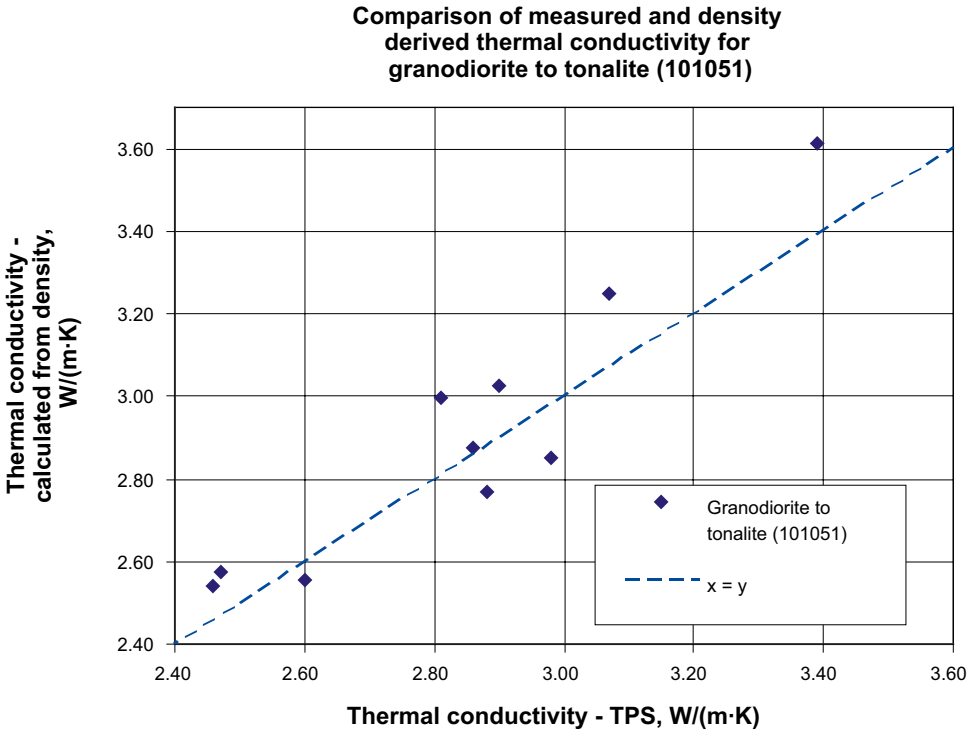

Figure 3-9. *Comparison of measured (TPS) thermal conductivity and thermal conductivity calculated from density logging data for granodiorite to tonalite (101051). The correlation coefficient for these variables is 0.935.*

and field testing at a smaller scale /Sundberg et al. 2007b/. The investigations were carried in the vicinity of drill site 7, situated in the outer margins of the Forsmark tectonic lens. The rock at this site is characterised by a relatively intense tectonic foliation, striking NNW and steeply dipping. Laboratory measurements at the centimetre scale using a modified TPS method indicate that thermal conductivity parallel with the foliation is, on average, a factor of 1.4 greater than conductivity perpendicular to the foliation. Field measurements, including the large-scale experiment, which measure larger volumes of rock have yielded anisotropy factors of approximately 1.15, considerably lower than for the laboratory measurements. A distinct scale dependence on anisotropy factor is indicated. A plausible explanation for the scale dependence is that the foliation is more clearly defined at the cm scale but is more variable at the dm to m scale.

The results of this investigation with regard to the scale dependence of anisotropy of thermal conductivity are summarised in Table 3-16.

Given that most of the sampled rock displays less intense deformation than that shown by the rock close to drill site 7, lower anisotropy factors would be expected for the greater part of the target volume.

Table 3-16. Results of investigation with regard to the scale dependence of thermal conductivity. Factor of anisotropy and the effective thermal conductivity (geometric mean of the two principal directions).

Scale	Thermal conductivity Mean factor of anisotropy $\lambda_{pa}/\lambda_{pe}$	Geometric mean W/(m·K)
Centimetre scale	1.40	3.45
Decimetre to metre scale	1.15	3.42

$\lambda_{pa}/\lambda_{pe}$ = thermal conductivity parallel to the foliation divided by thermal conductivity perpendicular to the foliation.

It should be noted that the thermal conductivity measurements by the TPS method presented in Section 3.2 were calculated based on the assumption of isotropy. The values represent the effective thermal conductivity of the measured volume, without reference to any particular direction. Thus, there may be some uncertainty in these TPS data due to anisotropy.

3.6 Heat capacity

Heat capacity has been determined indirectly from thermal conductivity and diffusivity measurements using the TPS (Transient Plane Source) method, and directly by calorimetric measurement. The methods are described in, for example, /Adl-Zarrabi 2006b/. In Table 3-17, the results from all heat capacity calculations from TPS-measurements are summarised /Adl-Zarrabi 2003, 2004abcd, 2005ab, 2006abc/. Compared to modelling stage 2.1, the data include 53 new measurements, nine for tonalite to granodiorite (101051), 15 for rock granite to granodiorite (101057), six for granite (101058), four for pegmatite (101061), twelve for amphibolite (102017), two for felsic to intermediate volcanic rock (103076) and five for granite (111058). Observe that most samples of tonalite to granodiorite (101054) and granodiorite (101056)) were sampled in groups from short sections of core, 0.2–1 m, and thus the data may not be representative for these rock types.

Direct calorimetric measurement of heat capacity was performed on 39 samples /Adl-Zarrabi 2006bc, Lau 2007/. In Table 3-18, results are shown for samples for which both direct and indirect methods have been performed. The differences between the results of the two methods for the same sample are up to 15%. The results from the different methods are also shown in Figure 3-10.

Since the calorimetric measurements are considered to be more reliable, there is probably a bias in the determination of heat capacity from the TPS-method. The reason for this is probably to be found in the measurement method (TPS). The measurement of thermal conductivity and thermal diffusivity take different volumes into account. This has no importance if the sample is isotropic and homogeneous. However, in Forsmark many samples are considered to be lineated or foliated and, therefore, the orientation of the sample influences the results. The largest error is assumed to be in the determination of thermal diffusivity.

Table 3-17. Heat capacity, determined by the TPS-method (MJ/m^3·K).

Rock type	Sample location	Mean	Std dev.	Number of samples
Granite to granodiorite, 101057	KFM01A, KFM01C, KFM01D, KFM02A, KFM03A, KFM04A, KFM07A, KFM08A and surface samples	2.15	0.17	74
Tonalite to granodiorite, 101054	KFM03A and surface samples	2.12	0.20	5
Granodiorite and tonalite, 101051	KFM01A, KFM01C, KFM03A, KFM05A, KFM06A and KFM08A	2.21	0.11	12
Granodiorite, 101056	KFM04A	2.25	0.07	5
Diorite, quartz diorite and gabbro, 101033	Surface sample	2.33	–	1
Granite, metamorphic, aplitic, 101058	KFM06A and KFM08A	2.08	0.10	12
Pegmatite, pegmatitic granite, 101061	KFM07A and KFM08A	1.92	0.14	4
Amphibolite, 102017	KFM01A, KFM01C, KFM01D, KFM05A, KFM07A and KFM08A	2.45	0.09	12
Felsic to intermediate volcanic rock, 103076	KFM01C and KFM08	2.26	–	2
Granite, fine- to medium-grained, 111058	KFM01C, KFM04A, KFM05A and KFM06A	2.14	0.10	5

Table 3-18. Heat capacity, determined by TPS- and calorimetric method (direct measurement) (MJ/m³·K) on the same sample.

Rock type	Sample location	TPS mean	TPS std dev.	Calorimetric mean	Calorimetric std dev.	Number of samples
Granite to granodiorite, 101057	KFM01A, KFM01C, KFM01D, KFM07A and KFM08A	2.09	0.17	2.06	0.06	14*
Granodiorite and tonalite, 101051	KFM01A, KFM01C, KFM05A and KFM06A	2.23	0.13	2.15	0.05	8
Granite, metamorphic, aplitic, 101058	KFM06A	2.05	0.05	2.01	0.02	3
Amphibolite, 102017	KFM01A, KFM01C, KFM01D and KFM05A	2.43	0.05	2.41	0.11	8
Felsic to intermediate volcanic rock, 103076	KFM01C	2.33	–	2.42	–	1
Granite, fine- to medium-grained, 111058	KFM01C, KFM04A, KFM05A and KFM06A	2.34	0.10	2.31	0.05	5

* Includes three altered samples.

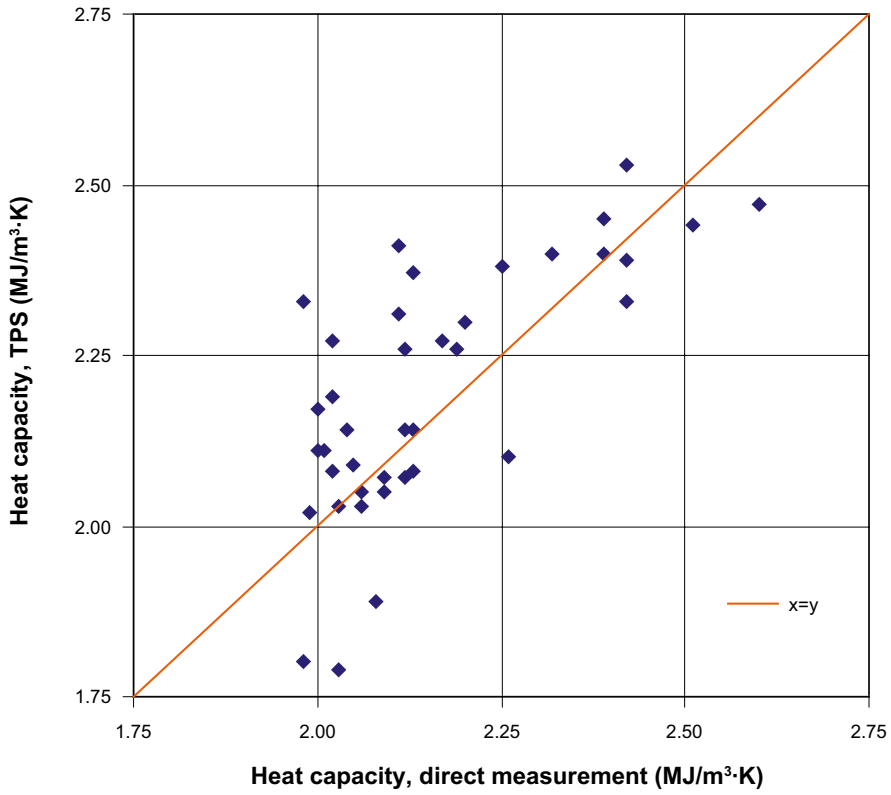

Figure 3-10. Comparison between heat capacity measured by different methods, TPS and direct measurement. Correlation coefficient = 0.709.

3.7 Thermal conductivity vs heat capacity

The relationship between thermal conductivity and density has been discussed in Section 3.4. It would be reasonable to assume a corresponding relationship between density and heat capacity. Such a relationship has been found earlier /Sundberg et al. 2003/. However, the relationship is weaker than that for thermal conductivity vs. density. Consequently, a relationship between thermal conductivity and heat capacity could be expected. In Figure 3-11 heat capacity from both TPS and calorimetric methods are plotted vs. thermal conductivity. The relationship between the more reliable heat capacity values from calorimetric measurements and the thermal conductivity measurements is described by a second order equation.

3.8 Temperature dependence in thermal properties

The temperature dependence of the thermal properties has been investigated earlier by measurement with the TPS-method on samples within rock type 101057, granite to granodiorite, at three different temperatures (20, 50 and 80°C) /Adl-Zarrabi 2004c/. No additional measurements have been performed in the data freeze for 2.2. Figure 3-12 illustrates the measuring results of thermal conductivity for each sample. With increasing temperature the thermal conductivity decreases by 9.8%/100°C temperature increase, calculated as mean value for the direction for functions fitted for each of the 18 samples. However, the decrease of thermal conductivity varies from 6.6% to 11.7% for the individual samples.

With increasing temperature the heat capacity increases by 28.9%/100°C temperature increase. However, the increase varies from 16.4% to 63.1% for the individual samples, see Figure 3-13.

For rock types with a lower quartz content compared to, granite to granodiorite (101057), the temperature dependence in thermal conductivity is expected to be less pronounced /Sundberg et al. 2005a/.

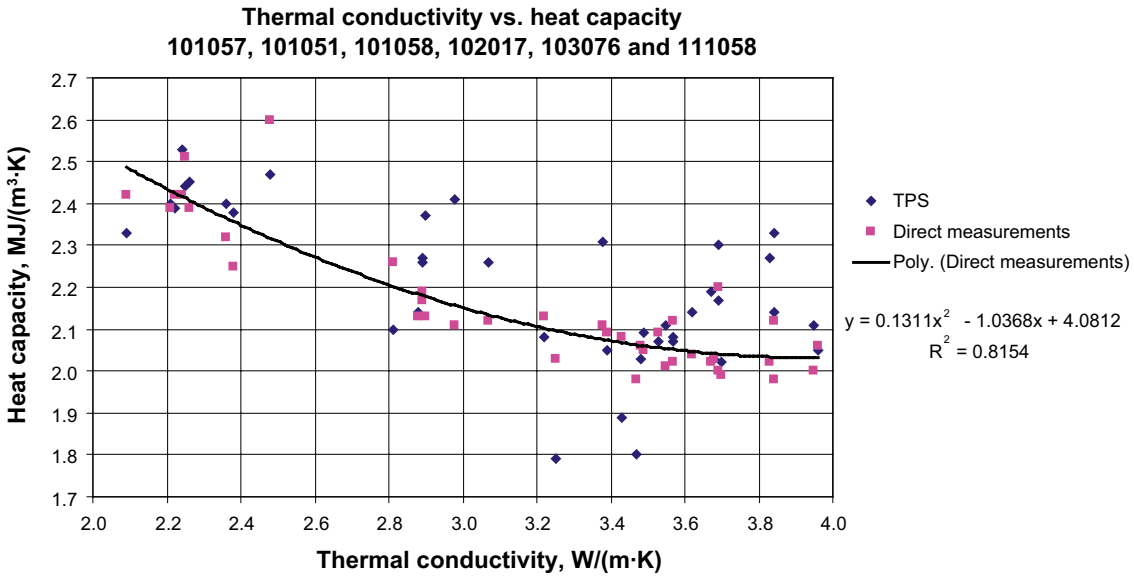

Figure 3-11. *Heat capacity vs. thermal conductivity. The heat capacity is calculated from TPS-determination and from calorimetric measurement. The second order relationship is based on calorimetric measurements only.*

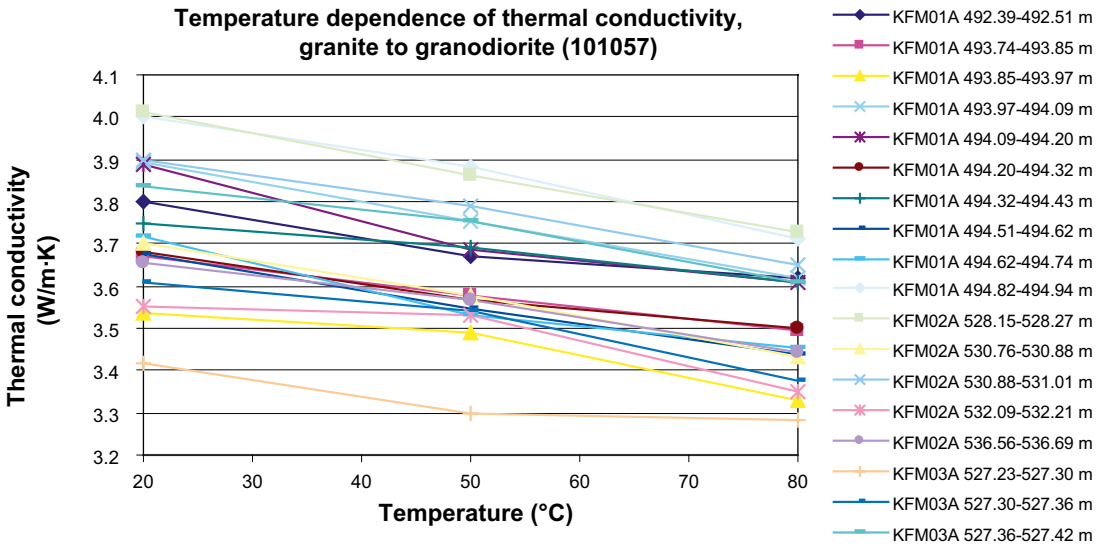

Figure 3-12. *Temperature dependence of thermal conductivity, rock type granite to granodiorite (101057).*

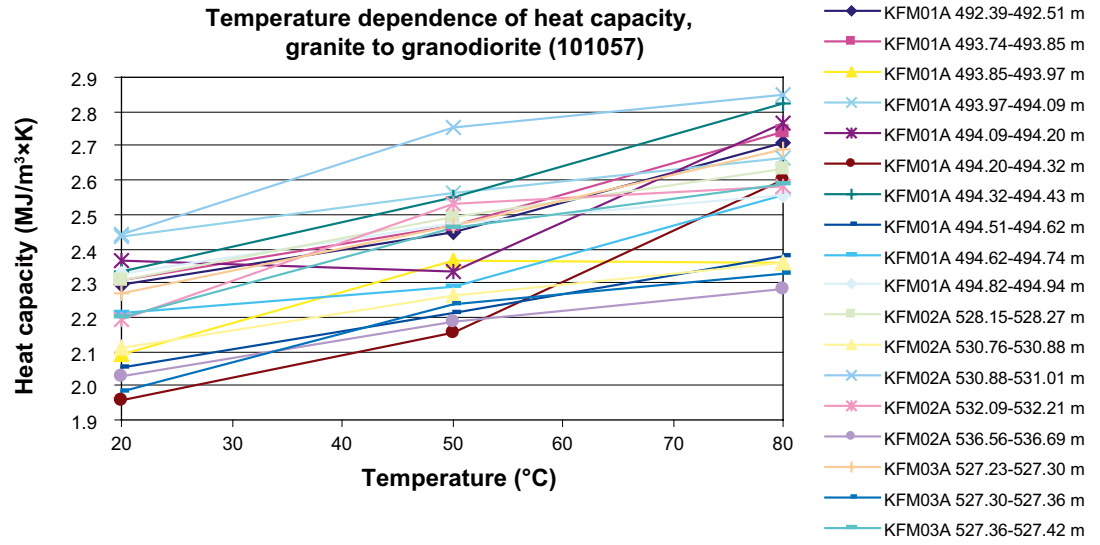

Figure 3-13. ***T****emperature dependence for heat capacity for granite to granodiorite, 101057 (based on TPS measurements).*

3.9 Coefficient of thermal expansion

The coefficient of thermal expansion has been measured on samples from five different rock types. Compared to previous investigations /SKB 2006b/ three additional samples of granodiorite to tonalite (101051) and three samples of granite (101058) have been measured. These, as well as previously performed measurements, divided according to rock type, are summarised in Table 3-19. The mean value of measured thermal expansion varies for the different rock types between $7.2 \cdot 10^{-6}$ and $8.1 \cdot 10^{-6}$ m/(m·K). For the dominant rock type (granite to granodiorite, 101057), the mean thermal expansion coefficient is $7.7 \cdot 10^{-6}$ m/(m·K). No samples of amphibolite (102017) has been investigated.

Table 3-19. Measured thermal expansion (m/(m·K)) on samples with different rock types from boreholes KFM01A, KFM02A, KFM03A, KFM04A, KFM05A and KFM06A (interval of temperature: 20–80°C).

Rock code	Rock name	Sample location	Arithmetric mean	St. dev.	Min	Max	Number of samples
101057	Granite to granodiorite	Borehole KFM01A, KFM02A, KFM03A, KFM04A	$7.7 \cdot 10^{-6}$	$2.2 \cdot 10^{-6}$	$2.1 \cdot 10^{-6}$	$1.5 \cdot 10^{-5}$	56
101056	Granodiorite	Borehole KFM04A	$8.1 \cdot 10^{-6}$	$3.4 \cdot 10^{-6}$	$5.2 \cdot 10^{-6}$	$1.4 \cdot 10^{-5}$	6
101054	Tonalite to granodiorite	Borehole KFM03A	$7.2 \cdot 10^{-6}$	$1.6 \cdot 10^{-6}$	$5.3 \cdot 10^{-6}$	$8.2 \cdot 10^{-6}$	3
101051	Granodiorite and tonalite	Borehole KFM03A, KFM05A, KFM06A	$7.8 \cdot 10^{-6}$	$1.2 \cdot 10^{-6}$	$6.5 \cdot 10^{-6}$	$1.0 \cdot 10^{-5}$	6
101058	Granite, aplitic	Borehole KFM06A	$7.5 \cdot 10^{-6}$	$5.4 \cdot 10^{-7}$	$6.9 \cdot 10^{-6}$	$8.0 \cdot 10^{-6}$	3

3.10 In situ temperature

3.10.1 Method

Fluid temperature and vertical temperature gradients have been measured in most cored boreholes at Forsmark. Temperature was measured by fluid temperature loggings at regular 10 cm intervals. The measured data were filtered and temperature gradients for 9 m sections were calculated.

Linear equations were fitted to down-hole temperature loggings. Linear equations were considered to be adequate, and higher degree equations were not calculated.

3.10.2 Results

Large differences in logged temperature for the same depth in different boreholes was noted in model stage 2.1 /SKB 2006b/. Uncertainties associated with the data were judged to be high. For this reason, the fluid temperature loggings for each borehole have been evaluated with regard to their reliability. The criteria considered were 1) errors associated with logging probe and 2) time between drilling and logging.

Different probes have been used by Ramböll for temperature logging, Century 8044, Century 8144, Century 9044 and Century 9042. Errors associated with Century 8044, 8144 and 9044 are particularly large, as much as ± 2°C. Therefore, fluid temperatures logged with these instruments are considered to be unreliable, and are omitted from subsequent analysis. The rejected data are from boreholes KFM05A, KFM06A and KFM07A. Boreholes logged using Century 9042 are considerably more accurate, less than ± 0.25°C /Stenberg 2006/.

The times between core drilling and temperature logging are about 6 months for KFM01A, 2 months for KFM01C, 3 weeks for KFM01D, 5 months for KFM02A, 6 weeks for KFM03A, KFM06C, KFK07C and KFM09B, 2 years for KFM04A, 10 weeks for KFM08C and 1 week for KFM10A. The period between the end of drilling activity and temperature logging should be sufficiently long in order to allow disturbances of the fluid temperature caused by drilling to stabilise. The drilling activity increases the temperature in the borehole but a temperature decrease probably occurs due to the added drilling fluid. However, also the drilling fluid can be of different temperature. Also a temperature equalisation occurs in the borehole when the drilling fluid is transported in the borehole. Times for core drillings and fluid temperature loggings for the boreholes are given in Table 3-20. A rough rule of thumb is that logging should preferably not be carried out within 2 months after the end of drilling, and definitely not within the first 3–4 weeks after drilling. Based on this approximation it can be deduced that logging data from KFM01D, KFM08A and KFM10A may have been collected before the water in the boreholes had stabilised. These data have also been omitted from subsequent calculations.

Table 3-20. Occasions for core drilling and fluid temperature loggings for boreholes at the Forsmark site.

Borehole	Core drilling Start time	Core drilling Stop time	Fluid temperature logging	Comment
KFM01A	2002-06-25	2002-10-28	2003-04-25	
KFM01C	2005-11-02	2005-11-29	2006-02-01	
KFM01D	2005-12-18	2006-02-18	2006-03-07	Short time between drilling and logging.
KFM02A	2003-01-08	2003-03-12	2003-08-05	
KFM03A	2003-04-16	2003-06-23	2003-08-08	
KFM04A	2003-08-25	2003-11-19	2005-11-12	
KFM06C	2005-04-26	2005-06-30	2005-08-10	The borehole was extended 0.48 m 2006-05-06.
KFM07C	2006-03-30	2006-08-08	2006-09-19	
KFM08A	2005-01-25	2005-03-31	2005-04-27	Short time between drilling and logging.
KFM08C	2006-01-30	2006-05-09	2006-07-18	
KFM09B	2005-11-16	2005-12-19	2006-01-30	
KFM10A	2006-03-14	2006-06-01	2006-06-08	Very short time between drilling and logging.

The temperature and gradient profiles has been investigated for the “approved” boreholes, namely KFM01A, KFM02A, KFM03A, KFM04A, KFM06C, KFM07C, KFM08C and KFM09B. KFM01C is also approved but to short to be used. The inclinations for the boreholes are given as intervals in Table 3-21. KFM01A, KFM02A, KFM03A and KFM07C are almost vertical, while the angles for the other boreholes are smaller. The results from the temperature loggings, and the calculated gradients are presented in Figure 3-14 to Figure 3-18. Figure 3-14 illustrates a summary of all investigated boreholes while Figure 3-15 to Figure 3-18 shows temperature for the boreholes separately. The y-axis in the figures illustrates depth below sea level (not the borehole length). To the series with temperature measurements for the investigated boreholes, an equation was fitted, see Table 3-23. Linear equations where estimated to be good enough, and higher degree equations did not give larger correspondence.

In Table 3-21, the fluid temperature at depths 400 m, 500 m and 600 m in the boreholes are presented. The temperature at 500 metres depth is calculated to be in the interval 11.2–12.0°C for the boreholes KFM01A, KFM02A, KFM03A, KFM04A, KFM06C and KFM08C, see Figure 3-14. KFM01C and KFM09B do not reach 500 m depth and are therefore not included in the calculation of mean temperature in Table 3-21.

Sections with larger gradient anomalies are summarized in Table 3-22. This might be because of water bearing fractures in these parts of the boreholes.

Mean annual air temperatures recorded at meteorological stations close to the Forsmark area are between 5°C and 5.5°C /Johansson et al. 2005/.

Table 3-21. Temperature (°C) for the "approved" boreholes at the Forsmark site, at different levels. Borehole inclinations are also included for the boreholes, given as lowest and highest angle.

Borehole	Temperature at the depth 400 m	Temperature at the depth 500 m	Temperature at the depth 600 m	Inclination (°)
KFM01A	10.6	11.7	12.9	75–85
KFM01C*	–	–	–	46–50
KFM02A	10.8	11.8	12.9	80–86
KFM03A	10.8	12.0	13.1	83–86
KFM04A	10.4	11.5	13.1	44–63
KFM06C	10.2	11.3	12.5	45–60
KFM07C*	10.4	11.4**	–	84–85
KFM08C	10.1	11.2	12.5	59–60
KFM09B*	10.4	–	–	41–55
Arithmetic mean	10.5	11.6	12.8	

* KFM01C is about 330 m, KFM07C about 490 m, KFM09B about 470 m (vertical depth).

** At 493 m (vertical depth).

Table 3-22. Sections with gradient anomalies along the investigated boreholes.

Borehole	Gradient anomalies (metres above sea level)	Maximum borehole depth (metres above sea level)
KFM01A	–	–980
KFM01C	–170 to –330	–330
KFM01D	–100 to –610	–610
KFM02A	–	–980
KFM03A	–	–980
KFM04A	–	–790
KFM06C	–250 to –470, –740 to –780	–780
KFM07C	–	–490
KFM08A	–100 to –760	–760
KFM08C	–	–780
KFM09B	–100 to –220	–470
KFM10A	peak at –300	–340

Table 3-23. Equations fitted to the temperature profiles for the investigated boreholes.

Borehole	Equation (linear fit)
KFM01A	T = –0.0119662715 z + 5.935478909
KFM02A	T = –0.01132695 z + 6.313194551
KFM03A	T = –0.01156285813 z + 6.38750348
KFM04A	T = –0.01182276231 z + 5.720154531
KFM06C	T = –0.01101015342 z + 6.00130687
KFM07C	T = –0.0104655901 z + 6.188779113
KFM08C	T = –0.01137420669 z + 5.723908337
KFM09B	T = –0.01086572982 z + 6.083668899

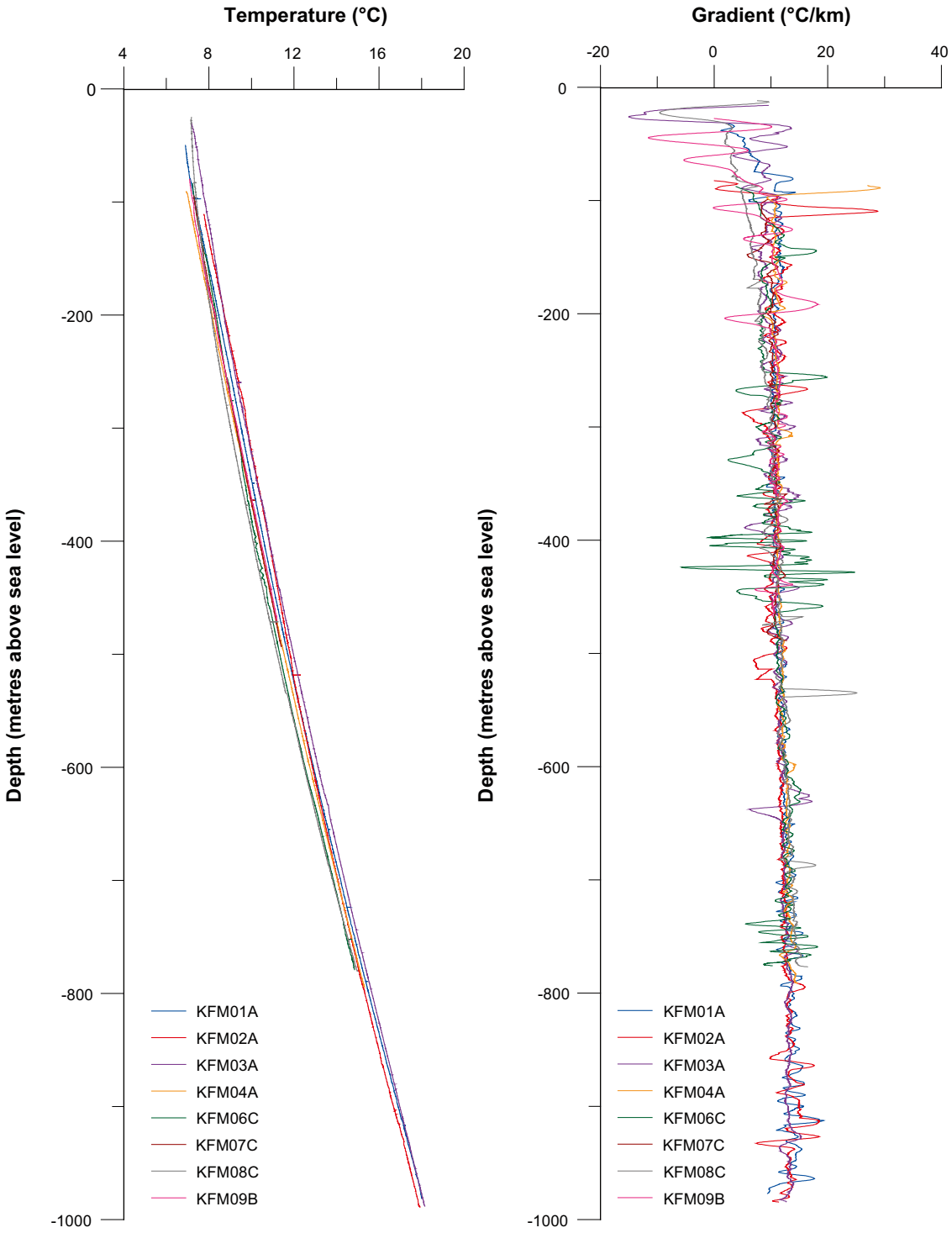

Figure 3-14. *Summary of temperature (a) and gradient calculated for nine metre intervals (b) for the eight boreholes at Forsmark. Results from fluid temperature loggings.*

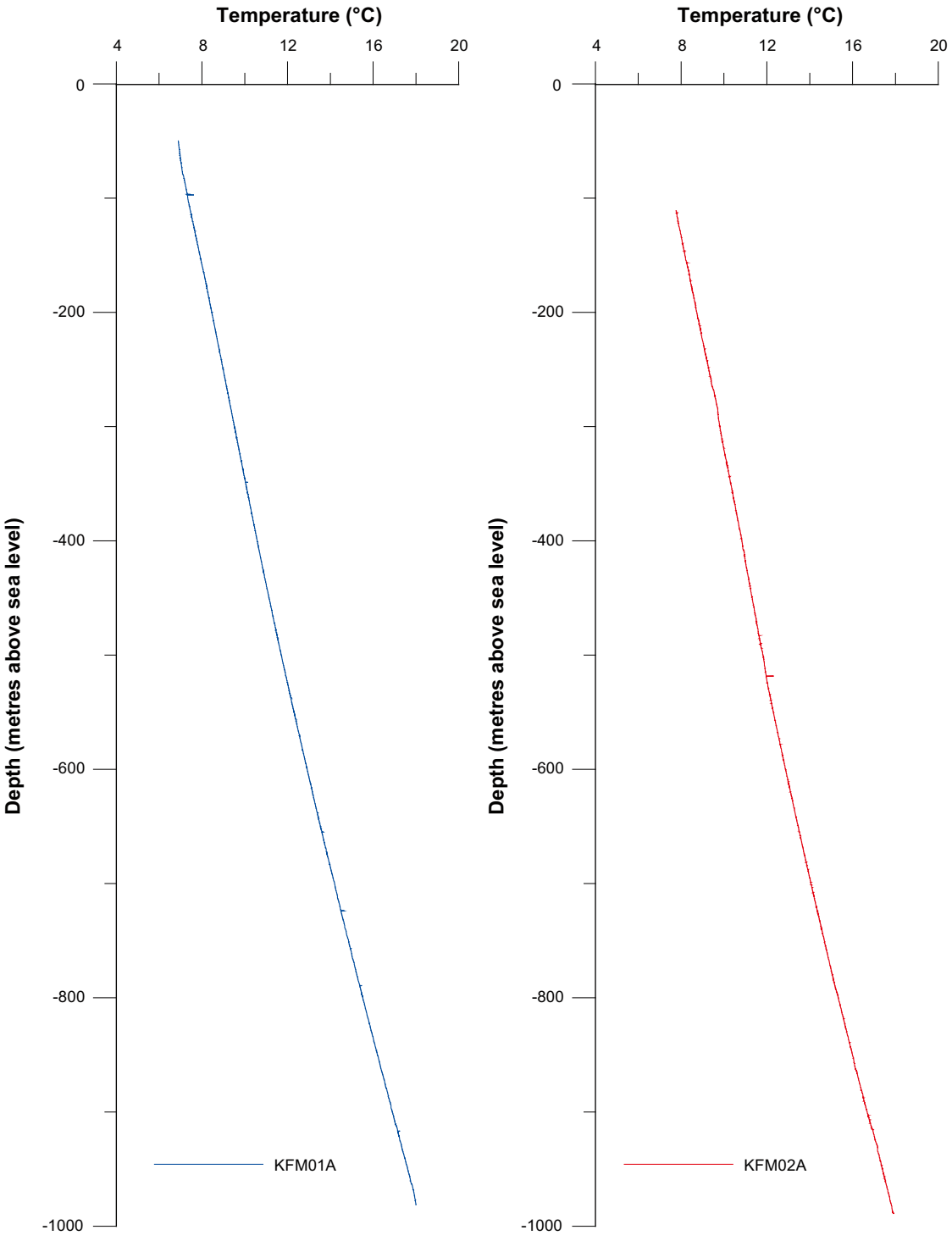

Figure 3-15. *Temperature from fluid temperature loggings, for KFM01A and KFM02A.*

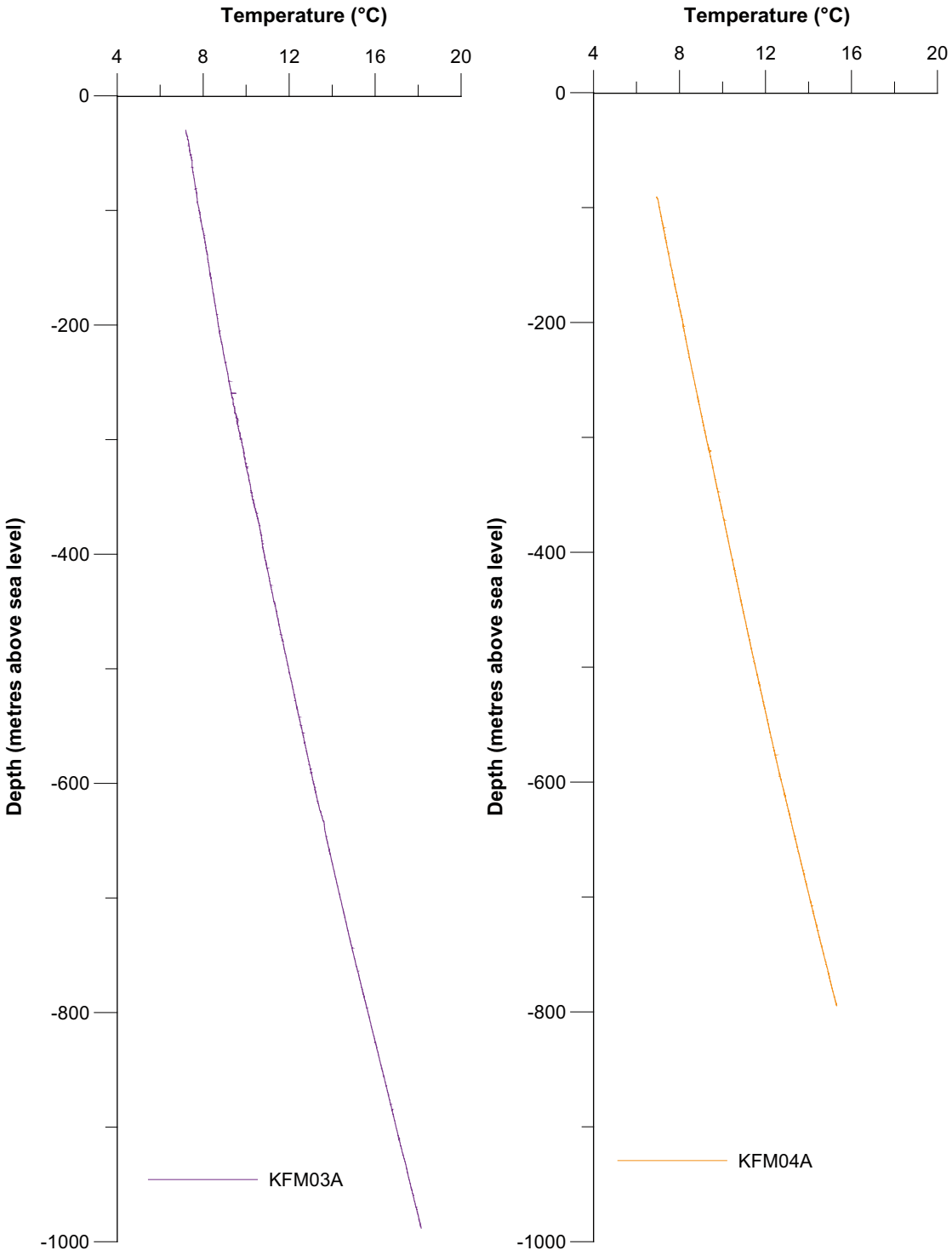

Figure 3-16. *Temperature from fluid temperature loggings, for KFM03A and KFM04A.*

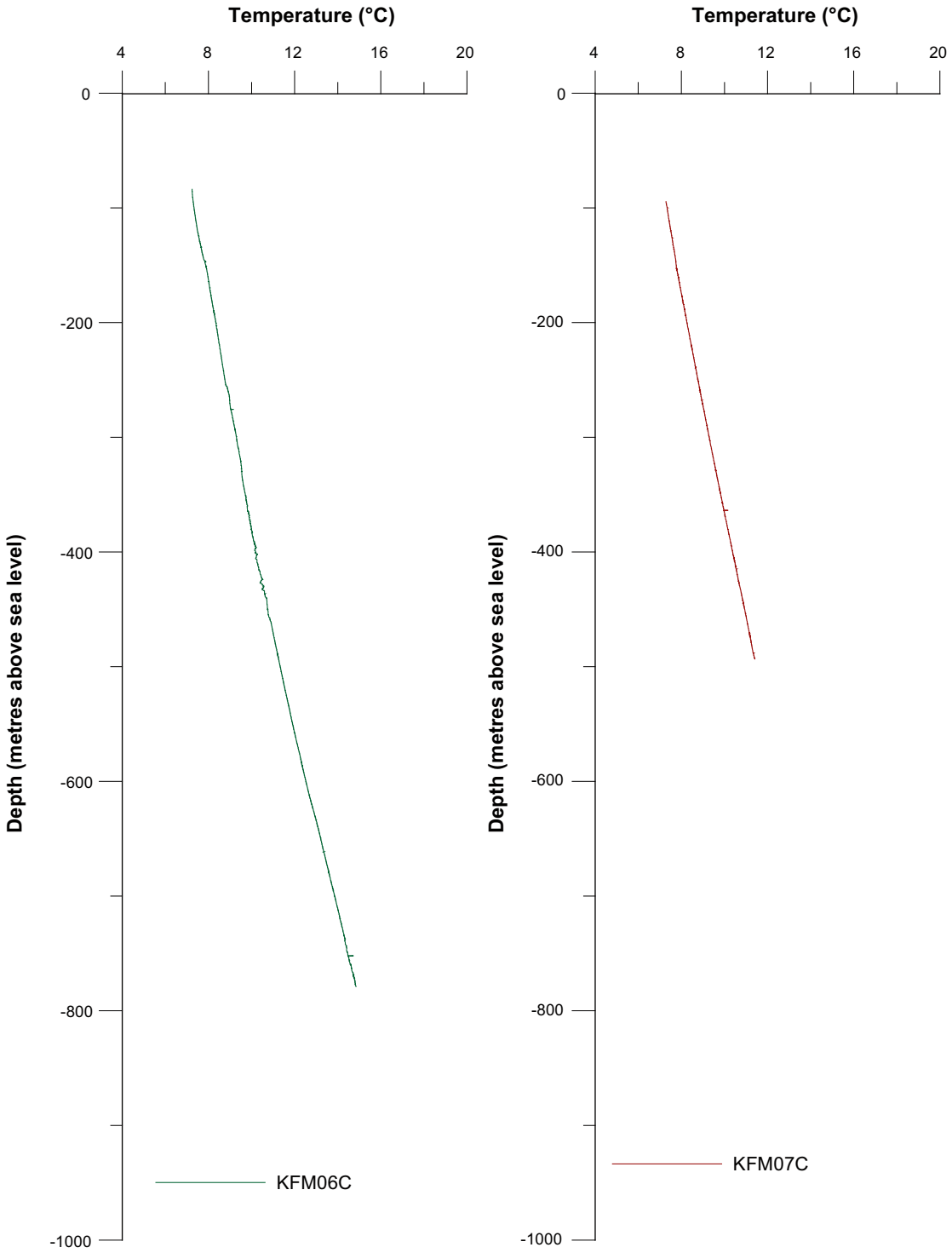

Figure 3-17. *Temperature from fluid temperature loggings, for KFM06C and KFM07C.*

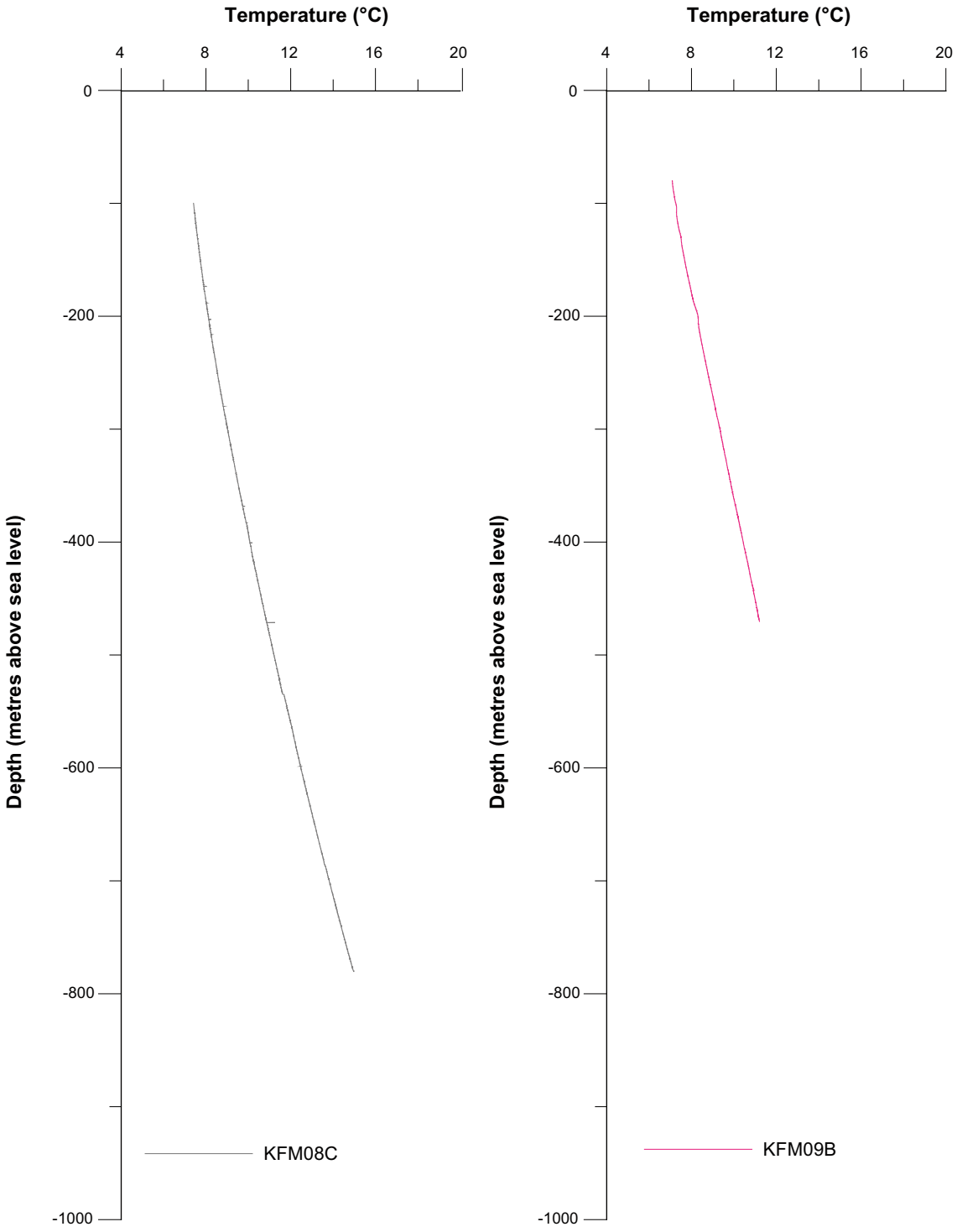

Figure 3-18. *Temperature from fluid temperature loggings, for KFM08C and KFM09B.*

3.11 Geology from boremap

The boundaries of the volume for which thermal modelling has been carried out during stage 2.2 is defined by the target volume /Stephens et al. 2007/. This volume is comprised of two rock domains RFM029 and RFM045. Boreholes intersecting these two domains inside the target volume, and which have been investigated with a view to using them in the geological simulation, are listed in Table 3-24.

Geological borehole data describing rock type (> 1 m) and rock occurrences (< 1 m), together with a lithological domain classification of boreholes, form the basis for the stochastic simulation of lithologies, an important component of the thermal modelling methodology described in Section 4.2 and /Back and Sundberg 2007/. Boreholes KFM02A, KFM03A and KFM09A have been omitted from the analysis, since they lie wholly or partly outside the target volume. Borehole KFM06B, with a length of 100 m, is very short and was excluded for this reason.

The borehole data representing each domain have been further analysed in order to select appropriate data for the stochastic simulation of the geology. This selection procedure is described in Section 5.1.

Table 3-24. Boreholes belonging to domains RFM029 and RFM045, and used as input to the geological simulation. The rock domain classification of boreholes is from /Stephens et al. 2007/.

Domain	Borehole
RFM029	KFM01A, 01B, 01C, 01D, KFM04A (500–1,001 m), KFM05A, KFM06A (102–751 m), KFM06C (102–411 m), 07A (102–793 m), 07B (5–298 m), 7C (85–498 m), 08A (102–781 m), 08B (6–200 m), 08C (102–342 m and 546–949 m), 9B (9–616 m), 10A (63–500 m)
RFM045	KFM06A (751–998 m), KFM06C (411–898 m), KFM08C (342–546 m)

4 Strategy for thermal modelling

4.1 Conceptual model

4.1.1 General

The methodology employed for thermal modelling in stage 2.2 has been fundamentally revised compared to previous model versions, and has been documented in a separate strategy report /Back and Sundberg 2007/. The strategy for thermal modelling is based on a conceptual model considering e.g. lithology, thermal properties of rock types, spatial variability and correlation, alteration of rock etc. The conceptual model mainly deals with the different types of heterogeneity (in terms of variability) and anisotropy, and related aspects. A short description of the conceptual model is given below.

The modelling approach presented in the Section 4.2 considers the main aspects of the conceptual model, most importantly the lithology (variability due to different rock types), the spatial variability and correlation within each rock type, and the anisotropy due to subordinate rock bodies (see below).

4.1.2 Heterogeneity

Thermal properties, especially thermal conductivity, vary significantly between different rock types but also within rock types. The spatial variability of thermal conductivity can thus be separated into:

1. "between rock type" variability, and
2. "within rock type" variability.

The "between rock type" variability is a result of the different compositions of the igneous rock types, resulting from different types of magma. The "within rock type" variability is a result of variations in the mineralogical composition, which is also intimately related to magma composition, but also post-crystallisation processes such as hydrothermal alteration. "Within rock type" variability is also a function of the way rocks have been classified; for example, a particular rock type may include two or more subvarieties or facies.

The total variability within a rock domain thus depends on the lithology and the thermal properties of each rock type. Although the thermal conductivity of a single rock type may be normally (Gaussian) or close to normally distributed, the statistical distribution of thermal conductivity for the domain as a whole is far from normally distributed. Depending on their fraction of the total volume, the low-conducting rock types may determine the lower tail of the thermal conductivity distribution (see Section 1.2 for a discussion of why the lower tail is of importance).

Thermal properties exhibit spatial correlation within a rock type but not between rock types. However, this spatial correlation may be weak or non-existent within some sections of a rock type, for several reasons. One reason is that the rock at a particular location may have been generated by incomplete mixing of magmas with different origins and compositions, resulting in weak correlation. Another reason is that some rock types may be grouped together as a single rock type due to practical difficulties of distinguishing between them during geological mapping work. There may be no correlation at all between such variants of rock (the relatively fine-grained granodiorite to tonalite (101051) is an example of this).

Although there is no reason to believe that there is spatial correlation between different rock types, there may be spatial within rock type correlation between one section of rock type A, across an intrusion of rock type B, to the next section of rock type A.

4.1.3 Anisotropy

The rock mass at Forsmark may have anisotropic thermal properties. There are two main types of thermal anisotropy to consider:

1. Anisotropy due to foliation/lineation.
2. Anisotropy due to orientation of subordinate rock bodies.

The first type is a structural anisotropy caused by foliation and lineation which occur within a rock type. The foliation and lineation imply a directional orientation of the minerals in the rock mass. The thermal conductivity is generally higher parallel with the mineral foliation and lower perpendicular to the foliation plane.

This is because conductive minerals will control the heat flow parallel to the foliation; the minerals extend longer in this plane and are not interrupted to the same extent by less conductive minerals. Perpendicular to the foliation there is a higher density of transitions between different minerals, resulting in less conductive minerals having greater influence. This is accentuated by the crystallographic orientation of the commonly occurring minerals in a rock, such as quartz and biotite.

The second type of anisotropy is a result of the spatial orientation of magmatic rock bodies, primarily subordinate rocks. These bodies may have preferential directions in space, resulting in anisotropy of the thermal properties. Amphibolites parallel to the foliation at Forsmark are typical examples of this anisotropy /SKB 2005a/.

In addition to these types of anisotropy there are also other types that could occur, at least theoretically. Anisotropy may be caused by heterogeneity within a rock type, i.e. by different spatial trends in the composition of a rock type in different directions. This anisotropy could be modelled by directional variograms, i.e. separate variograms for the three principal directions. However, there is no geological evidence to indicate that this anisotropy is of significant importance in Forsmark. Therefore, it is not further analysed in the report.

4.2 Modelling approach

4.2.1 Introduction

The strategy for the thermal site descriptive modelling is to produce spatial statistical models of both lithologies and thermal properties and perform stochastic simulations to generate a spatial distribution of thermal properties that is representative of the modelled rock domain. The focus of the modelling approach described in this chapter is on thermal conductivity. Stochastic simulation is commonly used as a tool to perform uncertainty analysis or risk analysis. A number of equally probable realisations are produced. These realisations are used to represent the rock domain statistically. There is no prerequisite that data need to be normally distributed or follow a specific statistical distribution. On the contrary, the strategy can handle data from any type of distribution. The methodology is described in detail in /Back and Sundberg 2007/.

The aim of the thermal modelling is to model the thermal properties spatially for a rock domain. There are three specific objectives for which the modelling approach can be used:

- Description: statistical description of the thermal properties of a rock domain.
- Prediction: prediction of thermal properties in a specific rock volume.
- Visualisation: visualisation of the spatial distribution of thermal properties.

In this report the focus is on description. Of special interest for the description is to:

- determine the low percentiles of thermal conductivity and the associated uncertainty,
- model how the thermal conductivity varies with scale,
- produce realisations of thermal conductivity that can be used for subsequent modelling work, such as numerical temperature simulations.

For the description problem, no concern is given to specific locations in the rock mass; only the statistics of the rock domain of interest are addressed, including the uncertainty of statistical parameters. The methodology for this type of problem is based on unconditional stochastic simulation. In principle, conditional stochastic simulation could be used instead but this would require simulation of the large rock volumes. Because of computer limitations only small parts of a rock domain can be simulated and therefore unconditional simulation is used. Furthermore, conditional simulation would only affect the distribution of thermal properties close to the investigated boreholes, whereas the majority of the potential repository volume can only be described statistically at this point. The expected result of the unconditional simulations is a set of realisations of spatially distributed thermal properties. These realisations can be used for subsequent temperature calculations. In this report, the realisations are described statistically.

4.2.2 Outline of the methodology

The methodology for thermal modelling is presented in Figure 4-1 and consists of the following steps:

1. Choice of simulation scale.
2. Preparation of lithological data (hard data).
3. Defining Thermal Rock Classes (TRCs) within the rock domain.
4. Preparation of thermal data (hard data).
5. Change of support.
6. Specifying expert knowledge (soft data).
7. Estimating the spatial statistical structure of the TRCs.
8. Stochastic simulation of TRCs.
9. Estimating spatial statistical thermal model for each TRC.
10. Stochastic simulation of thermal conductivity.
11. Merging of realisations.
12. Upscaling of simulation results.
13. Presentation of results.

The methodology in Figure 4-1 is applied separately for each rock domain. Starting at the upper part of Figure 4-1, the simulation scale (1) is defined as one of the first steps in the methodology. This scale determines how lithological data (2) should be prepared and if a change of support (5) is required for the thermal data (4). The lithological data acquired from boreholes and mapping of the rock surface need to be reclassified into thermal rock classes, TRCs (3). The main reason is to simplify the simulations; only a limited number of classes can be handled in the simulations.

The lithological data are used to construct models of the transition between different TRCs, thus describing the spatial statistical structure of each TRC (7). The result is a set of transition probability models that are used in the simulation of TRCs (8). The intermediate result of this first stochastic simulation is a number of realisations of the geology, each one equally probable.

Based on the thermal data, a spatial statistical thermal model is constructed for each TRC (9). It consists of a statistical distribution and a variogram for each TRC. These are used in the stochastic simulation of thermal conductivity (10) and the result is a number of equally probable realisations of thermal conductivity for the domain. Steps 9/10 can be carried out in parallel with steps 7/8 because they are independent of each other, provided that the TRCs (step 3) have been defined properly.

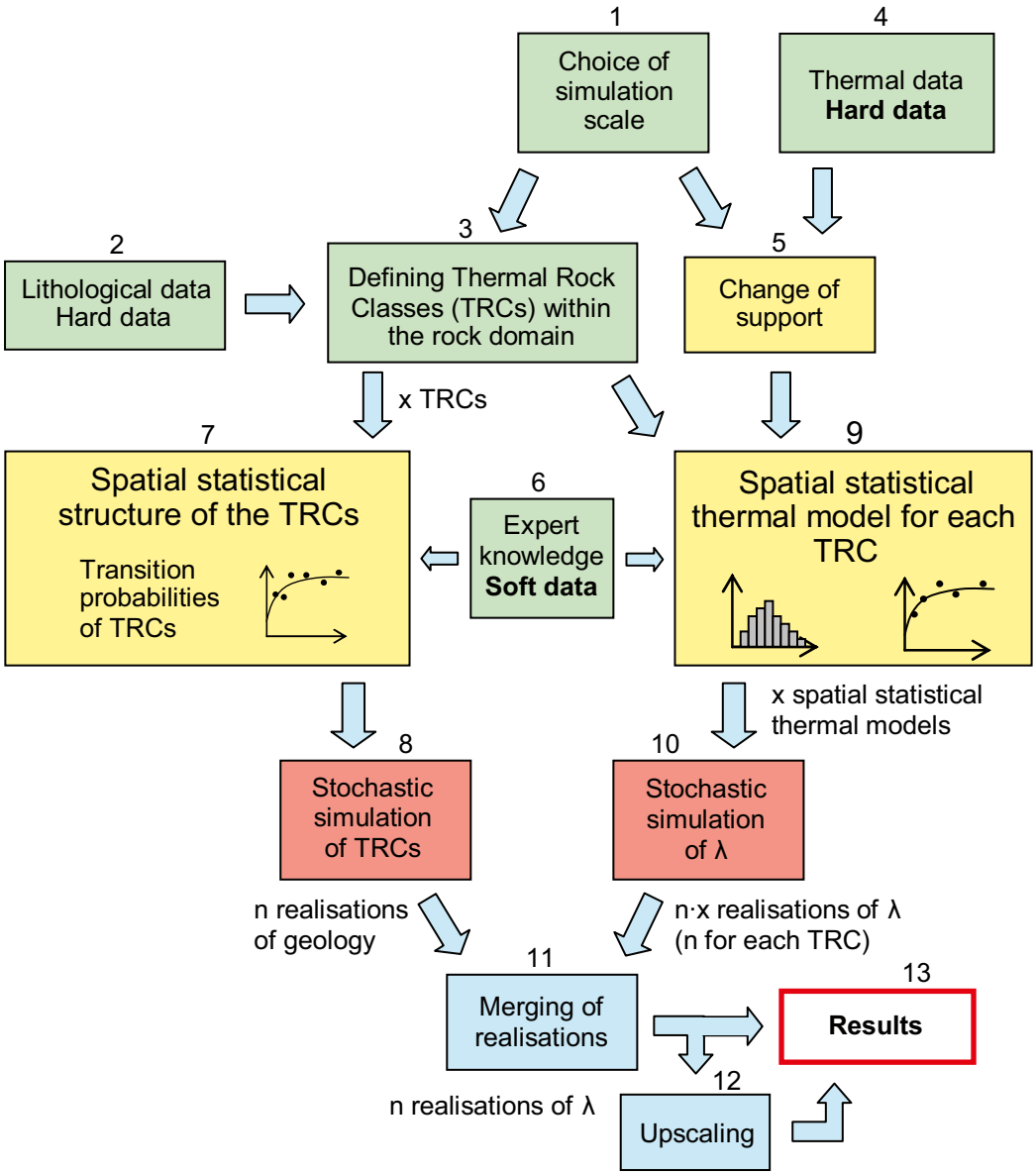

Figure 4-1. *Schematic description of the approach for thermal modelling of a rock domain (λ represents thermal conductivity).*

In the next step, the realisations of TRCs (lithology) and thermal conductivity are merged (11), i.e. each realisation of geology is filled with simulated thermal conductivity values. The result is a set of realisations of thermal conductivity that considers both the difference in thermal properties between different TRCs, and the variability within each TRC. If the result is desired in a scale different from the simulation scale, upscaling of the realisations can be performed (12). Upscaling can be performed up to a scale not larger than the size of the simulation domain. In practice, upscaling should be made to a much smaller scale, preferable the canister scale. The results (13) can be presented in a number of ways, for example as 3D illustrations, histograms and statistical parameters for the rock mass, probabilities of encountering low thermal conductivity data etc.

How each step in the procedure was applied in Forsmark is described briefly in the following sections. For specific details of the methodology the reader is referred to /Back and Sundberg 2007/ and references therein. Details on the Forsmark-specific implementation of the modelling strategy can be found in Chapter 5 and 6 using Table 4-1.

Table 4-1. Steps in the thermal modelling strategy and where the Forsmark-specific implementation can be found in the report.

Step in the thermal modelling strategy (Ch. 4)	Report section with application to Forsmark
1. Choice of simulation scale	5.4.1
2. Preparation of lithological data (hard data)	5.2
3. Defining Thermal Rock Classes within the rock domain	5.2
4. Preparation of thermal data (hard data)	5.3
5. Change of support	5.4.1
6. Specifying expert knowledge (soft data)	5.3
7. Estimating the spatial statistical structure of the TRCs	5.3
8. Stochastic simulation of TRCs	5.4.2
9. Estimating spatial statistical thermal model for each TRC	5.3
10. Stochastic simulation of thermal conductivity	5.4.3
11. Merging of realisations	6.1
12. Upscaling of simulation results	6.1
13. Presentation of results	6.1

4.2.3 Choice of simulation scale – step 1

The scale used in the simulations is decided at an early stage. The simulation scale is here defined as the size of a grid cell in the simulation. The simulation domain is defined as all the grid cells in a realisation. Due to practical restrictions, such as computer capacity and time limitations, the practical limit for the number of grid cells is currently in the order of 10^6 in a simulation domain.

The following considerations are taken into account when choosing the simulation scale:

- Preferably, the simulation scale should be equal to the scale (support) of measurements. This will make change of support unnecessary.
- The simulation scale must be sufficiently small to reflect small-scale variations in lithology and thermal properties that may be of importance.
- For 3D simulations representing large rock volumes, the simulation scale must be sufficiently large so that the number of grid cells does not become too large.
- The data requirements in SKB's design work must be considered when the simulation scale is defined.

Some of the issues above are contradictory. For example, the simulation scale should be sufficiently small to reflect small-scale variations but sufficiently large to make possible simulation of large rock volumes, which are two contradicting objectives. It may therefore be necessary to perform thermal simulations in two steps, starting with a small simulation scale. After a change of support, according to Section 4.2.7 a simulation at the larger scale can be performed.

In order to take small-scale rock occurrences into account a simulation scale of 0.1 m is recommended. This scale is sufficiently small to approximately coincide with the measurement scale for thermal laboratory data (TPS method). Change of support is therefore not required for such data.

4.2.4 Preparation of lithological data – step 2

The lithological information mainly consists of data from cored boreholes. All drill cores have been mapped to assess the lithology. The disadvantage of the available data from boreholes is that they mainly describe a vertical transect. Horizontal continuity is difficult to assess because only data for separate distant boreholes are available. However, inclined boreholes can supply information for the horizontal continuity, as well as surface data from rock outcrops. The lithological data are complemented with expert opinion when required (Figure 4-1).

The resolution in boremap data is 1 cm, but the resolution should match the simulation scale. Therefore, the lithological data (Section 3.11) must be processed before being used. Both dominant and subordinate rock types are considered but a problem is how to handle subordinate rock types with an apparent thickness less than the cell size. Here, a probabilistic approach is used: When a simulation scale of 1 m is desired, each 1 m section in a borehole is assigned a rock type that is randomly taken from the 1 m section (due to the high resolution in boremap there may be several rock types within that 1 m section but only one of them is randomly selected to represent the whole section). This means that all subordinate rock types are properly represented if the data set is sufficiently large. However, there may be a considerable discretisation error if the rock occurrences are close to, or smaller than, a metre. It is especially important how low-conductive rocks are discretised, such as amphibolites.

Details on lithological data and other geological information of importance for the thermal modelling in Forsmark are presented in Section 5.1.

4.2.5 Defining Thermal Rock Classes within the rock domain – step 3

The purpose of this step is to define, for each rock domain, the lithological classes or Thermal Rock Classes (TRCs) that will be used in the stochastic simulations. Each TRC comprises one or more rock types having similar thermal and lithological properties, see Section 5.3.1. The reason that TRCs need to be defined instead of using the rock types directly is that the number of rock types present may exceed five, which is the number of classes that can be handled in the simulations. By defining TRCs the complexity of the simulations can be kept at a reasonable level. The TRCs implies a cruder classification than rock types but the TRCs are sufficiently detailed to handle the thermal properties. It should be noted that this step and the subsequent simulations do not imply a revision of the rock domain model, but is an attempt to describe the lithological variation within a rock domain in a statistical sense.

4.2.6 Preparation of thermal data – step 4

The data type that is believed to best represent small-scale thermal conductivity is the TPS data. In addition SCA data and calculated thermal conductivity from density loggings can also be used.

The most important information about spatial variability is believed to be density logging data, i.e. for those rock types where a relationship exists between density and thermal conductivity. Even for rock types where such a relationship is not evident, density logging data are used as input to the variogram modelling (Section 4.2.11).

The different types of thermal conductivity data for Forsmark are presented in Chapter 3.

4.2.7 Change of support – step 5

A change of support, i.e. a change in scale, is performed for each TRC using stochastic simulation and upscaling with the SCA method; see /Sundberg et al. 2005b/. The principle is simple:

1. 3D unconditional stochastic simulation is performed at a simulation scale of 0.1 m, which is close to the scale of measurements.
2. The simulation volume is divided into cubes of the size of the desired larger scale, e.g. 1 m.
3. The effective thermal conductivity for each cube is calculated, using the SCA method by iteration.

A principle sketch of the change of support is illustrated in Figure 4-2. The result of a change of support is a reduced variance.

A spatial statistical thermal model (statistical distribution and variogram) of the upscaled thermal conductivity is fitted after the change of support is performed, according to Section 4.2.11. This is made by calculating a histogram based on the upscaled or "change of support" values and a new variogram. The variogram for the 1 m scale is affected by the upscaling in the following way compared to the 0.1 m scale:

- The nugget is almost completely eliminated (a change of support from 0.1 m to 1 m implies a volume increase by a factor of 1,000, and correspondingly a reduction of the nugget by the same factor /Dowd 2007/).
- The range is increased by 0.9 m /Dowd 2007/.

Stochastic simulation is then performed for each TRC at the 1 m scale (Section 4.2.12).

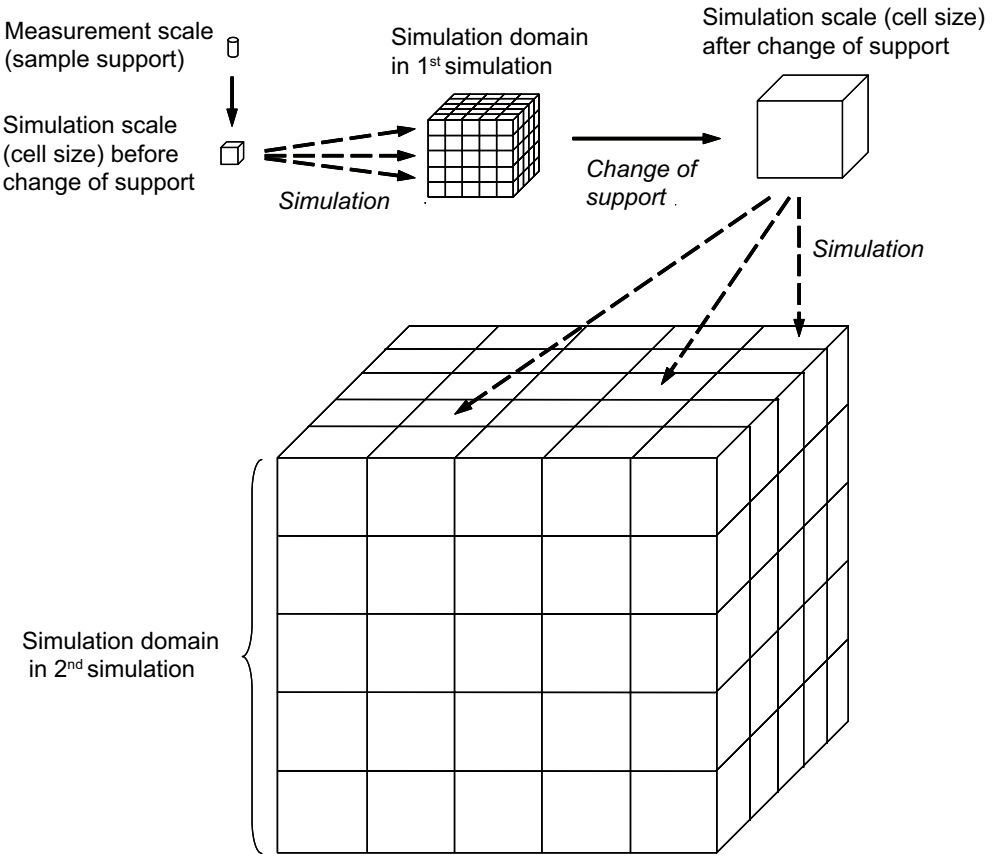

Figure 4-2. *Schematic description of sample support, simulation scale, simulation domain (simulation volume) and change of support. A two-step simulation procedure is used; the first at the 0.1 m scale and the second at the 1 m scale.*

4.2.8 Specifying expert knowledge (soft data) – step 6

Expert knowledge was required as a complement in order to complete the spatial statistical structure of TRCs (lithology) and the spatial statistical thermal models; see Section 4.2.9 and Section 4.2.11, respectively. Existing hard data from boreholes and observations at the ground surface provide important but partial knowledge of the geological conditions in a rock domain. Modelling of the spatial statistical structure of TRCs can be much improved and made more realistic with the inclusion of geological expert knowledge. Geological interpretations of typical geometries of rock types, their orientation and mutual relations and correlation structure, are necessary inputs. The conceptual description of geology in Section 5.3 is therefore important.

The spatial statistical thermal models (statistical distribution and variogram) required expert knowledge concerning the reasonable shape of histograms and the proper values for variogram parameters, especially for TRCs with small data sets. For example, theoretical lower and upper limits of thermal conductivity for rock types can be approximated from expert judgements of "extreme", but possible, mineral compositions.

Expert knowledge is also needed when different thermal data sets for one TRC have different statistics, such as TPS and SCA data. In such cases, TPS data are primarily relied on but for TRCs with very small data sets a mixture TPS and SCA data can be used.

4.2.9 Spatial statistical structure of the TRCs (lithology) – step 7

Approach

Stochastic three-dimensional (3D) simulations of lithology are used as input into the thermal modelling at Forsmark. Before the lithology can be simulated, the spatial structure for the different thermal rock classes (TRCs) has to be modelled. Traditionally, in spatial statistical analysis for geological applications the following approach is used:

1. Calculate values of a spatial statistic (usually the semivariogram) at regularly-spaced lags (separation vectors).
2. Fit a mathematical function (e.g. spherical, exponential) through the variogram measurements.
3. Implement various estimation (e.g. kriging) or simulation (e.g. sequential simulation, simulated annealing) procedures.

Geologic or "subjective" knowledge does not necessarily enter directly into this procedure.

Another approach to modelling spatial conditions in geological systems is Markov chain analysis, where the transitional trends between geological materials are analyzed. This approach is used in the report. Spatial modelling using Markov chain analysis makes it possible to more directly and explicitly consider factors with geological significance, such as:

- volumetric proportions of rock categories,
- mean lengths (e.g. mean thickness in the vertical direction),
- juxtapositional tendencies (how one category tends to locate in space relative to another),
- anisotropy directions, i.e. caused by preferred orientation and geometry of subordinate rock bodies, e.g. dykes,
- spatial variations of the above.

Because of the importance of fully acknowledging both hard and soft geological information for the lithological modelling, the Markov chain analysis approach is recommended here. Markov methods have previously been used for predictions in the Swedish nuclear waste repository programme; see e.g. /Rosén and Gustafson, 1995ab, 1996, Norberg et al. 2002/.

Transition probabilities and spatial variability

The modelling consists of calculating transition probabilities (see Section 5.4.1) followed by expert adjustments based on geological interpretations. /Carle and Fogg 1997/ describe how transition probabilities can be used to model the spatial structure, using Markov chains. An example is illustrated in Figure 4-3.

The probability of a transition from one TRC to another is described in each of the 16 graphs. The example illustrates four different TRCs, i.e. there are 16 different possible transitions. One such transition is from class A to class A, i.e. the TRC is the same when we move one grid cell in the strike direction (left graph in upper row). Another such transition is from class A to class B (second left graph in upper row) and from class B to class A (left graph in second upper row). The probability of a transition from one TRC to another is represented on the y-axis in each graph and the distance between two points is represented on the x-axis.

The transition probability example in Figure 4-3 is for one-dimensional (1D) simulation in the x-direction. For 3D simulations, similar sets of graphs are required also for the y- and z-directions. This results in a total of 3×16 = 48 transition probability graphs when four TRCs are present. The hard input data for the transition probability modelling will consist of lithological data, mainly from boreholes. The resolution in input data should be the same as the simulation scale.

In practice, software is required for creating the transition probability plots in Figure 4-3. One such software is described below.

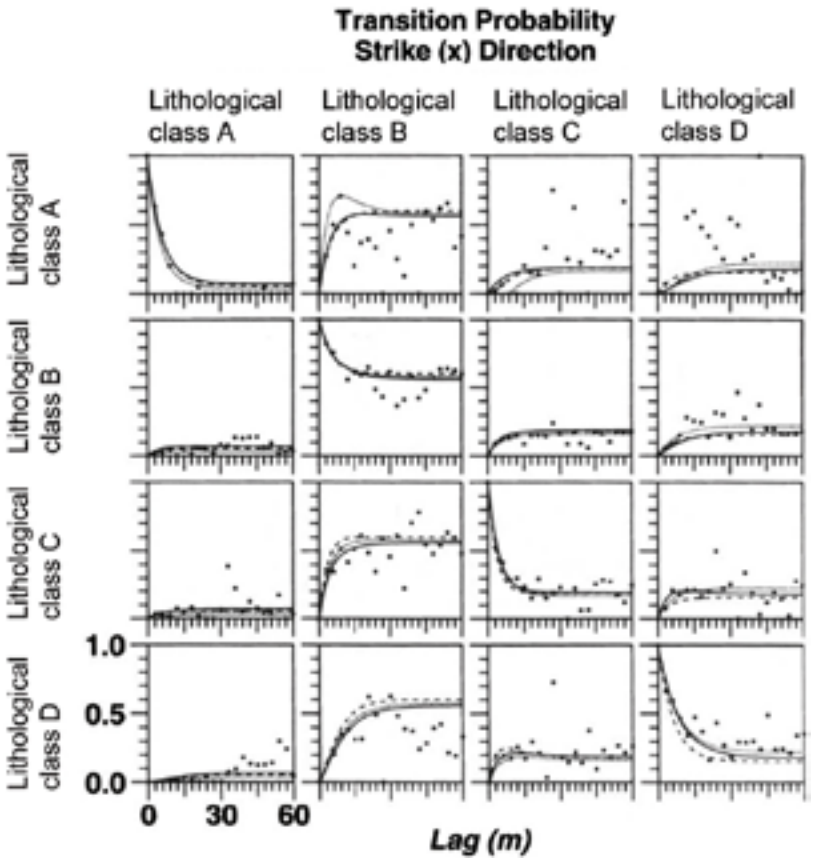

Figure 4-3. *Principle for transition probabilities using Markov chains for 1D simulation /after Carle and Fogg 1997/. The graphs present the probability of transition from one thermal rock class to another when moving from one cell to the next in the x-direction.*

The software T-PROGS

The T-PROGS (Transition PRObability GeoStatistics) /Carle 1999, GMS 2006/ software has been used for the transition probability analysis and the stochastic simulations. This software utilizes a transition probability-based geostatistical approach to:

1. model spatial variability of categorical data, e.g. rock classes, by 3D Markov Chains,
2. set up indicator co-kriging equations for predicting rock categories at positions where observations have not been made, and
3. formulate the objective function for simulated annealing for finding the global maximum of the predicted model, i.e. for finding the optimal spatial configuration given the selected input parameters.

T-PROGS facilitates stochastic modelling of lithology based on Markov chain analysis for describing the spatial conditions of lithological categories. The major steps in T-PROGS are:

1. calculation of transition probability measurements,
2. modelling spatial variability with Markov chains, and
3. stochastic simulation.

These steps are performed using five different modules; Figure 4-4.

The spatial dependency of material categories are estimated by classical Markov chain analysis. The analysis starts with calculations of the number of transitions between material categories at equally spaced distances (lags). For our case, the material classes are equal to the TRCs. The frequencies are transformed to transition probabilities for the specific lag distance. The probability calculations are displayed in a transition probability matrix, such as:

$$\mathbf{T}\,(\Delta h_z = 1.5\ \text{m}) = \begin{bmatrix} t_{11}(\Delta h_z) & \cdots & t_{1K}(\Delta h_z) \\ \vdots & \ddots & \\ t_{K1}(\Delta h_z) & \cdots & t_{KK}(\Delta h_z) \end{bmatrix} = \begin{bmatrix} 0.63 & 0.11 & 0.0 & 0.04 & 0.22 \\ 0.16 & 0.48 & 0.04 & 0.0 & 0.32 \\ 1.0 & 0.0 & 0.0 & 0.0 & 0.0 \\ 0.14 & 0 & 0.14 & 0.57 & 0.14 \\ 0.05 & 0.11 & 0.03 & 0.0 & 0.81 \end{bmatrix}$$

Transition probability matrices are calculated for different lag distances. For each transition category, these “experimental” probabilities are plotted against the lag distance. For each transition category, a curve is fitted to the experimental data to model the spatial dependency. Transition probability matrices are estimated for each principal direction in the modelling volume to facilitate three dimensional modelling of spatial dependency. Anisotropy in the geometry of subordinate rock bodies is accounted for by using different transition probability matrices for different directions.

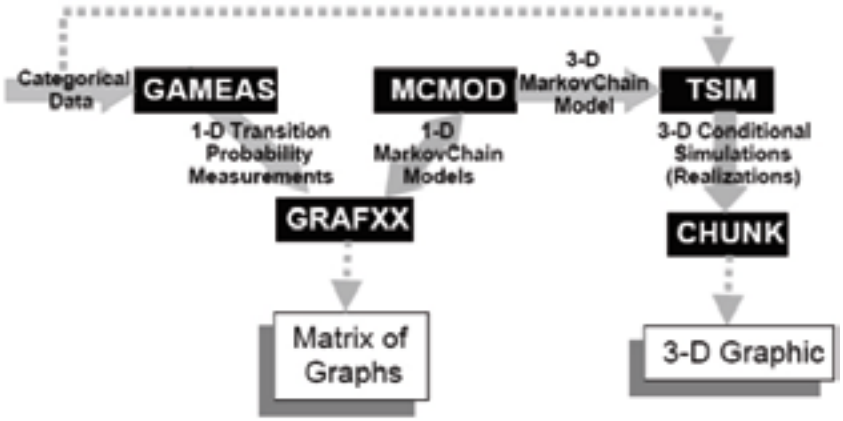

Figure 4-4. *The T-PROGS modelling procedure /GMS 2006/.*

The transition probability analysis thus provides the spatial dependency structure between categories (e.g. TRCs) in the system. The proportion and the typical length of each category are derived from the transition probability structure; see /Carle 1999/.

Most Markov chain analyses in geological applications have been performed in the form of so called embedded analyses /Carle 1999/, in which transition probabilities of occurrences from one discrete occurrence of a category to another, are considered, irrespective of the lag distance. The embedded analysis thus provides the probabilities of entering other categories when leaving a specific category and does not directly give information about the spatial dependencies of the categories. T-PROGS links the embedded Markov chain analysis to the development of *continuous-lag* (spatially dependent) Markov chain models. The reason this is important is that geologists are more inclined to think and work in the embedded framework /Carle 1999/.

4.2.10 Stochastic simulation of TRCs (lithology) – step 8

The stochastic simulation of TRCs is performed with the software T-PROGS presented in previous section. An overview of the methodology is given here. For details, the reader is referred to the cited references.

Based on the transitional properties analysed by Markov chain analysis, stochastic simulations (conditional or unconditional) of categorical configurations, such as TRCs, are made through a two-step procedure of:

1. Generating an "initial configuration" using a co-kriging-based version of the sequential indicator simulation (SIS) algorithm /Deutsch and Journel 1998/ where a transition probability-based indicator co-kriging estimate is used to approximate local conditional probabilities by:

$$\Pr\{k \text{ occurs at } \mathrm{x}_0 \mid i_j(\mathrm{x}_\alpha);\ \alpha = 1,...,N;\ j = 1,...,K\} \approx \sum_{\alpha=1}^{N}\sum_{j=1}^{K} i_j(\mathrm{x}_\alpha)\, w_{jk,\alpha}$$

where N is the number of data, K is the number of categories, $w_{jk,\alpha}$ represent a weighting coefficient, and $i_j(x_\alpha)$ represents the value of an indicator variable:

$$i_j(x_\alpha)\ \{\ \begin{matrix} 1\ if\ category\ j\ occurs\ at\ x_\alpha \\ 0\ otherwise \end{matrix} \quad ; \quad j = 1,...,K$$

Use of co-kriging instead of the traditional indicator kriging approach improves consideration of spatial cross-correlations.

2. Iteratively improving the conditional simulation in terms of matching simulated and modelled transition probabilities by applying the simulated quenching (zero-temperature annealing) algorithm:

$$\min\left\{ O = \sum_{l=1}^{M}\sum_{j=1}^{K}\sum_{k=1}^{K}[t_{jk}(h_l)_{MEAS} - t_{jk}(h_l)_{MOD}]^2 \right\}$$

where O denotes an objective function, the h_l denote $l = 1,\ldots, M$ specified lag vectors, and *MEAS* and *MOD* distinguish measured and simulated (measured from the realization) transition probabilities, respectively /Aarts and Korst 1989, Deutsch and Journel 1998, Deutsch and Cockerham 1994, Carle 1997/. The simulated quenching algorithm is implemented by repeatedly cycling through each nodal location of the conditional simulation and inquiring whether a change to another category will reduce O; if so, the change is accepted. This iterative improvement procedure continues until O is minimized, or a limit on the number of iterations is reached. Conditioning is maintained by not allowing changes of categories at conditioning locations. "Artifact discontinuities" /Deutsch and Cockerham 1994/ are avoided by generation of the initial configuration and including consideration for anisotropy and limiting the number of lags in formulation of the objective function /Carle 1997/.

This procedure is used for each equally probable stochastic realization being performed. T-PROGS can produce up to 999 realizations in one batch of simulation. T-PROGS assumes statistical homogeneity throughout the modelling volume. The proportions of the material categories calculated in the Markov chain analysis is kept stationary in all realizations.

4.2.11 Spatial statistical thermal model for each TRC – step 9

A spatial statistical thermal model was developed for each TRC. This model describes the statistics and the spatial correlation structure of thermal conductivity for a TRC. Development of the model is performed in three steps:

1. Qualitative trend analysis.
2. Fitting a distribution model to the histogram.
3. Variogram modelling (structural analysis).

To develop spatial statistical thermal models is maybe the most important step in the thermal modelling approach. The specific models developed for Forsmark are described in detail in Chapter 5.

Qualitative trend analysis

There may be large spatial trends of thermal conductivity for some rock types. Qualitative trend analyses is performed to reveal trends that can be significant for the thermal modelling. An example is rock type 101051 (granodiorite to tonalite) in Forsmark, for which trends within and between the boreholes make it necessary to develop separate spatial statistical thermal models for the various subtypes of the rock; see Section 5.4.2.

Fitting a distribution model

A distribution model is fitted to the histogram of each TRC. This is performed by smoothing the histogram with the smoothing algorithm in the geostatistical software Gslib /Deutsch and Journel 1998/. This algorithm uses a simulated annealing procedure that honours the sample statistics. Smoothing is required because of small data sets. The smoothing requires a decision of stationarity to be made for the model. This is a reasonable decision for individual TRCs. A proper decision of stationarity is critical for the representativeness and reliability of the geostatiscal tools used /Deutsch and Journel 1998/.

A very important aspect to consider is how to model the tails of the histogram where there are no data. The following principles are suggested for setting lower and upper limits of thermal conductivity in the distribution models for each TRC.

1. The distribution model should cover the range of the data.
2. Since the number of data is limited it can be assumed that values outside the range of the data exist.
3. Where possible, and where justified, a theoretical lower limit (minimum value) can be approximated from assumptions regarding the mineral compositions of “extreme” cases. By “extreme” it is meant mineral compositions which produce the lowest thermal conductivities.

The distribution model of a TRC should reflect all rock types belonging to that TRC.

Variogram modelling (structural analysis)

The spatial correlation within each TRC is modelled by a variogram. Variogram analysis is performed in order to construct a variogram model which characterises the essential features of a TRC's spatial variability/dependence. The principles used in variogram modelling are listed in geostatistical textbooks; see e.g. /Journel and Huijbregts 1978, Isaacs and Srivastava 1989, Deutsch and Journel 1998/. Thermal conductivity data for most rock types are too few to produce any reliable variograms. For this reason, density loggings can be employed. In the thermal modelling strategy it is assumed that density and thermal conductivity exhibit similar, although not identical, correlation structure; see the discussion in Chapter 5. Experimental variograms are created for the main rock type in each TRC. It is assumed that the spatial correlation structure of the main rock type is representative for the TRC as a whole.

The variogram modelling is a very important step in the thermal modelling because it will dictate how the variance is reduced when the scale increases. This is important for the tails of the thermal conductivity distribution at different scales. The variogram model is associated with modelling uncertainty, which is an important uncertainty to consider in the strategy.

4.2.12 Stochastic simulation of thermal conductivity – step 10

Sequential Gaussian Simulation (SGS) is used for simulating the thermal properties within each TRC; see /Back and Sundberg 2007/ for details. Consequently, one simulation is performed for each TRC. The basis for the SGS is the spatial statistical thermal model; see Section 4.2.11. The result of the simulation is a set of equally probable realisations of thermal conductivity.

The stochastic simulations of thermal conductivity are performed unconditionally in 3D and with the same cell sizes and simulation volumes as the geological simulations described in Section 4.2.10. One thermal realisation is created for each realisation of geology (TRCs). This implies that the same number of realisations is produced as described in Section 4.2.10.

The number of realisations is decided based on the objective of the simulation. Because the lower tail of the thermal conductivity distribution is of great concern (see Section 1.2), the number of realisations is selected to be relatively large for the simulation scale 1 m. The main objective of simulations at the 0.1 m scale is different (to perform change of support) and therefore the number of realisations is lower.

4.2.13 Merging of realisations – step 11

The realisations of TRCs (the geology) and thermal conductivity are merged so that thermal values from each TRC are assigned to a position in space determined by the realisation of geology. Thus, a geological realisation works as a mask for the thermal realisations. The principle is illustrated in Figure 4-5 for 2D-realisations. The result of the merging is one set of realisations of thermal conductivity. These realisations consider both variability due to different TRCs (lithology) and variability within each TRC. All realisations are equally probable.

4.2.14 Upscaling of simulation results – step 12

Upscaling of the simulation results can be performed if results are desired for a scale different from the simulation scale. Such upscaling can also be used to study how the result varies with the scale, plotted on a graph. This was performed for evaluation of the simulations (see Section 6.2).

The upscaling is performed with the SCA approach /Sundberg 1988; Back and Sundberg 2007/ and the effective thermal conductivity λ_e is calculated by iteration.

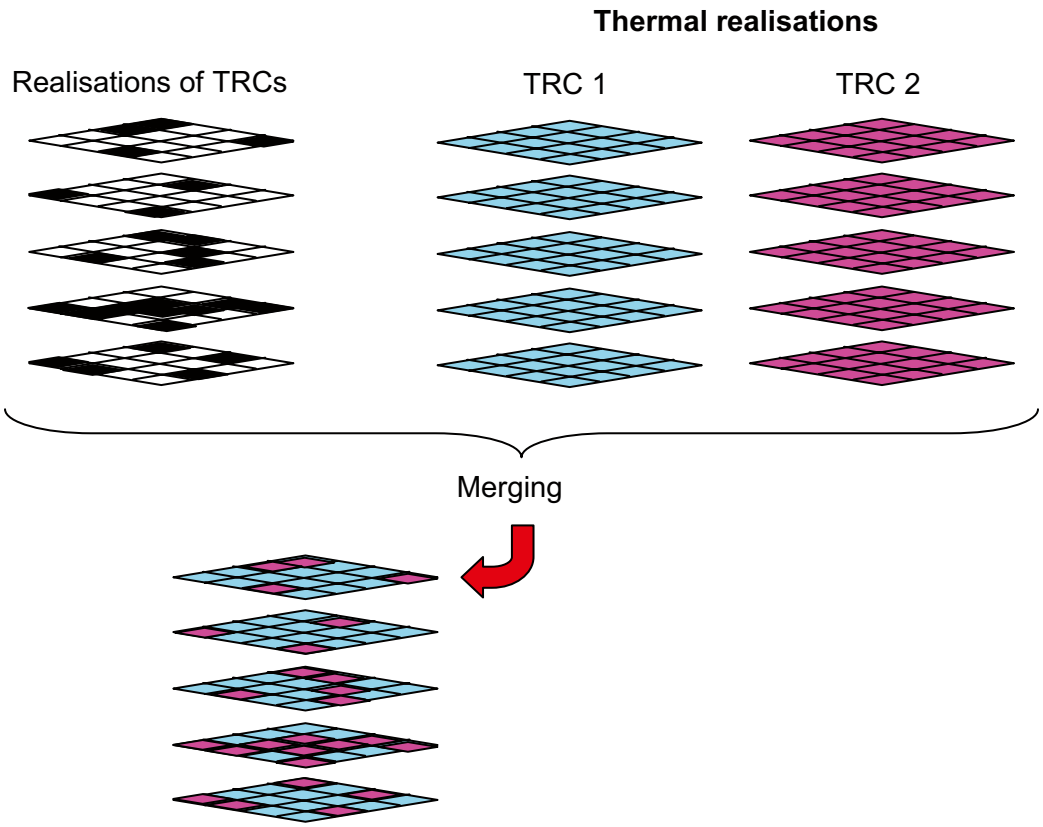

Figure 4-5. *Schematic description of the merging of TRC realisations (lithology) and thermal realisations for two TRCs (2D realisations). The same principle applies also to 3D-realisations and when there are additional TRCs. The spatial variability of thermal conductivity within each TRC is not illustrated in the figure.*

4.2.15 Presentation of results – step 13

The main results of the simulations are a set of equally probable realisations of thermal conductivity for each rock domain. These realisations are used to determine:

- Histograms of simulated thermal conductivity, representing the rock domain of interest. Of special interest is the lower tail of the histogram, as discussed in Section 1.2.
- Statistical parameters, such as the mean, the 0.1-percentile, the 1-percentile and the 2.5-percentile.
- Estimates of the uncertainty in statistical parameters, e.g. confidence intervals of the mean and the percentiles.

5 Statistical analyses and stochastic simulation

5.1 General

The application to Forsmark of the methodology for thermal modelling outlined in Chapter 4 is presented in this chapter. First, in Section 5.2, the modelling assumptions are identified. Next, in Section 5.3, the geological input, both hard and soft data, is described. This is followed in 5.4 by the establishment of spatial statistical models for both lithologies and thermal conductivity. Finally, Section 5.5 presents the results of lithological and thermal simulations. These results include

- the spatial distributions of TRCs in rock domains 29 and 45, and
- thermal conductivity distributions of the individual TRCs.

5.2 Modelling assumptions

The modelling approach requires a number of modelling assumptions in various steps of the modelling process. The most important ones are believed to be the following:

- It is assumed that TPS data (and modal analysis data to some extent) represent the 0.1 m scale so that simulations could be performed at this scale.
- The 1 m scale is assumed to be sufficiently small to properly represent the subordinate rock types; see Section 6.2 for a discussion of this assumption.
- The simulation volumes ($5\times5\times5$ m^3 for scale 0.1 m and $50\times50\times50$ m^3 for scale 1 m) are assumed to be sufficiently large for the objectives of the simulations.
- Borehole information and core samples are assumed to be representative for the rock domain.
- Water movements are not considered in the modelling. It is assumed that modelling such effects could lead to non-conservative estimates of thermal properties.
- The modelling is performed using effective values of thermal conductivity (isotropic assumption). This also applies to the upscaling methodology where effective values are calculated using the SCA approach. Anisotropy, both due to foilation/lineation and orientation of subordinate rock types, was evaluated separately.
- Expert opinion is used as an important source of information for determining the spatial statistical structure of a TRC (lithology); see Section 5.1.
- It is assumed that spatial statistical structure of a TRC (lithology) is the same for all rock types that belong to that TRC.
- Various assumptions of the shapes of histograms and variograms for the thermal conductivity of TRCs are required. This is further discussed in Chapter 5.
- It is assumed that the spatial statistical thermal model for a TRC (statistical distribution and variogram) is the same for all rock types that belong to that TRC.
- Thermal conductivity is assumed to exhibit correlation from one section of a TRC to the next section of the same TRC, i.e. a different type of rock separating to the sections does not “break” the correlation.

Detailed information regarding the assumptions made for the lithological and the spatial statistical thermal models for each TRC is provided in the following sections.

5.3 Conceptual description of geology

5.3.1 Method

Geological borehole data form the basis for the stochastic simulation of lithologies, an important component of the thermal modelling procedure. Geological data must be available at the same resolution as the scale of simulation, which is defined as the size of a grid cell in the simulation. For this reason, the lithological boremap data was processed to match the two simulation scales chosen, namely 0.1 m and 1 m. The resolution in boremap is 1 cm. For 0.1 m data, each borehole section belonging to a domain is divided into 0.1 m sections and each section is assigned a rock type according to the dominant lithology. In this threshold approach, occurrences less than 0.05 m are disregarded. For 1 m data, a slightly different approach was used. Each 1 m section was assigned a rock type randomly selected from the 0.1 m sections within the 1 m section. This selected rock type is assumed to represent the whole 1 m section. This probabilistic approach was considered appropriate in order to deal with the low conductivity amphibolites, which commonly occurs as borehole lengths of less than 1 m. Using the threshold approach would have lead to a gross underestimation of the proportion of amphibolite in the rock mass.

The geological simulation can deal with a maximum of five lithological classes. For this reason, the rock types are grouped into classes, called thermal rock classes (TRC). Rock types with similar thermal and lithological properties were assigned to the same class, The TRCs were defined primarily based on the thermal properties, e.g. thermal conductivity, of the rock types. However, consideration was also taken of a rock type's geological properties, such as mineral composition, mode of occurrence and age. The next step is to convert rock type codes to the appropriate TRC code. Five TRCs were defined. The classification of rock types into TRCs for domain 29 and domain 45 are presented in Table 5-1 and Table 5-2 respectively. Some of the rock types for which thermal data is available, e.g. tonalite to granodiorite (101054) and granodiorite (101056), are rare or absent altogether in the investigated rock domains, and have therefore not been assigned to a TRC.

The code for a TRC is defined by using the two last digits of the rock code for the dominating rock type in that class. Each domain consists of four TRCs. Three TRCs are common to both domains. TRC 57, which is dominated by granite to granodiorite (101057), is unique for domain 29. Rock type granite (101058) is of very minor importance in this TRC. TRC 58 is dominated by granite (101058), but also has a substantial component of granite to granodiorite (101057).

Table 5-1. Division of rock types into TRCs for domain RFM029. Proportions of different rock types and geological characteristics are according to /Stephens et al. 2007/.

TRC	Rock name/code	Proportion in domain 29, %	Mean thermal conductivity (TPS)	Composition, mode of occurrence, etc
57	Granite to granodiorite, 101057	74%	3.68	Both felsic group B rocks. Dominating granites.
	Granite, aplitic, 101058	1%	3.85	
51	Granodiorite to tonalite, 101051	5%	2.85	Felsic to more intermediate group A and C rocks.
	Felsic to intermediate volcanic rock, 103076	0.4%	2.54	
61	Pegmatite, pegmatitic granite, 101061	13%	3.33	Both felsic group D rocks. Late tectonic dykes, segregations, veins.
	Granite, 111058	2%	3.47	
17	Amphibolite, 102017	4%	2.33	Both mafic group B rocks. Dykes and small irregular bodies.
	Diorite, quartz diorite and gabbro, 101033	0.2%	2.28	

Table 5-2. Division of rock types into TRCs for domain RFM045. Proportions of different rock types and geological characteristics are according to /Stephens et al. 2007/.

TRC	Rock code	Proportion in domain 45, %	Mean thermal conductivity (TPS)	Composition, mode of occurrence, etc
58	Granite to granodiorite, 101057	18%	3.68	Both felsic group B rocks. Dominating granites commonly affected by albitization.
	Granite, aplitic, 101058	49%	3.85	
51	Granodiorite to tonalite, 101051	9%	2.85	Felsic to more intermediate group A and C rocks.
	Felsic to intermediate volcanic rock, 103076	1%	2.54	
61	Pegmatite, pegmatitic granite, 101061	14%	3.33	Both felsic group D. rocks. Late tectonic dykes, segregations, veins.
	Granite, 111058	1%	3.47	
17	Amphibolite, 102017	6%	2.33	Both mafic group B rocks. Dykes and small irregular bodies.
	Diorite, quartz diorite and gabbro, 101033	0.2%	2.28	

To model the geometrical distribution of different TRCs, Markov chain analysis is used. This method allows the incorporation of both hard and soft geological information. The hard data are the borehole data referred to above, the processing of which involves the steps listed below.

1. Data from rock type (> 1 m borehole length) and rock occurrence (< 1 m borehole length) are merged.
2. Each 0.1 m section of borehole is assigned a rock type according to the dominant lithology.
3. The appropriate TRC code is assigned to each 0.1 m section.
4. Coordinates (northing, easting and elevation) are assigned to each 0.1 m section. These coordinates were obtained from geophysical logging data files in the Sicada database.
5. Data rows which have not been assigned a TRC are removed. This is the case when unusual rock types which have not been assigned a TRC code occur.
6. Boreholes and parts of boreholes are grouped according to the domain classification of boreholes /Stephens et al. 2007/. Only two domains were considered here, namely RFM029 and RFM045. The deformation zones were not removed since the geology inside and outside such zones was not considered to differ significantly /Stephens 2007/.

The soft data consist of expert geological interpretations, for example, typical geometries of rock types, their orientation and mutual relations. These are discussed in the subsequent sections.

5.3.2 Borehole characterisation of domains RFM029 and RFM045

The spatial orientation of subordinate rock bodies may result in anisotropy of the thermal properties. In order to take into account the preferential spatial orientations of the subordinate rock bodies, in particular amphibolite, a judgement of the typical orientation and geometries of these bodies is required. For a particular simulation, all occurrences of a particular rock type are modelled with the same orientation and geometry. Therefore, it is important that the boreholes used to represent a particular rock volume are rather homogenous with regard to the orientation and geometries of these rock bodies.

At Forsmark, amphibolite occurs as small, irregular and dyke-like bodies. Furthermore, this rock type has thermal conductivities considerably lower than the dominant granitoid host rocks. For these reasons, priority was given to modelling the directional properties of amphibolite.

It is generally the case that amphibolite contacts (strike and dip) coincide with the dominant foliation direction /Stephens et al. 2007/. Thus, in the absence of data for amphibolites, foliation directions have been investigated.

The investigated rock volume is situated within a tectonic lens. The internal part of this lens is dominated by rocks with a lower ductile strain, which are more lineated than foliated. The margins of the lens are characterised by more intense foliation. In domain RFM029 the amphibolites have been affected by these different deformation styles, and the rocks should therefore be treated as either:

1. foliated (margins of tectonic lens) or
2. more lineated than foliated (internal part of the tectonic lens).

It is also possible to distinguish between

a) boreholes sections in which both foliation and amphibolite contacts are predominantly NW to NNW striking with moderate to steep dips to the W, (typical) and

b) boreholes sections in which both foliation and amphibolite contacts are variable but predominantly E-W striking, and S dipping. (Anomalous).

This analysis was based on boremap mapping P-reports and consultations with geologists /Stephens 2007/.

Based on the criteria defined above, boreholes belonging to domain RFM029 (see Table 3-24) were divided into two categories:

- margins of tectonic lens with typical anisotropy directions (1a),
- internal part of the tectonic lens with typical anisotropy directions (2a).

Boreholes/borehole sections with anomalous foliation/amphibolite contact directions (b above) were excluded from the analysis. These include KFM01B and KFM08A.

A similar analysis was performed for the boreholes sections assigned to domain RFM045. The rocks of domain 45 are generally more lineated than foliated. Borehole sections with generally ESE-WNW striking amphibolite contacts with moderate dips to the south were selected to characterise the rocks of this domain.

Table 5-3 summarises boreholes used to characterize different parts of domain 029 and domain 045.

5.3.3 Orientation and geometry of subordinate rock types in domain RFM029

Expert judgements of the orientation and typical geometries of subordinate rock types were required as input to the modelling work. These interpretations were solicited from the geological modelling team, and complemented by data analysis presented in boremap reports for individual boreholes. As regards the dimensions/geometry of different rock types, it is emphasised here that judgements are based on impressions gained by geologists in the field and not on any hard data. Orientation data on rock type contacts and foliation are available both from boreholes and the surface. Mineral stretching lineations have been recorded from outcrops only.

Amphibolite contacts in the boreholes assigned to categories 1a and 2a above strike NNW with dips steeply to the west /Stephens 2007, Stephens et al. 2007/. More plentiful foliation data from the same boreholes show the same general orientation, e.g. /Petersson et al. 2005b/

Based on surface data given in the domain property tables, the mean trend and plunge of the mineral stretching lineation for domain 29 is 141º/39º. The lineation appears to be rather constant in orientation throughout the area, i.e. it does not appear to be folded like the foliation /Stephens 2007/. The axis of maximum elongation of amphibolite bodies in the internal part of domain 29 is assumed to be parallel to the mineral stretching lineation for domain 29.

Table 5-3. Boreholes used to characterise domains RFM029 and RFM045. Note that the classification of domain 29 into internal and marginal parts has been done for the purposes of thermal modelling and should be considered as a simplification.

Domain	Borehole	Borehole interval (from geology model 2.2)	Borehole length used as input for modelling	Comment
RFM029 (margin)	KFM01A	102–1,001 m	102–380 m (below 380 m foliation generally dips E)	Ductile deformation typified by foliation. Amphibolite contacts and foliation generally NNW striking with moderate to steep dips to the W
	KFM01C	12–450 m	12–450 m	
	KFM04A	500–1,001 m	500–1,001 m	
	KFM07A	102–793 m	102–793 m	
	KFM07B	5–298 m	5–298 m	
	KFM07C	85–498 m	85–498 m	
	KFM08C	102–342 m and 546–949 m	102–300 m (below 300 m orientation of foliation is anomalous and variable)	
	KFM09B	9–616 m	9–616 m	
	KFM10A	63–500 m	63–500 m	
RFM029 (internal)	KFM01D	92–800 m	92–800 m	Ductile deformation typified by lineation. Amphibolite contacts and foliation generally NNW striking with moderate to steep dips to the W
	KFM05A	102–1,000 m	102–1,000 m	
	KFM08B	6–200 m	6–200 m	
RFM045	KFM06A	751–998 m	751–998 m	Ductile deformation typified by lineation. Amphibolite contacts and foliation generally ESE-WNW striking with moderate dips to the S
	KFM06C	411–898 m	411–898 m	

One of the assumptions made when describing the geometry and orientation of bodies of subordinate rock types is that the axis of maximum stretching (lineation) lies on the plane of foliation. For this reason, some adjustments have been made to the estimated mean orientations of amphibolite contacts and lineations. The values given in Table 5-4 are consistent with this assumption. The adjustments are well within the range of variation measured in the field and in borehole cores.

A judgement by site geologists /Stephens 2007/ of the geometry of the amphibolites in the margins of the tectonic lens is that they extend in both a strike and dip direction approximately 2 to 3 times their thickness. As regards the internal part of the tectonic lens it was proposed that the amphibolites be modelled as rod-like bodies, extending parallel to the mineral stretching lineation, approximately 3–4 times their thickness, and approximately twice their thickness in the intermediate direction.

Table 5-4 summarises assumptions made regarding the orientation and geometry of amphibolite bodies.

Regarding the orientation of thermal rock classes 51 and 61 (granodiorite to tonalite (101051) and pegmatite (101061) respectively), it has been assumed, following consultations with site geologists /Stephens 2007/, that they have the same rock contact orientations (strike and dip) as amphibolite. For pegmatites (101061), this is corroborated by stereoplots of orientations given in some boremap reports, e.g. for KFM05A /Petersson et al. 2004b/ and KFM07A /Petersson et al. 2005b/. The rather sparse data for granodiorite to tonalite (101051) indicate more variable rock contact orientations; see e.g. /Petersson et al. 2004b, Petersson et al. 2005b/.

Table 5-4. Assumed orientation and geometry of amphibolite bodies in domain RFM029.

	Orientation of amphibolite bodies		Orientation of longest axis. Based on mineral stretching lineation		Ratio between shortest, intermediate and longest axes
	strike	dip	trend	plunge	
Domain 29, margin	150°	80°W			1:3:3
Domain 29, internal	150°	80°W	157°	38°	1:4:2

Granodiorite to tonalite (101051) is considered to have been affected by lineation rather than foliation throughout the whole of domain 29 /Stephens 2007/. These bodies were subjected to stretching and boudinage in a similar way to the amphibolites in the internal part of the tectonic lens. For simulation purposes, they were modelled as rod-like bodies with the same geometry as assumed for the amphibolites in the internal part of the tectonic lens. Like the amphibolites, their longest axis is assumed to be parallel to the mineral stretching lineation. This assumption applies to both the internal and marginal parts of domain 29.

Pegmatites (101061), the main rock type in TRC 61, are assumed to be dyke or disc-like bodies with a diameter 5–10 times their thickness, i.e. dimensions along strike and down dip equally long. Because of the limitations related to the small simulation volume, an anisotropy factor of anisotropy greater than 3:1 could not be accommodated in simulations at 0.1 m scale. For this reason, this factor was used. This assumption was taken to be valid for both the internal and marginal parts of domain 29.

Since separate geological simulations were performed for the different parts of domain 29 it was necessary to decide on the relative importance of each part so that the appropriate number of realisations could be chosen. The marginal part of domain 29 was considered to comprise one-third, and the internal part two-thirds of the domains total volume. The number of realisations for the respective parts were weighted accordingly /Stephens 2007/.

5.3.4 Orientation and geometry of subordinate rock types in domain RFM045

Domain RFM045 is considered to possess a deformation style typical of the internal part of the tectonic lens at Forsmark /Stephens et al. 2007/, which means that lineation is assumed to be the dominant form of ductile deformation. The amphibolites appear as lenses and boudins at the surface /Stephens 2007/. This may not be entirely true with respect to borehole KFM06C, which displays a slight predominance of foliation /Petersson et al. 2006/.

Amphibolite contacts in KFM06A and 06C generally strike ESE-WNW (112.5°) with dips about 60 to the south /Petersson et al. 2005c, Stephens 2007/. Foliation data from these borehole sections confirm this general pattern /Petersson et al. 2005c, 2006/.

There is no mineral stretching data available for domain RFM045. Since the lineation appears to be rather constant in orientation throughout the Forsmark area (surface data only), the data from domain RFM029 are used. The mean trend and plunge of the mineral stretching lineation for domain RFM029 is 141/39 based on surface data.

The geometry of the amphibolites is assumed to be the same as for the internal part of domain RFM029, i.e. is modelled as rod-like bodies. Table 5-5 summarizes assumptions about orientation and geometry. TRCs 51 and 61 are modelled in the same way as in domain RFM029.

Table 5-5. Assumed orientation and geometry of amphibolite bodies in domain RFM045 in the simulations.

	Orientation of amphibolite bodies		Orientation of longest axis. Based on mineral stretching lineation		Ratio between shortest, intermediate and longest axes
	strike	dip	trend	plunge	
Domain 45	112.5°	60°S	141°	39°	1:4:2

5.3.5 Rock type proportions

Rock type proportions for domains RFM029 and RFM045 are presented in Table 5-6 and Table 5-7. Proportions based on the boreholes used in this study are compared with proportions estimated by geologists /Stephens et al. 2007/. The reason for the discrepancies are the somewhat fewer boreholes used for the thermal modelling.

Table 5-6. Quantitative estimates in volume % of different TRCs in domain RFM029.

TRC	Proportions of TRCs from boreholes used in 1 m simulations (%)		Proportions from geological model v. 2.2 /Stephens et al. 2007/ (%)	Comment
	Domain 29 internal	Domain 29 marginal	Domain 29 whole	
57	78.7	79.5	74.8	Comprises Granite to granodiorite, 101057, and Granite, aplitic, 101058
51	4.5	2.3	5.0	Comprises Granodiorite to tonalite, 101051, and Felsic to intermediate volcanic rock, 103076
61	13.1	13.1	14.8	Comprises Pegmatite, pegmatitic granite, 101061, and Granite, 111058
17	3.8	5.1	4.6	Comprises Amphibolite, 102017, and Diorite, quartz diorite and gabbro, 101033

Table 5-7. Quantitative estimates in volume % of different TRCs in domain RFM045.

TRC	Proportions of TRCs from boreholes used in 1 m simulations (%)	Proportions from geological model v. 2.2 /Stephens et al. 2007/ (%)	Comment
58	57.7	67.3	Comprises Granite to granodiorite, 101057, and Granite, aplitic, 101058
51	18.9	10.2	Comprises Granodiorite to tonalite, 101051, and Felsic to intermediate volcanic rock, 103076
61	16.1	15.2	Comprises Pegmatite, pegmatitic granite, 101061, and Granite, 111058
17	7.3	6.5	Comprises Amphibolite, 102017, and Diorite, quartz diorite and gabbro, 101033

5.3.6 Alteration

Studies of alteration in boreholes by the geology modelling group have shown that most alteration occurs within the recognised deformations zones /Stephens et al. 2007/. Oxidation and albitization are by far the most abundant forms of alteration. Outside the deformation zones, oxidation comprises approximately 7% and 20% of the rock mass in domain 29 and domain 45 respectively. Most of the oxidation outside the deformation zones is defined as being faint to weak in character, in contrast to inside deformation zones where a significant proportion of altered rock exhibits medium to strong alteration. In domain 29, an additional 3% is made up of albitised rock, an alteration type more common in domain 45, where it comprises over 50% of the rock mass /Stephens et al. 2007/.

The main mineralogical changes associated with oxidation are saussuritization of plagioclase, chloritization of biotite and the development of hematite, which imparts a red-colouring to the rock /Stephens et al. 2003, 2005, Sandström and Tullborg 2006/. Thermal conductivities (both TPS and SCA data) of samples of altered granite to granodiorite (101057) and granodiorite to tonalite (101051) have been presented in Sections 3.2 and 3.3. The available data indicate that oxidation has resulted in slightly higher thermal conductivities than in the unaltered equivalents. This is presumably due to the alteration minerals commonly having higher thermal conductivities than their parent minerals (see Section 3.3).

The relatively minor proportion of the rock mass outside the deformation zones that is affected by oxidation, combined with its relatively weak character and the tendency for alteration to produce slightly higher conductivities than fresh rock, do not justify separate modelling of the thermal properties of altered rock. Instead, where available, the data from altered samples are combined with the data from unaltered samples, in order to statistically characterise the thermal properties of the rock types.

5.3.7 Amphibolite

At Forsmark, amphibolite, which occurs as small, irregular and dyke-like bodies, comprise approximately 5% of the rock mass. Having little or no quartz, the amphibolites have thermal conductivities considerably lower than the dominant granitoid host rocks. An assessment of the true thickness of amphibolites is reported by /Stephens et al. 2007/. The amphibolites are predominantly thin geological entities with numerically relatively few occurrences with a true thickness greater than 0.9 m; see Figure 5-1. A somewhat different picture emerges when the volume of each true thickness class is plotted; Figure 5-2. This plot shows that mafic rocks with a true thickness of 1 m or more make up approximately 1% of the total rock volume based on the borehole data. Analysis of individual rock domains has not been performed. However, an anomalously large amphibolite body, present along a borehole length of about 40 m in borehole KFM06C (745–785 m), occurs in domain 45. This occurrence is equivalent to approximately 15% of all amphibolite with borehole lengths longer than 1 m in 16 boreholes.

5.4 Spatial statistical models of lithology and thermal conductivity

5.4.1 Lithological models

Spatial properties

Spatial dependency was modelled from borehole data. The typical lens length, and interactions of TRCs were calculated through the transition probability analysis of borehole data. Anisotropy due to subordinate rock bodies was taken into account based on geological interpretations by the site geologists at Forsmark. In the context of the lithological simulation, anisotropy refers

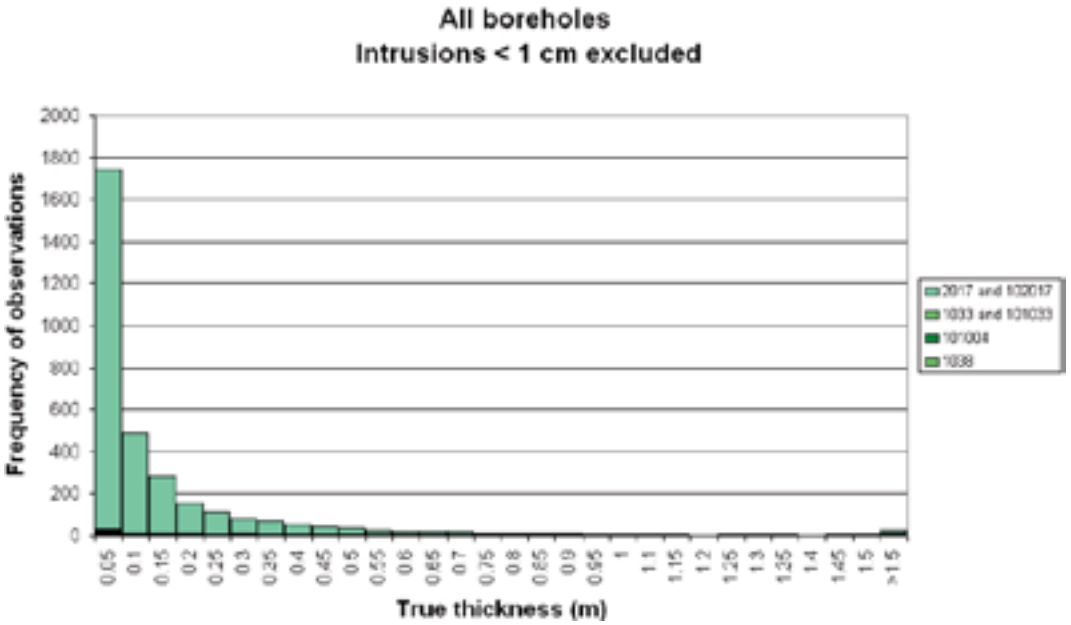

Figure 5-1. *Thickness distribution of mafic rocks (mainly amphibolite – code 102017) based on data from all cored boreholes excluding KFM07C, KFM08C, KFM10A /Stephens et al. 2007/.*

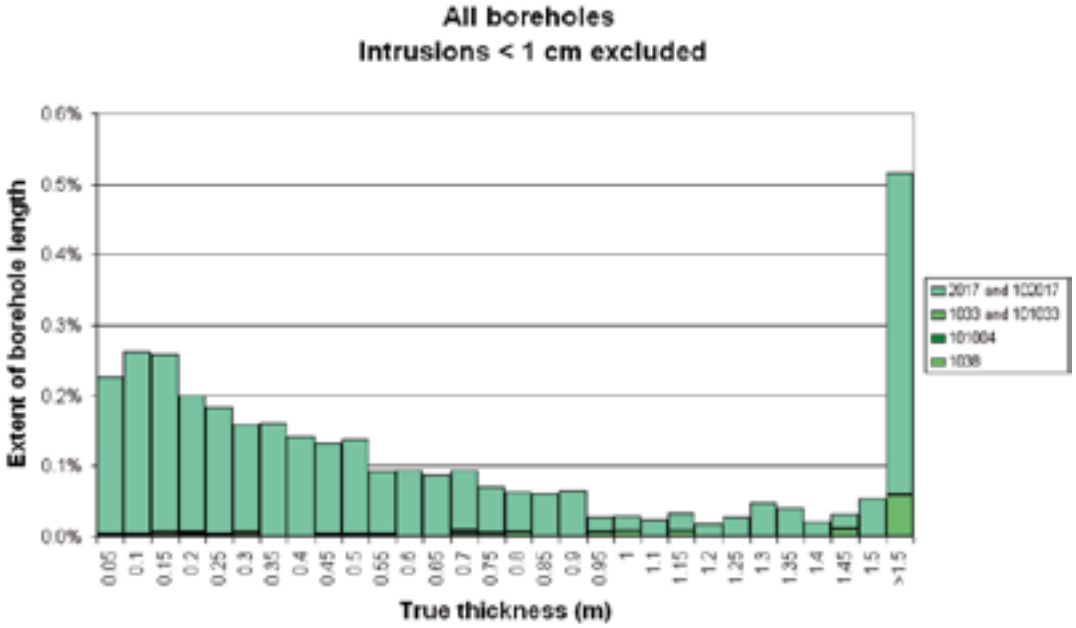

Figure 5-2. *Percentage of borehole length in each thickness class for mafic rocks (mainly amphibolite – code 102017) based on data from all cored boreholes excluding KFM07C, KFM08C, KFM10A /Stephens et al. 2007/. The y-axis can also be considered as a measure of volume percent.*

to subordinate rock types having dimensions in a particular direction that are different to another direction. For example, an amphibolite body may have a much longer extension in one direction, perhaps because of its original mode of emplacement as a dyke, or due to subsequent deformation which may have stretched, compressed or flattened rock bodies.

The spatial analysis was made stepwise for each domain as follows:

1. Initial transition probability analysis of TRCs from borehole data. This initial analysis is based on all borehole data selected to characterise each domain (Table 5-3), and without any consideration of anisotropy.
2. Transformation of borehole data into the anisotropy orientation of the TRCs (subordinate rock bodies). This means that anisotropy of typical lengths, and thus also continuous-lag transition probabilities, was accounted for. The proportions of TRCs were assumed to be isotropic. The simulations need to be oriented in the principal direction of anisotropy to properly represent the spatial properties of the domain. Existing boreholes are typically not oriented in the anisotropy direction, and a transformation of borehole data to the orientation of the anisotropy of the system is therefore necessary. Geological information describing anisotropy was given as: (1) the trend and plunge of the mineral stretching orientation and (2) the strike and dip of the foliation (Table 5-4 and Table 5-5). The orientation of rock units is a function of these.

A local coordinate system (x’’’, y’’’, z’’’) is developed for each domain, governed by the principal direction of anisotropy and an origin defined by minimum easting, minimum northing, and maximum elevation from positions in borehole records. The local coordinate system is obtained through rotations:

1. To the trend direction of the mineral orientation, i.e. rotation of the xy-plane around the z-axis. This produces the principal axes x’, y’ and z’.
2. To the plunge of the mineral orientation, i.e. rotation of the x’-z’ plane around the y’-axis. This produces the principal axes x’’, y’’ and z’’.
3. To the foliation of the rocks, i.e. rotation of the y’’-z’’ plane around the x’’-axis. This produces the principal axes x’’’, y’’’ and z’’’.

This results in a transformed coordinate system with main axis (x’’’) parallel to the principal direction of anisotropy, see Figure 5-3.

A detailed mathematical description of the transformation of borehole data to a coordinate system oriented in the principal direction of anisotropy as a function of the mineral stretching and foliation plane is given in Appendix I.

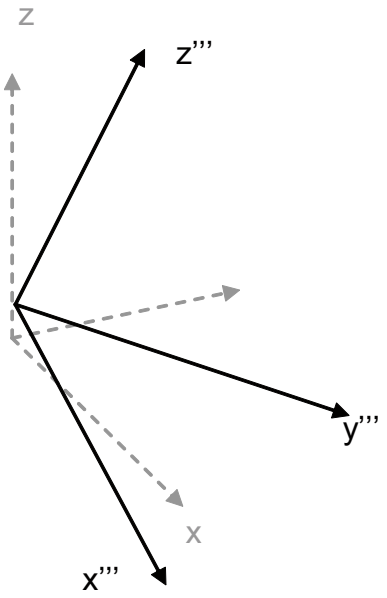

Figure 5-3. *Principal directions x’’’, y’’’ and z’’’ of the local transformed coordinate system, where x’’’ is parallel to the principal direction of anisotropy.*

Calculation of typical lengths of TRCs for the x’’’, y’’’ or z’’’ directions of anisotropy were made on the transformed borehole data. To minimize errors due to borehole deviations from anisotropy directions only the boreholes with orientation close to one of the axes x’’’, y’’’ or z’’’ were used. The boreholes used for each domain are as follows:

Domain 045: Borehole KFM06C.

Domain 029 internal: Borehole KFM05A.

Domain 029 marginal: Boreholes KFM01C, KFM07B, KFM07C, KFM09B.

The typical lengths in remaining directions were obtained from geometry relationship information for TRCs, given by the geological interpretations of the domains.

Calculation of the transition probability structure were made with respect to the typical lengths calculated for x’’’, y’’’ and z’’’. By adjusting the typical lengths, the transition probability matrix was updated for each direction x’’’, y’’’ and z’’’. The proportions of TRCs were assumed to be isotropic and thus identical to those calculated in Step 1.

Results

The anisotropy factors, i.e. the relative lengths of TRCs in the x’’’, y’’’ and z’’’ directions, estimated by geological interpretations of the TRCs are given in Table 5-8. The same anisotropy factors were used for 1 dm and 1 m simulations. The results of the spatial analysis for each domain for decimetre data are given in Table 5-9 to Table 5-11. Transition probabilities are presented as embedded probabilities.

Table 5-8. Anisotropy factors (relative lengths) for TRCs for the geological domains in the Forsmark simulations.

	Domain RFM045			Domain RFM029 internal			Domain RFM029 marginal		
	TRC17	TRC51	TRC61	TRC17	TRC51	TRC61	TRC17	TRC51	TRC61
X’’’	4	4	5–10	4	4	5–10	3	4	5–10
Y’’’	2	2	5–10	2	2	5–10	3	2	5–10
Z’’’	1	1	1	1	1	1	1	1	1

Table 5-9. Proportions, transition probabilities and typical lengths for domain RFM045, 1 dm simulations. Transition probabilities are shown as embedded probabilities of going from one TRC to other TRCs. Diagonal terms show the typical lengths of TRCs based on all boreholes and without consideration of anisotropy. “Typical TRC lengths” show the typical anisotropic lengths for directions x’’’, y’’’ and z’’’ calculated from transformed borehole data and geological interpretations.

TRC	Proportion (%)	Isotropic transition probabilities to TRCs (embedded) and typical lengths (m). (Lengths shown in bold)				Typical TRC lengths (m)		
		TRC 17	TRC 51	TRC 58	TRC 61	X’’’	Y’’’	Z’’’
TRC 17	9.8	**1.67**	0.11	0.52	0.37	4.07	2.03	1.01
TRC 51	25.9	0.02	**2.60**	0.58	0.40	3.90	1.95	0.98
TRC 58	53.0	0.09	0.14	**1.51**	0.78	b.g.	b.g.	b.g.
TRC 61	11.3	0.08	0.14	0.79	**0.34**	0.31	0.31	0.10

b.g. = background material, not calculated for anisotropy directions.

Table 5-10. Proportions, transition probabilities and typical lengths for domain RFM029 internal, 1 dm simulations. Se also text in Table 5-9.

TRC	Proportion (%)	Isotropic transition probabilities to TRCs (embedded) and typical lengths (m). (Lengths shown in bold)				Typical TRC lengths (m)		
		TRC 17	TRC 51	TRC 57	TRC 61	X'''	Y'''	Z'''
TRC 17	5.4	**0.63**	0.03	0.84	0.13	1.26	0.63	0.32
TRC 51	5.6	0.03	**1.67**	0.55	0.41	3.04	1.52	0.76
TRC 57	80.5	0.20	0.05	**2.27**	0.75	b.g.	b.g.	b.g.
TRC 61	8.5	0.04	0.05	0.91	**0.29**	0.26	0.26	0.08

b.g. = background material, not calculated for anisotropy directions.

Table 5-11. Proportions, transition probabilities and typical lengths for domain RFM029 marginal, 1 dm simulations. Se also text in Table 5-9.

TRC	Proportion (%)	Isotropic transition probabilities to TRCs (embedded) and typical lengths (m). (Lengths shown in bold)				Typical TRC lengths (m)		
		TRC 17	TRC 51	TRC 57	TRC 61	X'''	Y'''	Z'''
TRC 17	4.5	**0.50**	0.00	0.81	0.19	0.52	0.52	0.17
TRC 51	2.2	0.03	**1.18**	0.60	0.37	2.23	1.12	0.56
TRC 57	76.0	0.21	0.04	**2.18**	0.75	b.g.	b.g.	b.g.
TRC 61	17.3	0.06	0.02	0.93	**0.60**	0.58	0.58	0.19

b.g. = background material, not calculated for anisotropy directions.

The relative lengths for TRC61 in all domains were subject to large uncertainties in the geological interpretations. During simulations it was not possible to use anisotropy factors as large as 5–10 in the x''' and y''' directions as shown in Table 5-8, and these had therefore to be limited to 3 in x''' and y''' directions for all domains.

The results of the spatial analysis for each domain for metre data are given in Table 5-12 to Table 5-14.

Table 5-12. Proportions, transition probabilities and typical lengths for domain RFM045, 1 m simulations. Transition probabilities are shown as embedded probabilities of going from one TRC to other TRCs. Diagonal terms show the typical lengths of TRCs based on all boreholes and without consideration of anisotropy. "Typical TRC lengths" show the typical anisotropic lengths for directions x''', y''' and z''' calculated from transformed borehole data and geological interpretations.

TRC	Proportion (%)	Isotropic transition probabilities to TRCs (embedded) and typical lengths (m). (Lengths shown in bold)				Typical TRC lengths (m)		
		TRC 17	TRC 51	TRC 58	TRC 61	X'''	Y'''	Z'''
TRC 17	7.3	**6.01**	0.38	0.50	0.13	28.28	14.14	7.07
TRC 51	18.9	0.13	**5.96**	0.54	0.33	5.92	2.96	1.48
TRC 58	57.7	0.09	0.19	**7.63**	0.72	b.g.	b.g.	b.g.
TRC 61	16.1	0.02	0.19	0.79	**2.42**	2.86	2.86	0.95

b.g. = background material, not calculated for anisotropy directions.

Table 5-13. Proportions, transition probabilities and typical lengths for domain RFM029 internal, 1 m simulations. Se also text in Table 5-12.

TRC	Proportion (%)	Isotropic transition probabilities to TRCs (embedded) and typical lengths (m). (Lengths shown in bold)				Typical TRC lengths (m)		
		TRC 17	TRC 51	TRC 57	TRC 61	X'''	Y'''	Z'''
TRC 17	3.8	**1.89**	0.03	0.89	0.08	4.10	2.05	1.03
TRC 51	4.5	0.07	**3.00**	0.67	0.26	6.52	3.26	1.63
TRC 57	78.7	0.16	0.08	**6.97**	0.76	b.g.	b.g.	b.g.
TRC 61	13.1	0.01	0.06	0.93	**1.42**	1.12	1.12	0.37

b.g. = background material, not calculated for anisotropy directions.

Table 5-14. Proportions, transition probabilities and typical lengths for domain RFM029 marginal, 1 m simulations. Se also text in Table 5-12.

TRC	Proportion (%)	Isotropic transition probabilities to TRCs (embedded) and typical lengths (m). (Lengths shown in bold)				Typical TRC lengths (m)		
		TRC 17	TRC 51	TRC 57	TRC 61	X'''	Y'''	Z'''
TRC 17	5.1	**1.66**	0.01	0.79	0.20	1.89	1.89	0.63
TRC 51	2.3	0.03	**2.18**	0.64	0.33	6.05	3.02	1.51
TRC 57	79.5	0.26	0.08	**8.10**	0.66	b.g.	b.g.	b.g.
TRC 61	13.1	0.06	0.04	0.90	**1.77**	2.01	2.01	0.67

b.g. = background material, not calculated for anisotropy directions.

5.4.2 Thermal conductivity models – 0.1 m scale

Approach

Spatial statistical thermal conductivity models are required for each TRC in order to perform simulations at the 0.1 m scale. These models, and the upscaled realisations to 1 m scale, are used to define thermal models for the 1 m scale. The latter are required for the 1 m simulations.

Once the thermal models for the 0.1 m scale are defined, the thermal models for the 1 m scale are fairly easy determined; see Section 5.4.3. Therefore, the focus of the presentation of the thermal models is on the 0.1 m scale, which forms the basis for the models at the 1 m scale.

Statistical distribution models – 0.1 m scale

Simulation of thermal conductivity requires two types of models for each TRC: a statistical distribution model and a model describing spatial correlation. The statistical distribution of thermal conductivity for each TRC is modelled by a histogram. Histograms for individual rock types and the models for different TRC are given in Appendix C. The histogram variation represents heterogeneity in thermal conductivity, without consideration of anisotropy.

Thermal data consist of TPS and SCA data. For the dominant granite to granodiorite, (101057), only the more reliable TPS data were used. For other rock types, SCA values were used together with TPS data to produce the histograms. Declustering was applied to some rock types in cases where spatially clustered data may be producing a bias in the statistics. This applies to rock types, amphibolite (102017) and granodiorite to tonalite (101051). Even the dominant granitoid, 101057, consist of much spatially clustered data. However, a comparison of declustered statistics with those of the clustered data showed no significant difference. For this reason, the clustered data set was used.

The TRC distribution models are constructed from data values from the constituent rock types. For example, TRC 57 combines data from both granite to granodiorite (101057) and granite (101058). The data are weighted according to the relative proportions of each rock type as well as the number of data values available for each rock type. For the TRCs common to both domains 29 and 45 the data are weighted according to the proportions of each rock type in domain 29, which is broadly similar to those in domain 45.

Values determined from oxidised samples of granite to granodiorite (101057) (4 samples) and granodiorite to tonalite (101051) (3 samples) were included in the data sets. These data correspond to 5% and 7% respectively of the complete data sets for these rock types. This is similar to the percentage (7%) of the rock mass outside the deformation zones which has been mapped as oxidised within domain 29 /Stephens et al. 2007/. For granite (101058), the dominant rock type in domain 45, both altered (mostly albitised) and unaltered samples were included in the TPS + SCA data set. The values on altered samples comprise approximately 60% of the total number of samples for this rock type. In domain 45, approximately 70% of the rock mass outside deformation zones is altered, mainly by albitization /Stephens et al. 2007/.

Data values based on modal analysis of borehole samples taken adjacent to the samples on which TPS measurements were made were removed from the data set used for histograms etc. This was relevant for granodiorite to tonalite (101051) only.

The TRCs are not assumed to be described by standard statistical distributions. Distribution models are instead based on smoothing of the sample histograms. This smoothing operation is performed in GSLIB. The smoothing operation requires input regarding the maximum and minimum values. Changing these values has a slight, but noticeable, effect on the shape of the distribution model. The principles for setting lower and upper limits of thermal conductivity in the distribution models for each thermal rock class (TRC) are given below.

1. The first and most important criterion is that the distribution model covers the range of the data for each TRC (both TPS and SCA data).
2. Theoretical lower and upper limits of thermal conductivity were approximated from SCA calculations based on “extreme”, but possible, mineral compositions of each rock type. By “extreme” it is meant mineral compositions which produce the lowest (or highest) rock thermal conductivities. Estimates of extreme, but possible, compositions were made by rounding off the mineral percentages up or down to the nearest 10%, in as far as this was geologically sound /Stephens 2007/. The minimum values chosen are considered to be conservatively low.
3. For rock types for which the judgements of extreme, but possible, compositions are difficult or impossible to make, the maximum and minimum limits set for compositionally similar rock types should be used as guidelines.

Table 5-15. Upper and lower limits of thermal conductivity in distribution models compared to TPS/SCA data.

TRC	Min	Max	Min TPS/SCA	Max TPS/SCA
TRC 57	2.8	4.4	3.25	4.21
TRC 58	2.8	4.4	3.25	4.21
TRC 61	2.9	4.2	3.06	4.08
TRC 17	2.0	3.1	2.21	3.0
TRC 51	2.0	4.0	2.09	3.76
TRC 51A	3.0	4.0	3.19	3.76
TRC 51B	2.7	3.2	2.81	3.13
TRC 51C	2.0	2.9	2.09	2.77

TRC 57 makes up approximately 75% of domain 29 and consists of rock types, granite to granodiorite (101057) and granite (101058). Granite to granodiorite (101057) totally dominates this TRC. Histograms of the data for this TRC are shown in Figure 5-4. The histogram for granite to granodiorite is based on TPS data only, whereas that for granite is based on both TPS and SCA data.

TPS values determined from oxidised samples of granite to granodiorite (101057) (4 samples) were included in the data set for this rock type. For granite (101058), also the dominant rock type in domain 45, more than half the data are from altered (mostly albitised) samples.

The distribution model for the TRC based on smoothing of the sample histogram is depicted in Appendix C. The assumed minimum and maximum values of thermal conductivity are 2.8 W/(m·K) and 4.4 W/(m·K), respectively.

TRC 58 makes up approximately 67% of domain 45 and, like TRC 57, consists of granite to granodiorite (101057) and granite (101058). However, in contrast to TRC 57, rock type 101058 dominates this TRC. A histogram of the data for this TRC is shown in Figure 5-5. Histograms for the individual rock types are shown and described in Appendix C.

The distribution model for TRC 58, based on smoothing of the sample histogram, is depicted in Appendix C. The assumed minimum and maximum values of thermal conductivity are 2.8 W/(m·K) and 4.4 W/(m·K), respectively.

TRC 61, which comprises pegmatite (101061) and granite (111058), makes up approximately 15% of the rock mass in both domain 29 and 45. Pegmatite and pegmatitic granite is the dominant rock type in this class. Both rock types occur as dykes and minor bodies. Histograms of the data for this TRC, as well as the individual rock types are shown in Figure 5-6. Both TPS and SCA data have been used to characterise these two rock types. Nonetheless, the total number of data values available is small (n = 18).

The distribution model for TRC 61, based on smoothing of the sample histogram, is shown in Appendix C. The assumed minimum and maximum values of thermal conductivity are 2.9 W/(m·K) and 4.2 W/(m·K), respectively.

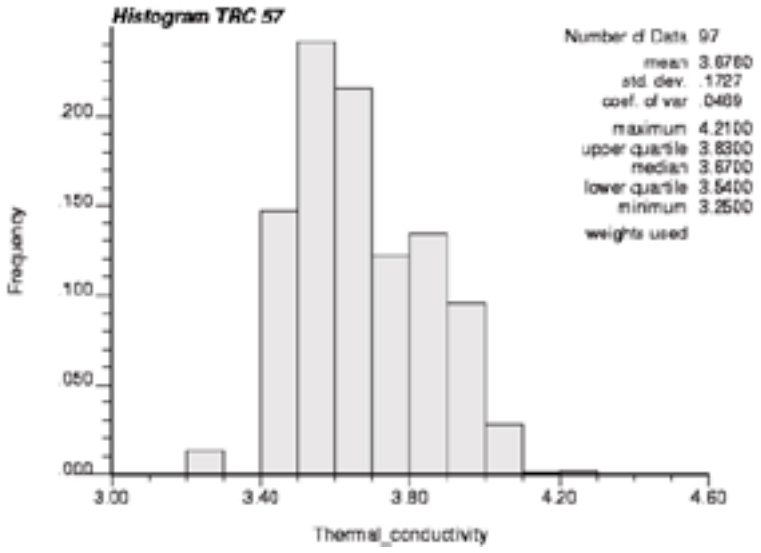

Figure 5-4. *Histogram of thermal conductivity derived for TRC 57.*

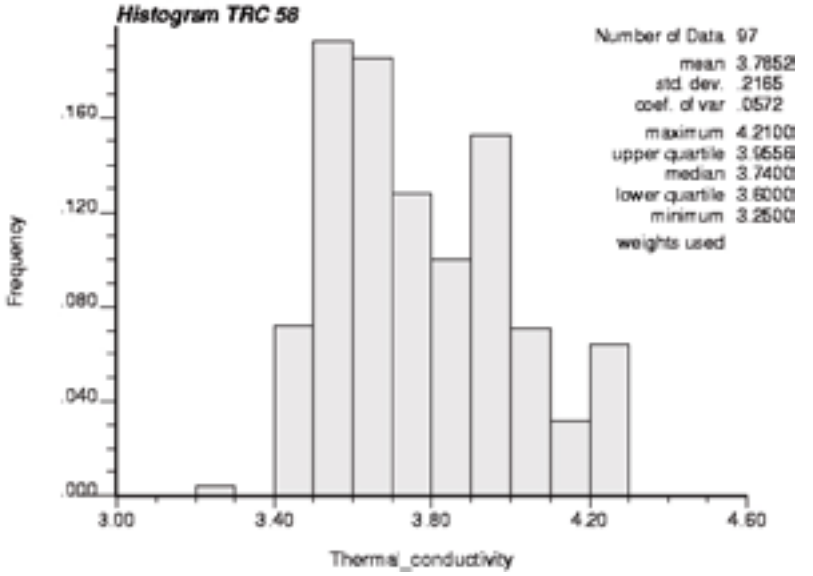

Figure 5-5. *Histogram of thermal conductivity derived for TRC 58.*

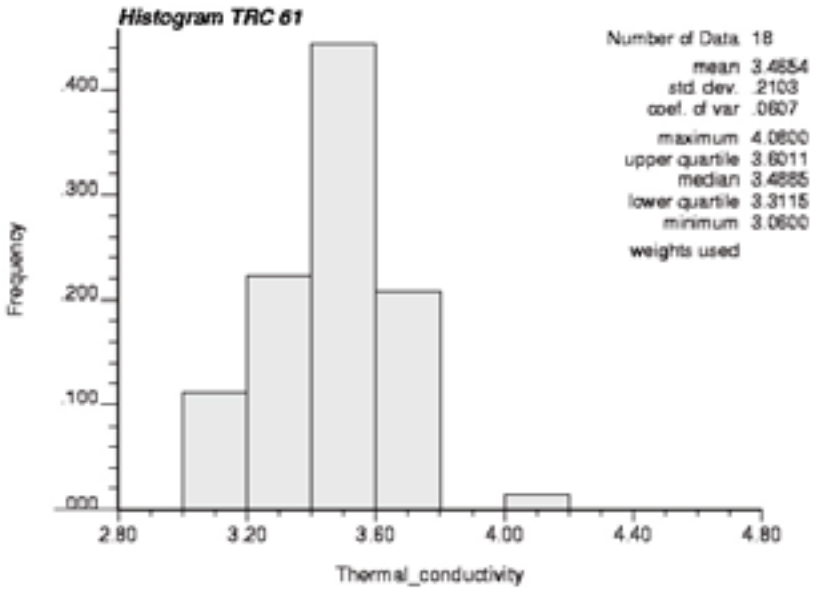

Figure 5-6. *Histogram of thermal conductivity derived for TRC 61.*

TRC 17 comprises amphibolite (102017) and subordinate gabbro, diorite and quartz diorite (101033). This TRC makes up between 4 and 5% of the rock mass in domain 29 and approximately 6% of domain 45 /Stephens et al. 2007/. Both rock types occur as dykes and irregular minor bodies. Histograms of the data for this TRC are shown in Figure 5-7. The data for amphibolite (102017) have been declustered to account for samples taken in groups within a borehole length of 1 m. Both TPS and SCA data have been used to characterise these two rock types. The amphibolites contain high contents of plagioclase and hornblende, with little or no quartz, which explains their low thermal conductivity values.

The distribution model for TRC 17, based on smoothing of the sample histogram, is shown in Appendix C. The assumed minimum and maximum values of thermal conductivity are 2.0 W/(m·K) and 3.1 W/(m·K), respectively.

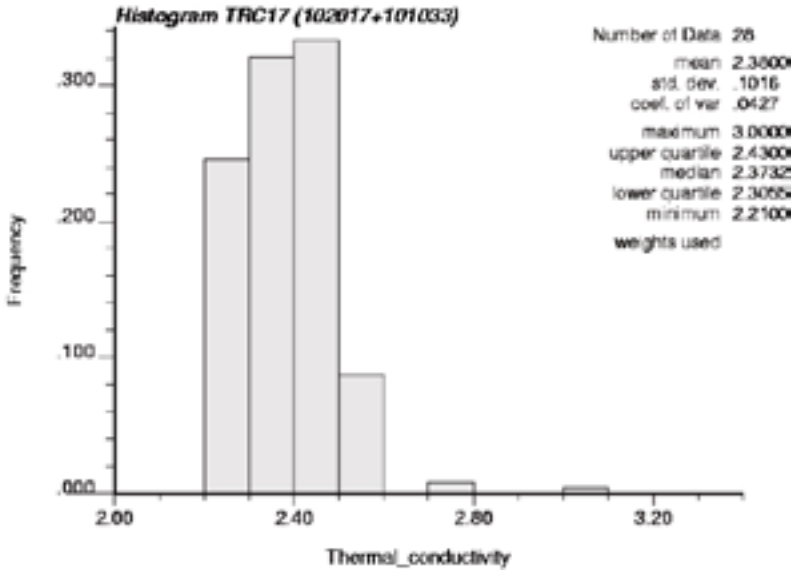

Figure 5-7. *Histogram of thermal conductivity derived for TRC 17.*

TRC 51 makes up c. 5% of domain 29 and c. 10% of domain 45. In both domains, granodiorite to tonalite (101051) comprises 90% of this class. Felsic to intermediate volcanic rock (103076) accounts for the remaining 10%.

Histograms of the data for this TRC are shown in Figure 5-8. Both TPS and SCA data have been used to characterise these two rock types. The data for both rock types have been declustered to account for samples taken close to one another (within a borehole length of 1 m). Three values from altered (oxidised) samples of granodiorite to tonalite (101051) have been included.

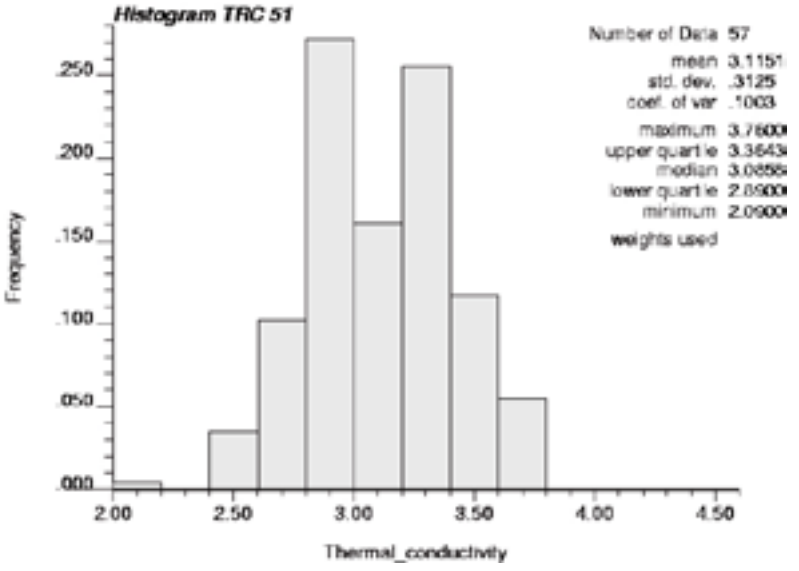

Figure 5-8. *Histogram of thermal conductivity derived for TRC 51.*

Results of attempts to create a variogram model which would describe the spatial correlation of granodiorite to tonalite (101051) were unsatisfactory (see below). This can be explained by the fact that granodiorite to tonalite (101051), the dominant rock type in this TRC, is not a single rock type. Compositionally rock type with code 101051 varies from tonalite and granodiorite to more subordinate granite /Stephens et al. 2007/. Calculations of thermal conductivity from density loggings, using the relationship established in 3.4.2, have shown that individual bodies of this rock type are rather homogenous with respect to thermal conductivity, but that there are quite large differences between these bodies. Histograms and box plots in Section 3.4 clearly show that there may be three or more modes present. For this reason, it was decided to divide granodiorite to tonalite (101051) into three groups. Firstly, borehole occurrences of granodiorite to tonalite (101051) having similar thermal conductivity calculated from density logging were grouped together as follows:

A. KFM01A (excluding occurrence at c. 250 m), KFM01B, KFM04A,

B. KFM01A (including occurrence at c. 250 m), KFM05A, KFM06A (below 620 m excluded), KFM08A

C. KFM03A

Secondly, the TPS and SCA values derived from samples from the above boreholes were assigned to their respective groups. The values were found to fall into three distinct groups: high (> 3.17 W/(m·K)), medium (2.8–3.18 W/(m·K)) and low (< 2.8 W/(m·K)). SCA values from surface samples were assigned to an appropriate group based on these divisions. The data for the minor rock type, felsic to intermediate volcanic rock (103076), were treated in the same way. Finally, histograms were constructed for each group (A, B and C) using TPS and SCA data from both rock types Figure 5-9. Distribution models are based on smoothing of these histograms.

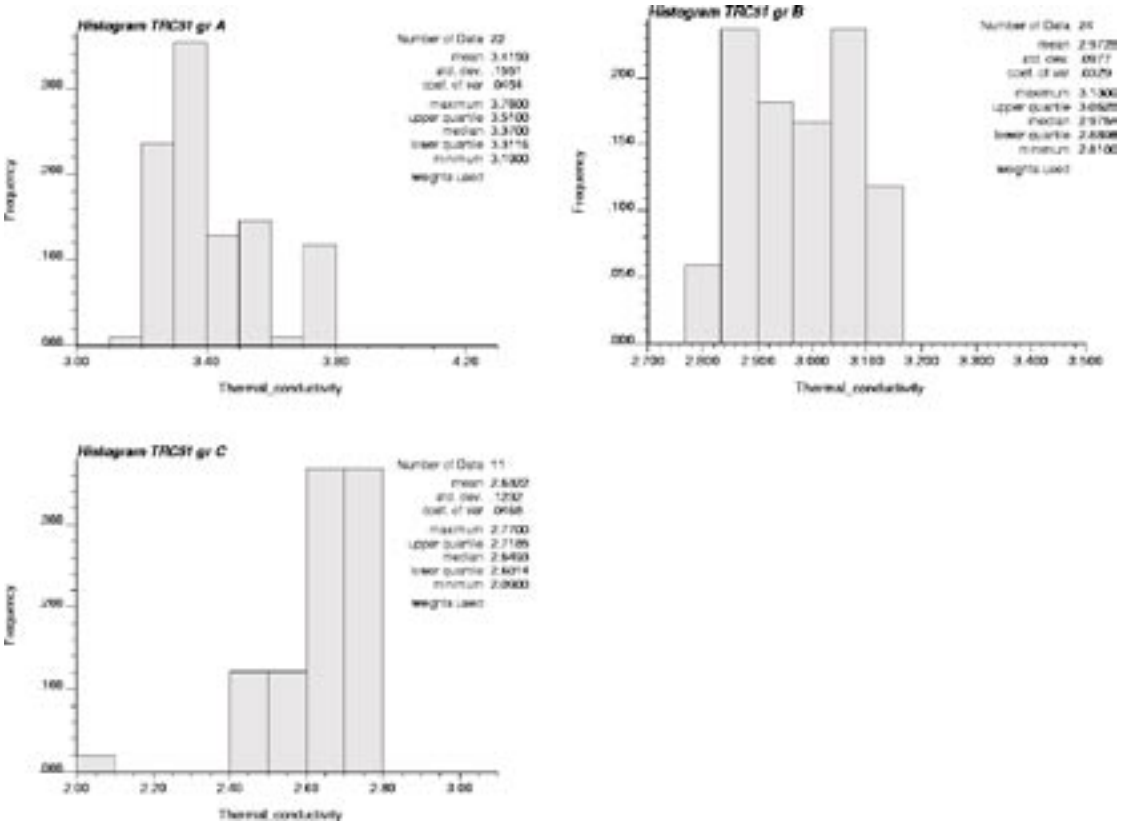

Figure 5-9. *Histogram for TRC 51A, B and C.*

The approach described above to deal with TRC 51 is not entirely satisfactory. The rather subjective cut-off limits used to divide the data into three groups produce histograms that do not overlap with each other. This is partly rectified in the distribution models by using smoothing functions together with maximum and minimum values that extend beyond the range of the data. Nevertheless, the overall result is an exaggerated trimodal distribution for TRC 51. This becomes apparent on analysing the simulation results; see Section 6.1. The advantage of this approach is that, using variograms, spatial dependence for the different types of TRC 51can now be modelled adequately. Furthermore, the total variability within TRC 51 can be accounted for, something that was difficult to achieve when the TRC was treated as one statistical population. So despite its drawbacks, this approach is considered better than the alternatives.

Thermal conductivities calculated from density loggings could have been used to create histograms for the different types of TRC 51. This was decided against because of the poor quality of the data for lower thermal conductivities; see Section 3.4. This is partly due to the large uncertainties associated with density data from borehole KFM03A, in addition to artefacts produced by the model (a second-order equation) describing the relationship between density and thermal conductivity.

The volume proportions of each group (A, B and C) within TRC 51 were based on density logging data in the boreholes investigated. The cut-off densities used between type A and B was 2,680 kg/m^3 and between type B and C, 2,730 kg/m^3. This gave the following proportions: A – 52%, B – 29%, C – 19%. These figures were rounded off to the nearest 10% and used as the proportions of each type of TRC 51 in the modelling of domains 29 and 45. The component represented by type C, tonalite in composition, occurs in boreholes KFM02A and 03A only, on the margins of, or outside, the target volume. However, since it is this component that exhibits the lowest thermal conductivity values, a conservative approach would require including this component in the modelling. This is considered a reasonable assumption since one can not exclude the possibility that rock with these compositions also occur within the target volume /Stephens 2007/.

Table 5-16 summarises the thermal conductivity statistics for each TRC.

Table 5-16. Statistics for each TRC of the empirical thermal conductivity data on which distribution models used for simulation are based.

TRC	Mean (W/m·K)	Standard deviation (W/m·K)	No. of samples
TRC 57	3.68	0.17	97
TRC 58	3.79	0.22	97
TRC 61	3.47	0.21	18
TRC 17	2.38	0.10	28
TRC 51A	3.42	0.16	22
TRC 51B	2.97	0.10	24
TRC 51C	2.63	0.12	11

Variogram models – 0.1 m scale

The spatial correlation within each TRC is modelled by a variogram. The procedure followed in order to create variograms for each TRC is described below.

1. Data were selected for the rock type representing each TRC. For TRC 57, the TPS data for granite to granodiorite (101057) were analysed. Data values from altered samples were removed, since they may disturb the pattern of spatial variation. For other TRCs, insufficient TPS and SCA data are available.
2. Variograms based on density logging data could be constructed for all TRCs; see the discussion below. First, it was necessary to process the borehole density logging data into a format suitable for variogram analysis.
   - Borehole data with high noise (> 20 kg/m^3) were excluded from the analysis. These included data from boreholes KFM06C and 08C.
   - Data from deformation zones, as defined in the geological model, stage 2.2 /Stephens et al. 2007/ were removed from the data set.
   - The data were sorted according to rock type and a separate file was created for the main rock type in each of the five TRCs.
   - Upper and lower limits of density were set for each rock type and values falling outside these limits were removed. These extreme values are likely to be due to random noise and interference from other rock types.
3. Normal scores transformation of the data was performed and variograms were calculated and plotted for different lag distances and lag tolerances; see /Deutsch and Journel 1998/.

A number of principles were defined for choosing suitable variogram models:

1. Because the data are restricted to boreholes, it is not possible to calculate reliable variograms in any directions other than in the direction of the boreholes, i.e. “down-hole” variograms. For this reason, directional variograms cannot be constructed. It is assumed that the spatial correlation within a particular rock type is isotropic. This is a reasonable assumption for the rocks at Forsmark (see Section 4.1.3).
2. The nugget (small-scale variability at a scale smaller than measurement scale) should be based, where possible, on TPS-data. If the nugget is uncertain, a conservative value should be chosen, which in this case means a value in the lower interval.
3. A rock with finer grains will have lower nugget than a coarse grained rock of similar composition. This is considered when the nugget is defined for a rock with sparse data.
4. The nugget constant is estimated by extrapolating the average linear behaviour of the first experimental points to the ordinate axis /Journel and Huijbregts 1978/. For density logging data, extrapolation is made from lag = 0.3 m because a value from shorter lags is unreliable due the filtering of data.
5. The resolution for the nugget is limited to steps of 0.1 or 0.05 (relative nugget effect).
6. The range (correlation length) should be based, where possible, on density log data, otherwise on TPS-data, and if such data are not available, on correlation lengths of similar rock types. The reason is that TPS data are usually too few to produce reliable variograms. If the range is uncertain, a higher value in the indicated interval should be chosen in order to be conservative.
7. If it is difficult to fit a variogram model, the selected type of model should be conservative (assuming the variogram can be described by one simple model). The most conservative is a Gaussian variogram model (S-shaped), which suggest high correlation at short distances.
8. If possible, the variogram structures should have a physical/geological explanation. The variogram model should always be guided by the geological knowledge of the phenomenon /Journel and Huijbregts 1978/. For example, the two different structures for granodiorite to tonalite (101051) (see Figure 5-14) could be interpreted as the short-range correlation and the mean distance between two rock bodies of different composition.

9. If there is no physical explanation for a feature of a variogram, an artefact of measurement should be suspected. In this case it may be best to ignore the feature and adopt the simplest model instead. In other cases, boreholes could be analysed separately if the created artefacts are a result of different measurement errors between boreholes (e.g. for rock type with code 101057).

Density logs were used to study spatial correlation, in particular the correlation length (range). A relationship between thermal conductivity and density has been established for some rock types. Even for rock types where no relationship is obvious, a relationship may still exist. In any case, it is reasonable to assume that any spatial dependence in density, as indicated by a variogram, also reflects spatial dependence in thermal conductivity /Sundberg et al. 2007a/. The opposite is probably not true. That is, an absence of spatial correlation in density does not mean that thermal conductivity does not exhibit spatial correlation. For example variations in quartz – feldspar content would not produce any marked variation in density, but the thermal conductivity would vary.

Because the density data are restricted to boreholes, it is not possible to calculate reliable variograms in any directions other than in the direction of the boreholes, i.e. "down-hole" variograms /Dowd 2007/. For rock types showing low overall variability in density, e.g. granite to granodiorite (101057), the difference between boreholes may appear significant, which produces variograms with apparently very long correlation lengths. These variograms are artefacts related to uncertainties in the density logging data, not a quantification of any real spatial variability. Therefore, for granite to granodiorite (101057), granite (101058) and pegmatite (101061), which display limited variability in density, variograms were calculated on individual boreholes. For granodiorite to tonalite (101051) and amphibolite (102017), which have a wider range of densities, using several boreholes together is justified.

The primary purpose of calculating variograms based on density loggings is to estimate the range, i.e. the separation distance over which spatial dependence is apparent. In other words, samples separated by distances closer than the range are spatially correlated.

Table 5-17. Noise in density loggings for different boreholes.

Borehole	Noise level in density logging kg/m^3	Reason for omission
KFM01A	17	
KFM01B	11	
KFM01C		No usable data
KFM01D	5	
KFM04A	9	
KFM05A	20	
KFM06A	12	
KFM06C	47	High noise
KFM07A	12	
KFM07B	5	
KFM07C	11	Data not available in Sicada database at time of analysis
KFM08A	14	
KFM08B	12	
KFM08C	30	High noise
KFM09A	6	Outside candidate area
KFM09B	6	
KFM10A	11	Data not available in Sicada at time of analysis

In the absence of sufficient TPS data, density variograms may also be used to roughly approximate the nugget. It is difficult to say whether the nugget estimated from density variograms underestimate or overestimate the nugget. The relatively high measurement error in the density logging data would give a higher nugget. On the other hand, the overlapping measurement volumes and the filtering procedure applied to the density logging data in order to dampen the random noise, means that the spatial dependence at distances less than about 0.4 m is strongly overestimated, giving a nugget which is too low. Compared to TPS values, the support of the density data is higher, which should give a lower nugget effect. The combined effect of these different phenomena is very difficult to evaluate.

It was discovered that borehole KFM09B had significantly higher density values for granite to granodiorite (101057) than other boreholes. This anomalous data from this borehole were removed from analysis.

For TRC 57, a choice of 25 m for the range is supported by covariogram plots based on data from boreholes KFM05A and KFM08A (Figure 5-10).

Variograms and covariograms for pegmatite (101061) are very erratic and unstable (Figure 5-11), which is probably partly due to the high nugget. The coarse grain size typical of pegmatite and pegmatitic granite should logically give a high nugget effect, since small-scale heterogeneities may not be evened out at the dm scale, so that proximal samples may be quite dissimilar. The experimental variograms shows that variability at short distances is high, almost as high as for long distances if one disregards the first lag distance which is affected by data processing (filtering). The range chosen for the variogram model is highly uncertain; there is no covariogram which unambiguously supports the adoption of 15 m as the range. However, given the high nugget, the choice of range is not very important.

Table 5-18. Nugget and range for TRCs. Nuggets and sills are normalised to the variance of the empirical data.

TRC	Rock code	Nugget	Basis for nugget	Range	Basis for range	Model	Comment
TRC 57	101057	0.6	< 0.71 (TPS)	25 m	Variograms and covariograms of density for KFM01A, KFM04A, KFM05A, KFM07A and KFM08A	Exponential	
TRC 58	101058	0.4	< 0.55 (TPS)	18 m	Range at 18 m was chosen to describe the first part of the sample variogram, in addition to extending the sill to 1	Exponential	
TRC 51A	101051	0.5	based on density logs	5 m	Based on judgement of variograms for several boreholes together	Spherical	A relation-ship exists between thermal conductivity and density
TRC 51B	101051	0.5	based on density logs	5 m		Spherical	
TRC 51C	101051	0.6	based on density logs	5 m		Spherical	
TRC 61	101061	0.75	Rough estimate based on density logging. Coarse grain size should logically give a high nugget effect, since proximal samples would be rather dissimilar	15 m	Variograms and covariograms of density for KFM01A, KFM05A and KFM08a	Spherical	
TRC 17	102017	0.35	< 0.45 based on density logs. Limited TPS data indicate very low variability at the dm-scale.	25 m	Based on judgement of several variograms and covariograms for density data from several boreholes together	Spherical	a) A relation-ship exists between thermal conductivity and density. b) Structures at distances longer than 25 m not modelled.

Translation of rock codes to rock names: 101057 = Granite to granodiorite, 101058 = Granite, 101051 = Granodiorite to tonalite, 102017 = Amphibolite.

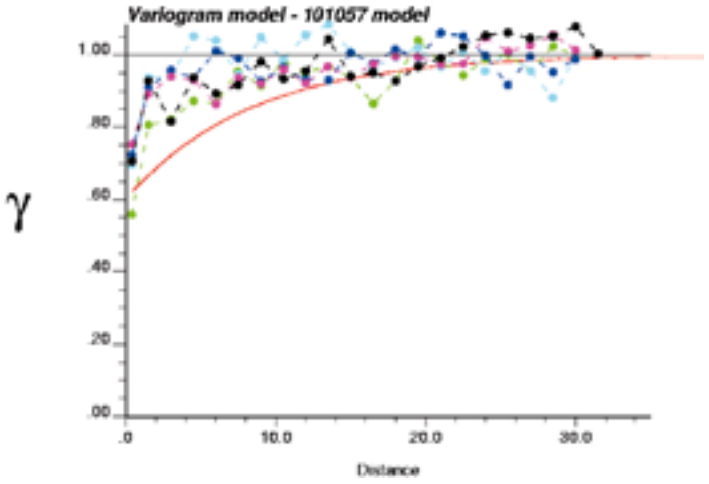

Figure 5-10. *Variogram model for TRC 57 based on sample variograms for granite to granodiorite (101057) produced from density logging data from 5 boreholes (KFM01A, KFM04A, KFM05A, KFM07A, KFM08A). Exponential variogram model fitted. Nugget is based on TPS data. Lag distance (x-axis) in metres (m). Variogram is normalised to the variance of the empirical data.*

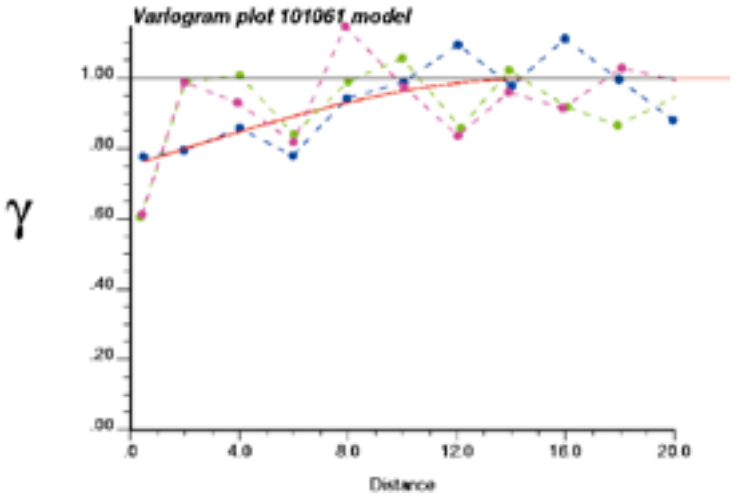

Figure 5-11. *Variogram model for TRC 61 based on sample variograms for pegmatite (101061) produced from density logging data from 3 boreholes (KFM01A, KFM05A, KFM08A). Spherical variogram model fitted. Lag distance (x-axis) in metres (m). Variogram is normalised to the variance of the empirical data.*

A relationship between density and thermal conductivity was indicated by laboratory measurements for amphibolite (102017); see Section 3.4. Thus more reliance can be placed on the nugget determined from density variograms for this rock type compared to rock types where no relationship is obvious. According to variograms with short lag distances the nugget based on the density logging data is as low as 0.40 (Figure 5-12). Given the measurement error associated with density logging data a lower nugget is possible. For this reason, a value of 0.35 was selected. A low nugget is consistent with the relatively fine-grained nature of this rock type, which should produce greater continuity, or less variability, at smaller scales. Furthermore, the limited amount of TPS data from samples taken in groups indicates very low variability at the dm-scale.

Granite (101058) displays a more complex variogram structure (Figure 5-13). A workable variogram model which describes the spatial correlation up to distances of 50 m was not established. For simulation at dm scale with a simulation volume of 5 m^3, a compromise was found by selecting a model which describes the experimental variogram rather well for separation distances up to 5 m, but not for longer distances.

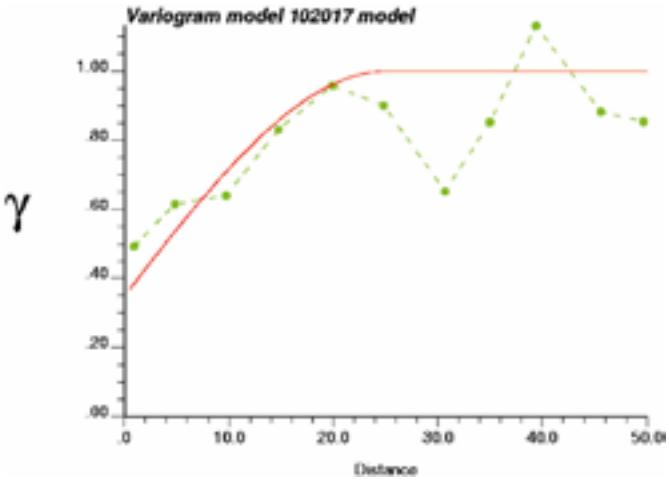

Figure 5-12. *Variogram model for TRC 17 based on sample variogram for amphibolite (102017) produced from density logging data from all investigated boreholes. Spherical variogram model fitted. Lag distance (x-axis) in metres (m). Variogram is normalised to the variance of the empirical data.*

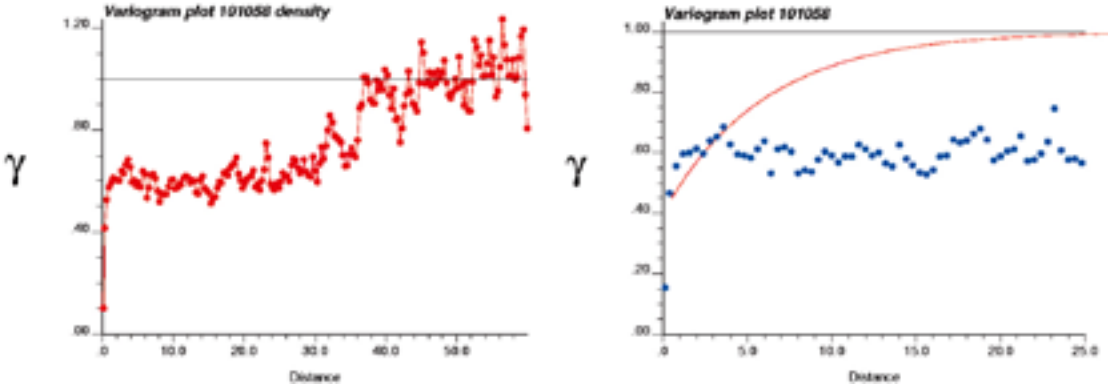

Figure 5-13. *Variogram model for TRC 58 based on sample variogram for granite (101058) produced from density logging data from all investigated boreholes. Exponential variogram model fitted. Lag distance (x-axis) in metres (m). Variogram is normalised to the variance of the empirical data.*

Two structures are apparent in the experimental variogram for granodiorite to tonalite (101051), a small-scale structure with a range of about 5 m and a larger structure with an apparent range of about 40 m (Figure 5-14). These two distinct variogram structures have plausible geological explanations. Occurrences of this rock type are typically between 2 and 30 m (borehole lengths), although occurrences of between 50 and 100 m (borehole lengths) have also been mapped. Petrographic studies and geophysical logging, e.g. /Carlsten et al. 2005/, have shown that individual bodies of this rock type are rather homogenous but that quite large differences exist between these bodies.

The spatial correlation structure exhibited by density logging data for granodiorite to tonalite (101051) could not be modelled satisfactorily using one variogram model. Instead it was decided to divide the rock into three subtypes and attempt to construct variograms for each group.

A relationship between density and thermal conductivity for granodiorite to tonalite (101051) has been established, see Section 3.4. The borehole density logging data for granodiorite to tonalite (101051) were divided into three subtypes, A, B and C on the basis of thermal conductivity calculated from density (see above).

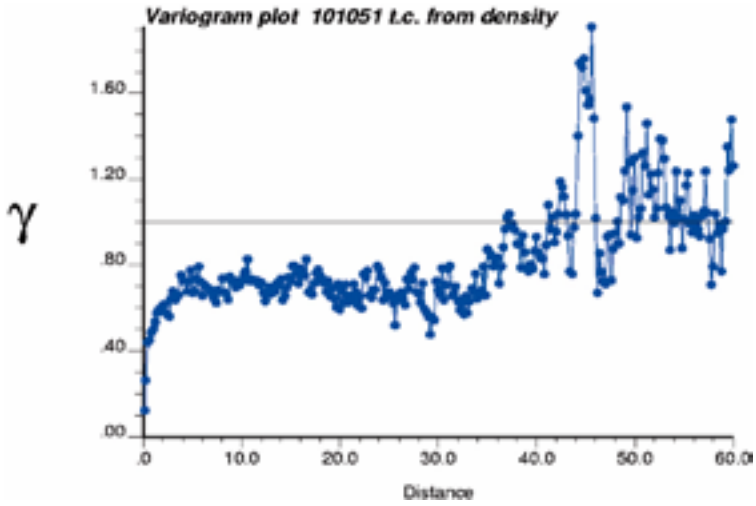

Figure 5-14. *Variogram for granodiorite to tonalite (101051) based on density data. Lag distance (x-axis) in metres (m). Variogram is normalised to the variance of the empirical data.*

For distances up to ca 10 m all three groups displayed some similarities in their experimental variograms (Figure 5-15). All three reach a semivariance of 1, which corresponds to the total sample variance, at about 5 m, and disregarding separation distances of 0.3 m or less, all three have a nugget of between 0.5 and 0.6. The range and nugget for the variogram models are selected accordingly. Group C is represented by density data from borehole KFM03A, which as pointed out in Section 3.4 suffer from high random noise. Nevertheless, the data display a spatial structure on a variogram plot similar to the other groups.

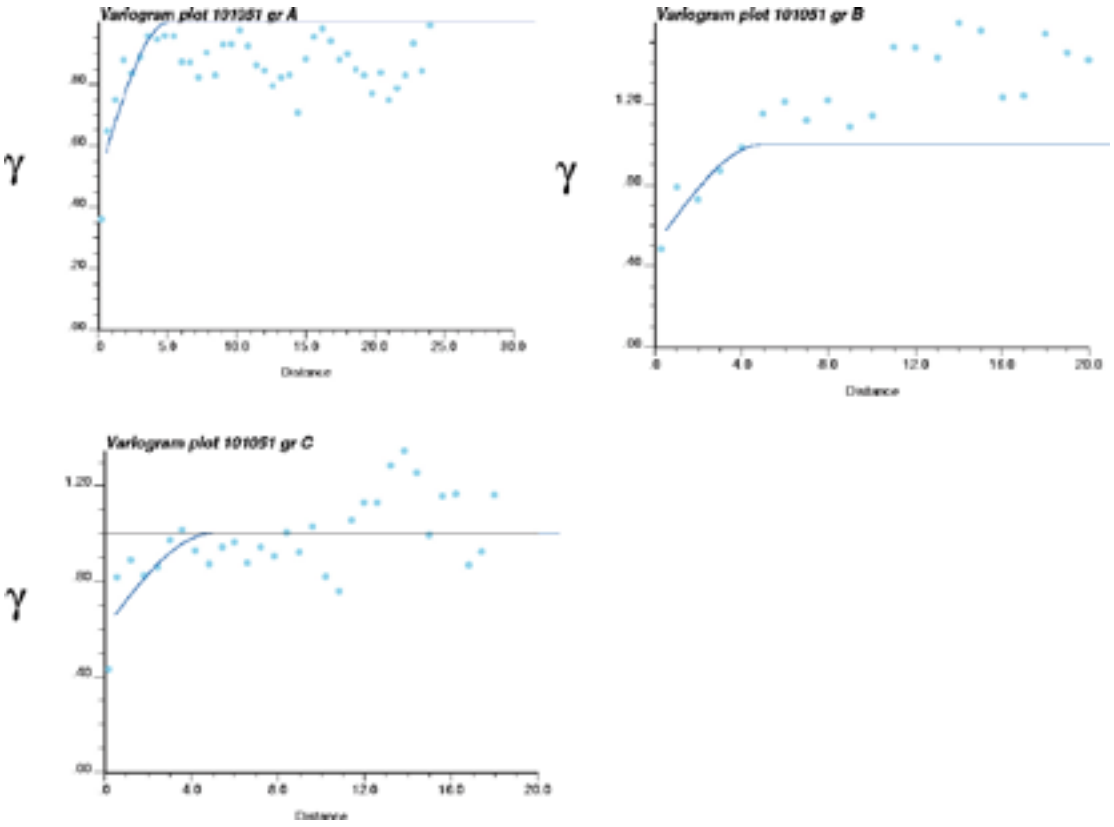

Figure 5-15. *Variogram model for TRC 51A, B and C based on sample variogram for granodiorite to tonalite (101051) produced from density logging data from all investigated boreholes. Spherical variogram model fitted. Lag distance (x-axis) in metres (m). Variogram is normalised to the variance of the empirical data.*

5.4.3 Thermal conductivity models – 1 m scale

Simulations at scale 1 m require a thermal model (histogram and variogram) for each TRC determined for this particular scale. In order to obtain a histogram for the 1 m scale, upscaling of the simulation results at 0.1 m scale is performed for each TRC. The histogram of the upscaled values (1 m scale) provides the basis for the statistical distribution for simulations at the 1 m scale. Details on how this was performed for the various TRCs are given in Section 5.5.3.

The variogram models for the 1 m scale are modified from the model used for the 0.1 m scale. The rules for this adjustment are listed in Section 4.2.7. The variogram parameters for modelling at 1 m scale for each TRC are shown in Table 5-19.

The spatial statistical thermal models for each TRC at the 1 m scale is thus defined by the variogram models (Table 5-19) and the statistical distribution models (Section 5.5.3).

5.5 Simulation results and validation

5.5.1 Choice of simulation scale and change of support

For the objective of description of the rock domains, a simulation scale of 1 m was selected, i.e. the simulation volume was divided into grid cells (cubes) of size $1\times1\times1$ m^3.

A simulation scale of 0.1 m (grid cell size $0.1\times0.1\times0.1$ m^3) was also used in the first unconditional simulation step. The purpose of this simulation was two-fold:

1. To perform change-of-support (upscaling) from the scale of thermal measurements to the simulations scale 1 m.
2. To perform high-resolution unconditional stochastic simulations at the 0.1 m scale, perform upscaling of the result to the 1 m scale, and compare the result with the result of the simulations performed directly at the 1 m scale.

Thus, simulation at 0.1 m is required in order to change the support to 1 m. After change of support, the simulation scale 1 m was used for the unconditional simulations with objective to describe the domain.

The simulation volumes for the two types of simulations were:

- $5\times5\times5$ m^3 for the 0.1 m simulations, i.e. a total number of 125,000 cells in each realisation.
- $50\times50\times50$ m^3 for the 1 m simulations, i.e. a total number of 125,000 cells in each realisation.

The implications of these limited simulation volumes are discussed later.

Table 5-19. Variogram parameters for modelling at 1 m scale for each TRC.

TRC	Rock Type	Nugget	Range	Model	Comment
TRC 57	101057	0	25 m	exponential	
TRC 58	101058	0	40 m	spherical	Range chosen to fit the large-scale structure.
TRC 61	101061	0	15 m	spherical	
TRC 51A	101051 gr A	0	6 m	spherical	
TRC 51B	101051 gr B	0	6 m	spherical	
TRC 51B	101051 gr C	0	6 m	spherical	
TRC 17	102017	0	25 m	spherical	

Translation of rock codes to rock names: 101057 = Granite to granodiorite, 101058 = Granite, 101051 = Granodiorite to tonalite, 102017 = Amphibolite.

5.5.2 Geology

Introduction

Stochastic unconditional simulations were performed using the spatial properties derived from the analysis described in Section 3.3.1. The simulations were made as follows:

- 0.1 m simulations:
  - Domain RFM045: 100 realisations.
  - Domain RFM029 internal: 100 realisations.
  - Domain RFM029 marginal: 100 realisations.
- 1 m simulations:
  - Domain RFM045: 400 realisations.
  - Domain RFM029 internal: 667 realisations.
  - Domain RFM029 marginal: 333 realisations.

For both 0.1 m and 1 m simulations the model dimensions were 50×50×50 cells, i.e. a total of 125,000 cells.

Example results

Figure 5-16 gives an example of 1 dm realisations for domain RFM029 internal and Figure 5-17 gives an example of 1 m realisations for domain RFM045.

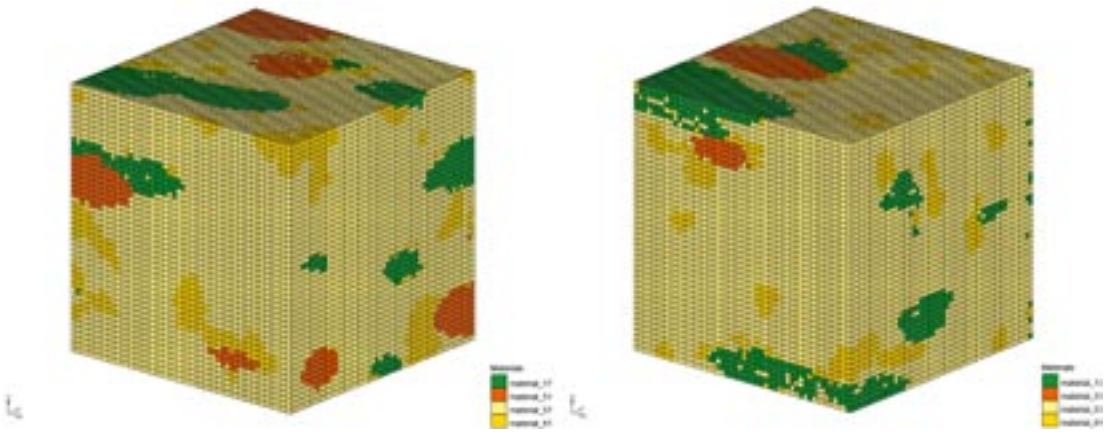

Figure 5-16. *Two 0.1 m realisations of domain RFM029 internal. The simulated rock volume has dimensions 5×5×5 metres. The simulated TRCs are TRC57 (yellow), TRC61 (orange), TRC51 (red) and TRC17 (green).*

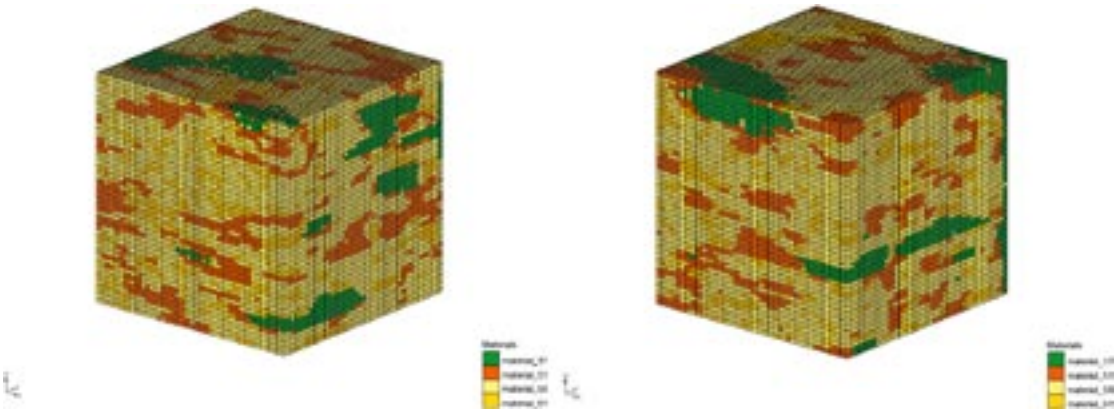

Figure 5-17. *Two 1 m realisations of domain RFM045. The simulated rock volume has dimensions 50×50×50 metres. The simulated TRCs are TRC58 (yellow), TRC61 (orange), TRC51 (red) and TRC17 (green).*

Analysis and verification of results

Methodology

The statistical properties, i.e. the proportions of categories (TRCs), the typical lengths of categories and the spatial properties of categories are assumed to be stationary for all realisations. The relevance of the results of the simulations have been analysed and verified by means of statistical analysis with respect to the ability of T-PROGS to reproduce:

- the proportions of the TRCs from input data,
- typical (mean) lengths of TRCs calculated by transition probability analysis, and
- the distribution of TRC lengths observed in borehole data.

As input into the T-PROGS modelling, the proportions and typical TRC lengths were calculated through transition probability analysis of borehole data. The typical lengths for different directions of the model volume were then calculated from the relative length information provided by the geological interpretations of anisotropy; see Sections 5.3.3 and 5.3.4.

The 1 m and 0.1 m simulations for domains RFM029 internal and RFM045 were selected for the verification analysis, which was made for as follows:

- The proportions of TRCs were made for 10 randomly selected realisations and compared to the proportions calculated from borehole data.
- The typical lengths were calculated from "borings" through 10 randomly selected realisations. Calculations were made for x, y and z-directions and for TRCs 17, 51 and 61. The 90% confidence interval was calculated for each of the typical lengths.
- Histograms of the lengths of the TRCs were made from "borings" in 20 randomly selected realisations. For each realisation 49 "borings" were made in each of the x, y and z-directions.

Results 1 m simulations domain RFM029 – Proportions

Table 5-20 shows the proportions of TRCs in 10 randomly selected realisations for domain 029 internal.

As can be seen from Table 5-20, T-PROGS nearly exactly reproduces the proportions of the TRCs for all realisations.

Results 1 m simulations domain RFM029 – Typical lengths

Calculations of typical lengths of TRCs 17, 51 and 61 were made from "borings" through 10 randomly selected realisations for domain RFM029 internal. TRC 57 constitutes the "background" in the simulations and is therefore not relevant to include in the analysis.

Table 5-20. Proportions of TRCs in 10 randomly selected realisations for domain RFM029 internal.

Category	Proportions from boreholes (%)	Proportion in realisation no. (%)									
		1	5	19	48	75	120	167	199	201	302
TRC17	3.8	3.8	3.8	3.8	3.8	3.8	3.8	3.8	3.8	3.8	3.8
TRC51	4.5	4.5	4.6	4.6	4.6	4.6	4.6	4.6	4.6	4.5	4.5
TRC57	78.7	78.6	78.5	78.6	78.6	78.6	78.6	78.6	78.6	78.6	78.6
TRC61	13.1	13.1	13.1	13.1	13.1	13.1	13.1	13.1	13.1	13.1	13.1

The typical lengths of the TRCs in the data obtained from the "borings" were calculated by transition probability analysis. The results of the calculations of the typical length m for directions x, y and z are presented in Table 5-21 to Table 5-23. The confidence interval is given for each calculation and a comparison is made with the nominal value (input value in the T-PROGS model) calculated from borehole data.

As can be seen from the analysis T-PROGS can reproduce the typical lengths of TRCs very well if the typical lengths are approximately 2.3 metres or longer. For shorter lengths T-PROGS seems to overestimate the typical lengths. The reason for this overestimation of shorter lengths is the discretisation of the model, where 1 metre is the shortest length that can be represented by this model.

Results 1 m simulations domain RFM029 – Distribution of lengths

From 49×3 = 147 borings in each of 10 randomly selected realisations histograms were prepared for each TRC in x, y and z-directions. The results are shown in Figure 5-18 to Figure 5-21.

Due to the large number of "borings" in the simulated volumes it is assumed that the histograms give a good representation of the simulated lengths of TRCs. A visual comparison was made of the histograms from the "borings" with lengths observed in the actual borehole data (KFM05A), see Figure 5-22. The comparison indicates that T-PROGS is able to realistically represent TRC lengths registered in the borehole data.

Table 5-21. Typical lengths of TRC17.

Typical length (m)	Nominal value (m)	Comment to simulated values
μ_x = 3.80 ± 0.81	4.10	OK
μ_y = 2.46 ± 0.37	2.05	Somewhat high
μ_z = 1.54 ± 0.14	1.03	High

Table 5-22. Typical lengths of TRC51.

Typical length (m)	Nominal value (m)	Comment to simulated values
μ_x = 5.90 ± 1.40	6.52	OK
μ_y = 3.58 ± 0.78	3.26	OK
μ_z = 2.00 ± 0.23	1.63	Somewhat high

Table 5-23. Typical lengths of TRC61.

Typical length (m)	Nominal value (m)	Comment to simulated values
μ_x = 1.81 ± 0.13	1.12	High
μ_y = 1.83 ± 0.15	1.12	High
μ_z = 1.19 ± 0.04	0.37	High

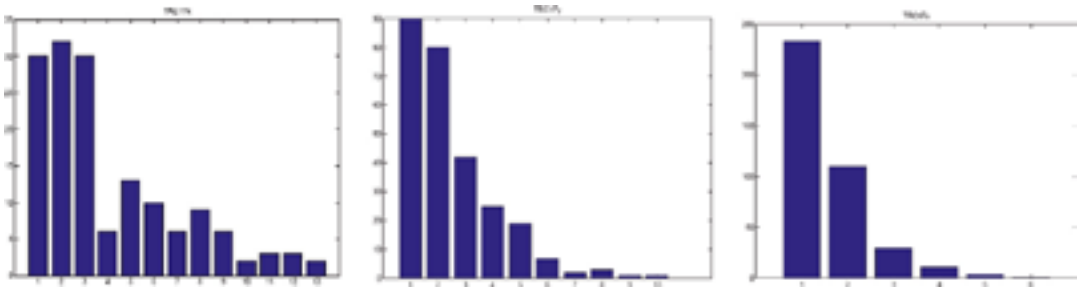

Figure 5-18. *Histogram from 10 randomly selected realisations of TRC 17 in x-, y- and z-direction (x-axis in metres).*

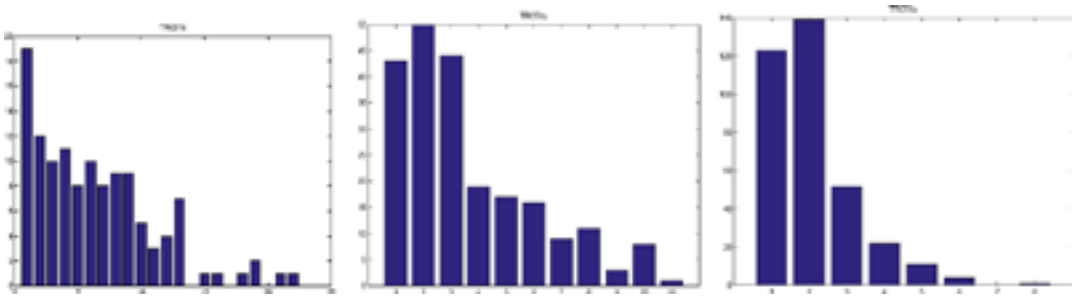

Figure 5-19. *Histogram from 10 randomly selected realisations of TRC 51 in x-, y- and z-direction (x-axis in metres).*

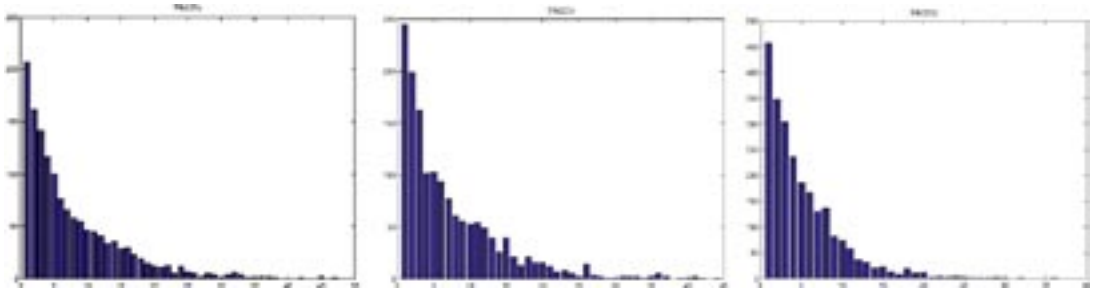

Figure 5-20. *Histogram from 10 randomly selected realisations of TRC 57 in x-, y- and z-direction (x-axis in metres).*

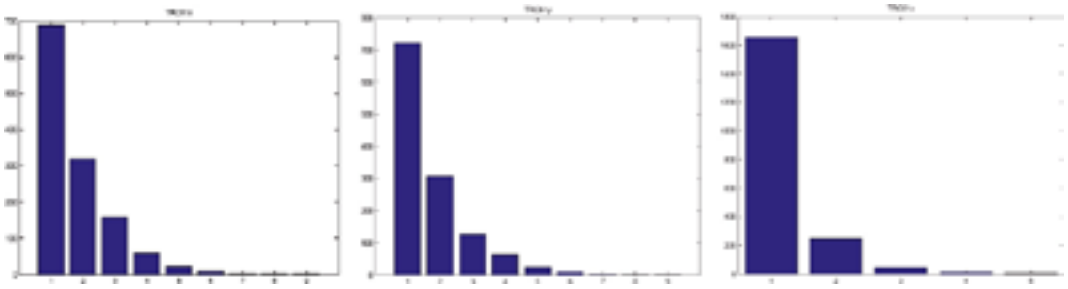

Figure 5-21. *Histogram from 10 randomly selected realisations of TRC 61 in x-, y- and z-direction (x-axis in metres).*

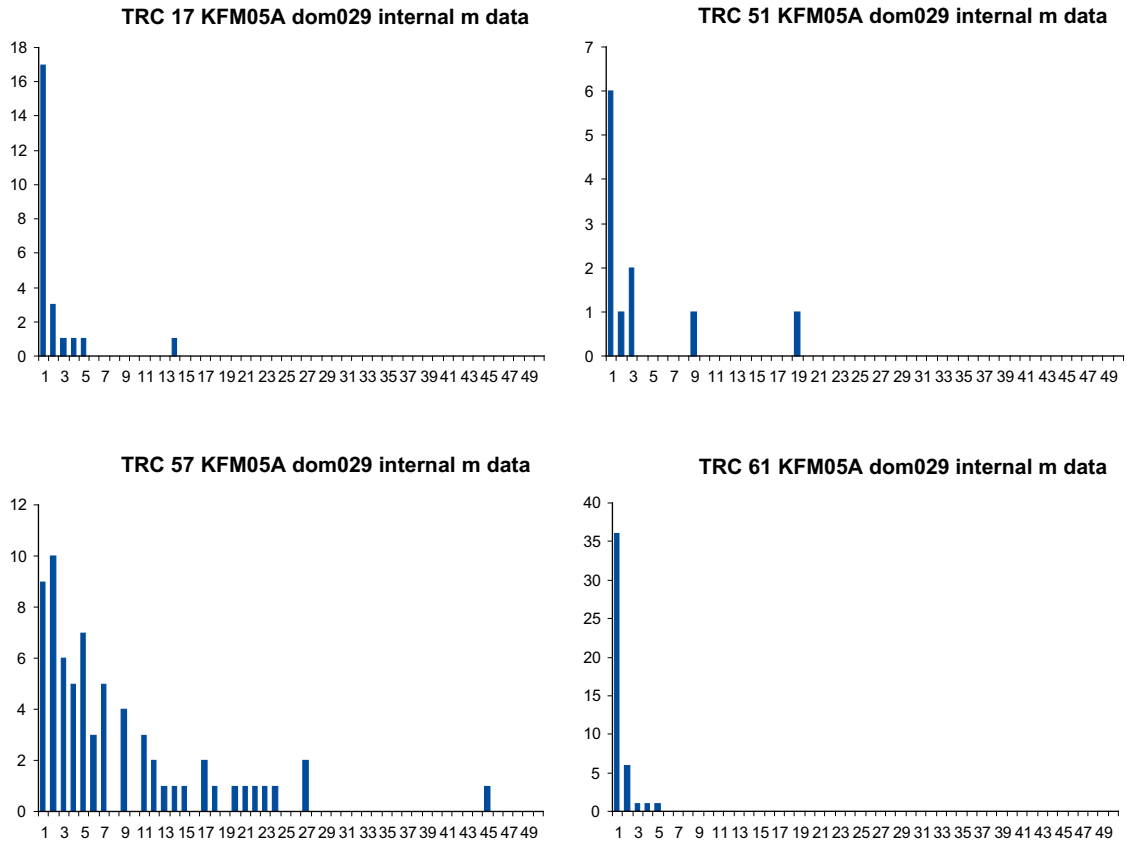

Figure 5-22. *Histograms of TRC lengths in borehole KFM05A.*

Results 1 m simulations domain RFM045 – Proportions

Table 5-24 shows the proportions of TRCs in 10 randomly selected realisations for Domain 045.

As can be seen from Table 5-24 T-PROGS nearly exactly reproduces the proportions of the TRCs for all realisations.

Results 1 m simulations domain RFM045 – Typical lengths

Calculations of typical lengths of TRCs 17, 51 and 61 were made from "borings" through 10 randomly selected realisations for domain RFM045. TRC 58 constitutes the "background" in the simulations and is therefore not relevant to include in the analysis.

The typical lengths of the TRCs in the data obtained from the "borings" were calculated by transition probability analysis. The results of the calculations of the typical length m for directions x, y and z are presented in Table 5-25 to Table 5-27. The confidence interval is given for each calculation and a comparison is made with the nominal value (input value in the T-PROGS model) calculated from borehole data.

Table 5-24. Proportions of TRCs in 10 randomly selected realisations for domain RFM045.

Category	Proportions from boreholes (%)	Proportion in realisation no. (%)									
		301	312	314	334	352	358	361	389	392	399
TRC17	7.3	7.6	7.6	7.8	7.6	7.5	7.5	7.9	7.7	7.5	7.9
TRC51	18.9	18.8	18.8	18.8	18.8	18.9	18.8	18.8	18.8	18.9	18.8
TRC58	57.7	57.6	57.2	57.4	57.5	57.6	57.6	57.3	57.4	57.6	57.3
TRC61	16.1	16.0	16.0	16.0	16.0	16.0	16.0	16.0	16.0	16.0	16.0

Table 5-25. Typical lengths of TRC17.

Typical length (m)	Nominal value (m)	Comment to simulated values
μ_x = 11.55 ± 4.84	28.28	Low
μ_y = 6.61 ± 1.98	14.14	Low
μ_z = 3.52 ± 0.42	7.07	Low

Table 5-26. Typical lengths of TRC51.

Typical length (m)	Nominal value (m)	Comment to simulated values
μ_x = 5.09 ± 0.76	5.92	Somewhat low
μ_y = 3.32 ± 0.31	2.96	Somewhat high
μ_z = 2.08 ± 0.15	1.48	Somewhat high

Table 5-27. Typical lengths of TRC61.

Typical length (m)	Nominal value (m)	Comment to simulated values
μ_x = 3.51 ± 0.36	2.86	Somewhat high
μ_y = 3.55 ± 0.38	2.86	Somewhat high
μ_z = 1.61 ± 0.09	0.95	High

As can be seen from the analysis T-PROGS can reproduce the typical lengths of TRCs reasonably well if the typical lengths are between approximately 2–5 metres. For shorter lengths T-PROGS seems to overestimate the typical lengths. The reason for this overestimation of shorter lengths is the discretisation of the model, where 1 metre is the shortest length that can be represented by this model. For longer lengths T-PROGS seems to underestimate the typical lengths for domain 45. Although a reasonable correspondence can be seen for domain 45 simulations, the simulated typical lengths for domain 45 correspond less well to the nominal values than the simulations for domain 29 internal.

Results 1 m simulations domain RFM045 – Distribution of lengths

From 49×3 = 147 borings in each of 10 randomly selected realisations histograms were prepared for each TRC in x, y and z-directions. The results are shown in Figure 5-23 to Figure 5-26.

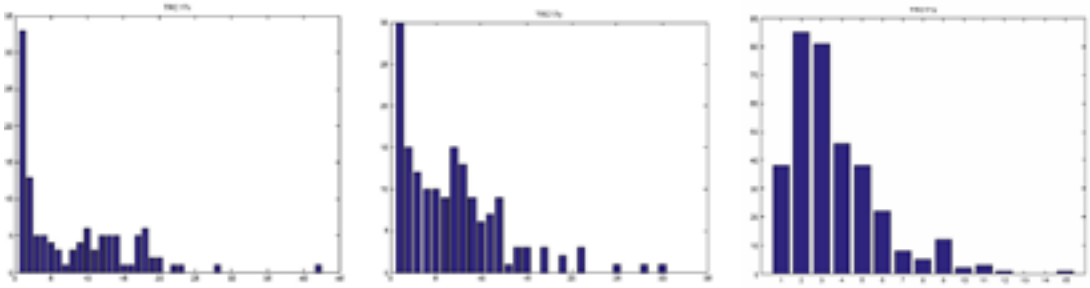

Figure 5-23. *Histogram from 10 randomly selected realisations of TRC 17 in x-, y- and z-direction (x-axis in metres).*

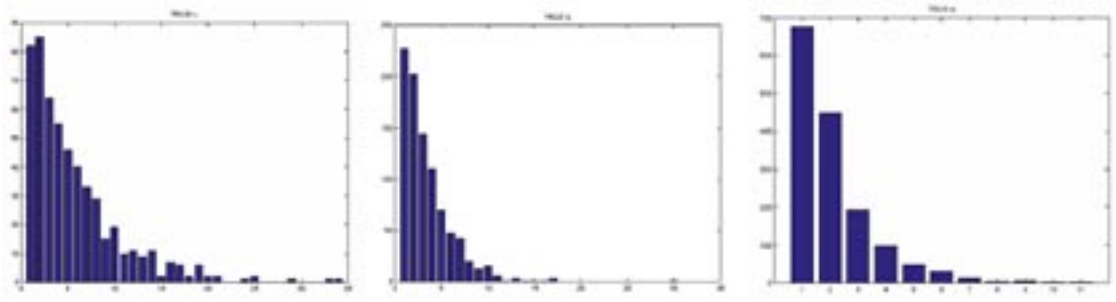

Figure 5-24. *Histogram from 10 randomly selected realisations of TRC 51 in x-, y- and z-direction (x-axis in metres).*

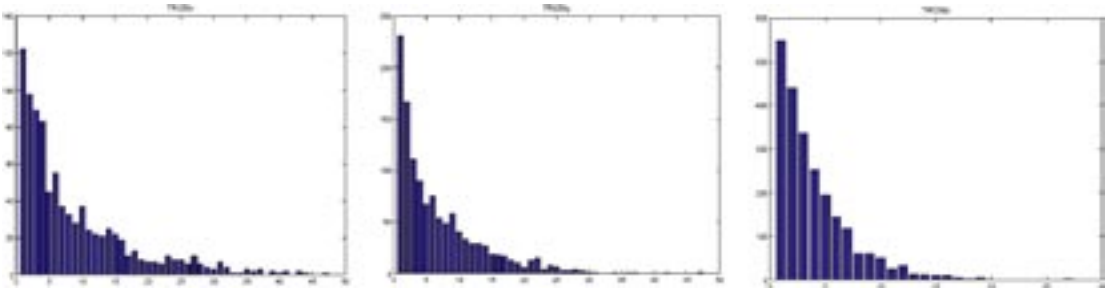

Figure 5-25. *Histogram from 10 randomly selected realisations of TRC 58 in x-, y- and z-direction (x-axis in metres).*

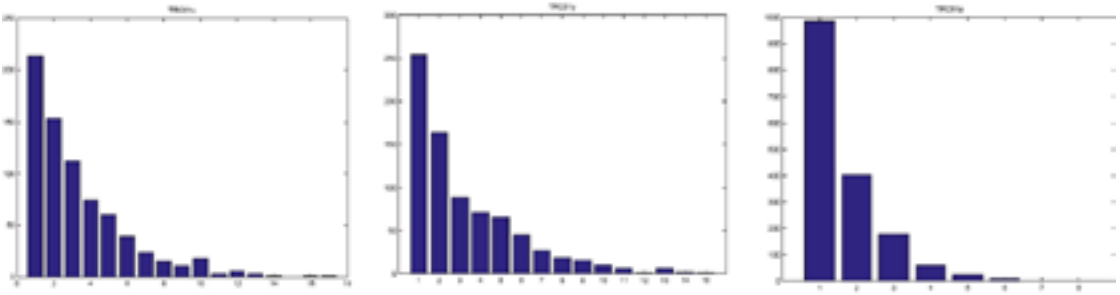

Figure 5-26. *Histogram from 10 randomly selected realisations of TRC 61 in x-, y- and z-direction (x-axis in metres).*

Due to the large number of "borings" in the simulated volumes it is assumed that the histograms give a good representation of the simulated lengths of TRCs. A visual comparison was made of the histograms from the "borings" with lengths observed in the actual borehole data (KFM06C), see Figure 5-27. The comparison indicates that T-PROGS is able to realistically represent TRC lengths registered in the borehole data.

5.5.3 Thermal conductivity

Introduction

Stochastic simulation of thermal conductivity was performed for each TRC. Unconditional simulation was performed at two scales, 0.1 m and 1 m. The simulation volume for the 0.1 m scale is a cube with dimensions 5×5×5 m, and that for the 1 m scale is a cube with dimensions 50×50×50 m. The numbers of realisations run for the 0.1 m and 1 m scales were 150 and 1,000 for domain 29, and 100 and 400 for domain 45, respectively.

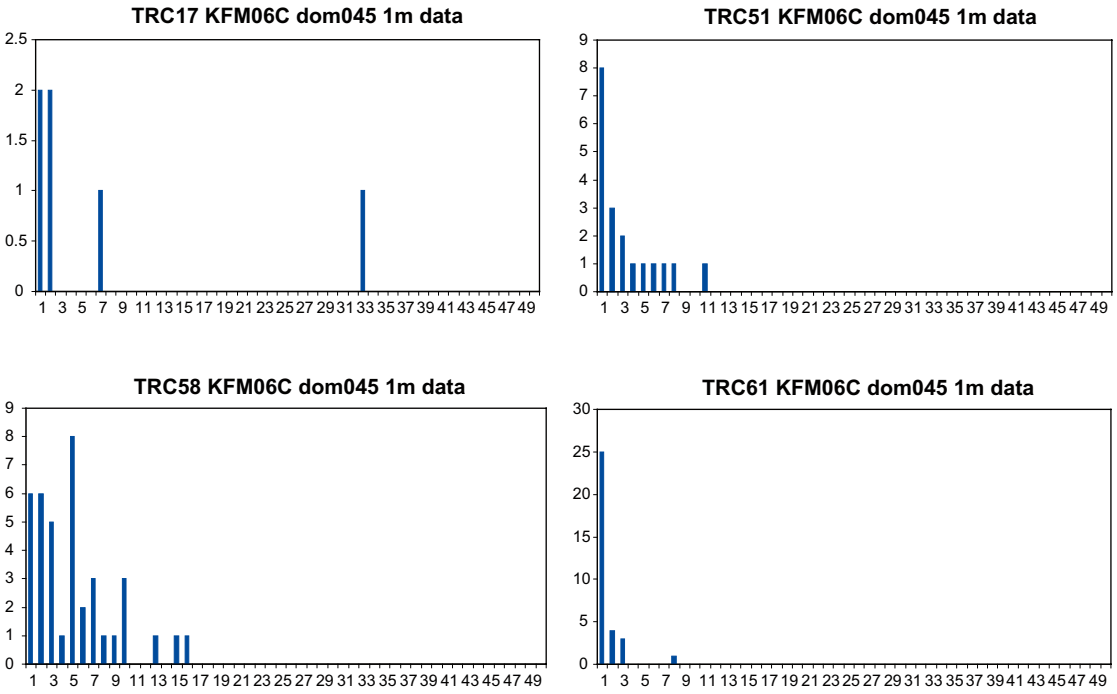

Figure 5-27. *Histograms of TRC lengths observed in borehole KFM06C.*

Procedure

The software used to perform the simulations is GSLIB. Each TRC is simulated using the histogram and variogram models defined in Section 5.4.2. For the 1 m scale, the distribution model is based on the results of 0.1 m simulation upscaled to 1 m.

The simulation programme includes a number of search options. Varying these parameters influences how well the variogram model is reproduced from the individual realisations. The most important parameters are:

- Search radius – defines the size of the data search neighbourhood used for simulating a value at a particular node.
- Multiple grid search – performs search operations in two or more steps using different sizes of data neighbourhood. Since the search must extend at least as far as the distance to which the variogram is to be reproduced, this is a useful function if there are problems recreating the model variogram for longer separation distances. This is often the case when the simulation volume is small compared to the correlation lengths, which is true for several of the TRCs.
- Number of simulated nodes – is the maximum number of previously simulated nodes to use for the simulation of another node. In practice the program allows any number between 12 and 48. Experience has shown that around 30 was optimal for most TRCs. Choosing a higher number increases the simulation time considerably with little or no improvement on the results.

The search options required a great deal of experimentation in order to produce satisfactory simulation results. Only by trial and error could suitable search options be decided upon.

Verification of simulations was performed in a number of ways.

1. Variogram reproduction. The main test of the suitability of the search options was the closeness of fit of the variograms produced by the individual realisations to the input variogram model /Deutsch and Journel 1998/.
2. Histogram reproduction. Each individual realisation should not be expected to reproduce the statistics (histogram) of the model. However, a large number of realisations together should do so /Deutsch and Journel 1998/. The small simulation volume used in 0.1 m scale simulations was in this respect less than optimal. The model statistics can be described by running the simulation (1 realisation) using a pure nugget (nugget = 1).

Results of simulation of thermal conductivity

For each TRC the following plots and diagrams have been produced to illustrate the results and validate the method.

1. Histogram of simulated values from 150 realisations combined for simulations at 0.1 m scale. Figure 5-28, Figure 5-30, Figure 5-32, Figure 5-34, Figure 5-36, Figure 5-38 and Figure 5-40 illustrate the results for 0.1 m scale. The statistics should be similar to the model statistics.
2. Histogram of simulation results at 0.1 m scale upscaled to 1 m for each TRC; see Figure 5-29, Figure 5-31, Figure 5-33, Figure 5-35, Figure 5-37, Figure 5-39 and Figure 5-41. These histograms show the degree to which variability within each TRC is evened out on upscaling from 0.1 m to 1 m.
3. Histogram of simulated values from 1,000 realisations combined for simulations at 1 m scale (Appendix G).
4. Statistics of distribution model at 0.1 m scale (Appendix C).
5. Histogram of individual realisations at 0.1 m scale (Appendix D).
6. Variogram reproduction plots for 0.1 m and 1 m scales based on individual realisations (Appendix F).
7. Visual representation of simulation results at both 0.1 and 1 m scales. 2D slice through a 3D realisation (Appendix D).

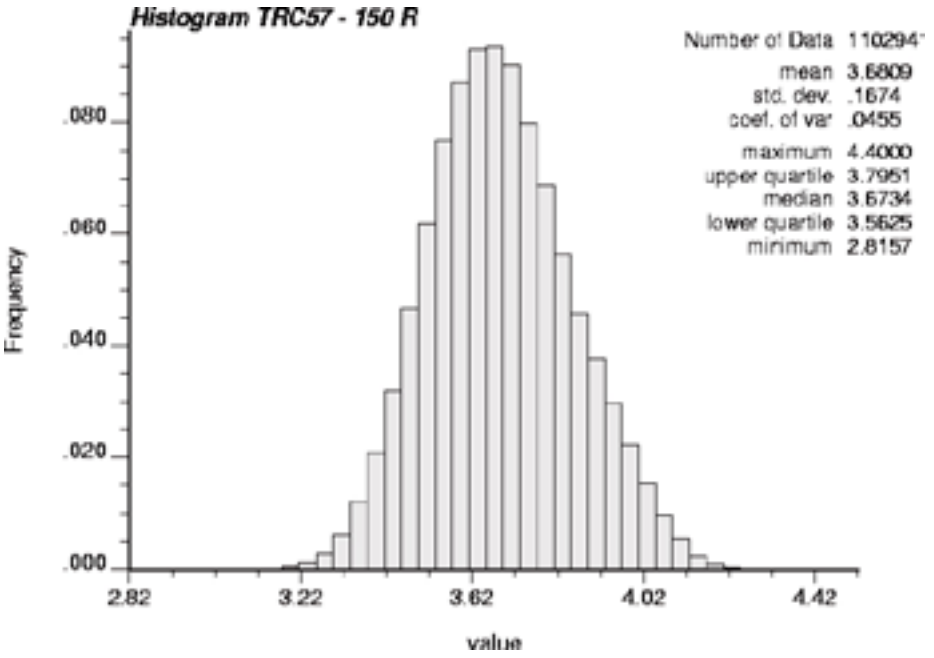

Figure 5-28. *Histogram of simulation results of TRC 57 at 0.1 m scale based on 150 realisations.*

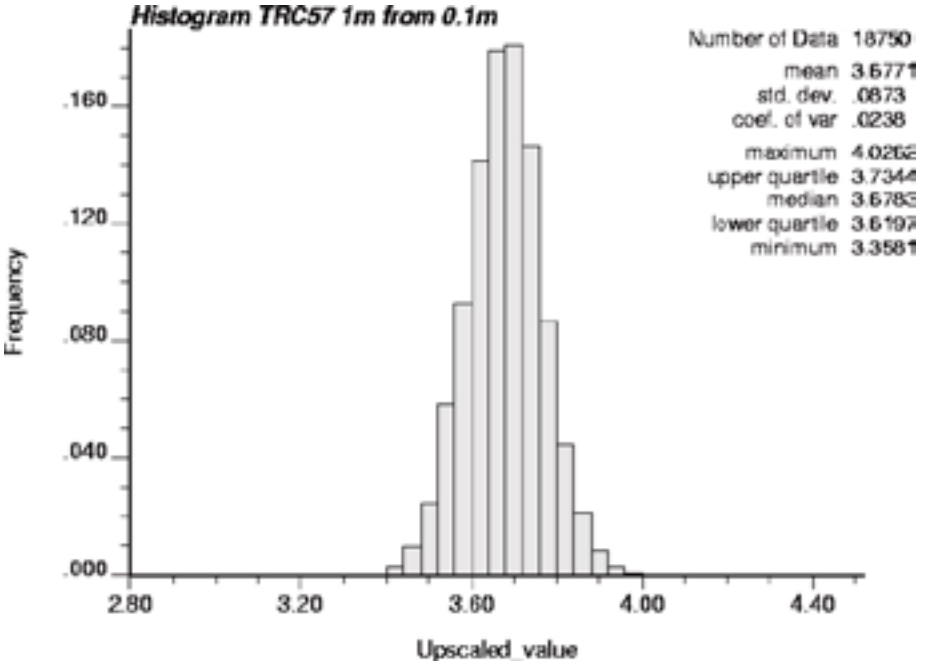

Figure 5-29. *Histogram of simulation results at 0.1 m scale upscaled to 1 m for TRC 57. Based on 150 realisations.*

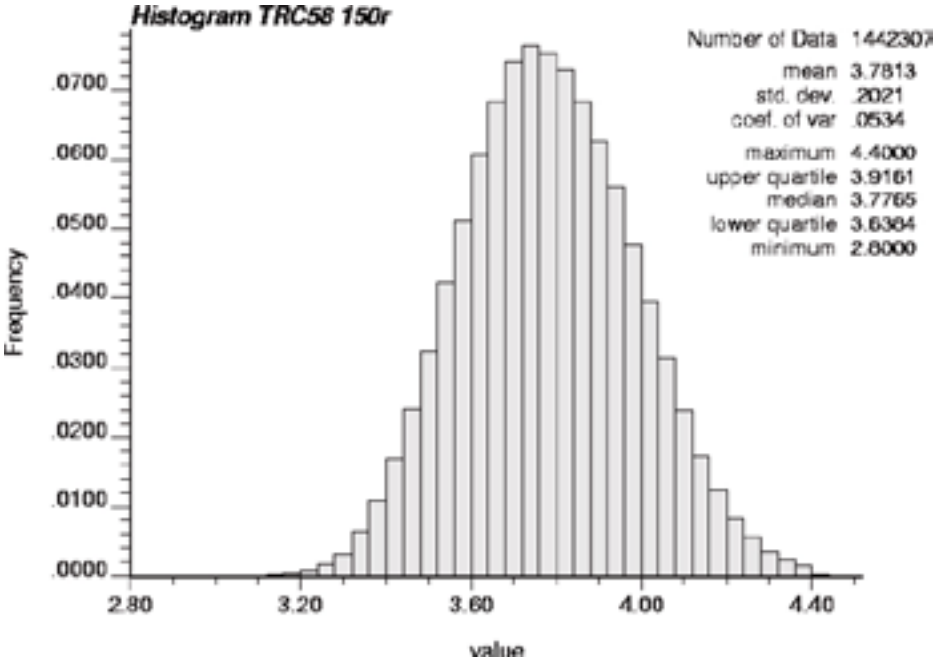

Figure 5-30. *Histogram of simulation results of TRC 58 at 0.1 m scale based on 150 realisations.*

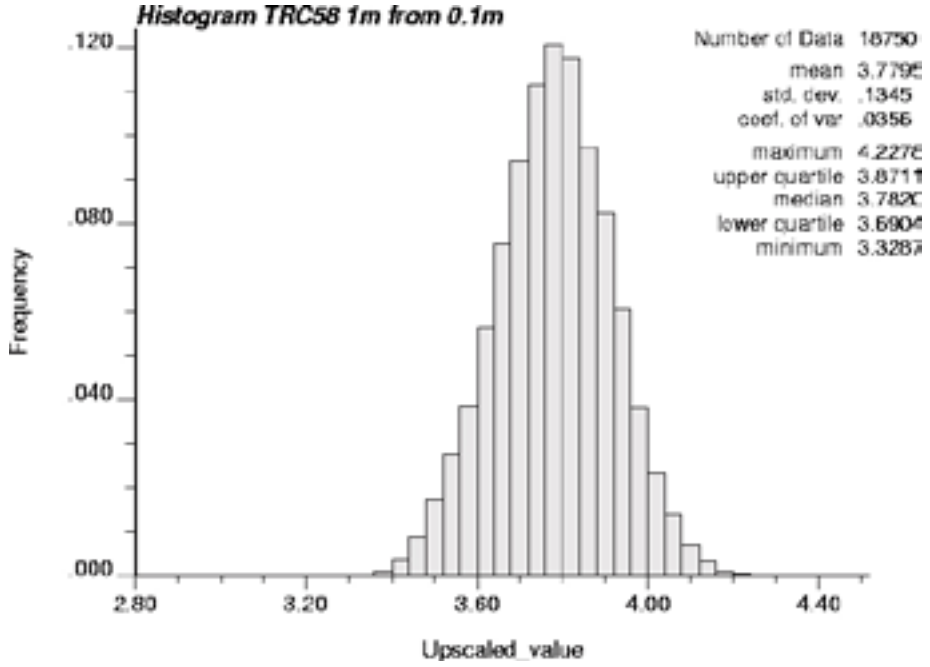

Figure 5-31. *Histogram of simulation results at 0.1 m scale upscaled to 1 m for TRC 58. Based on 150 realisations.*

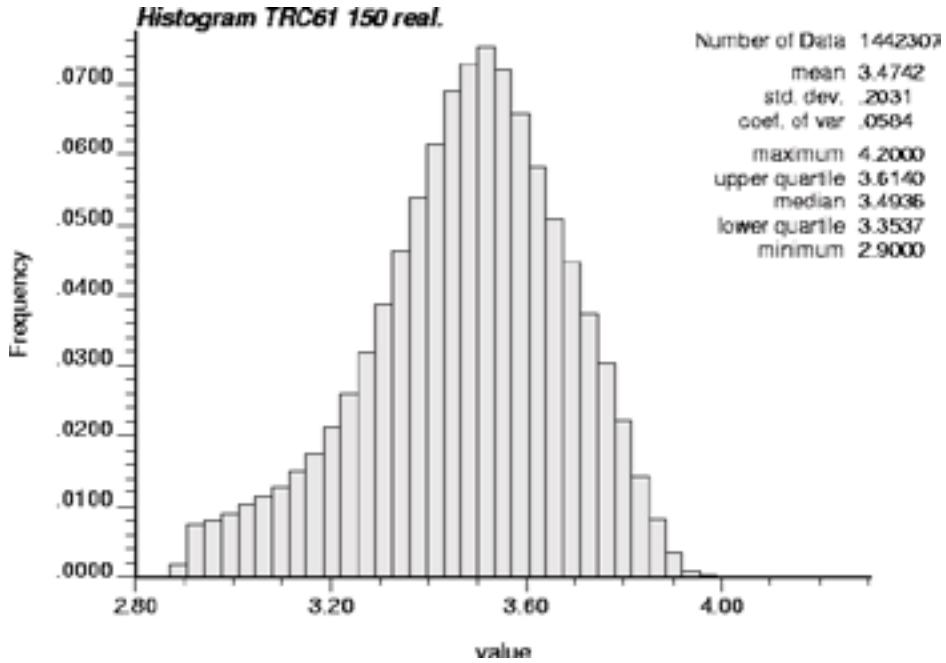

Figure 5-32. *Histogram of simulation results of TRC 61 at 0.1 m scale based on 150 realisations.*

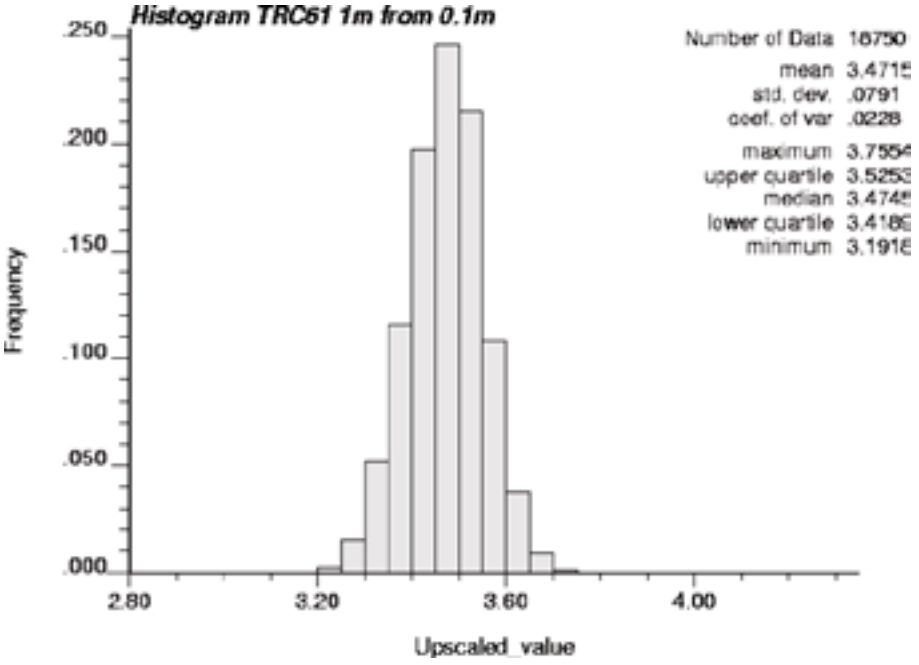

Figure 5-33. *Histogram of simulation results at 0.1 m scale upscaled to 1 m for TRC 61. Based on 150 realisations.*

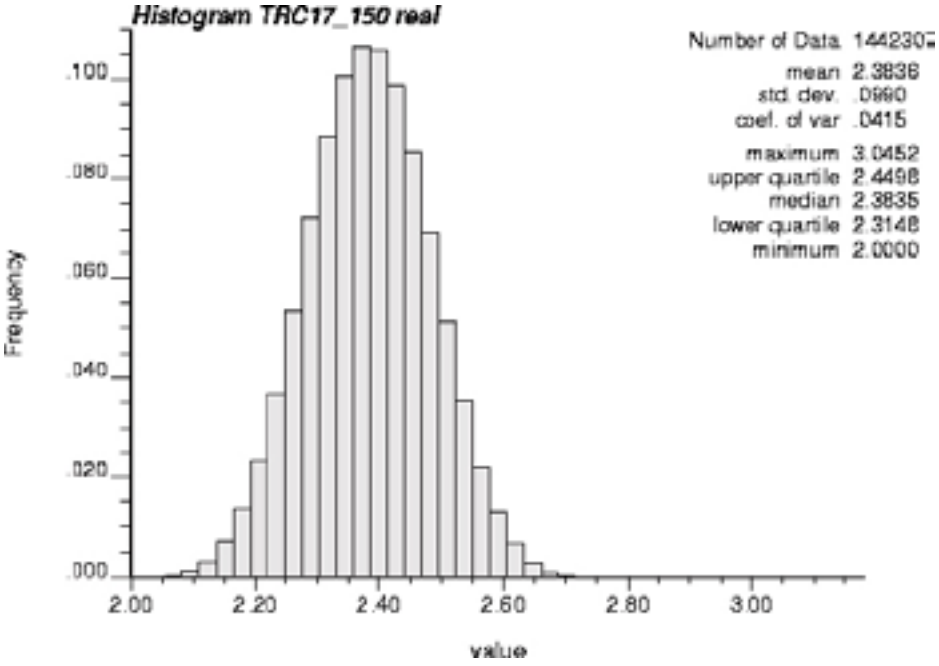

Figure 5-34. *Histogram of simulation results of TRC 17 at 0.1 m scale based on 150 realisations.*

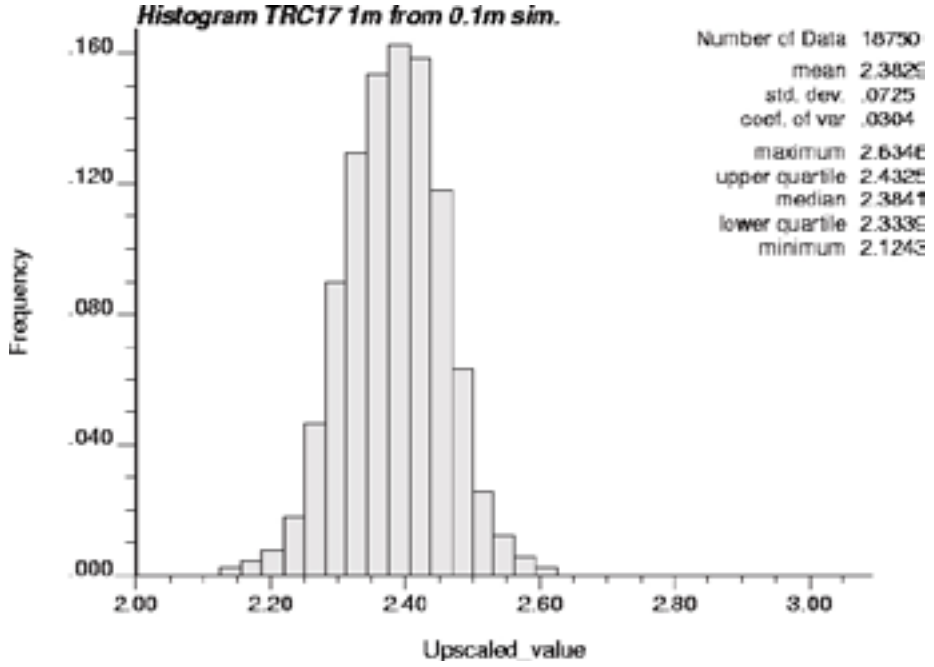

Figure 5-35. *Histogram of simulation results at 0.1 m scale upscaled to 1 m for TRC 17. Based on 150 realisations.*

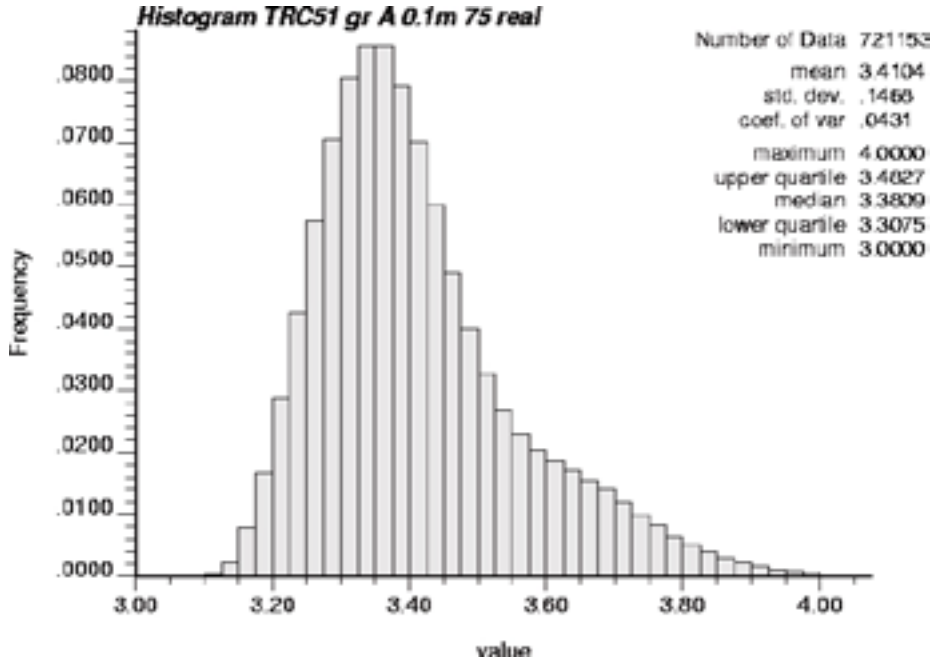

Figure 5-36. *Histogram of simulation results of TRC 51, type A, at 0.1 m scale based on 75 realisations.*

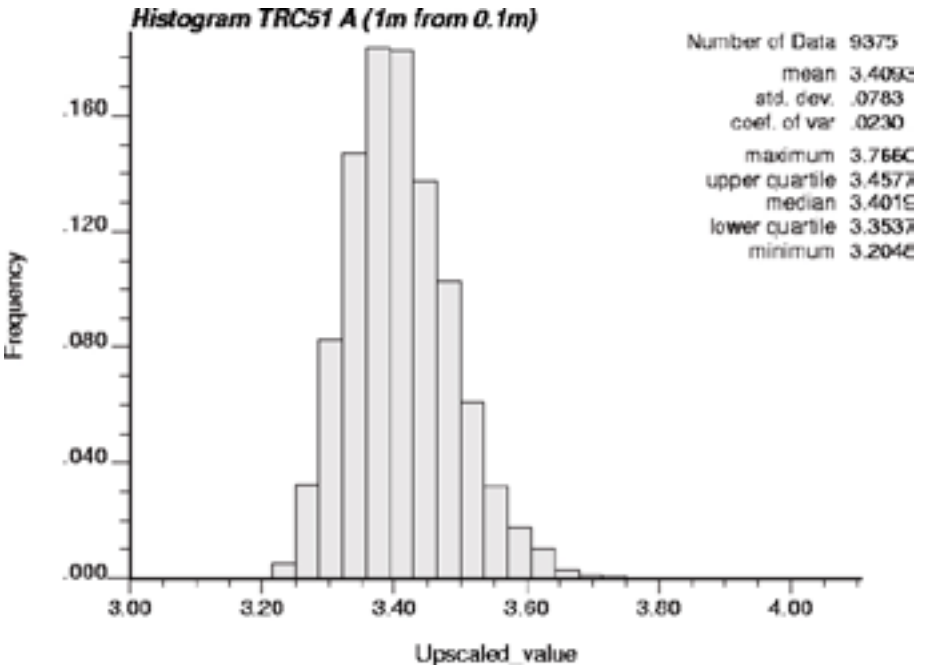

Figure 5-37. *Histogram of simulation results at 0.1 m scale upscaled to 1 m for TRC 51, type A. Based on 75 realisations.*

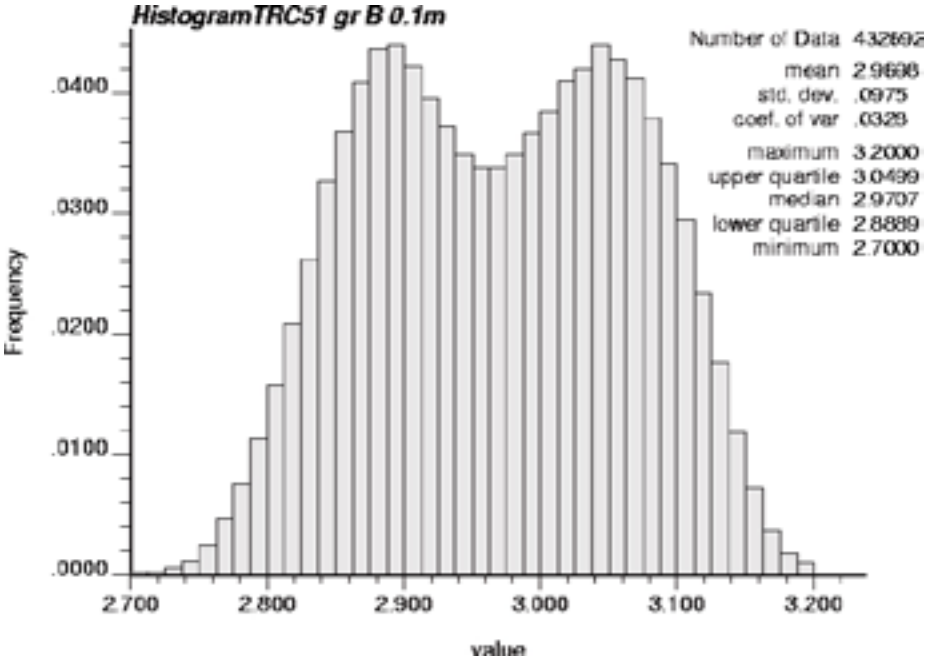

Figure 5-38. *Histogram of simulation results of TRC 51, type B, at 0.1 m scale based on 45 realisations. The apparently bimodal distribution is a result of the empirical data (Figure 5-9) on which the statistical distribution model was based. It may be an effect of a small number of data values (24).*

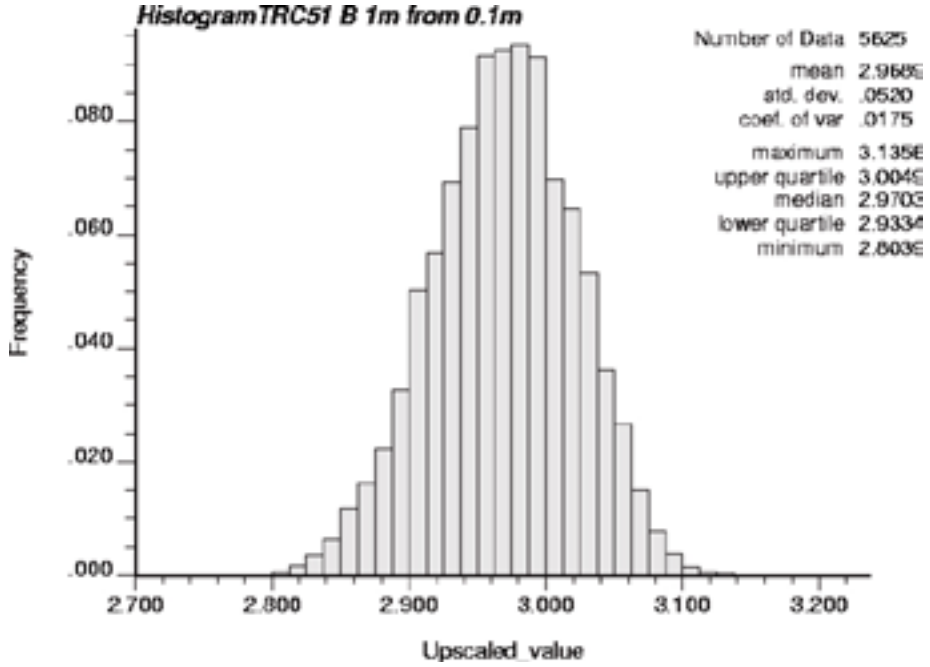

Figure 5-39. *Histogram of simulation results at 0.1 m scale upscaled to 1 m for TRC 51, type B. Based on 45 realisations.*

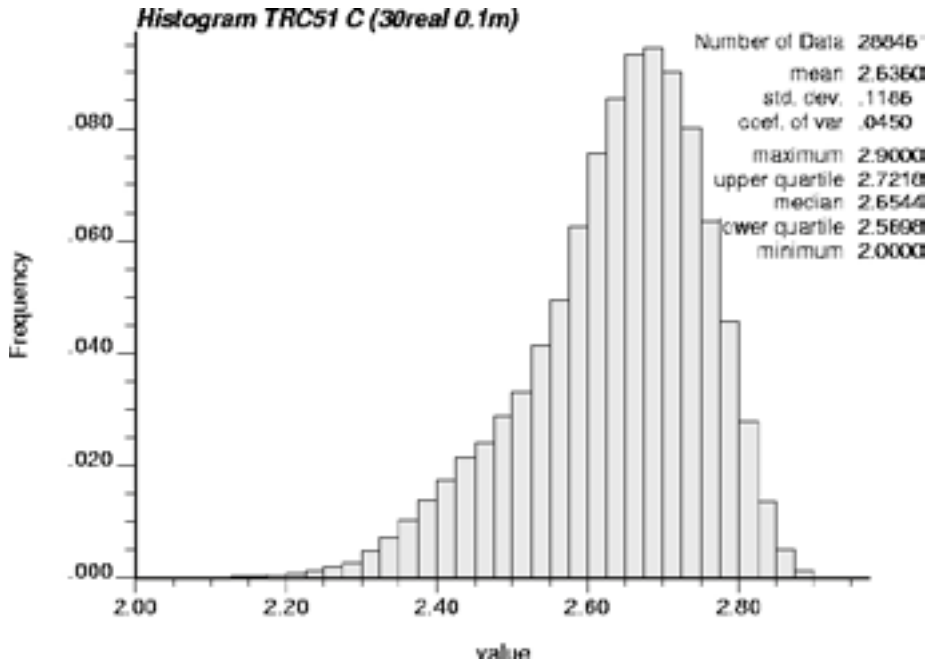

Figure 5-40. *Histogram of simulation results of TRC 51, type C, at 0.1 m scale based on 30 realisations.*

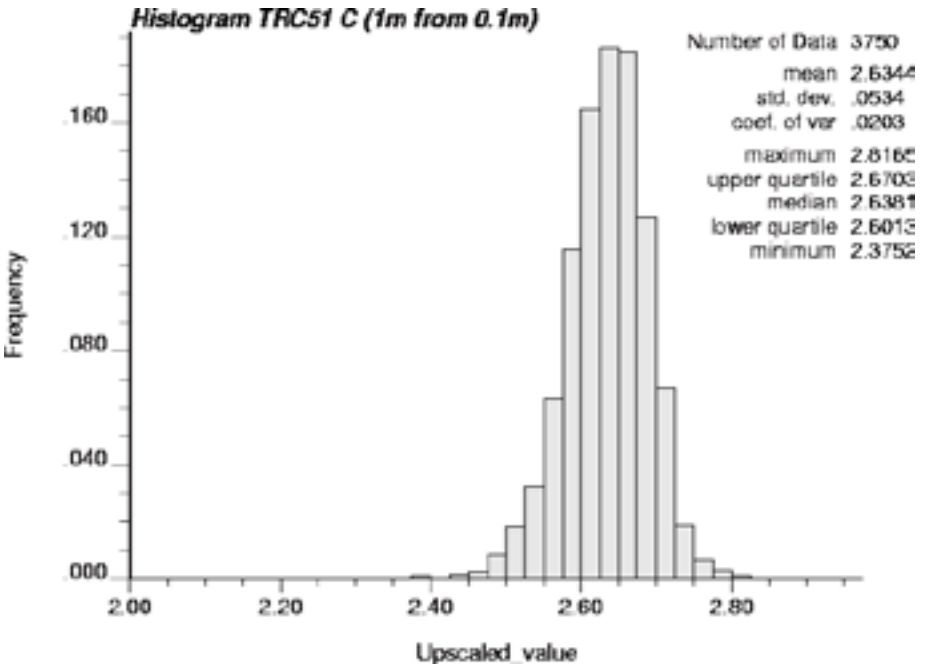

Figure 5-41. *Histogram of simulation results at 0.1 m scale upscaled to 1 m for TRC 51, type C. Based on 30 realisations.*

Statistics of all thermal simulations are summarised in Table 5-28.

Analysis of results

- The combined realisations honour rather well the histogram and variogram models. There is very close correspondence between the means of the realisations and the underlying models. The variances of the combined realisations are slightly lower than the variances of the model. This is observed in the simulation results at both 0.1 m and 1 m scales.
- The results of variogram reproduction are presented in Appendix F. Plots compare the variograms calculated from the realisations with the model variograms on which simulations were based. Generally speaking, variograms reproduced from the 1 m scale simulations show a better fit with the variogram models than for the 0.1 m scale. For the latter, this is most likely due to the small simulation volumes compared to the correlation ranges.
- The statistics, e.g. the mean, of each realisation from simulation at 0.1 m scale fluctuates around the model statistics. Furthermore, the variance of individual realisations is almost always somewhat lower than the variance of the distribution model. This is to be expected since the volume being simulated (a 5 m large cube) is small with respect to the range of correlation (up to 25 m).
- Upscaling of simulation results at 0.1 m scale to 1 m produces a marked reduction in variance, in particular for TRCs that show a low degree of spatial continuity, e.g. TRC 57 and TRC 61. Results indicate that for the dominant TRC in domain 029, approximately 70% of the variability present at the cm-dm scale is evened out at the 1 m scale.
- There is a higher degree of spatial continuity with increasing support size. This is illustrated by comparing the 2D visualisations of realisations at both 0.1 m and 1 m scales (Appendix D).

Table 5-28. Thermal conductivity statistics for all simulated TRCs. Statistics for the distribution model used for simulation at 0.1 m scale are also shown for comparison. Simulation at 1 m scale uses the distribution of upscaled 0.1 m values as a distribution model.

TRC	Scale (m)		Mean (W/m·K)	Standard deviation (W/m·K)	Variance reduction* (%)
57	0.1	Model	3.678	0.176	
	0.1	150 realisations	3.681	0.167	
	1	Upscaled from 0.1 m sim.	3.677	0.087	73
	1	1,000 realisations	3.673	0.081	
58	0.1	Model	3.785	0.217	
	0.1	150 realisations	3.781	0.202	
	1	Upscaled from 0.1 m sim.	3.780	0.135	56
	1	1,000 realisations	3.779	0.127	
61	0.1	Model	3.469	0.209	
	0.1	150 realisations	3.474	0.203	
	1	Upscaled from 0.1 m sim.	3.472	0.079	85
	1	1,000 realisations	3.475	0.073	
17	0.1	Model	2.380	0.107	
	0.1	150 realisations	2.384	0.099	
	1	Upscaled from 0.1 m sim.	2.383	0.073	46
	1	1,000 realisations	2.385	0.063	
51 A	0.1	Model	3.416	0.156	
	0.1	75 realisations	3.410	0.147	
	1	Upscaled from 0.1 m sim.	3.409	0.078	72
	1	500 realisations	3.411	0.073	
51 B	0.1	Model	2.970	0.098	
	0.1	45 realisations	2.970	0.098	
	1	Upscaled from 0.1 m sim.	2.969	0.052	72
	1	300 realisations	2.977	0.049	
51 C	0.1	Model	2.633	0.125	
	0.1	30 realisations	2.636	0.119	
	1	Upscaled from 0.1 m sim.	2.634	0.053	80
	1	200 realisations	2.636	0.049	

* Variance reduction due to upscaling from 0.1 m to 1 m.

6 Thermal domain model

6.1 Domain modelling results

The results of the final modelling steps (11, 12 and 13 in Section 4.2.2 and Figure 4-1) are presented below for two rock domains, RFM029 and RFM045. First, the results of the lithological simulations and the thermal conductivity simulations are merged as described in Section 4.2.13. Then upscaling to larger scales is performed as described in Section 4.2.14. Histograms and tables are used to illustrate the results of thermal modelling for different scales.

6.1.1 Rock domain RFM029

The results of merging lithological simulations and thermal conductivity simulations, as well as subsequent upscaling, for rock domain RFM029 are presented in this section.

The main result of the thermal modelling for domain RFM029 is the set of 1,000 realisations of thermal conductivity from the 1 m-simulations. A histogram of these realisations combined is shown in Figure 6-1. Summary statistics of the realisations are presented in Table 6-1. The lower tail is a result of the low-conductive rocks, mainly amphibolite. As discussed below and in Section 6.2, there are reasons to believe that the lower tail is too large in Figure 6-1 and Table 6-1 due to discretisation error.

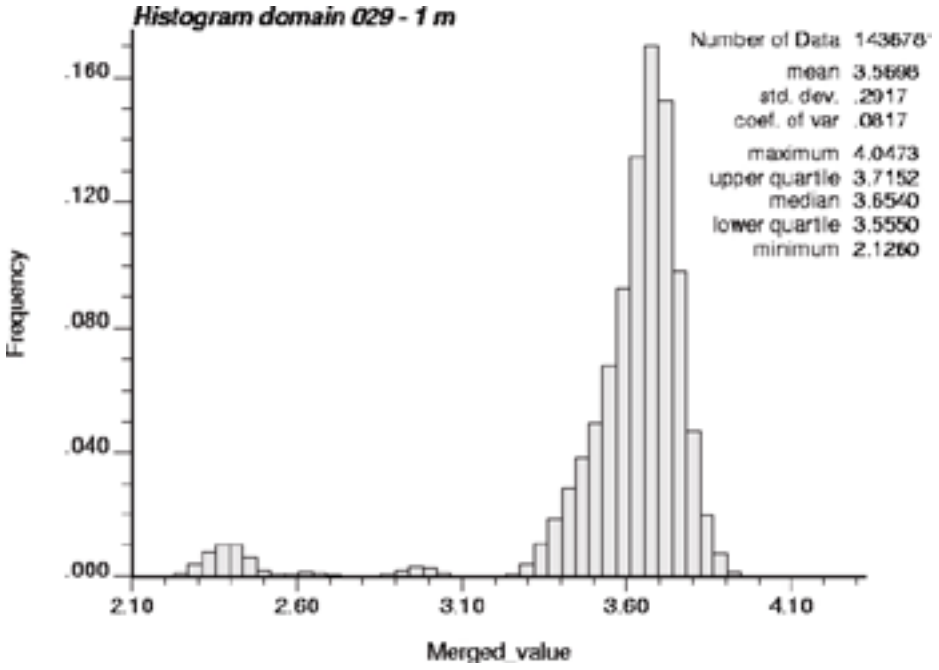

Figure 6-1. *Histogram of thermal conductivity of domain RFM029 simulated at the 1 m scale.*

Table 6-1. Summary statistics for domain RFM029 based on simulations at the 1 m scale. The indicated uncertainty (±) is calculated as a two-sided 95% confidence interval, based on the variability between the 1,000 realisations, each realisation representing a volume of rock of 50×50×50 m³.

Statistical parameter	Value	Unit
Mean	3.58 ± 0.03	W/(m·K)
Variance	0.084 ± 0.031	[W/(m·K)]²
Standard deviation	0.29 ± 0.05	W/(m·K)
Min	2.16 ± 0.05	W/(m·K)
Max	4.00 ± 0.06	W/(m·K)
0.1-percentile (0.001-quantile)	2.26 ± 0.04	W/(m·K)
1-percentile (0.01-quantile)	2.34 ± 0.03	W/(m·K)
2.5-percentile (0.025-quantile)	2.40 ± 0.04	W/(m·K)

Upscaling of the realisations has the effect of smoothing the histogram, as illustrated in Figure 6-2 and Figure 6-3 for the scales 2 m and 5 m, respectively. In the 5 m scale, the pronounced lower tail of the distribution has more or less disappeared.

These results of the 1 m-simulations can be compared to the results based on the 0.1 m simulation; see Figure 6-4 and Figure 6-5. The upscaled 0.1 m values to the 1 m scale in Figure 6-5 give a somewhat different picture than Figure 6-1. During upscaling of the 0.1 m values, the lower tail is rapidly reduced. The main reason is that the volumetric proportions of the different TRCs for the domain are maintained in the small simulation volume of 150 m³ for the lithological simulations at scale 0.1 m. During upscaling, this results in a rapid reduction of the variability during upscaling. This is further analysed in Section 6.2.

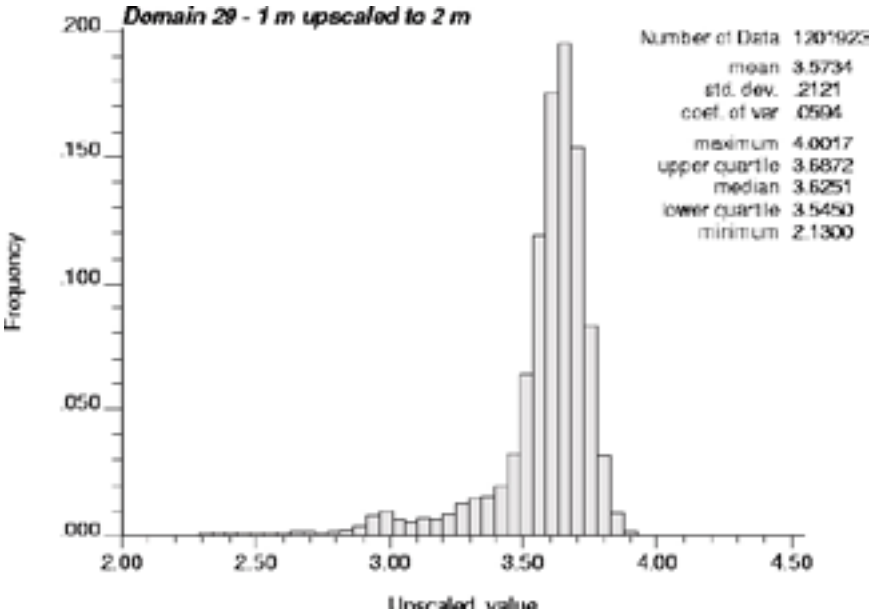

Figure 6-2. *Histogram of thermal conductivity of domain 029 simulated at the 1 m scale but upscaled to 2 m.*

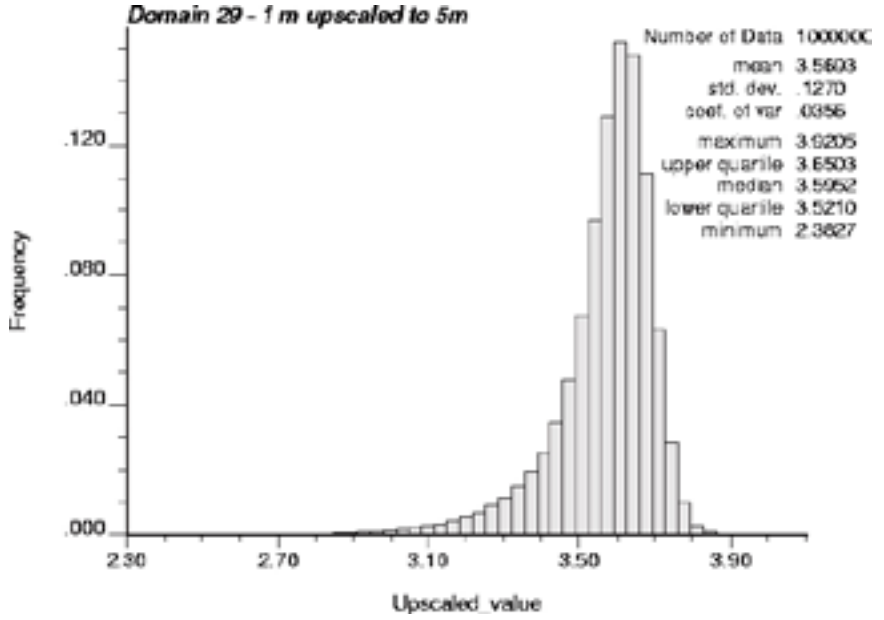

Figure 6-3. *Histogram of thermal conductivity of domain 029 simulated at the 1 m scale but upscaled to 5 m.*

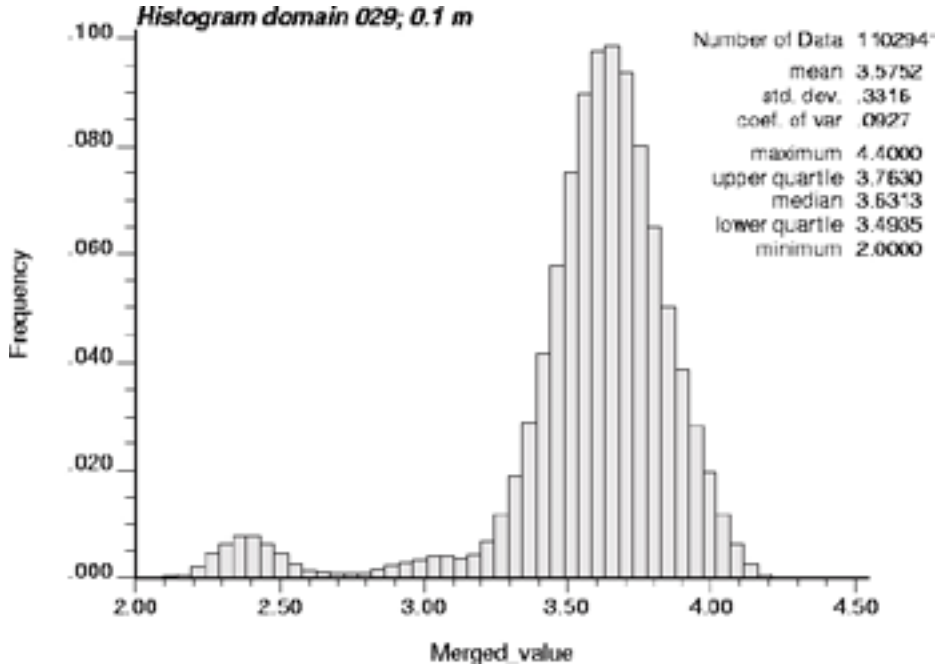

Figure 6-4. *Histogram of thermal conductivity of domain RFM029 simulated at the 0.1 m scale.*

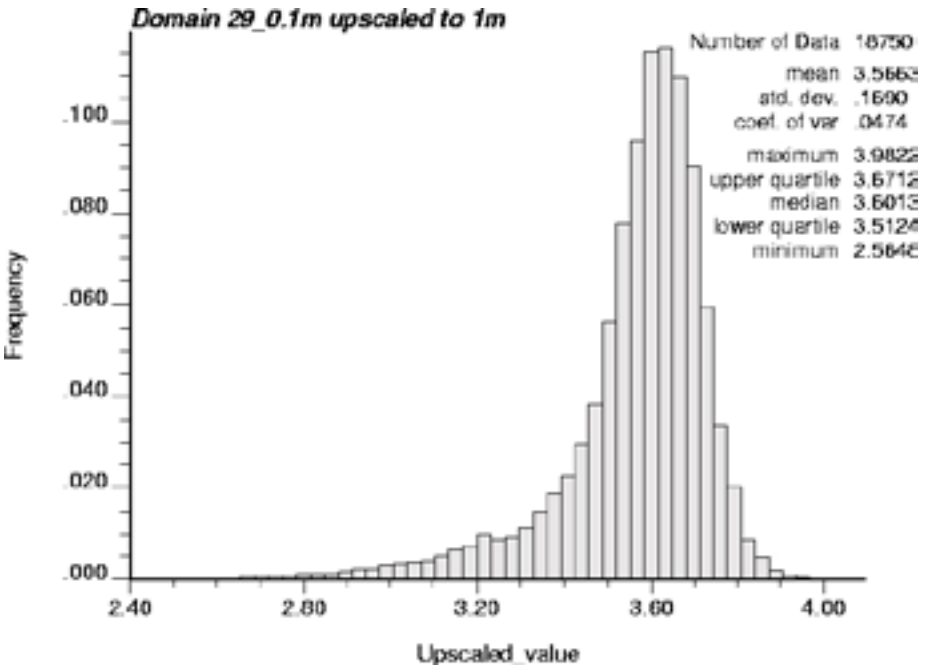

Figure 6-5. *Histogram of thermal conductivity of domain RFM029 simulated at the 0.1 m scale but upscaled to 1 m.*

6.1.2 Rock domain RFM045

The results of merging lithological simulations and thermal conductivity simulations, as well as subsequent upscaling, for rock domain RFM045 are presented in this section.

The main result of the thermal modelling for domain 45 is the set of 400 realisations of thermal conductivity from the 1 m-simulations. A histogram of these realisations combined is presented in Figure 6-6. Summary statistics of the realisations are presented in Table 6-1. The pronounced lower tail and its strange shape is a result of low-conductive rock, mainly amphibolite (TRC17) and granodiorite to tonalite (TRC51). Amphibolite is modelled to occur in larger bodies in

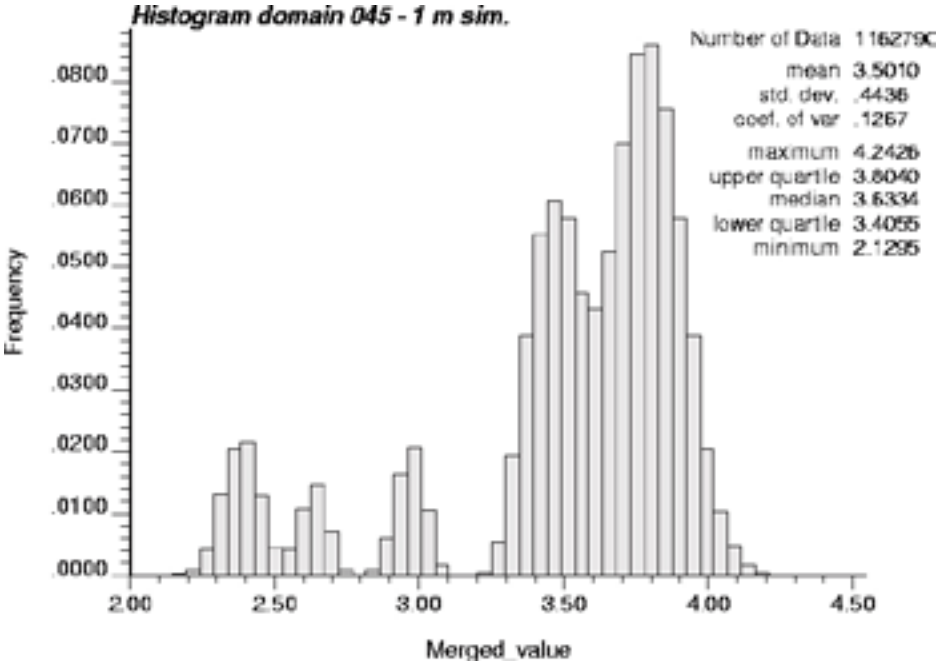

Figure 6-6. *Histogram of thermal conductivity of domain RFM045 simulated at the 1 m scale.*

domain 45 compared to domain 29; see also the lithological realisations in Appendix A. A result of these larger rock bodies of amphibolite is that the discretisation error is expected to be lower for domain 45 than for domain 29.

The summary statistics in Table 6-2 indicate that rock domain RFM045 is more heterogeneous than domain 29, having much higher standard deviation. The variability between the different realisations is considerable.

Upscaling of the realisations has a smoothing effect of the histogram, as illustrated in Figure 6-7 for the scale 5 m. However, even at this scale there is a pronounced lower tail of thermal conductivity values, indicating that there are large bodies of low-conductive rock in domain RFM045; compare Figure 6-3 for domain RFM029.

Table 6-2. Summary statistics for domain 045 based on simulations at the 1 m scale. The indicated uncertainty (±) is calculated as a two-sided 95% confidence interval, based on the variability between the 400 realisations, each realisation representing a volume of rock of 50×50×50 m³.

Statistical parameter	Value	Unit
Mean	3.50 ± 0.13	W/(m·K)
Variance	0.19 ± 0.10	[W/(m·K)]²
Standard deviation	0.44 ± 0.11	W/(m·K)
Min	2.17 ± 0.05	W/(m·K)
Max	4.16 ± 0.10	W/(m·K)
0.1-percentile (0.001-quantile)	2.25 ± 0.05	W/(m·K)
1-percentile (0.01-quantile)	2.31 ± 0.04	W/(m·K)
2.5-percentile (0.025-quantile)	2.35 ± 0.04	W/(m·K)

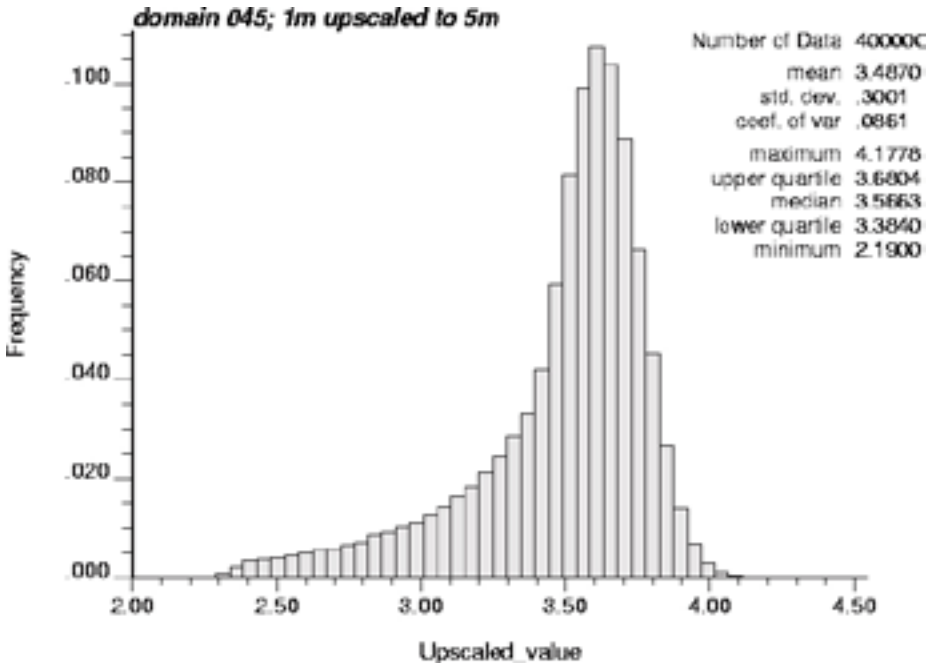

Figure 6-7. *Histogram of thermal conductivity of domain RFM045 simulated at the 1 m scale but upscaled to 5 m.*

These results of the 1 m-simulations can be compared to the results based on the 0.1 m simulation; see Figure 6-8 and Figure 6-9. The upscaled 0.1 m values to the 1 m scale in Figure 6-9 give a somewhat different picture than Figure 6-6 and have a lower variance. The reason is the same as for domain RFM029; the small simulation volume for the 0.1 m simulations, which results in a too large variance reduction during upscaling.

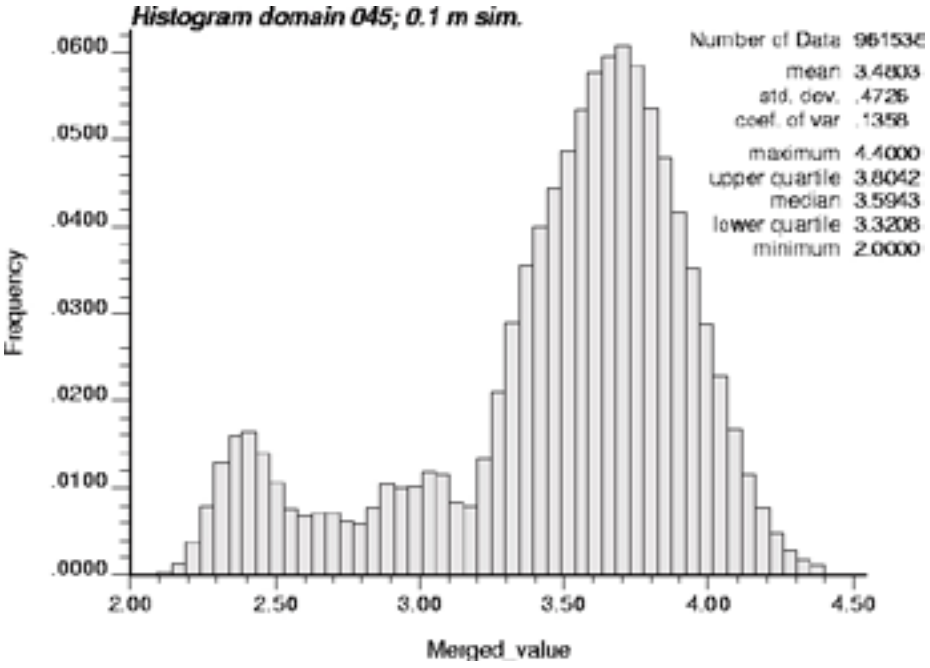

Figure 6-8. *Histogram of thermal conductivity of domain RFM045 simulated at the 0.1 m scale.*

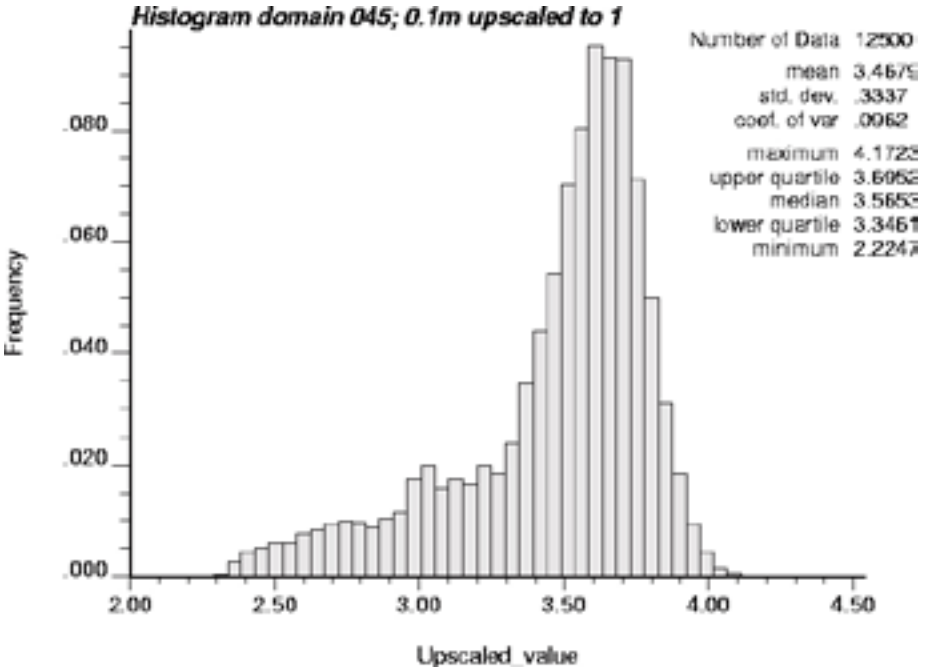

Figure 6-9. *Histogram of thermal conductivity of domain RFM045 simulated at the 0.1 m scale but upscaled to 1 m.*

6.2 Evaluation of domain modelling results

6.2.1 Domain RFM029

The lower tail of the thermal conductivity distribution is of great importance for the design of a repository. The modelling results were therefore analysed in detail in this respect. The analysis was performed on the 0.1-percentile, 1-percentile and 2.5-percentile of the thermal conductivity distribution for the domain. In addition, a range of scales, from 0.1 m to 5 m, were analysed. The results are presented in Figure 6-10 to Figure 6-12 for the three percentiles, respectively. The plots illustrate how the lower percentiles increase when the scale increases. This is a way of describing how the variance reduction affects the lower percentiles and how sensitive they are to the choice of scale.

Results are presented for both simulations performed at the dm scale and the metre scale. The simulated values represent the 0.1 m scale (red dot) and the 1 m scale (blue dot). Values for larger scales are calculated (upscaled) using the Self-Consistent Approximation (SCA) Approach; see /Sundberg 1988, Sundberg et al. 2007a/. It is evident from Figure 6-10 to Figure 6-12 that there is a large difference between the two simulation scales. For example, simulations performed at the 0.1 m scale and upscaled to the 1 m scale results in significantly higher thermal conductivity values than simulations performed directly at the 1 m scale. This conclusion is valid for all three analysed percentiles.

The reason for the deviation between the two simulations is mainly a result of two phenomena:

1. The discretisation of 1 m cells for the 1 m simulations results in a significant error when a rock occurs at sections less than, or close to 1 m (either a full cubic metre is assigned or nothing at all).
2. The thermal conductivity rapidly approaches the mean of the domain when upscaling is performed on larger and larger scales. This is because the mean thermal conductivity of the simulated volume is close to the mean of the domain.

The first phenomenon indicates that the thermal conductivity of the blue dots is too low at scales close to 1 m. However, the discretisation error is reduced during upscaling. It is reasonable to believe that the error has more or less disappeared at a scale of at least 5 m. The blue dots representing the 5 m scale in Figure 6-10 to Figure 6-12 are therefore reliable.

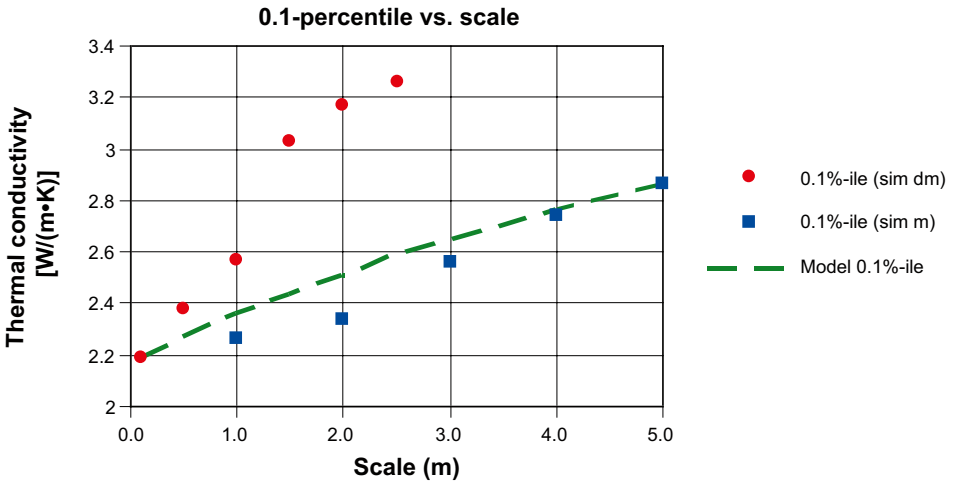

Figure 6-10. *The 0.1-percentile (0.001 quantile) versus the scale for domain 29. Upscaling was performed on simulated values at the 0.1 m scale (red) and simulated values at the 1 m scale (blue). A model (green) was fitted to the most reliable values.*

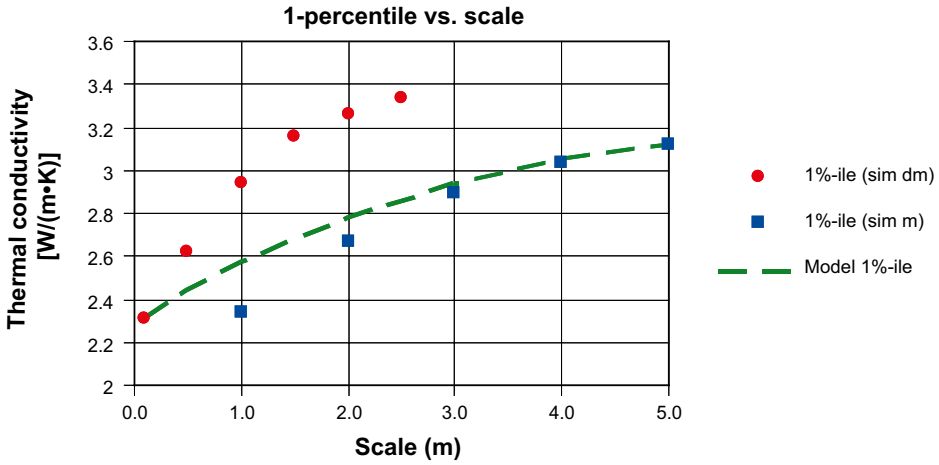

Figure 6-11. *The 1-percentile (0.01 quantile) versus the scale for domain 29. Upscaling was performed on simulated values at the 0.1 m scale (red) and simulated values at the 1 m scale (blue). A model (green) was fitted to the most reliable values.*

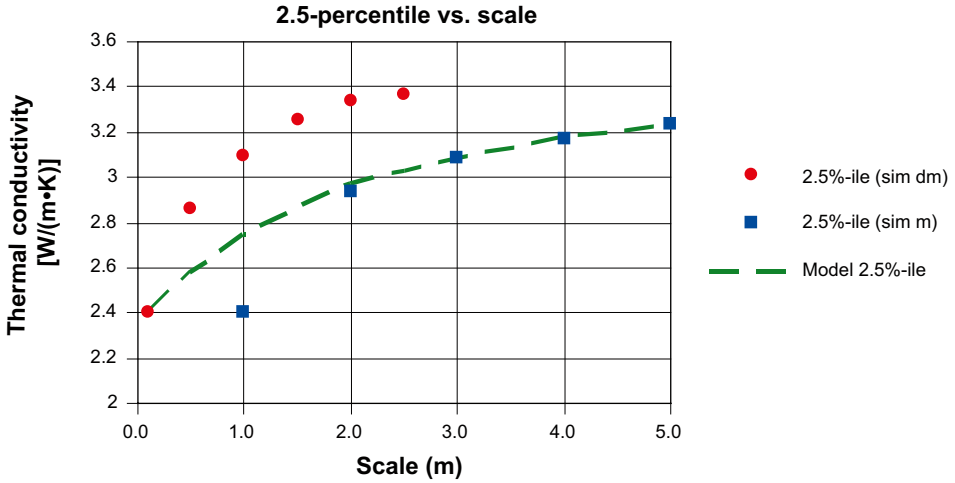

Figure 6-12. *The 2.5-percentile (0.025 quantile) versus the scale for domain 29. Upscaling was performed on simulated values at the 0.1 m scale (red) and simulated values at the 1 m scale (blue). A model (green) was fitted to the most reliable values.*

The red dots, based on simulation at the 0.1 m scale, represent a higher resolution than the 1 m simulations. The first red dot, representing the 0.1 m scale, is therefore reliable. However, during upscaling the second phenomenon listed above is pronounced because the simulation volume is only 5×5×5 m^3. Upscaling of 0.1 m values rapidly approaches the domain mean. Therefore, upscaled values based on the 0.1 m simulation will overestimate the thermal conductivity and cannot be relied on (a much larger simulation volume would be required to eliminate this phenomenon). However, the purpose of the 0.1 m simulation was change of support within a single TRC, not representative modelling of all TRCs in a whole domain. The latter was achieved by 1 m simulations.

In each of Figure 6-10 to Figure 6-12, a model is fitted to the two most reliable values in the graphs, assuming a parabolic shape of the model. An infinite number of models could be fitted to these two points but the values based on the 1 m simulations (blue dots) are much more reliable than the red dots and therefore a fit close to the blue dots are made. However, the shape of the curve is not known and the deviation from the blue dots could in reality be even smaller. The graphs indicate that the discretisation error is reduced when the scale increases, which is reasonable. For the 2.5-percentile (Figure 6-12) the discretisation error seems insignificant already at the 2 m scale. However, it should be borne in mind that the fit of the models are performed subjectively.

The described problem of deviating results between simulations performed at the 0.1 m scale and the 1 m scale could be overcome by selecting the simulation scale (cell size) and the simulation volume more carefully. A lesson learned from the performed simulations is that the simulation scale should be significantly lower than the scale at which the most important rock types (from a thermal perspective) occurs.

6.2.2 Domain RFM045

Percentiles and scales were evaluated in a similar manner for domain RFM045 as for domain RFM029. The results are presented in Figure 6-13 to Figure 6-15. The discretisation error at simulation scale 1 m is much lower for domain 45 than for domain 29. The reason is that the low-conductive amphibolite is modelled to occur at much larger sections in domain 45. This is illustrated in the presented realisations in Appendix H.

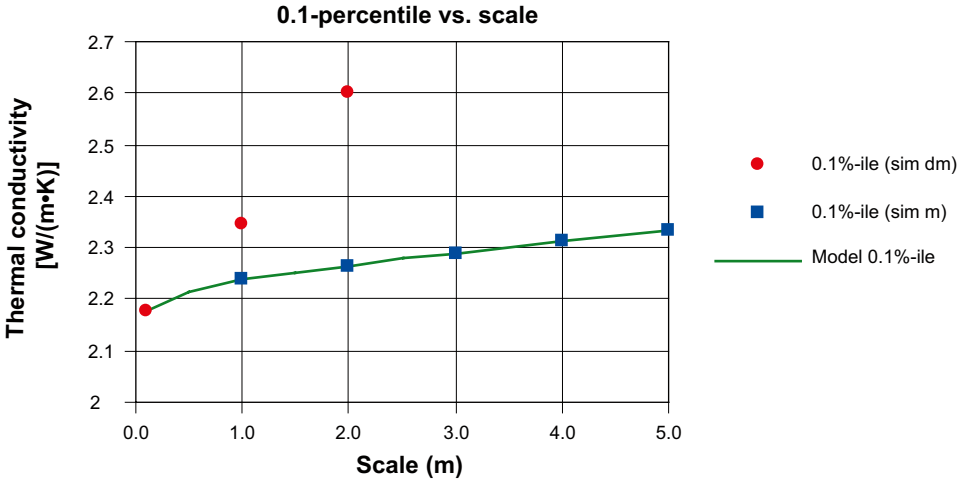

Figure 6-13. *The 0.1-percentile (0.001 quantile) versus the scale for domain 45. Upscaling was performed on simulated values at the 0.1 m scale (red) and simulated values at the 1 m scale (blue). A model (green) was fitted to the most reliable values.*

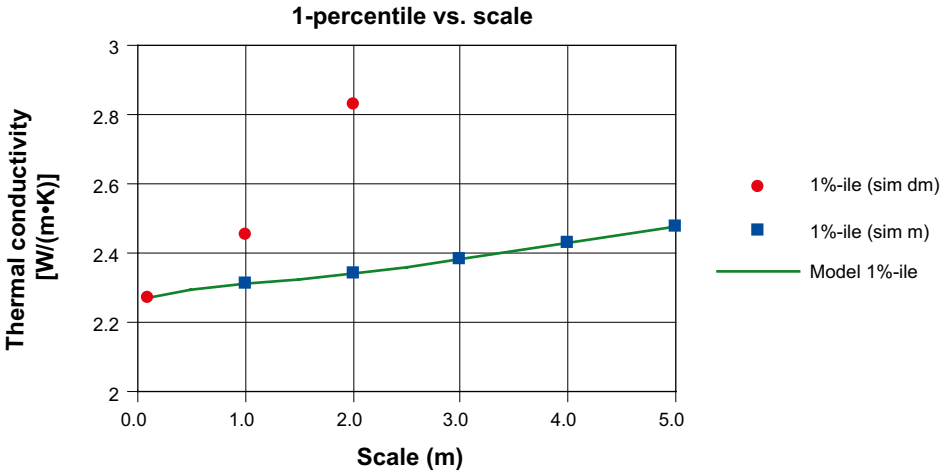

Figure 6-14. *The 1-percentile (0.01 quantile) versus the scale. Upscaling was performed on simulated values at the 0.1 m scale (red) and simulated values at the 1 m scale (blue). A model (green) was fitted to the most reliable values.*

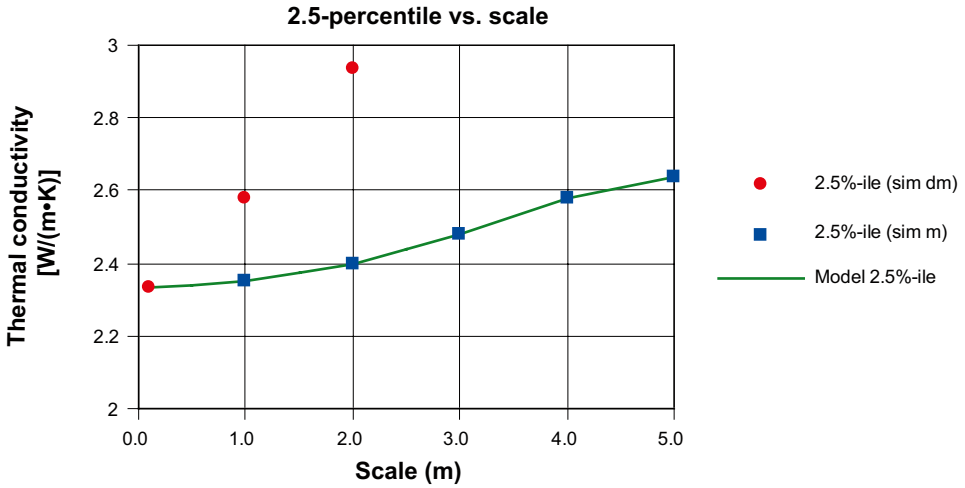

Figure 6-15. *The 2.5-percentile (0.025 quantile) versus the scale for domain 45. Upscaling was performed on simulated values at the 0.1 m scale (red) and simulated values at the 1 m scale (blue). A model (green) was fitted to the most reliable values.*

Because of small discretisation errors, the green models in Figure 6-13 to Figure 6-15 are fitted through all blue dots. The models are also extended to the red dot representing the 0.1 m scale, which is regarded as reliable. The red dots representing larger scales are not reliable due to the upscaling phenomenon described in the previous section.

6.2.3 Anisotropy due to subordinate rock bodies

The anisotropy of thermal conductivity due to spatial orientation of subordinate rock bodies was analysed at domain level for domain RFM029 based on the simulation results. All 1 m realisations (1,000) were divided into a 5×5×5 m^3 cubes and the thermal conductivity in the x'''-, y'''- and z'''-directions of each cube was calculated (for simplicity, these directions are denoted by x, y and z throughout this section, including Figure 6-16 to Figure 6-20).

The upper and lower bounds for thermal conductivity for each 125 m^3 cube could be calculated as the arithmetic mean and the harmonic mean, respectively. The thermal conductivity value for a specific direction through the cube is somewhere within this range. Estimates of the thermal conductivity for each of the principal directions were made using the following approach:

1. Divide the cube into "rods" extending in the direction of interest; see Figure 6-16 for an example for the y-direction. Calculate the thermal conductivity of the rod as the harmonic mean of the cells in the rod.
2. Calculated the thermal conductivity of all rods as the arithmetic mean[1].
3. Perform 1 and 2 for all three principal directions.

Note that this approach does not necessarily provide theoretically correct values of thermal conductivity in the various directions, only rough approximations. However, the calculated values are believed to be sufficiently accurate to evaluate the thermal conductivity in the principal directions relative to each other. More advanced approaches, such as numerical modelling of heat flow, are required in order to improve the accuracy.

The result of the anisotropy analysis is presented in histograms in Figure 6-17 to Figure 6-19 for the x-, y- and z-directions, respectively. As indicated, the lower tail is most pronounced for the z-direction. This can be explained by the fact that the low-conductive amphibolite is modelled as having its greatest cross-sectional area in the xy-plane.

[1] The SCA method for 2-dimensions is more theoretically sound but the arithmetic mean is a good approximation.

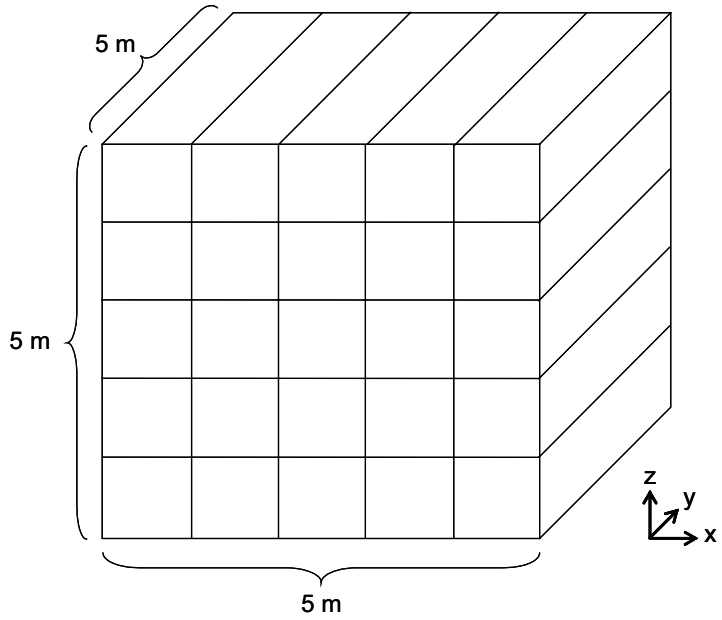

Figure 6-16. *Evaluation of thermal conductivity in the y-direction. Each 5×5×5 m³ cube was divided into 1×1×5 m "rods", each rod made up of five 1 m cells oriented in the y-direction. The thermal conductivity of the rod was calculated as the harmonic mean of the five cells. The thermal conductivity in the y-direction of the whole 5×5×5 m³ cube was calculated as the arithmetic mean of the 5×5 rods.*

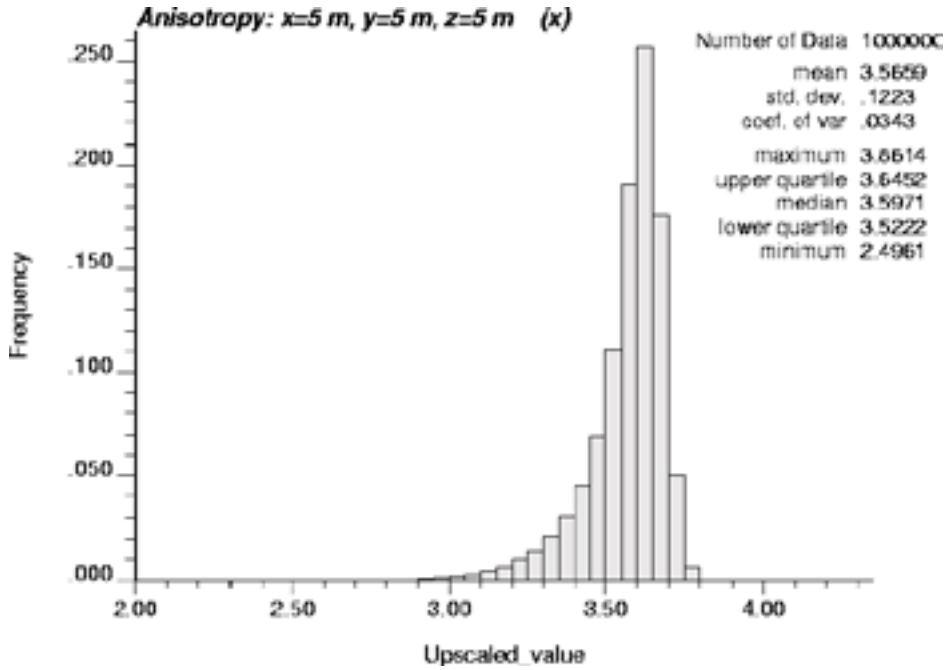

Figure 6-17. *Thermal conductivity of 5×5×5 m³ cubes in the x-direction for domain RFM029.*

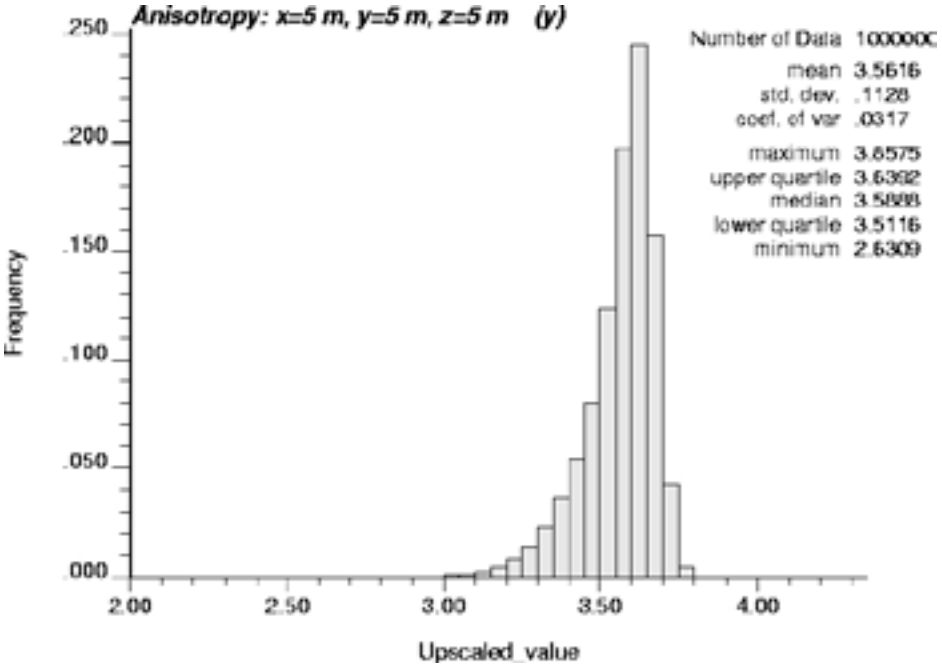

Figure 6-18. *Thermal conductivity of 5×5×5 m³ cubes in the y-direction for domain RFM029.*

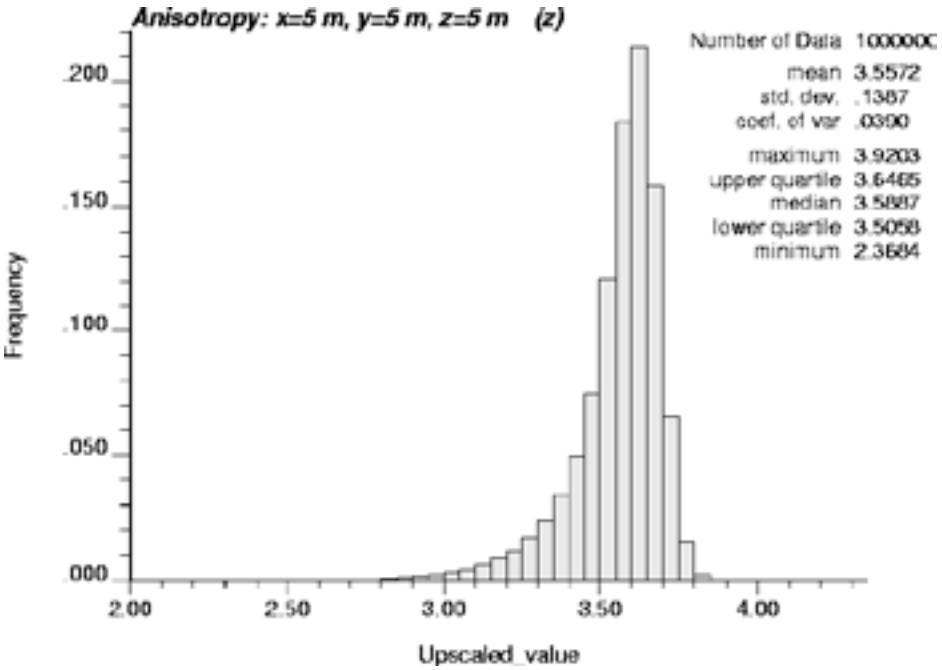

Figure 6-19. *Thermal conductivity of 5×5×5 m³ cubes in the z-direction for domain RFM029.*

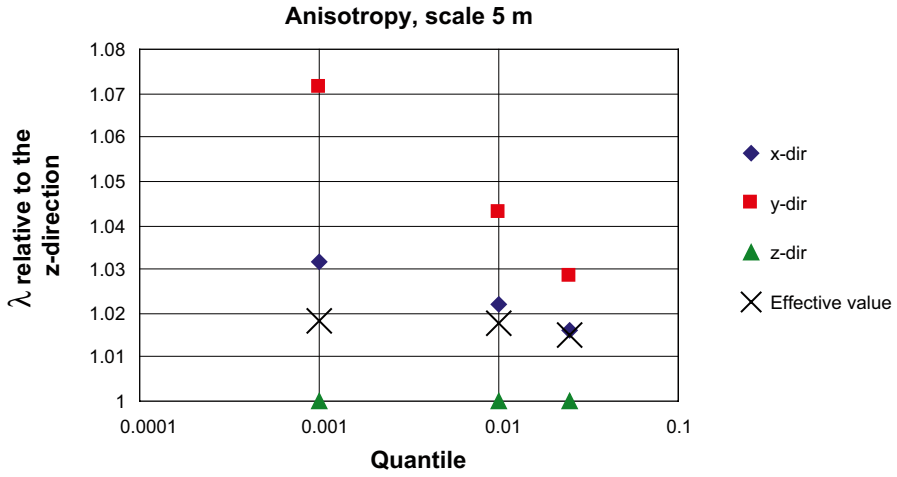

Figure 6-20. *Anisotropy factors for of the lower tail of the thermal conductivity distribution in the three principal directions of 5×5×5 m³ cubes relative to the z-direction (domain RFM029). Note the logarithmic scale of the quantiles.*

A quantitative comparison of the three principal directions is given in Figure 6-20 for the three evaluated quantiles, expressed as anisotropy factors. The thermal conductivity has been normalised with the thermal conductivity in the z-direction (the most low-conductive direction). Effective values (isotropic assumption) calculated with the SCA approach /Sundberg et al. 2005b/ are also indicated for comparison. The largest calculated relative difference from the z-direction was found for the y-direction, where the thermal conductivity at the 0.001 quantile (0.1 percentile) was found to be more than 7% larger than the z-direction (anisotropy factor 1.07). The anisotropy factor decreases for higher percentiles. The reason that the anisotropy is strongest in the far end of the lower tail is because this part of the tail is dominated by amphibolite. Figure 6-20 also indicates that the thermal conductivity in the x-direction is close to the mean (effective value) for all directions.

Similar evaluations of anisotropy could be performed also for other scales than the 5 m scale. However, this has not been performed but it is reasonable to assume that the anisotropic effect becomes weaker as the scale increases. Correspondingly, a stronger anisotropic effect can be assumed for scales less than 5 metres.

6.3 Domain properties

6.3.1 Thermal conductivity

The main result of the thermal modelling is a set of realisations of thermal properties for the two rock domains. These realisations can be used for further processing, most importantly for numerical temperature simulations for design of repository layout (distances between deposition holes).

The thermal properties at domain level is summarised in Table 6-3 and Table 6-4 for rock domains RFM029 and RFM045, respectively. For domain 29, the estimates for scale 1 m are uncertain due to a possible discretisation error for the low-conductive amphibolite. This error is evened out at the 5 m scale. For domain 45 the corresponding error is negligible.

The interval of thermal conductivity for the 1 m scale for the lower percentiles in Table 6-1 is based on Figure 6-10 to Figure 6-12. An estimated “best” value is given in this interval.

Table 6-3. Properties for domain RFM029 based on simulations at the 1 m scale. The "best" estimates and the intervals for the 1 m scale are based on the evaluation of the domain results in Section 6.2.

Statistical parameter	1 m scale W/(m·K)	5 m scale W/(m·K)
Mean	3.58	3.57
Standard deviation	0.29	0.13
0.1-percentile	2.30* (2.26–2.4)	2.87
1-percentile	2.45* (2.34–2.6)	3.12
2.5-percentile	2.55* (2.40–2.8)	3.23

* Best estimate based on the evaluation in Section 6.2. To set a realistic upper limit on the percentile intervals for 1 m scale, the difference between the lower limit and the best estimate is added to the best estimate and rounded off upwards to the nearest first decimal place.

Table 6-4. Properties for domain RFM045 based on simulations at the 1 m scale.

Statistical parameter	1 m scale W/(m·K)	5 m scale W/(m·K)
Mean	3.50	3.49
Standard deviation	0.44	0.30
0.1-percentile	2.25	2.33
1-percentile	2.31	2.48
2.5-percentile	2.35	2.64

The properties in Table 6-4 are strongly affected by how the spatial structure of TRC17 (amphibolite) was modelled. The low thermal conductivities, even for the 5 m scale, are a result of the large bodies of amphibolite produced in the lithological simulations; see uncertainty analysis below.

The values above are valid at 20°C. With increasing temperature the thermal conductivity of the dominant granitoid rock decreases by about 10%/100°C temperature increase, calculated as mean value.

Thermal anisotropy

Anisotropy due to foliation/lineation in the dominant granite to granodiorite has been measured in situ at one site. Field measurements indicate that thermal conductivity parallel to the foliation plane is higher, by a factor of approximately 1.15, than conductivity perpendicular to the foliation.

Evaluation of anisotropy due subordinate rock bodies, primarily amphibolite, indicates a slightly lower thermal conductivity in the 5 m scale in a direction perpendicular to the plane of maximum flattening of the amphibolites (the z´´´-direction). The largest calculated relative difference from the z´´´-direction was found for the y´´´-direction, where the thermal conductivity at the 0.1 percentile was found to be more than 7% larger than the z-direction (anisotropy factor 1.07). The anisotropy factor decreases for higher percentiles. The reason that the anisotropy is strongest in the far end of the lower tail is because this part of the tail is dominated by amphibolite. A stronger anisotropic effect is assumed for scales less than 5 metres.

Comparison with previous model versions

The above results for domain RFM029 can be compared with previously reported results. In Table 6-5, results presented in version 1.2 /Sundberg et al. 2005a/ are compared with the results of the latest modelling work. The mean thermal conductivity is similar in both versions, but the standard deviations and estimates of the 2.5 percentile are significantly different. The reason for these discrepancies is that the present model has incorporated data on amphibolite rock, something which was unavailable in version 1.2. In model stage 2.1 /SKB 2006b/, this shortcoming was recognised, but as little modelling work was performed, there are no results with which to make a direct comparison. Modelling of domain RFM045 has not been previously performed.

6.3.2 Heat capacity

The mean heat capacity of the dominant granitoid rock (101057) in domain 29 is 2.15 MJ/(m^3·K). For domain 45, the dominant granite (101058) has a mean heat capacity of 2.08 MJ/(m^3·K). These values are based on calculations from TPS measurements and are valid at 20°C. With increasing temperature the heat capacity of the dominant granitoid rock increases by about 29%/100°C temperature increase as a mean value.

Domain modelling was not performed. However, a relationship, described by a second order equation, between heat capacity from direct measurements and thermal conductivity has been established. Using this relationship, together with the output from simulation of thermal conductivity, permits the estimation of heat capacity distributions at domain level.

6.3.3 Thermal expansion coefficient

The mean thermal expansion coefficient for the investigated rock types within the target volume varies between $7.2 \cdot 10^{-6}$ and $8.1 \cdot 10^{-6}$ m/(m·K). For the dominant granite to granodiorite (101057), the mean thermal expansion coefficient is $7.7 \cdot 10^{-6}$ m/(m·K). Data is not available for amphibolite (102017). Domain modelling has not been performed. The conclusion presented in model stage 1.2 /Sundberg et al. 2005a/, i.e. a mean coefficient of thermal expansion of $7 \cdot 10^{-6} – 8 \cdot 10^{-6}$ m/(m·K) for the different rock domains, is still valid.

6.3.4 In situ temperature

The mean in situ temperature measured at 400 m, 500 m and 600 m depth, based on 8 boreholes, is estimated at 10.5°C, 11.6°C, and 12.8°C respectively. The uncertainties reported in model stage 2.1 /SKB 2006b/ regarding the quality of in situ temperature measurements have now been identified. The mean values reported here are based on borehole loggings that are considered to be reliable.

Table 6-5. Comparison of modelling results for thermal conductivity (W/(m·K)) at the 1 m scale with previous model versions for domain RFM029.

Statistical parameter	F1.2	F2.2
Mean	3.55	3.58
Standard deviation	0.22	0.29
2.5-percentile	2.9	2.55

6.4 Uncertainty analyses

6.4.1 Data uncertainty

The main data uncertainties are described below:

Thermal conductivity and heat capacity

The TPS and SCA data for the dominant rock types and the most important subordinate rock types such as amphibolite (102017) and granodiorite to tonalite (101051) are considered to be reasonably representative. Data for some rock types may not be representative, either because they are too few or are from samples taken in groups from a short length of drill core. The latter is the case for tonalite to granodiorite (101054) and granodiorite (101056). These uncertainties are not considered to have a significant impact on the thermal model, since the rock types with less than satisfactory representativness are of minor importance within the modelled domains, or have thermal properties similar to the dominant granite.

The TPS measurements on isotropic samples are considered to be quite reliable, especially the thermal conductivity. The measurement of thermal conductivity and thermal diffusivity take different volumes into account. This has no influence on the results when the samples are isotropic. However, if the samples have thermal anisotropic behaviour, which in some degree is normally the case in the Forsmark area (foliated or lineated samples), there may be impact on the results. The largest error is assumed to be in the determination of thermal diffusivity. This has impact on the determined heat capacity that is calculated from the thermal conductivity and diffusivity from the TPS measurements. However, the heat capacity has also been determined directly by a calorimetric method. These measurements are considered to be more reliable. The uncertainty in thermal conductivity associated with SCA data is significantly larger than for TPS data.

Uncertainties are also associated with the thermal anisotropic properties of the dominant granite (lineation/foliation), mainly due to few determinations. The mean values of the thermal anisotropy factor may be quite reliable but the spatial distribution has large uncertainties.

Thermal expansion coefficient

The representativeness of samples selected for thermal expansion measurements can be questioned. The samples are few and concentrated to certain parts of the rock volume.

Temperature

In earlier model versions rather large uncertainties have been associated with the temperature loggings. In the current model version the reliability of temperature loggings has been evaluated concerning calibration error and disturbance from drilling. The uncertainties are therefore much smaller than in earlier model versions.

Boremap data

Uncertainties in the geological properties, including proportions of different rock types, of domains RFM029 and RFM045 are considered to be low /Stephens et al. 2007/. For reasons outline in Section 5.3, some boreholes were excluded from the input data to the geological simulations. The effect of this is slightly different proportions of rock types, and in the case of domain RFM045 in particular an overestimation of the size of typical amphibolite bodies.

6.4.2 Model uncertainty

Major model uncertainties

The thermal stochastic modelling, according to the strategy in Chapter 4, mainly concerns thermal conductivity. There are several uncertainties associated with the different steps of this modelling. The importance of the uncertainties differs significantly between the different steps. Some uncertainties do only have a minor effect on the result or no effect at all, whereas others are fundamental. Here, a summary is given of the five uncertainties that are believed to be most important for the results at rock domain level.

The modelling approach that was applied in Forsmark makes it possible to study each uncertainty quantitatively by varying the uncertain parameters and study the effect on the output result. However, this is a time consuming process that has not been performed due to limited resources. Therefore, the uncertainties are evaluated qualitatively, although in principle quantitative estimates could be given.

The major uncertainties are associated with:

1. the simulation scale,
2. the simulation volume,
3. the spatial statistical structure of TRCs (lithology),
4. the spatial statistical thermal models,
5. the simulation technique.

Uncertainties 3 and 4 are dependant on uncertainties associated with the representativeness of boreholes and samples, as well as lack of data.

The simulation scale

The effect of using a simulation scale of 1 m to represent subordinate rock types is not fully known. The evaluation in Section 6.2 indicates that the 1 m simulations give a too conservative estimate of the lower percentiles for rock domain RFM029 due to discretisation errors. The magnitude of this uncertainty could be quantified by performing simulations at other scales but this has not been performed due to practical limitations. A qualitative analysis of this uncertainty is however performed in Section 6.2; see the green models in the graphs for domain RFM029. The analysis indicates that for the 1 m scale, the calculated percentiles underestimate the true values due to the discretisation error for domain RFM029.

This uncertainty is believed to be the largest one of the five listed above for domain RFM029, at least for the 1 m scale. However, it is reasonable to assume that this uncertainty is more or less eliminated at the 5 m scale.

The simulation volume

The limited simulation volumes have an affect on the simulation results but the effect is not fully known. There are two situations when this could be a problem: (1) when the lithological simulation is performed at a scale so small that the true statistics of this volume deviates from the domain statistics, and (2) when the correlation lengths of thermal properties are similar to the length of the simulation volume or longer. Both these situations exist for the 0.1 m simulations for Forsmark. However, the uncertainty is small when the 0.1 m realisations are used only for upscaling of thermal conductivity to the 1 m scale for individual TRCs (the lithology is not included in this phase). On the other hand, when the lithology is included the uncertainty becomes significant during upscaling of the 0.1 m realisations. The reason is that the simulation technique makes each lithological realisation resemble the domain statistics, a situation that can be questioned for this small volume ($5\times5\times5$ m^3). The spatial variability is therefore evened out rapidly during upscaling.

These uncertainties are much smaller for the 1 m realisations because the simulation volume is larger (50×50×50 m^3). Therefore, upscaling of the 1 m realisations are more realistic. One remaining uncertainty is how well each 50×50×50 m^3 block in the rock mass in reality resembles the domain statistics, as is assumed in the lithological simulations. This uncertainty can be reduced by increasing the simulation volume.

The spatial statistical structure of TRCs (lithology)

There are several uncertainties associated with the developed models of the spatial statistical structure of the TRCs (lithology). Most of these are coupled to the lack of knowledge concerning detailed geological information, such as typical lengths of rock bodies in the three spatial directions, representativeness of the borehole information for the whole rock domain, trends in the statistics of the lithology within the rock domain etc. These uncertainties could in principle be evaluated by including different sets of soft data (expert opinion) and study the variation in output. However, no such structured analysis has been performed due to practical limitations. Instead, "best estimates" have been determined in cooperation with the geologists; see Section 5.3. Thus, potential bias in the expert knowledge is transferred to the simulations of the lithology.

Although no quantitative uncertainty analysis was performed regarding the lithology, a qualitative analysis of the statistics of different boreholes was performed; see Section 5.5.1. Geological heterogeneities within domain 29 were dealt with by dividing the domain into two sub-domains in the simulations. This is believed to have reduced the uncertainty significantly.

The proportions of each TRC in the lithological simulations deviate somewhat from the proportions of different rock types estimated as part of the modelling carried out by the geological team /Stephens et al. 2007/. TRCs with low thermal conductivities, TRC 17 and TRC 51, are slightly underestimated in domain 29, whereas for domain 45, the proportions of these TRCs appear to be overestimated. The reason for these discrepancies is that a fewer number of boreholes were used as input for the modelling of the spatial structure of TRCs compared to the geological modelling work.

Probably the most important uncertainty for the result for domain 45 is associated with how the amphibolite was modelled. In the lithological simulation of domain 45, analysis of typical lengths of amphibolite rock bodies indicate the presence of significantly larger bodies than in domain 29. One particularly long interval (c. 40 m) of amphibolite in borehole KFM06C has most certainly had a disproportionate influence on the thermal modelling results for rock domain 45. More specifically, it may have resulted in a too large lower tail of the distribution of thermal conductivity.

In addition, the anisotropy due to subordinate rock bodies is mainly a result of how the amphibolite was modelled. Limitations in the spatial statistical structure of amphibolite results in uncertainty regarding the estimated anisotropy factors.

The spatial statistical thermal models

Limited data for some TRCs result in uncertain spatial statistical thermal models. When data are few and show large variability, the shape of a distribution model cannot only be based on hard data. In addition, the low limit of thermal conductivity of a TRC is usually not known and must be determined based on expert opinion. The variogram models require more data than the distribution models. Since there is a relationship between density and thermal conductivity /Sundberg et al. 2007a/ it has been assumed that thermal conductivity exhibits a similar correlation structure as density and density data is therefore used. This is a reasonable assumption but the associated uncertainty is not known.

In spite of these uncertainties, the spatial statistical thermal conductivity models are believed to be more reliable than in previous versions of the thermal site descriptive modelling. They do not rely on any particular statistical distribution and the correlation structure is included in the model, which was not the case in previous model versions.

The heat capacity distribution has not been modelled on domain level. However, from the result of the thermal conductivity modelling and the relationship between thermal conductivity and heat capacity such a modelling can be done. Uncertainties associated with the thermal conductivity modelling are in such a case also present in the modelled heat capacity distribution. In addition, uncertainties related to the relationship between thermal conductivity and heat capacity can be included.

The simulation technique

The simulation technique is a source of uncertainty. This uncertainty is closely related to the simulation scale and the simulation volume. The advantage of this uncertainty compared to the others is that it can easily be identified. The principle is simple: The result of a simulation is compared against the input models. Deviations indicate that there is uncertainty.

This type of verification was performed both for the lithological and the thermal simulations. The conclusion is that the output resembles the input relatively well but there is not an exact match. For example, the variance in simulated thermal conductivity for a TRC is generally slightly lower than what is suggested by the input distribution (histogram). The reason is probably the restricted simulation volumes, which implies that the whole domain variance cannot be reproduced in a single realisation. However, when all realisations together are analysed the deviation from the domain statistics is smaller, but there is still a deviation, probably due to inability to reproduce variograms for small simulations volumes. Experience indicates that variograms are difficult to reproduce if simulation volumes are small /Dowd 2007/.

This uncertainty is believed to have only a minor influence on the results. To reduce the uncertainty, it would probably be necessary to increase the simulation volume and to assure that the variograms are reproduced better. However, this would probably not have any significant effect on the domain result.

6.4.3 Summing up

Most of the identified uncertainties would have a minor impact on the resulting thermal model, whereas the modelling of the amphibolite may have resulted in an excessively large lower tail of the distribution of thermal conductivity. In conclusion, the resulting models are judged to represent the modelled domain and its variability, but may overemphasise the importance of the low conductive amphibolite.

7 Conclusions

7.1 Discussion

The performed modelling has provided valuable insight into the thermal properties at Forsmark. The modelling results are more realistic and reliable than previous model versions and uncertainties are easier to identify.

The main output result of the modelling is a set of realisations that can be used for various purposes, e.g. statistical analysis and numerical temperature simulations. However, the presented approach provides almost unlimited possibilities of different types of analyses and evaluations of the domain results. Only the most straight-forward analyses have been presented in this report.

In model stage 2.1, there were still considerable uncertainties associated with the thermal models for some rock types, in particular amphibolite (102017) and granodiorite to tonalite (101051). The statistical thermal distribution models for TRC 17 and TRC 51 (dominated by amphibolite (102017) and granodiorite to tonalite (101051) respectively) used in the present modelling work are based on considerably more data, and are more robust. This is particularly important since the lower tail of the thermal conductivity distribution of a domain is largely determined by these rock types. New for stage 2.2 is that the spatial correlation within each TRC has been modelled by means of variograms, a big improvement on the approach used in previous model versions.

Some problems have been recognised. The performed modelling has indicated a problem of capturing the wide span of scales involved in the thermal modelling. Measurements are performed in the cm-dm scale, subordinate rocks with importance for the thermal modelling occur down to the dm-m scale, correlation lengths range from dm to 50 m or longer, and the domain properties may require simulation volumes of 50–100 m or more. A too large simulation scale may result in discretisation errors regarding subordinate rock types. On the other hand, if the simulation scale is too small, the simulation volume is restricted by the capacity of the computer, which may result in a too small simulation volume. This may lead to other problems, e.g. difficulty of reproducing the variogram models during simulations, underestimation of the spatial variability in the lithology, and a too large variance reduction during upscaling. The thermal modelling in Forsmark indicates that great care should be taken when the simulation scale and the simulation volume is decided.

Because of the way in which amphibolite was modelled in domain 45, the distribution of thermal conductivity has a lower tail that is conservatively low. For the forthcoming investigation phase, it is recommended that the lithological simulation of domain 45 is revised in such a way that the size of amphibolite bodies produced by simulation is not as heavily influenced by the unusually large body of amphibolite present in borehole KFM06C. To achieve this, the occurrence in borehole KFM06C may be either excluded completely from the input to the lithological simulation, or down-weighted so that its influence is more consistent with other available geological data and expert judgements.

7.2 Conclusions

The main conclusions of the thermal modelling are:

- The spatial variability of thermal properties between and within different rock types was successfully modelled. The result is a set of realisations of the thermal properties for rock domains RFM029 and RFM045 generated by stochastic simulation.
- The statistics of thermal properties at domain level are summarised in Table 6-3 and Table 6-4 for rock domains RFM029 and RFM045 respectively. The choice of scale has a profound influence on the distribution of thermal conductivity values. The variance decreases and the lower tail percentiles increase significantly as the scale of observation increases from 1 to 5 m.

  Best estimates of the 0.1 percentile of thermal conductivity are:
  – Domain RFM029: 2.30 W/(m·K) for the 1 m scale and 2.87 W/(m·K)for the 5 m scale.
  – Domain RFM045: 2.25 W/(m·K) for the 1 m scale and 2.33 W/(m·K)for the 5 m scale.
- The discretisation error of amphibolite is believed to be the largest uncertainty for the 1 m scale for domain RFM029. This error results in conservative estimates (believed to be too low) of the lower percentiles for the 1 m scale for domain RFM029. However, this uncertainty has a much smaller effect in the 5 m scale.
- Low-conductive rocks, mainly amphibolite (102017) and the tonalitic varieties of granodiorite to tonalite (101051) are decisive for the lower tail of the thermal conductivity distribution of a domain. The shape of the tail, at various scales, is therefore mainly determined by how these rock types are modelled. One of the most important uncertainties for the result for domain RFM045 is how amphibolite was modelled in the stochastic simulation of lithologies. Based on relatively limited data, the typical lengths of amphibolite rock bodies are modelled as being significantly longer than in domain RFM029. This may have resulted in a too heavy lower tail of the distribution of thermal conductivity for domain RFM045.
- In addition to the above uncertainties, the uncertainties associated with the spatial structure of TRCs (lithology) and the spatial statistical thermal models of each TRC are believed to be important.
- Evaluation of anisotropy caused by the preferred orientation of amphibolite bodies in domain 45 indicates that thermal conductivity in a direction (z”’) perpendicular to the plane (x”’-y”’) of maximum flattening of the amphibolites is lower than in other directions. The thermal conductivity is highest in the y”’-direction. For the 5 m scale, an anisotropy factor of 1.07 was calculated for the 0.1 percentile. The anisotropy factor is lower for higher percentiles. A stronger anisotropic effect is expected for scales less than 5 metres.
- Ductile deformation fabrics have also produced anisotropy in thermal conductivity (foliation and lineation). Field measurements in foliated granite within the margins of domain 29 indicate that thermal conductivity parallel to the foliation plane are higher, by a factor of approximately 1.15, than conductivity perpendicular to the foliation. Given that the penetrative deformation fabrics in most of the target volume are less intense than observed at the site of the field measurements, the degree of anisotropy in thermal properties is expected to be generally lower in the greater part of the target volume.
- The temperature increase with depth is now well established. The mean in situ temperature at 400 m, 500 m and 600 m depth is estimated at 10.5°C, 11.6°C, and 12.8°C respectively.
- The mean thermal expansion coefficient for the dominant granitoid rock types within the target volume varies between $7.5 \cdot 10^{-6}$ and $7.8 \cdot 10^{-6}$ m/(m·K).

References

Aarts E, Korst J, 1989. Simulated annealing and Boltzmann machines: John Wiley & Sons, New York.

Adl-Zarrabi B, 2003. Determination of thermal properties by the TPS-method. SKB P-03-08, Svensk Kärnbränslehantering AB.

Adl-Zarrabi B, 2004a. Drill hole KFM01A Thermal properties: heat conductivity and heat capacity determined using the TPS method and mineralogical composition by modal analysis. SKB P-04-159, Svensk Kärnbränslehantering AB.

Adl-Zarrabi B, 2004b. Drill hole KFM02A Thermal properties: heat conductivity and heat capacity determined using the TPS method and mineralogical composition by modal analysis. SKB P-04-161, Svensk Kärnbränslehantering AB.

Adl-Zarrabi B, 2004c. Drill hole KFM03A Thermal properties: heat conductivity and heat capacity determined using the TPS method and mineralogical composition by modal analysis. SKB P-04-162, Svensk Kärnbränslehantering AB.

Adl-Zarrabi B, 2004d. Drill hole KFM04A Thermal properties: heat conductivity and heat capacity determined using the TPS method and mineralogical composition by modal analysis. SKB P-04-199, Svensk Kärnbränslehantering AB.

Adl-Zarrabi B, 2005a. Forsmark site investigation. Drill hole KFM06A. Thermal properties: heat conductivity and heat capacity determined using the TPS method. SKB P-05-123, Svensk Kärnbränslehantering AB.

Adl-Zarrabi B, 2005b. Forsmark site investigation. Borehole KFM07A. Thermal conductivity and thermal diffusivity determined using TPS method. SKB P-05-214, Svensk Kärnbränslehantering AB.

Adl-Zarrabi B, 2006a. Forsmark site investigation. Borehole KFM08A. Thermal conductivity and thermal diffusivity determined using the TPS method. SKB P-05-219, Svensk Kärnbränslehantering AB.

Adl-Zarrabi B, 2006b. Forsmark site investigation. Borehole KFM01C. Thermal properties of rocks using calorimeter and TPS method. SKB P-06-66, Svensk Kärnbränslehantering AB.

Adl-Zarrabi B, 2006c. Forsmark site investigation. Borehole KFM01A, KFM01C, KFM01D, KFM04A, KFM05A, KFM06A and KFM09A. Thermal properties of rocks using calorimeter and TPS method, and mineralogical composition by modal analysis. SKB P-06-233, Svensk Kärnbränslehantering AB.

Back P-E, Sundberg J, 2007. Thermal Site Descriptive Model. A Strategy for the Model Development during Site Investigations. Version 2.0. SKB R-07-42, Svensk Kärnbränslehantering AB. (In press)

Carle S F, 1997. Implementation schemes for avoiding artefact discontinuities in simulated annealing: Mathematical Geology, v. 29, no. 2, p. 231–244.

Carle S F, 1999. T-PROGS: Transition Probability Geostatistical Software. Version 2.1. Hydrologic Sciences Graduate Group. University of California, Davis.

Carle S F, Fogg G E, 1997. Modeling spatial variability with one- and multi-dimensional Markov chains: Mathematical Geology, v. 29, no. 7, 891–918.

Carlsten S, Gustafsson J, Mattsson H, Petersson J, Stephens M, 2005. Geological single-hole interpretation of KFM06A and KFM06B. SKB R-05-132, Svensk Kärnbränslehantering AB.

Deutsch C V, Cockerham P W, 1994. Practical considerations in the application of simulated annealing in stochastic simulation: Math. Geology, v. 26, no. 1, p. 67–82.

Deutsch C, Journel A, 1998. GS-LIB: Geostatistical Software Library and User´s Guide. Second edition. Oxford University Press, New York.

Dowd P A, 2007. University of Adelaide. Personal communication.

GMS (Groundwater Modeling System), 2006. Tutorials, Volume 1. Ver 6.0. Environmental Modeling Research Laboratory. Brigham Young University. USA.

Horai K, 1971. Thermal conductivity of rock-forming minerals. J. Geophys. Res. 76, p. 1,278–1,308.

Horai, Baldridge, 1972. Thermal conductivity of nineteen igneous rocks. Application of the needle probe method to the measurement of the thermal conductivity of rock. Estimation of the thermal conductivity of rock from the mineral and chemical compositions. Phys. Earth Planet. Interiors 5, p. 151.

Isaaks E, Srivastava M, 1989. An Introduction to Applied Geostatistics. Oxford University Press, New York

Johansson P-O, Werner K, Bosson E, Berglund S, Juston J, 2005. Description of climate, surface hydrology, and near-surface hydrogeology. Preliminary site description Forsmark area – version 1.2. SKB R-05-06, Svensk Kärnbränslehantering AB.

Journel A G, Huijbregts C J, 1978. Mining geostatistics. Academic Press, London.

Lau P, 2007. Drill holes KFM01A, KFM07A and KFM08A. Specific heat capacity of rocks using calorimetric measurements. Forsmark site investigation. SKB P-07-19, Svensk Kärnbränslehantering AB.

Mattsson H, Keisu M, 2004. Interpretation of borehole geophysical measurements in KFM04A, KFM06A (0–100 m), HFM10, HFM11, HFM12, HFM13, HFM16, HFM17 and HFM18. SKB P-04-143, Svensk Kärnbränslehantering AB.

Mattsson H, Keisu M, 2005. Interpretation of borehole geophysical measurements from KFM08A and KFM08B. SKB P-05-202, Svensk Kärnbränslehantering AB.

Mattsson H, Thunehed H, Keisu M, 2004. Interpretation of borehole geophysical measurements in KFM01A, KFM01B, HFM01, HFM02 and HFM03. SKB P-04-80, Svensk Kärnbränslehantering AB.

Munier R, Stenberg L, Stanfors R, Milnes A G, Hermanson J, Triumf C-A, 2003. Geological Site Descriptive Model. A strategy for the model development during site investigations. SKB R-03-07, Svensk Kärnbränslehantering AB.

Norberg T, Rosén L, Baran Á, and Baran S, 2002. On modelling discrete geological structures as Markov random fields. Mathematical Geology, 34(1), 63–77.

Olofsson I, Simeonov A, Stigsson M, Stephens M, Follin S, Nilsson A-C, Röshoff K, Lindberg U, Lanaro F, Fredriksson A, Persson L, 2007. Site descriptive modelling Forsmark, stage 2.2. A fracture domain concept as a basis for the statistical modelling of fractures and minor deformation zones, and interdisciplinary coordination. SKB R-07-15, Svensk Kärnbränslehantering AB.

Petersson J, Berglund J, Danielsson P, Wängnerud A, Tullborgh E-L, Mattsson H, Thunehed H, Isaksson H, Lindroos H, 2004a. Forsmark site investigation. Petrography, geochemistry, petrophysics and fracture mineralogy of boreholes KFM01A, KFM02A and KFM03A+B. SKB P-04-103, Svensk Kärnbränslehantering AB.

Petersson J, Berglund J, Wängnerud A, Danielsson P, Stråhle A, 2004b. Forsmark site investigation. Boremap mapping of telescopic drilled borehole KFM05A. SKB P-04-295, Svensk Kärnbränslehantering AB.

Petersson J, Berglund J, Danielsson P, Skogsmo G, 2005a. Forsmark site investigation. Petrographic and geochemical characteristics of bedrock samples from boreholes KFM04A-06A, and a whitened alteration rock. SKB P-05-156, Svensk Kärnbränslehantering AB.

Petersson J, Skogsmo G, Wängnerud A, Berglund J, Stråhle A, 2005b. Forsmark site investigation. Boremap mapping of telescopic drilled borehole KFM07A. SKB P-05-102, Svensk Kärnbränslehantering AB.

Petersson J, Skogsmo G, Berglund J, Wängnerud A, Stråhle A, 2005c. Forsmark site investigation. Boremap mapping of telescopic drilled borehole KFM06A and core drilled borehole KFM06B. SKB P-05-101, Svensk Kärnbränslehantering AB.

Petersson J, Skogsmo G, Berglund J, von Dalwigk I, Wängnerud A, Danielsson P, Stråhle A, 2006. Forsmark site investigation. Boremap mapping of telescopic drilled borehole KFM06C. SKB P-06-79, Svensk Kärnbränslehantering AB.

Rosén L, Gustafson G, 1995a. A Bayesian Markov Geostatistical Model for Canister Positioning in a Nuclear Waste Repository. Proceedings to IAH SOLUTIONS ’95 Conference. Edmonton, Alberta, Canada, June 4–10, 1995. 8 p.

Rosén L, Gustafson G, 1995b. Suitable Nearfield Design. Stage 2. Provisional Positioning Index (PPI) Predictions with respect to Lithology, Hydraulic Conductivity and Rock Designation Index along the TBM-tunnel. SKB PR 25-95-19, Svensk Kärnbränslehantering AB.

Rosen L, Gustafson G, 1996. A Bayesian Markov Geostatistical Model for Estimating Hydrogeological Properties. Ground Water, Vol. 34, No. 5, p. 865–875.

Sandström B, Tullborg E-L, 2006. Mineralogy, geochemistry, porosity and redox capacity of altered rock adjacent to fractures. Forsmark site investigation. SKB P-06-209, Svensk Kärnbränslehantering AB.

Sandström B, 2006. Personal communication. Göterborgs Universitet.

SKB 2002. Forsmark – site descriptive model version 0. SKB R-02-32, Svensk Kärnbränslehantering AB.

SKB 2004. Preliminary site description Forsmark area–version 1.1. SKB R-04-15, Svensk Kärnbränslehantering AB.

SKB, 2005a. Preliminary site description, Forsmark area – version 1.2. SKB R-05-18 (Updated 2005-11-09), Svensk Kärnbränslehantering AB.

SKB 2005b. Preliminary safety evaluation for the Forsmark area. Based on data and site descriptions after the initial site investigation stage. SKB TR-05-16, Svensk Kärnbränslehantering AB.

SKB 2005c. Programme for further investigations of geosphere and biosphere. Forsmark site investigation, SKB R-05-14, Svensk Kärnbränslehantering AB.

SKB 2006a. Long-term safety for KBS-3 repositories at Forsmark and Laxemar – a first evaluation. Main Report of the SR-Can project, SKB TR-06-09, Svensk Kärnbränslehantering AB.

SKB, 2006b. Site descriptive modelling Forsmark stage 2.1. Feedback for completion of the site investigation including input from safety assessment and repository engineering, SKB R-06-38, Svensk Kärnbränslehantering AB.

Stenberg L, 2006. Personal communication. Svensk Kärnbränslehantering AB.

Stephens M B, Lundqvist S, Bergman, T Andersson J, Ekström M, 2003. Bedrock mapping. Rock types, their petrographic and geochemical characteristics, and a structural analysis of the bedrock based on Stage 1 (2002) surface data. SKB P-03-75, Svensk Kärnbränslehantering AB.

Stephens M B, Lundqvist S, Bergman T, Ekström M, 2005. Bedrock mapping – Petrographic and geochemical characteristics of rock types based on stage 1 (2002) and stage 2 (2003) surface data. Forsmark site investigation. SKB P-04-87, Svensk Kärnbränslehantering AB.

Stephens M B, 2007. Personal communication. Sveriges geologiska undersökning (SGU).

Stephens M B, Fox A, Isaksson H, Öhman J, Simeonov A, 2007. Geology – Site descriptive modelling, Forsmark stage 2.2. SKB R-07-45 (in prep), Svensk Kärnbränslehantering AB.

Sundberg J, 1988. Thermal Properties of Soils and Rocks. Publ. A 57, Dissertation. Geologiska institutionen, Chalmers University of Technology, and University of Göteborg.

Sundberg J, 2003. A strategy for the model development during site investigations version 1.0. SKB R-03-10, Svensk Kärnbränslehantering AB.

Sundberg J, 2003b. Thermal properties at Äspö HRL. Analysis of distribution and scale factors. SKB R-03-17, Svensk Kärnbränslehantering AB, Stockholm, Sweden.

Sundberg J, Back P, Bengtsson A, Ländell M, 2005a. Thermal modelling. Preliminary site description Forsmark area – version 1.2. SKB R-05-31, Svensk Kärnbränslehantering AB.

Sundberg J, Back P-E, Hellström G, 2005b. Scale dependence and estimation of rock thermal conductivity. SKB R-05-82, Svensk Kärnbränslehantering AB.

Sundberg J, Back P-E, Ericsson L O, Wrafter J, 2007a. A method for estimation of thermal conductivity and its spatial variability in igneous rocks from in situ density logging. (Submitted to International Journal of Rock Mechanics and Mining Sciences, Elsevier)

Sundberg J, Wrafter J, Sundberg A, 2007b. Forsmark site investigation. Anisotropy of thermal properties in granite at Forsmark. Large-scale field measurements and comparison with small-scale field measurements and laboratory measurements. SKB P-07-194, Svensk Kärnbränslehantering AB.

Thunehed H, 2004. Interpretation of borehole geophysical measurements in KFM02A, KFM03A, KFM03B and HFM04 to HFM08. SKB P-04-98, Svensk Kärnbränslehantering AB.

Thunehed H, Keisu M, 2004. Interpretation of borehole geophysical measurements in KFM05A, HFM14, HFM15 and HFM19. SKB P-04-154, Svensk Kärnbränslehantering AB.

Wrafter J, Sundberg J, Ländell M, Back P, 2006. Thermal modelling. Site descriptive modelling. Laxemar 2.1. SKB R-06-84, Svensk Kärnbränslehantering AB.

Appendix A

Domain realisations of simulated TRCs (geology)

In this appendix, example realisations are presented in 2D for simulation scales 0.1 m and 1 m for rock domain RFM029 and RFM045. All 2D-realisations represent a slice in the centre of a 3D cube. For example, the 25th slice of the xy-plane is the 25th slice that can be cut in the z-direction (there are 50 slices).

Two realisations are presented for each type of simulation and direction.

Domain RFM029, 0.1 m scale

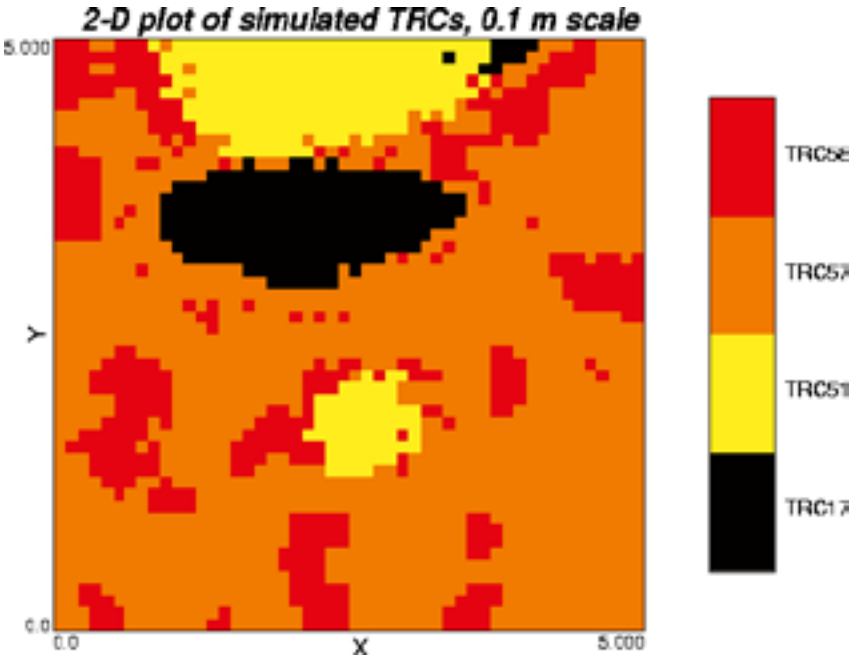

Domain RFM029, Realisation = 1, Slice = 25, xy-plane

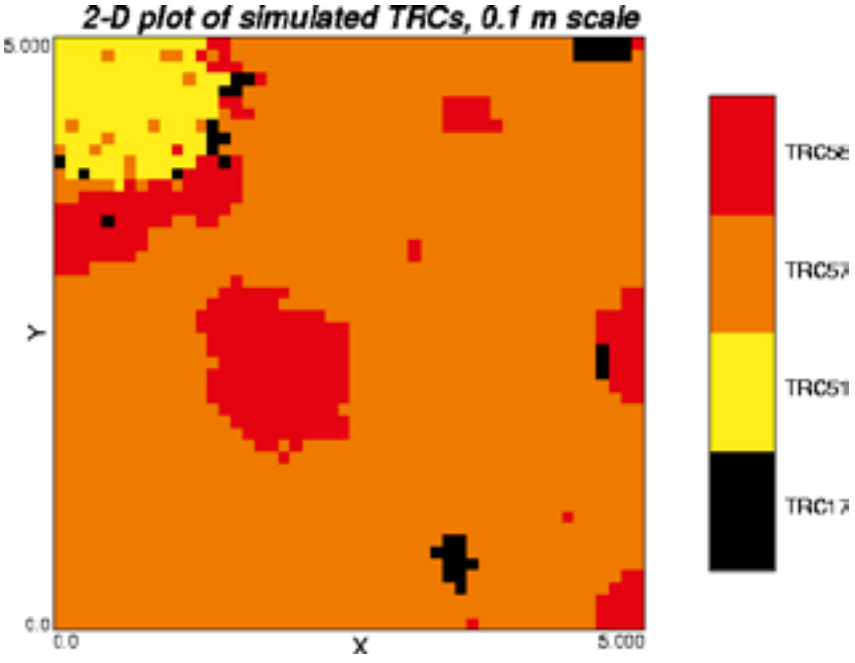

Domain RFM029, Realisation = 150, Slice = 25, xy-plane

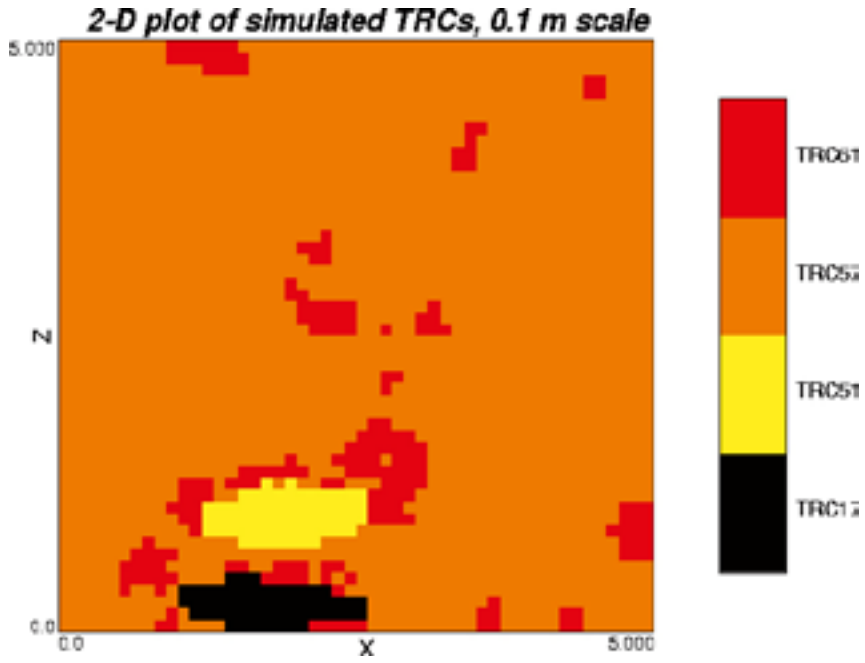

Domain RFM029, Realisation = 1, Slice = 25, xz-plane

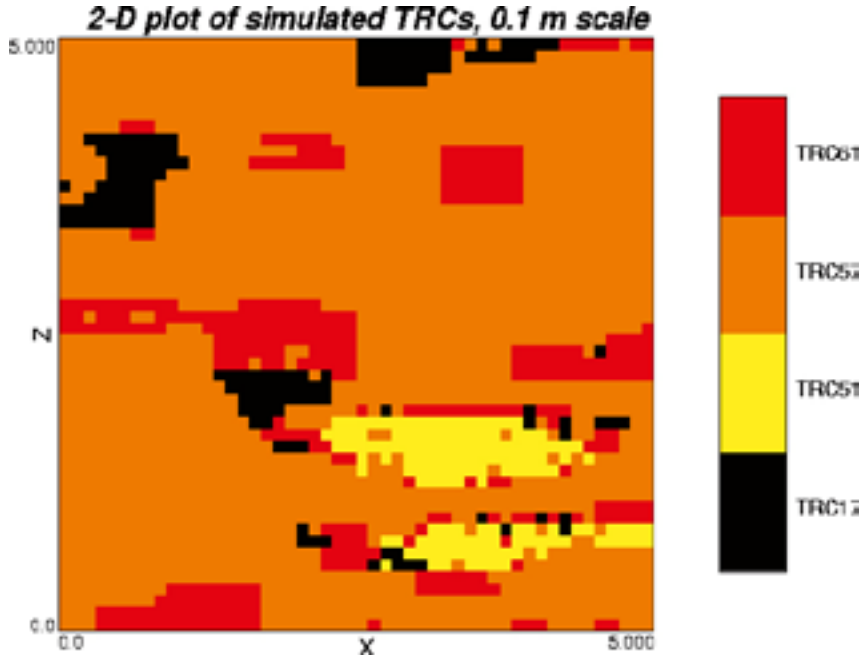

Domain RFM029, Realisation = 150, Slice = 25, xz-plane

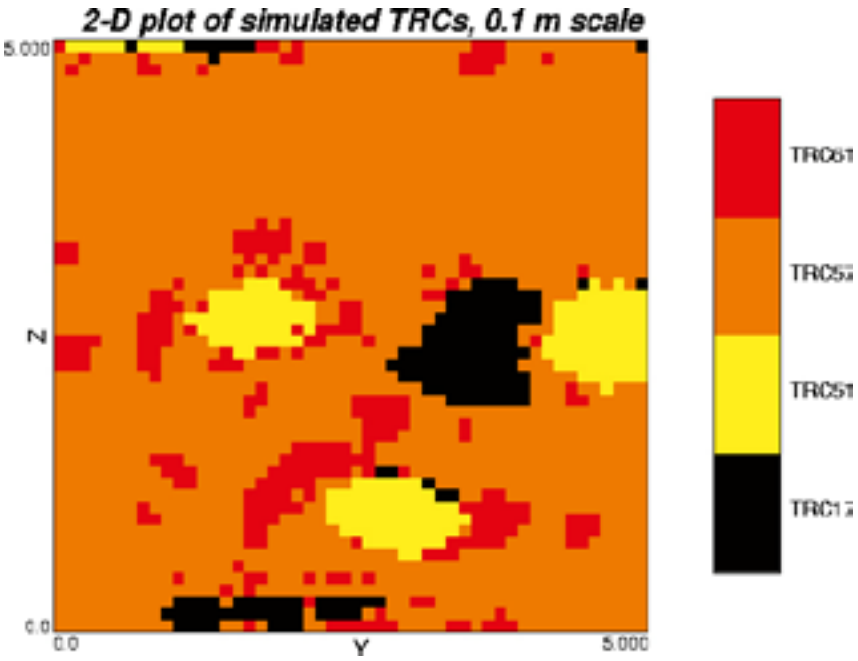

Domain RFM029, Realisation = 1, Slice = 25, yz-plane

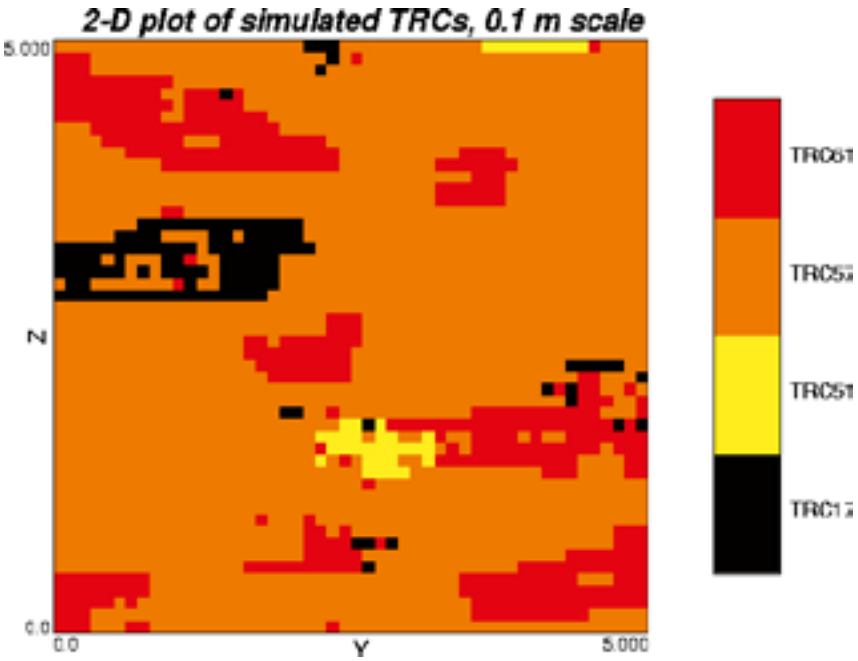

Domain RFM029, Realisation = 150, Slice = 25, yz-plane

Domain RFM029, 1 m scale

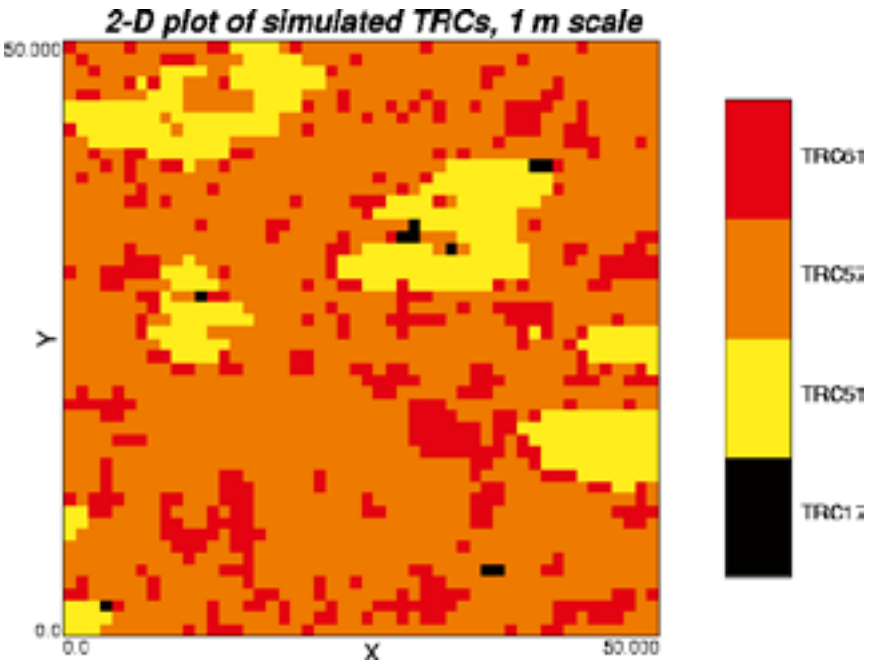

Domain RFM029, Realisation = 1, Slice = 25, xy-plane

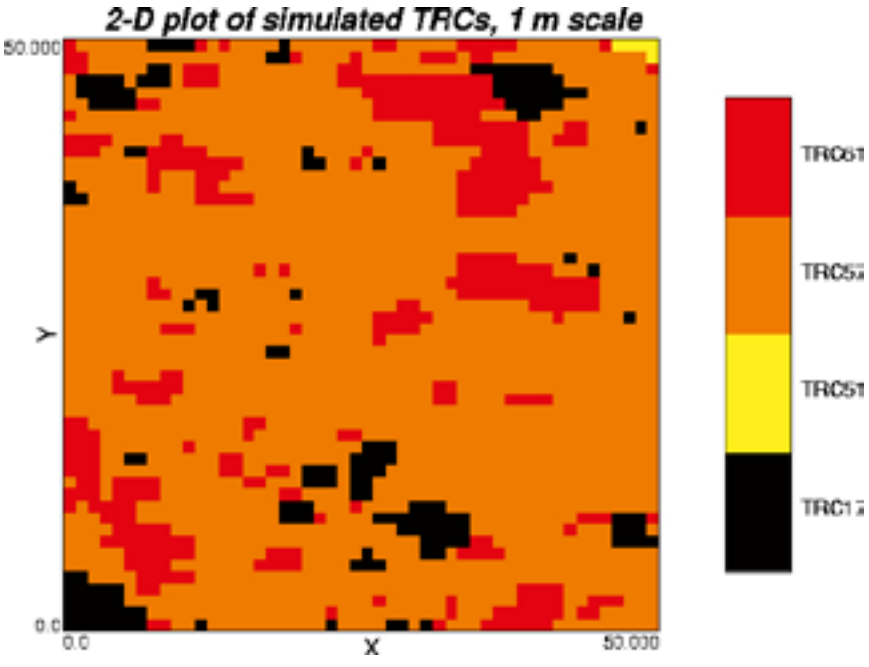

Domain RFM029, Realisation = 1,000, Slice = 25, xy-plane

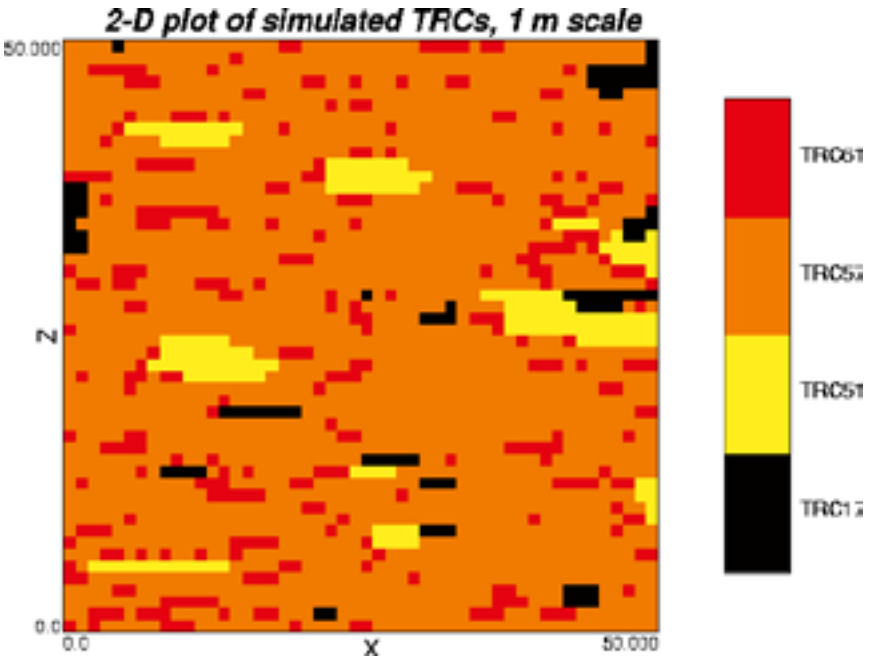

Domain RFM029, Realisation = 1, Slice = 25, xz-plane

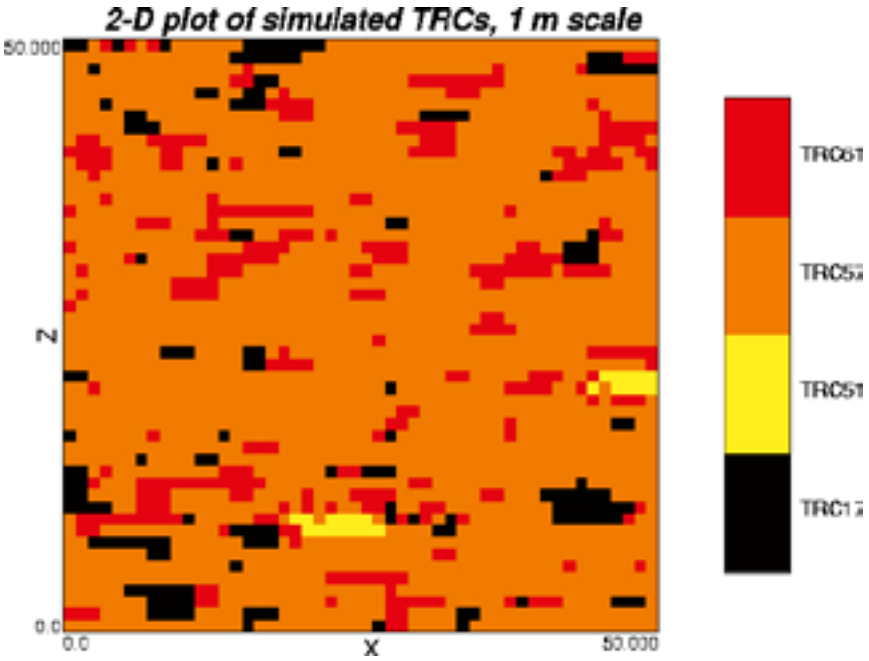

Domain RFM029, Realisation = 1,000, Slice = 25, xz-plane

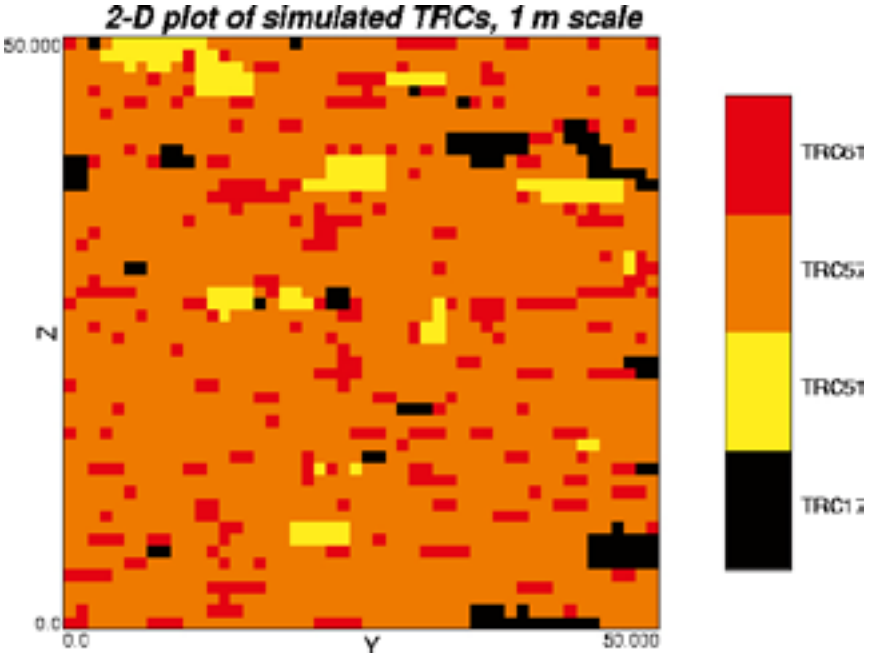

Domain RFM029, Realisation = 1, Slice = 25, yz-plane

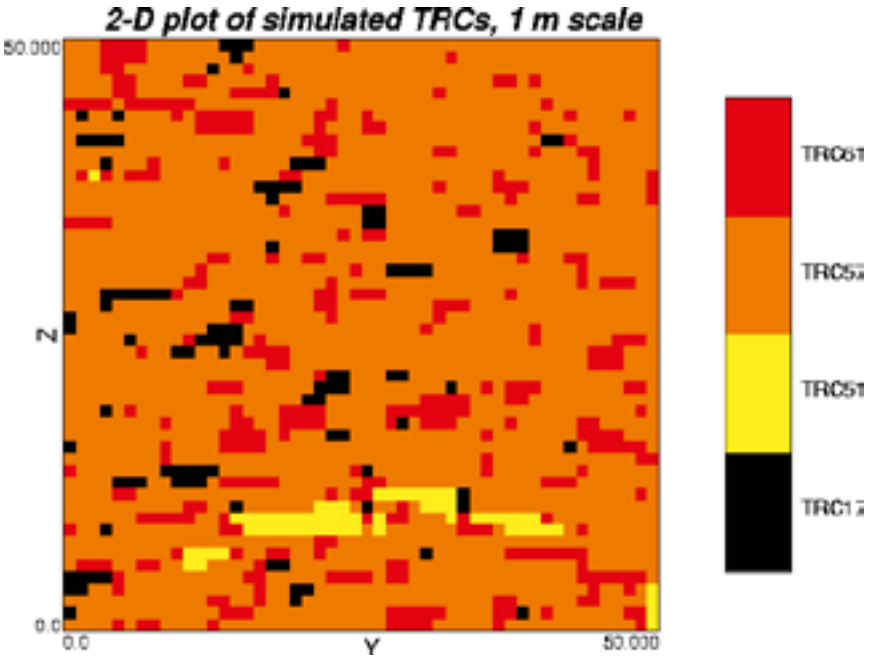

Domain RFM029, Realisation = 1,000, Slice = 25, yz-plane

Domain RFM045, 0.1 m scale

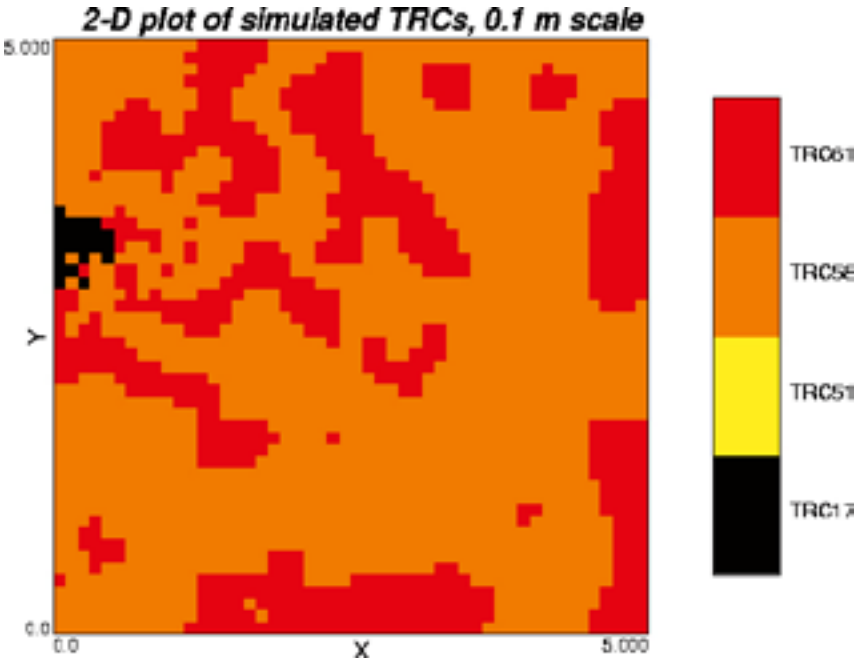

Domain RFM045, Realisation = 1, Slice = 25, xy-plane

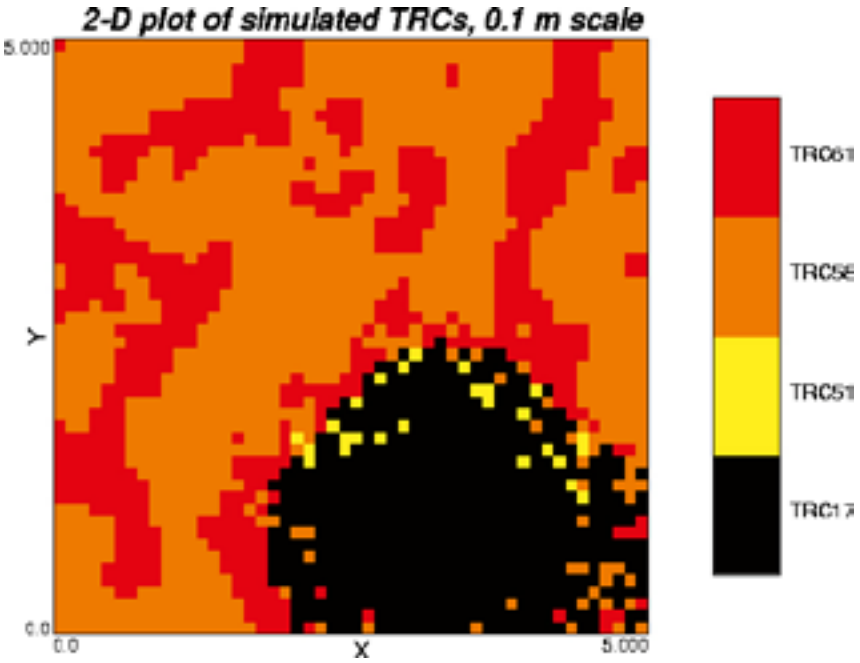

Domain RFM045, Realisation = 100, Slice = 25, xy-plane

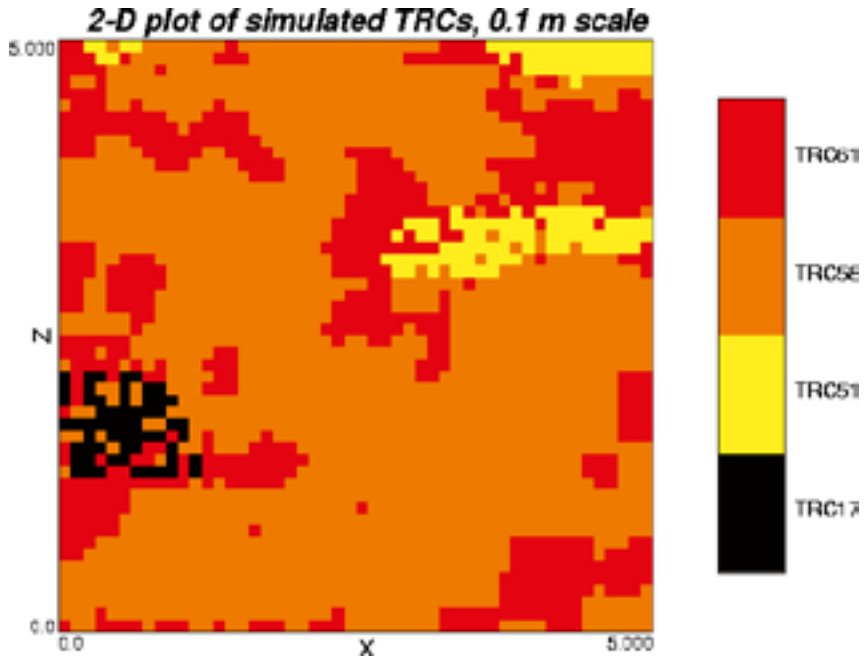

Domain RFM045, Realisation = 1, Slice = 25, xz-plane

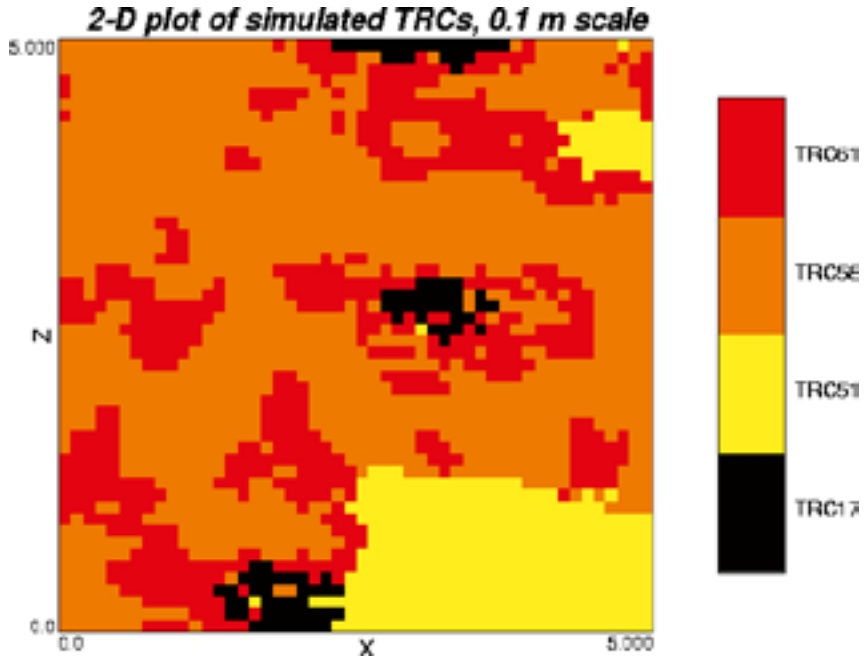

Domain RFM045, Realisation = 100, Slice = 25, xz-plane

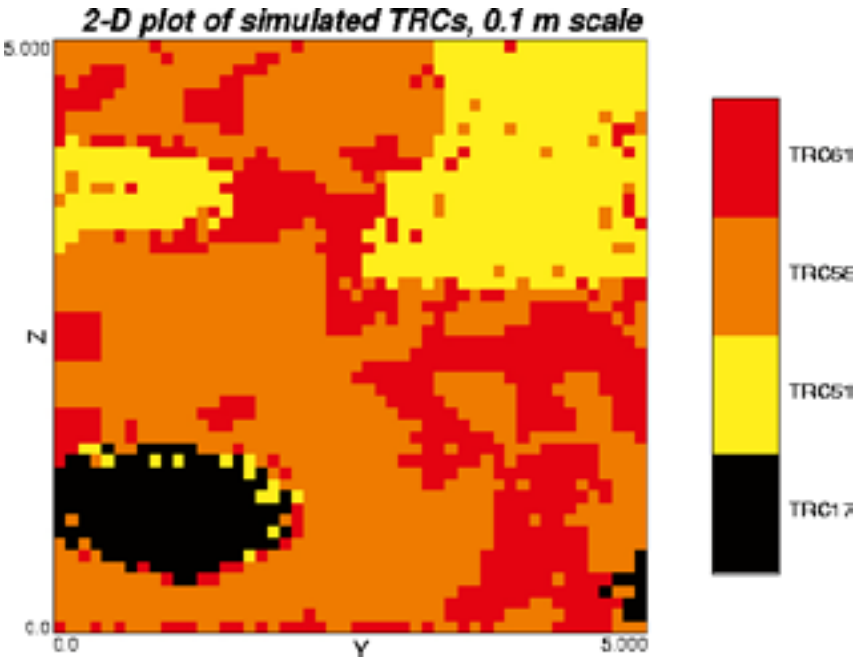

Domain RFM045, Realisation = 1, Slice = 25, yz-plane

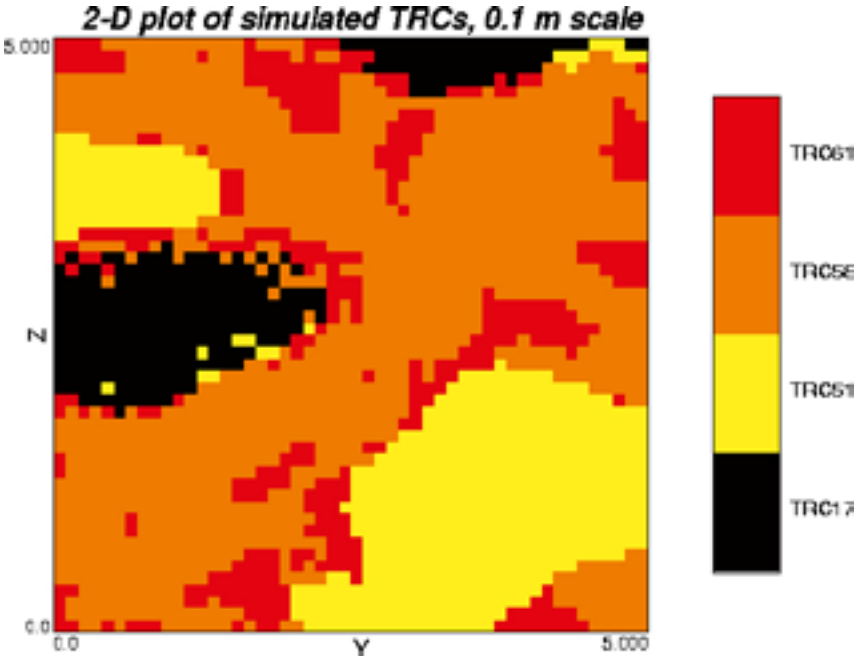

Domain RFM045, Realisation = 100, Slice = 25, yz-plane

Domain RFM045, 1 m scale

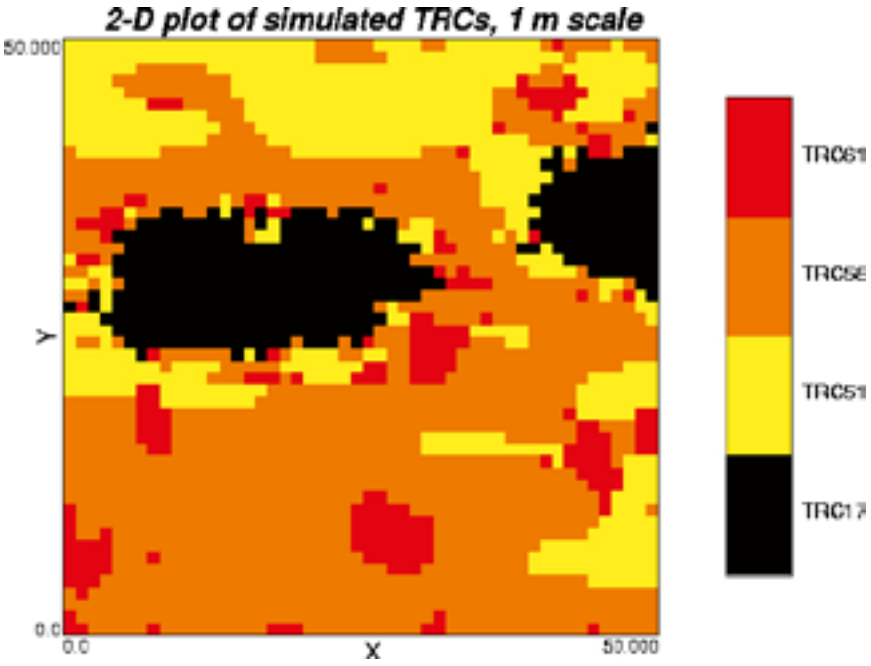

Domain RFM045, Realisation = 1, Slice = 25, xy-plane

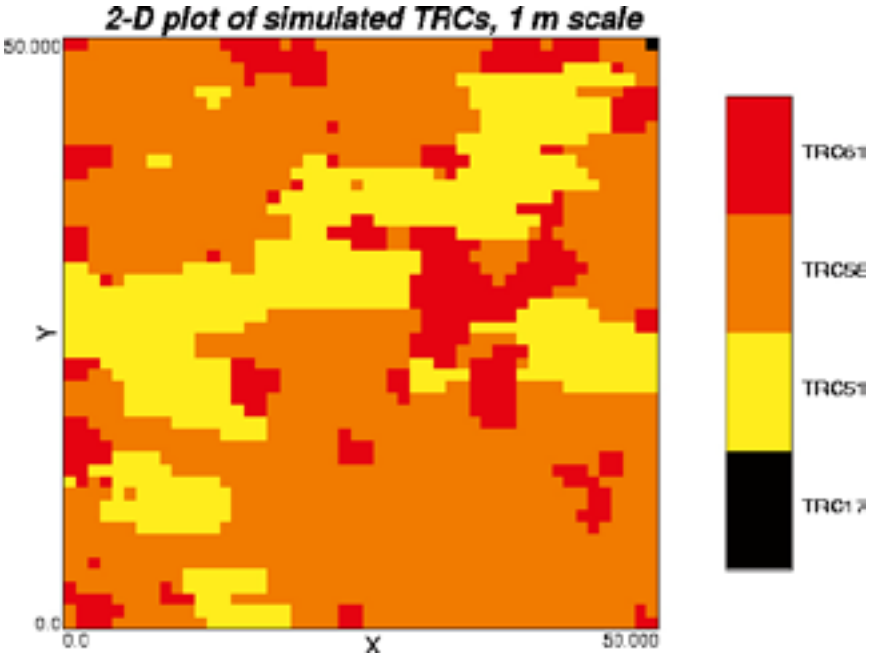

Domain RFM045, Realisation = 400, Slice = 25, xy-plane

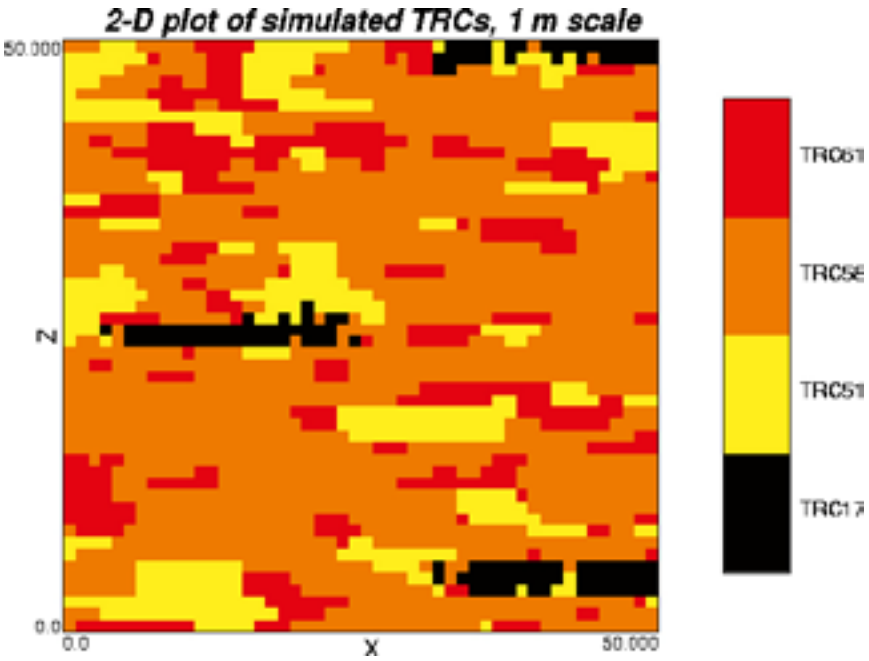

Domain RFM045, Realisation = 1, Slice = 25, xz-plane

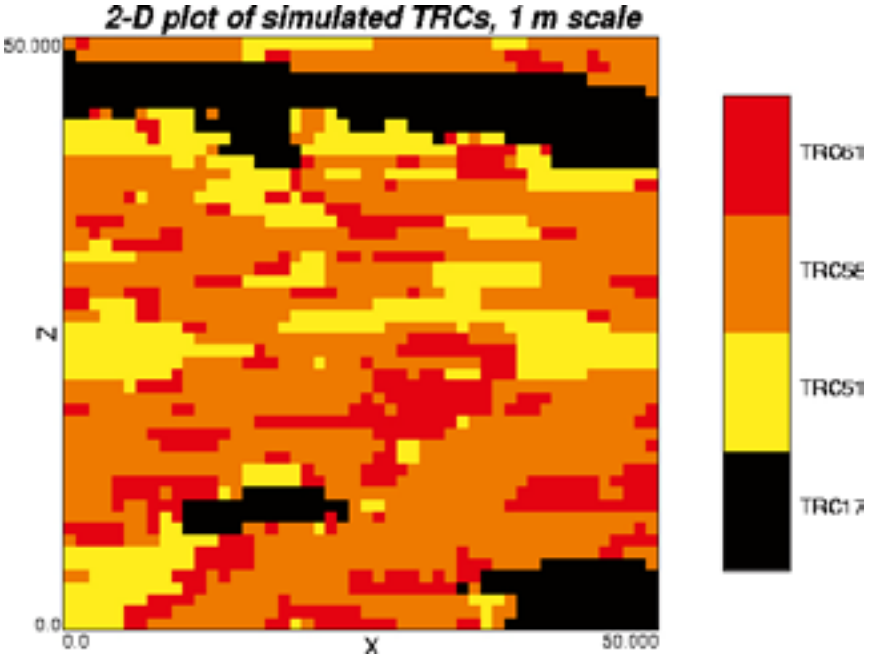

Domain RFM045, Realisation = 400, Slice = 25, xz-plane

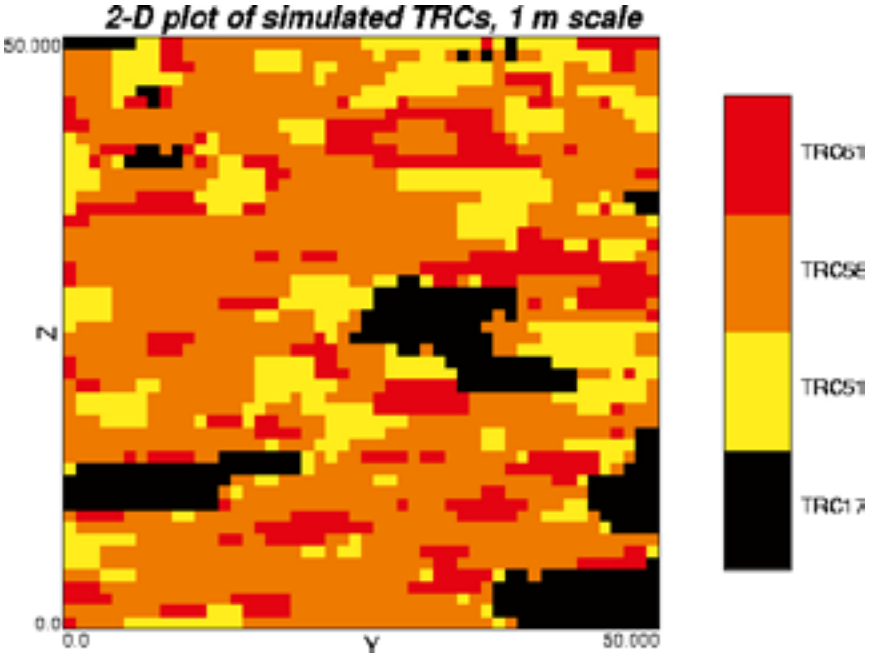

Domain RFM045, Realisation = 1, Slice = 25, yz-plane

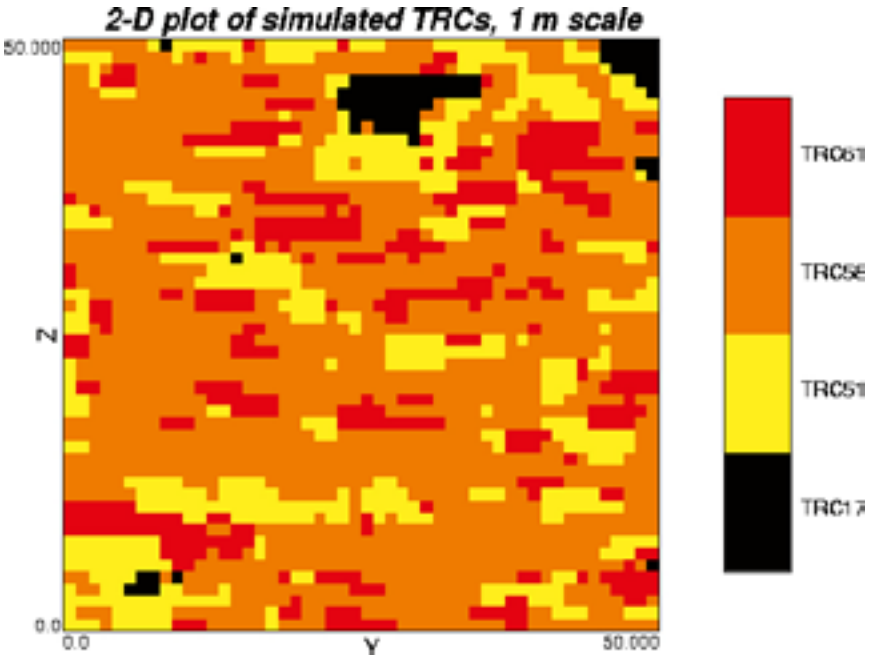

Domain RFM045, Realisation = 400, Slice = 25, yz-plane

Appendix B

Simulations of geology 1 dm scale – validation of results

Results 1 dm simulations domain 029 internal

Proportions

Table B-1 shows the proportions of TRCs in 10 randomly selected realisations for domain RFM029 internal.

As can be seen from Table B-1 T-PROGS nearly exactly reproduces the proportions of the TRCs for all realisations.

Typical lengths

Calculations of typical lengths of TRCs 17, 51 and 61 were made from "borings" through 10 randomly selected realisations for domain RFM029 internal. TRC 57 constitutes the "background" in the simulations and is therefore not relevant to include in the analysis.

The typical lengths of the TRCs in the data obtained from the "borings" were calculated by transition probability analysis. The results of the calculations of the typical length m for directions x, y and z are presented in Table B-2, Table B-3 and Table B-4. The confidence interval is given for each calculation and a comparison is made with the nominal value calculated from borehole data (KFM05A).

Table B-1. Proportions of TRCs in 10 randomly selected realisations for domain RFM029 internal.

Category	Proportions from borehole (%)	Proportions in realisation no. (%)									
		2	6	15	26	29	44	51	60	61	88
TRC17	5.4	5.4	5.6	5.8	5.5	5.6	5.7	5.4	5.8	5.7	5.7
TRC51	5.6	5.9	5.9	6.3	5.9	5.9	5.9	5.9	6	6.2	6.1
TRC57	80.5	80	79.8	79	79.9	79.9	79.5	80.1	79.5	79.3	79.5
TRC61	8.5	8.6	8.7	8.9	8.7	8.6	8.9	8.6	8.7	8.8	8.7

Table B-2. Typical lengths for TRC17.

Typical length (dm)	Nominal value (dm)	Comment to simulated values
μ_x = 3.50 ± 1.32	12.6	Low
μ_y = 4.67 ± 1.58	6.3	OK
μ_z = 3.10 ± 0.64	3.2	OK

Table B-3. Typical lengths for TRC51.

Typical length (dm)	Nominal value (dm)	Comment to simulated values
μ_x = 4.19 ± 2.08	30.4	Low
μ_y = 5.57 ± 2.22	15.2	Low
μ_z = 4.83 ± 1.16	7.6	Low

Table B-4. Typical lengths for TRC61.

Typical length (dm)	Nominal value (dm)	Comment to simulated values
μ_x = 2.83 ± 0.35	2.6	OK
μ_y = 2.82 ± 0.33	2.6	OK
μ_z = 2.87 ± 0.33	0.8	High

As can be seen from the analysis, T-PROGS does not reproduce the typical lengths and anisotropy of TRCs as well for decimetre data as it does for metre data. Longer lengths are typically underestimated and shorter lengths typically overestimated. In addition, the confidence intervals are higher (in relative terms) than for 1 metre data.

The reasons for these results have not been analyzed in detail, but may partly be due to nominal (input) lengths in some cases (especially for TRC51) being relatively long compared to the model dimensions (5 metres). This might cause boundary effects that restrict the ability to reproduce anisotropy. Another possible, but less likely reason is the fact that the T-PROGS algorithm does not accept nominal length values shorter than 0.25 metres, which made it necessary to use a higher input value for TRC61 in the z-direction than was calculated in the transition probability analysis.

Lengths

From 49×3 = 147 borings in each of 10 randomly selected realisations histograms were prepared for each TRC in x, y and z-directions. The results are shown in Figure B-1 to Figure B-12.

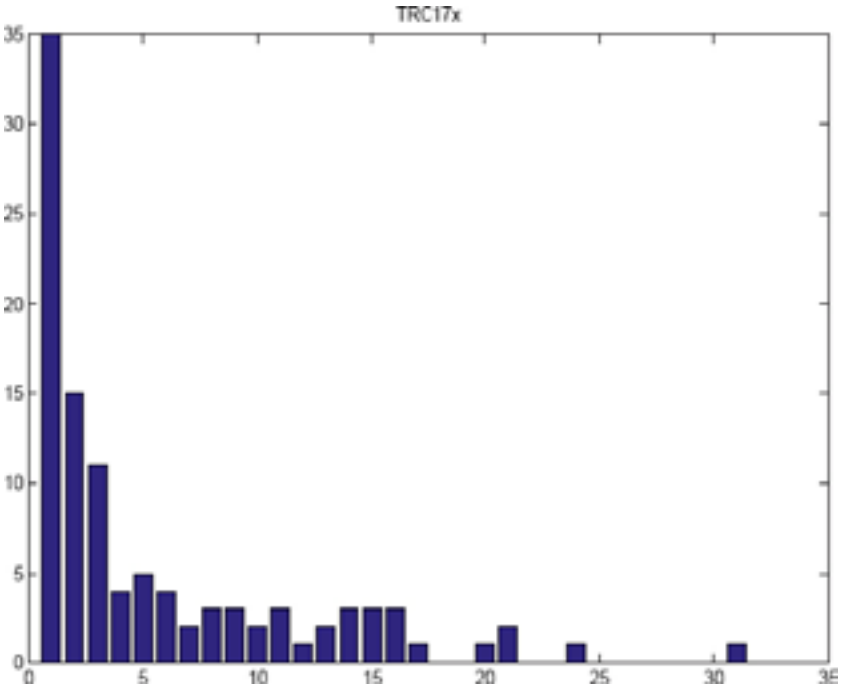

Figure B-1. *Histogram of TRC 17 in x-direction (x-axis in decimetres).*

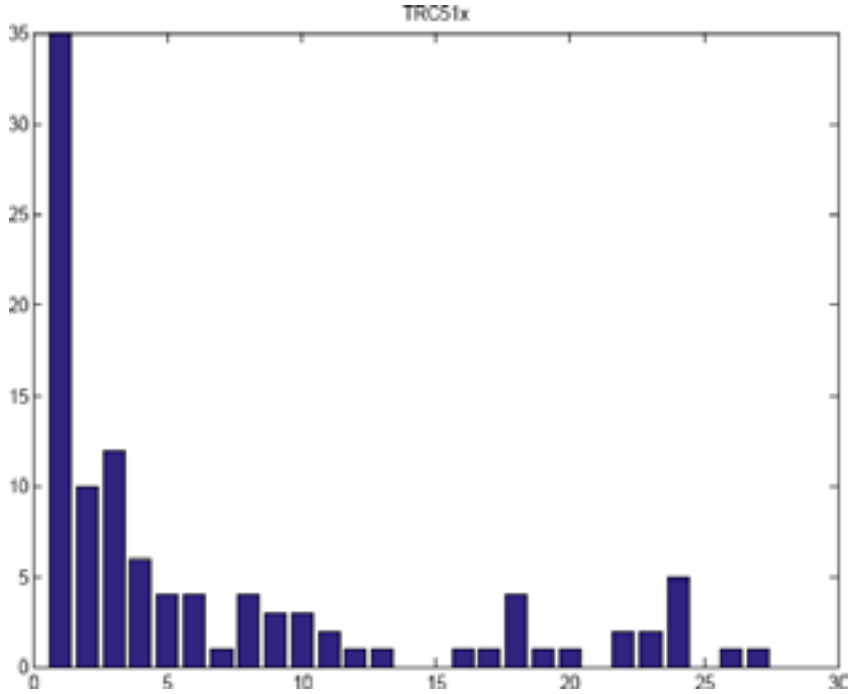

Figure B-2. *Histogram of TRC 51 in x-direction (x-axis in decimetres).*

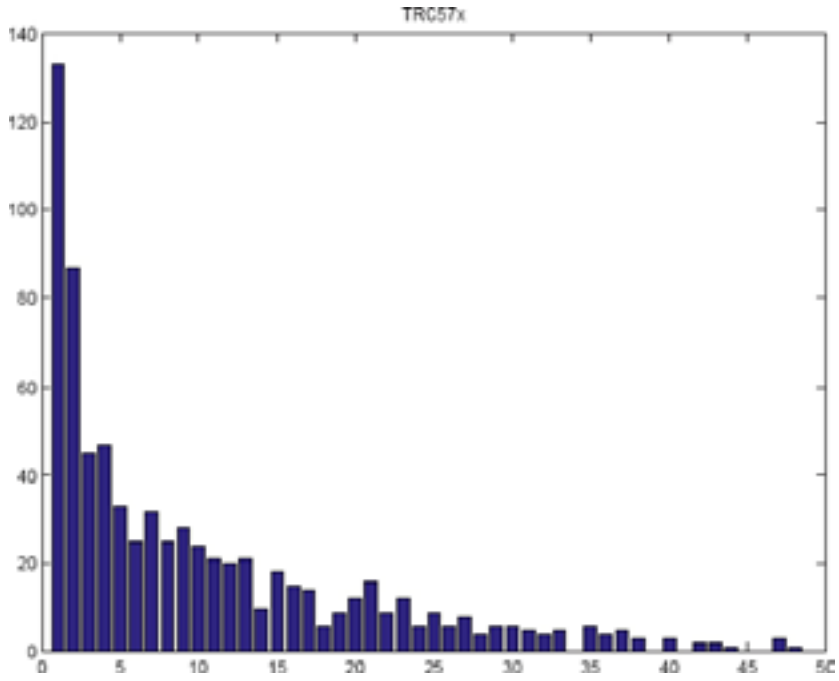

Figure B-3. *Histogram of TRC 57 in x-direction (x-axis in decimetres).*

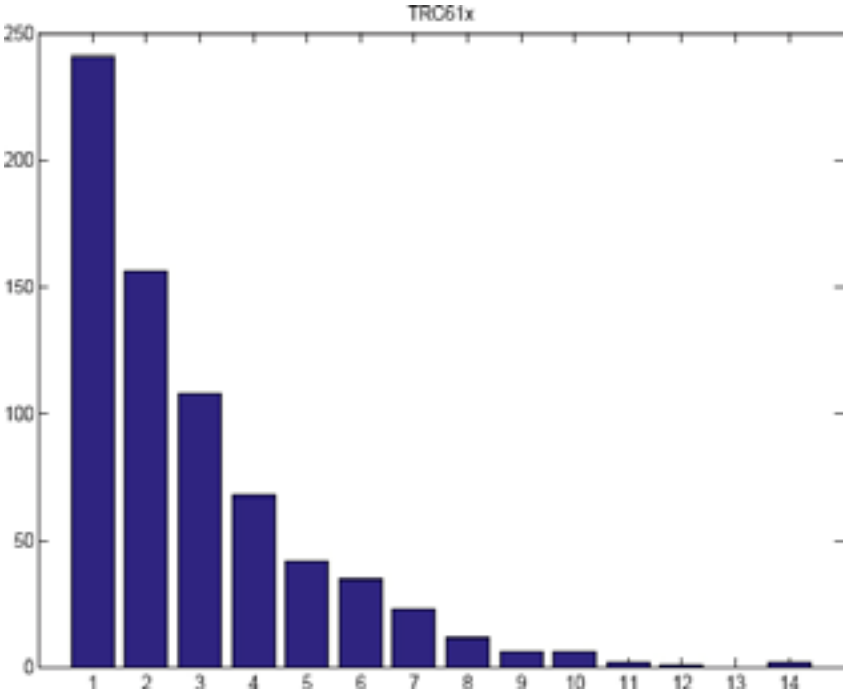

Figure B-4. *Histogram of TRC 61 in x-direction (x-axis in decimetres).*

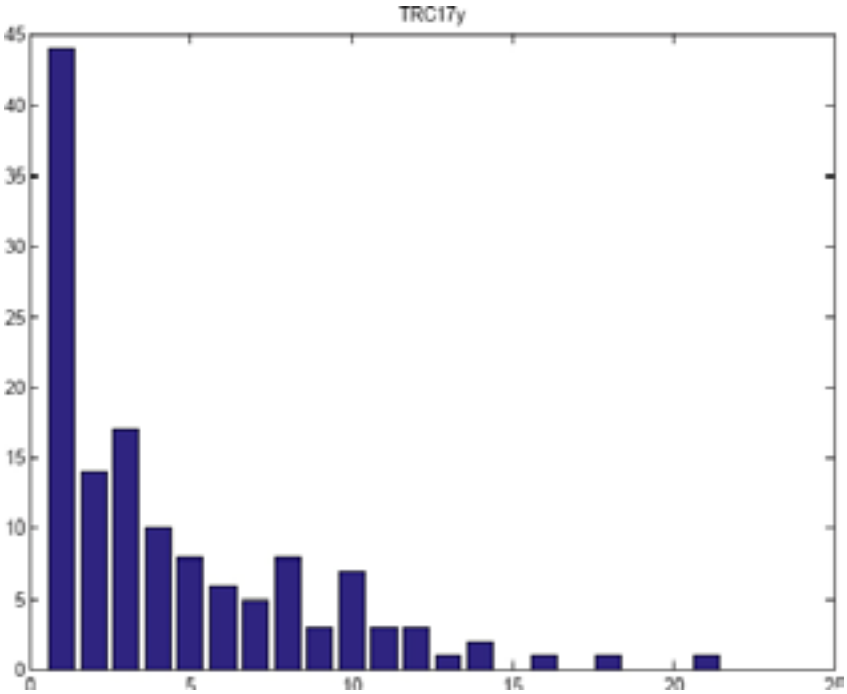

Figure B-5. *Histogram of TRC 17 in y-direction (x-axis in decimetres).*

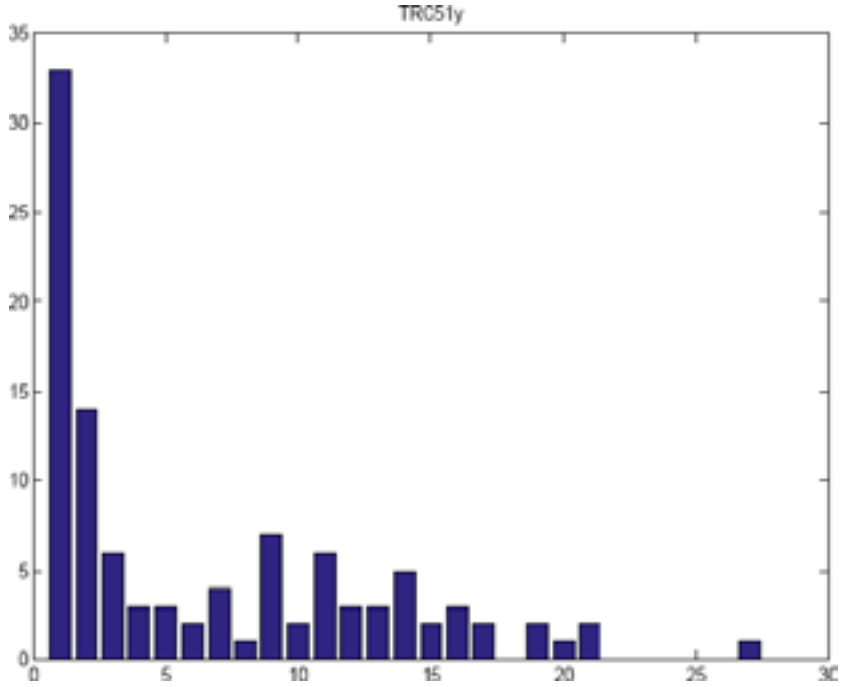

Figure B-6. *Histogram of TRC 51 in y-direction (x-axis in decimetres).*

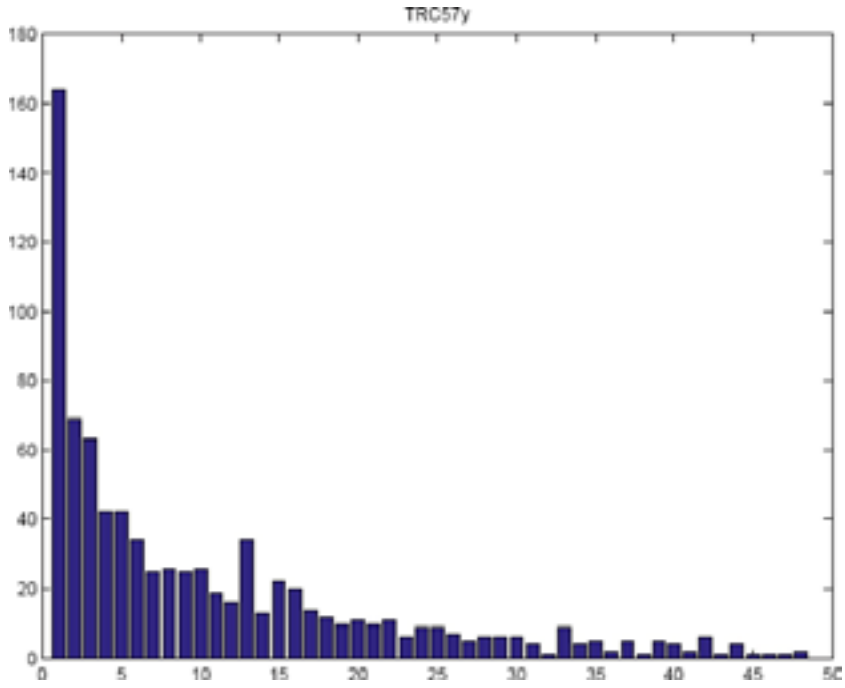

Figure B-7. *Histogram of TRC 57 in y-direction (x-axis in decimetres).*

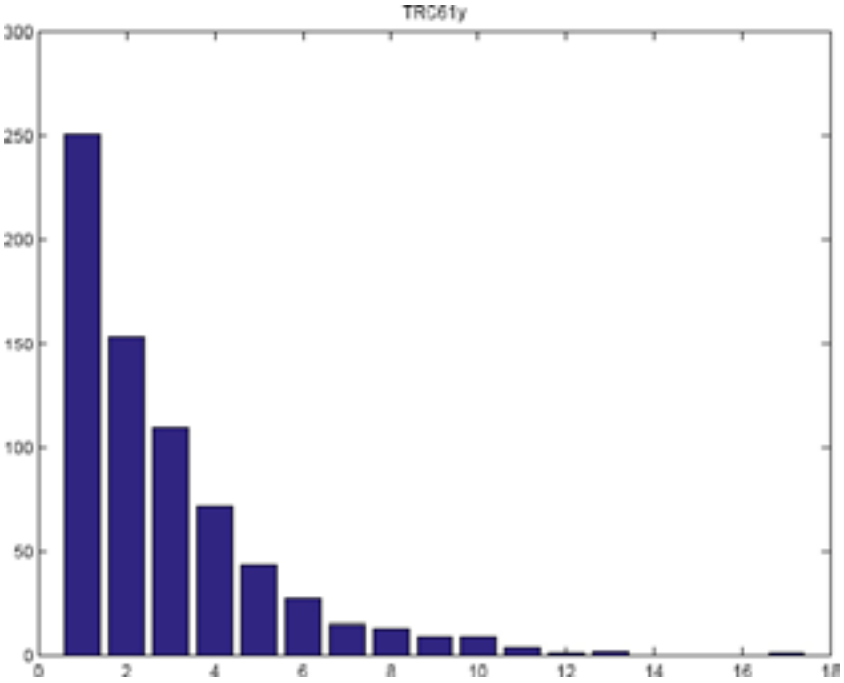

Figure B-8. *Histogram of TRC 61 in y-direction (x-axis in decimetres).*

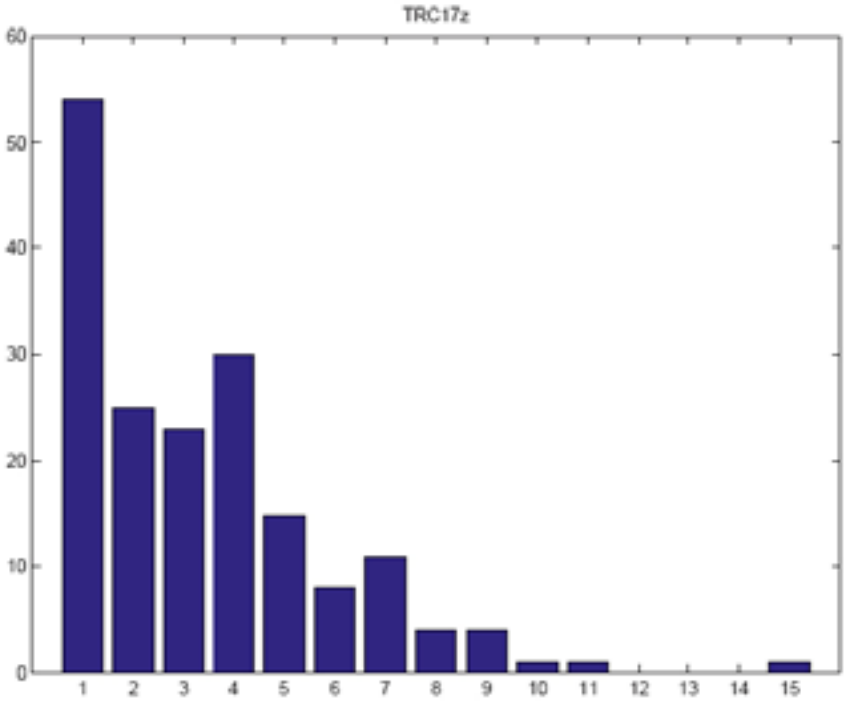

Figure B-9. *Histogram of TRC 17 in z-direction (x-axis in decimetres).*

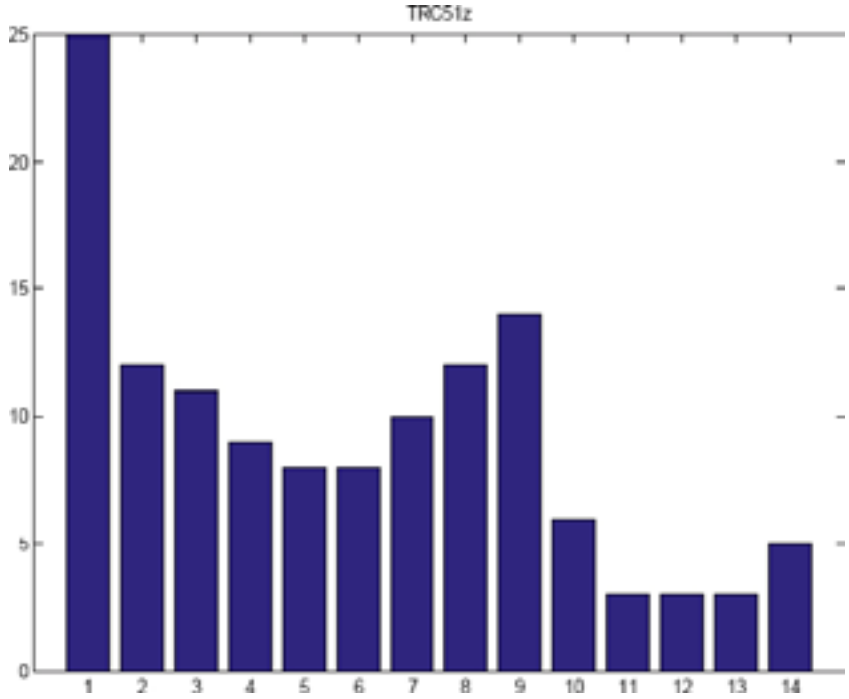

Figure B-10. *Histogram of TRC 51 in z-direction (x-axis in decimetres).*

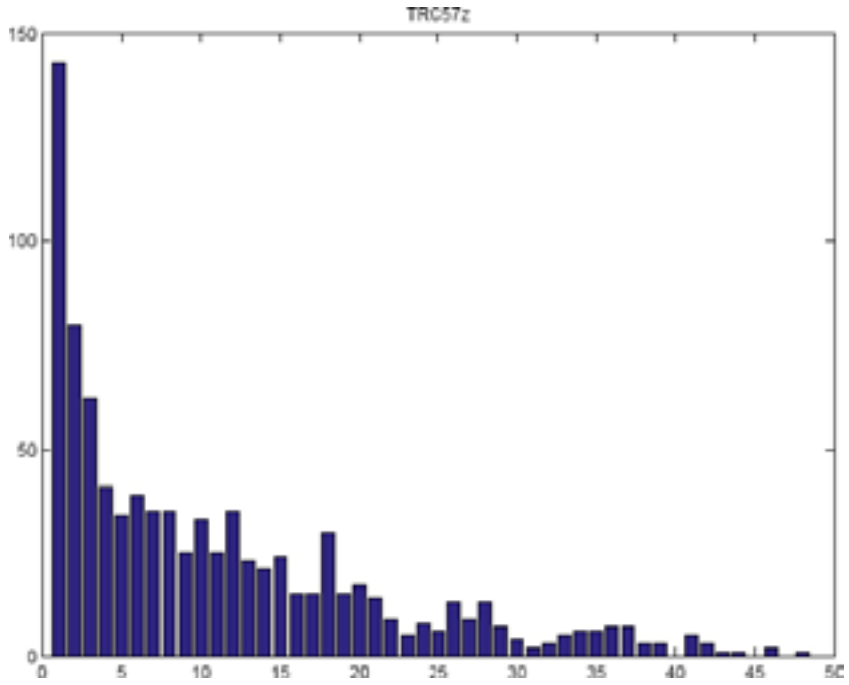

Figure B-11. *Histogram of TRC 57 in z-direction (x-axis in decimetres).*

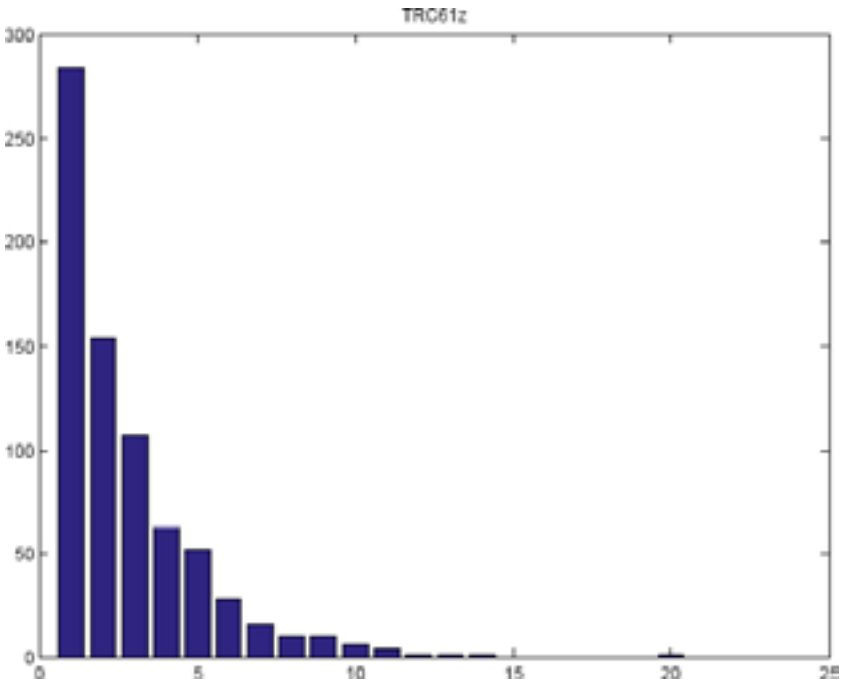

Figure B-12. *Histogram of TRC 57 in z-direction (x-axis in decimetres).*

Because of the large number of "borings" in the simulated volumes it is assumed that the histograms give a good representation of the simulated lengths of TRCs. A visual comparison of the histograms with lengths observed in the borehole data indicates that T-PROGS is able to realistically represent TRC lengths registered in the borehole data, see Figure B-13.

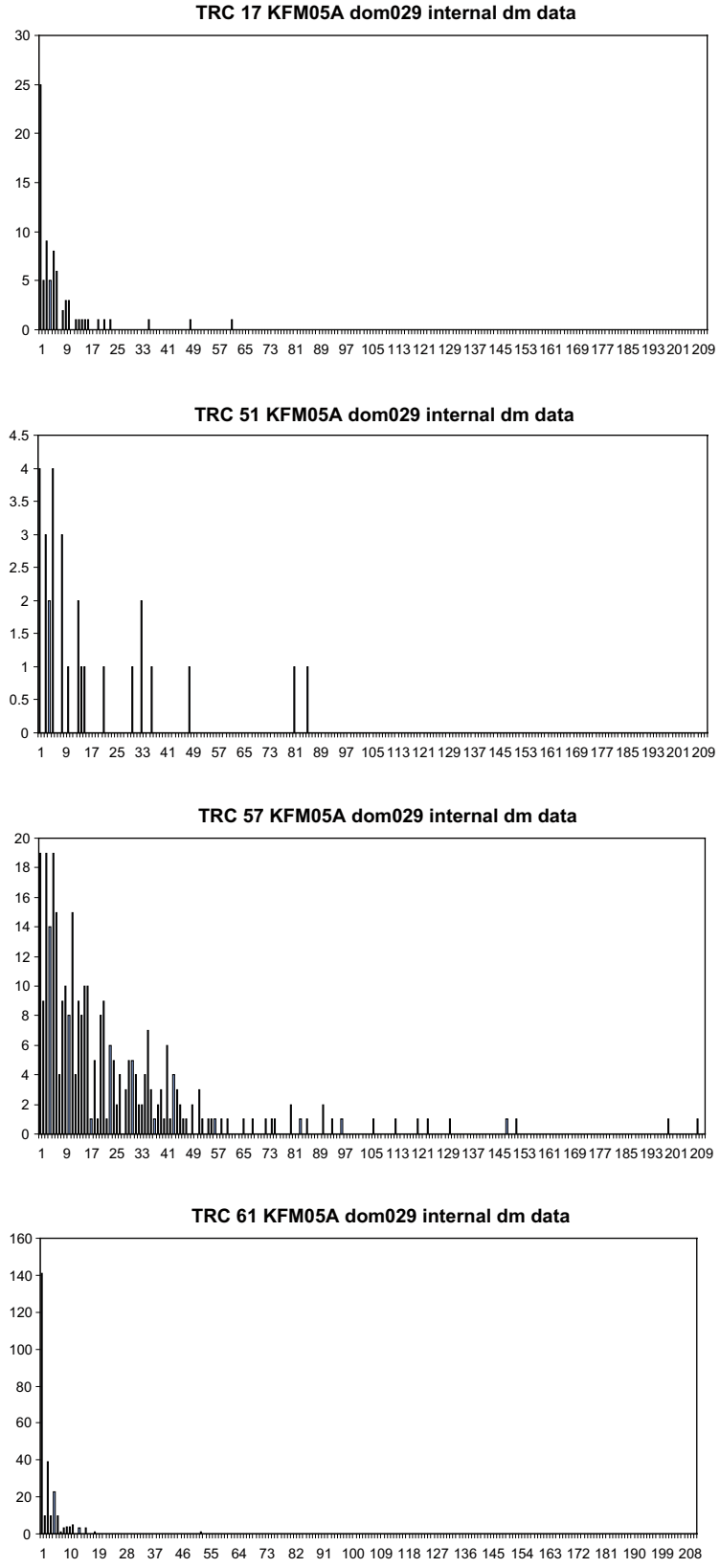

Figure B-13. *Histograms of TRC lengths in borehole KFM05A.*

Results 1 dm simulations domain 045

Proportions

Table B-1 shows the proportions of TRCs in 10 randomly selected realisations for domain RFM045.

As can be seen from Table B-5 T-PROGS reproduces the proportions of the TRCs very well for all realisations.

Typical lengths

Calculations of typical lengths of TRCs 17, 51 and 61 were made from "borings" through 10 randomly selected realisations for domain RFM045 internal. TRC 57 constitutes the "background" in the simulations and is therefore not relevant to include in the analysis.

The typical lengths of the TRCs in the data obtained from the "borings" were calculated by transition probability analysis. The results of the calculations of the typical length m for directions x, y and z are presented in Table B-6, Table B-7 and Table B-8. The confidence interval is given for each calculation and a comparison is made with the nominal value calculated from borehole data.

Table B-5. Proportions of TRCs in 10 randomly selected realisations for domain RFM029 internal.

Category	Proportions from borehole (%)	Proportions in realisation no. (%)									
		2	6	15	26	29	44	51	60	61	88
TRC17	9.8	11.3	10.7	10.7	11.7	10.5	10.7	10.8	10.9	11.3	10.9
TRC51	25.9	25.9	26.6	26.1	26.1	26.7	25.8	25.7	25.6	26.3	26.1
TRC58	53.0	51.3	51.5	51.4	51.3	51.4	51.7	52	51.9	50.9	51.8
TRC61	11.3	11.6	11.2	11.8	10.8	11.3	11.7	11.5	11.7	11.4	11.2

Table B-6. Typical lengths for TRC17.

Typical length (dm)	Nominal value (dm)	Comment to simulated values
μ_x = 5.52 ± 1.77	40.7	Low
μ_y = 5.45 ± 1.53	20.3	Low
μ_z = 4.81 ± 1.20	10.1	Low

Table B-7. Typical lengths for TRC51.

Typical length (dm)	Nominal value (dm)	Comment to simulated values
μ_x = 6.14 ± 1.75	39.0	Low
μ_y = 6.23 ± 1.49	19.5	Low
μ_z = 5.41 ± 0.98	9.75	Low

Table B-8. Typical lengths for TRC61.

Typical length (dm)	Nominal value (dm)	Comment to simulated values
μ_x = 3.13 ± 0.32	3.1	OK
μ_y = 2.95 ± 0.29	3.1	OK
μ_z = 2.83 ± 0.27	1.0	High

As can be seen from the analysis, T-PROGS does not reproduce the typical lengths and anisotropy of TRCs as well for decimetre data as it does for metre data. Longer lengths are typically underestimated and shorter lengths typically overestimated. In addition, the confidence intervals are higher (in relative terms) than for 1 metre data.

The reasons for these results have not been analyzed in detail, but may partly be due to nominal (input) lengths in some cases (especially for TRC 17 and TRC51) being relatively long compared to the model dimensions (5 metres). Some TRC lengths are longer than the dimensions of the simulated volume (5 metres) are present in borehole KFM06C, see Figure B-25 below. This might cause boundary effects that restrict the ability to reproduce anisotropy even more than for domain 029. As for domain 029 the effect of T-PROGS not accepting nominal length values shorter than 0.25 metres, may restrict the ability for reproducing the anisotropy for TRC61.

Lengths

From 49×3 = 147 borings in each of 10 randomly selected realisations histograms were prepared for each TRC in x, y and z-directions. The results are shown in Figure B-14 to Figure B-25.

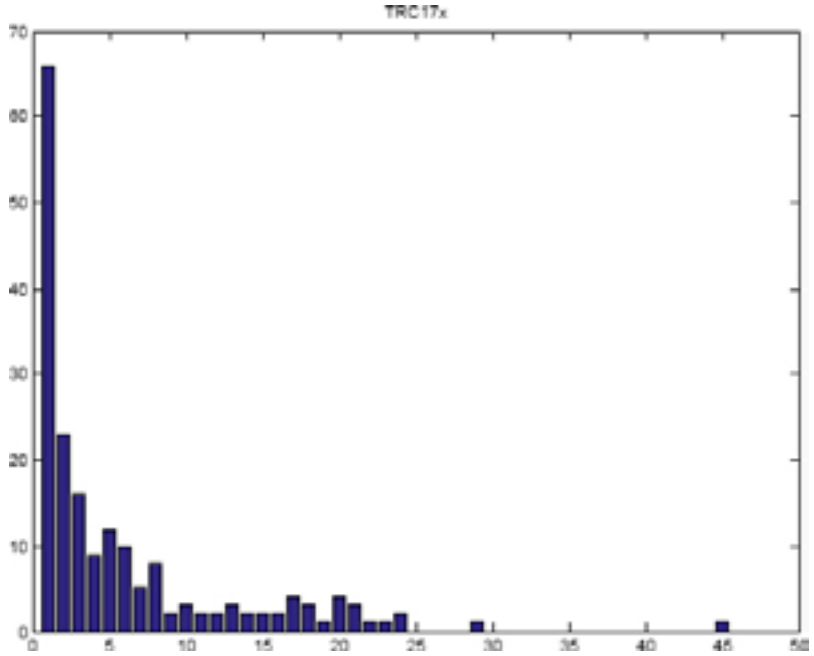

Figure B-14. *Histogram of TRC 17 in x-direction (x-axis in decimetres).*

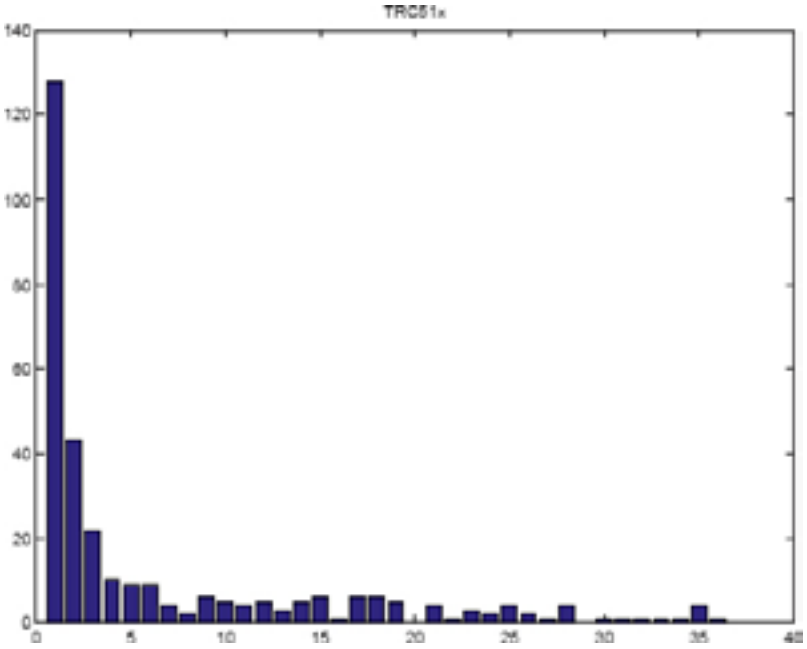

Figure B-15. *Histogram of TRC 51 in x-direction (x-axis in decimetres).*

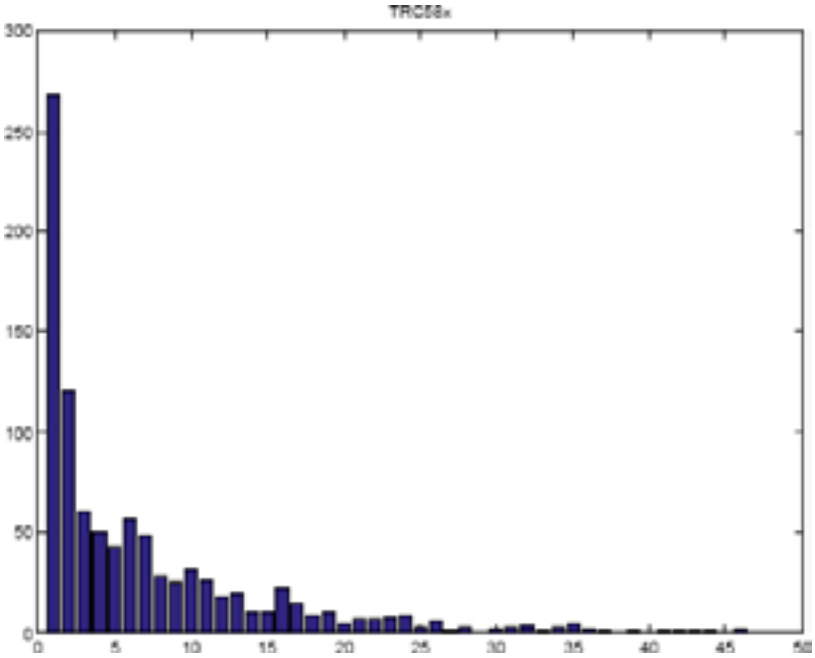

Figure B-16. *Histogram of TRC 58 in x-direction (x-axis in decimetres).*

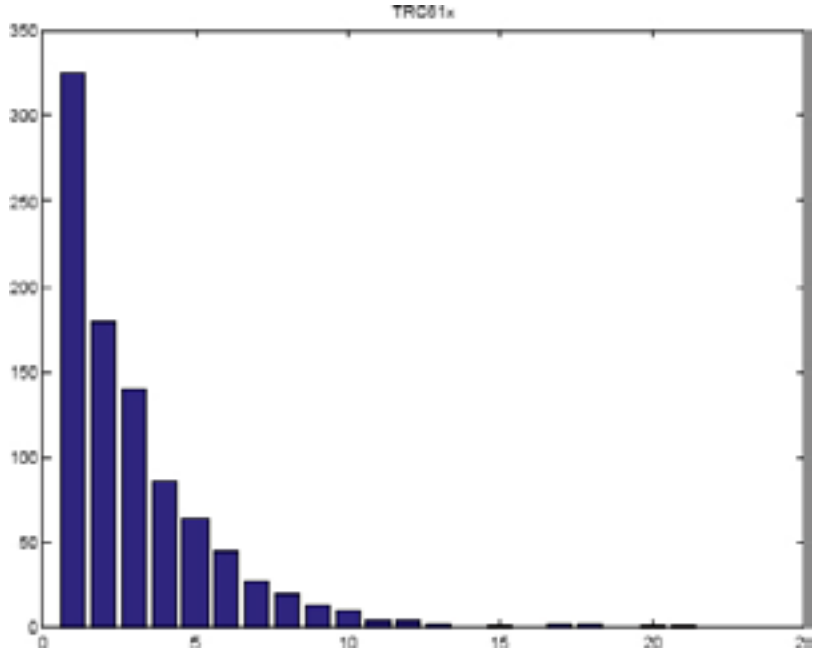

Figure B-17. *Histogram of TRC 61 in x-direction (x-axis in decimetres).*

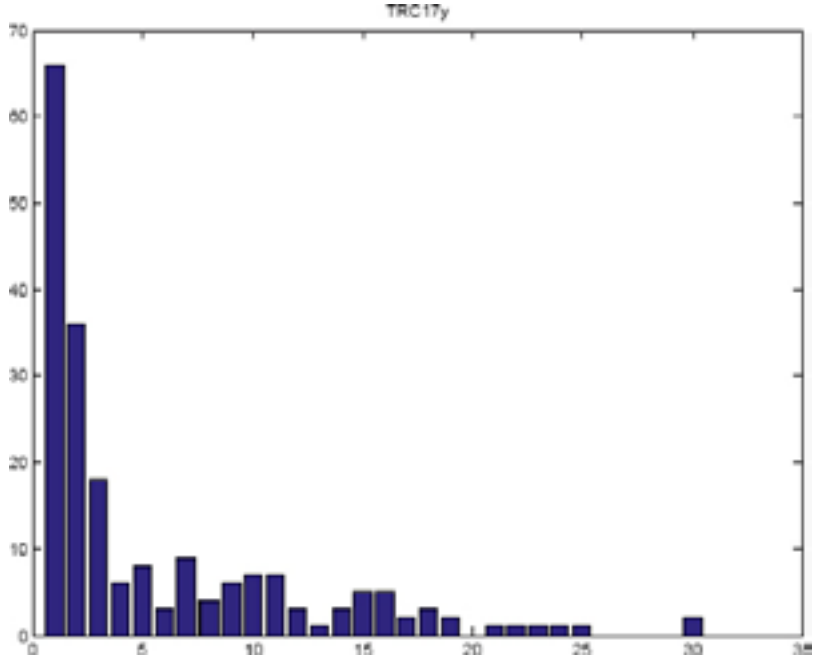

Figure B-18. *Histogram of TRC 17 in y-direction (x-axis in decimetres).*

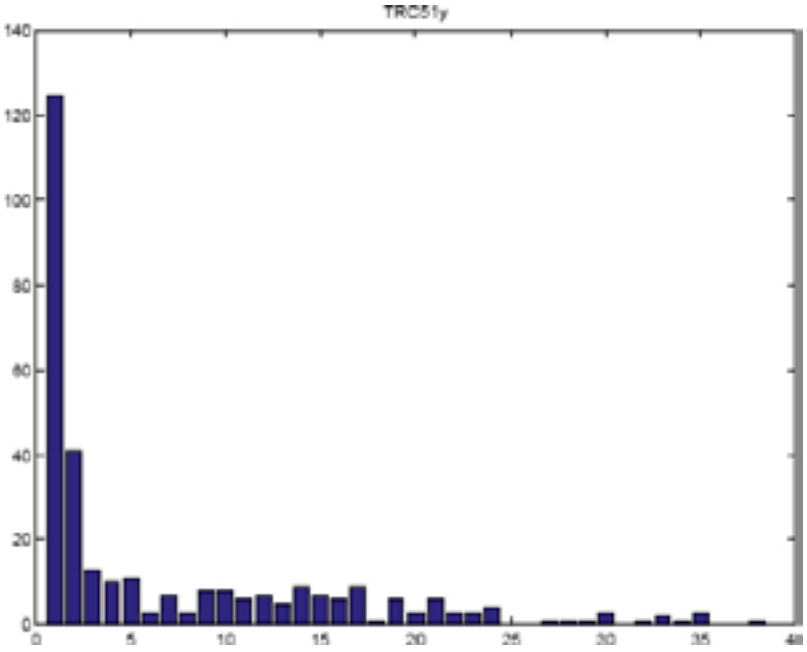

Figure B-19. *Histogram of TRC 51 in y-direction (x-axis in decimetres).*

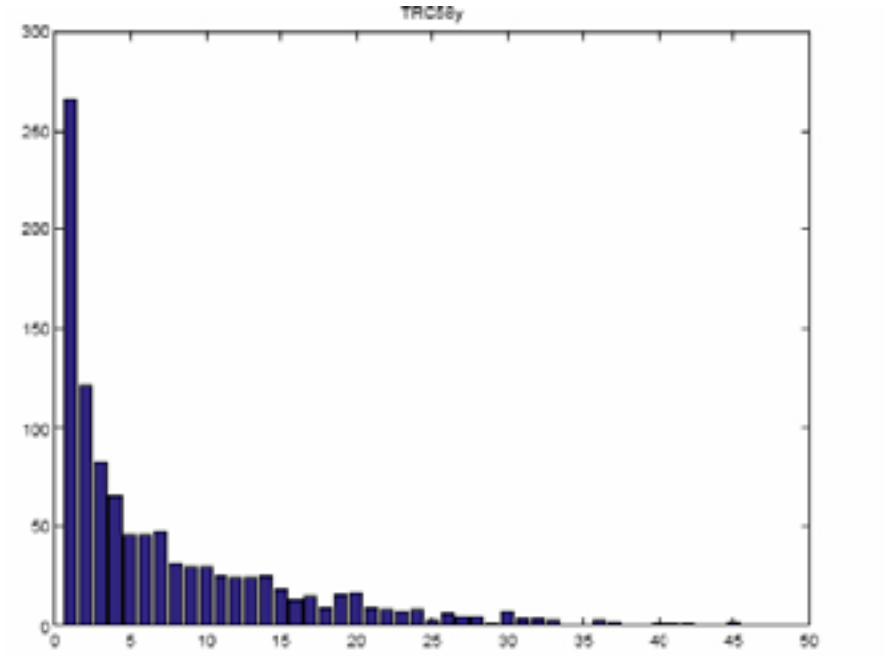

Figure B-20. *Histogram of TRC 58 in y-direction (x-axis in decimetres).*

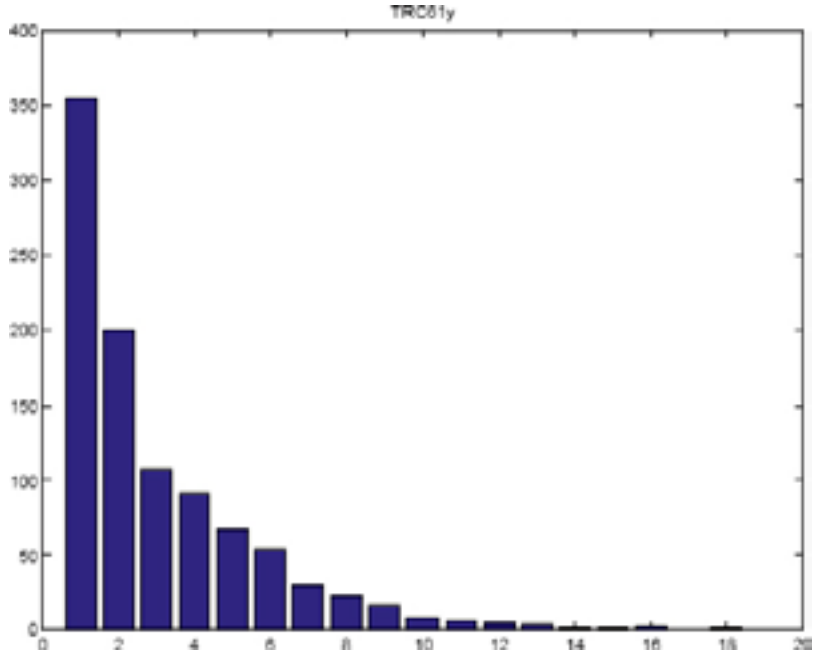

Figure B-21. *Histogram of TRC 61 in y-direction (x-axis in decimetres).*

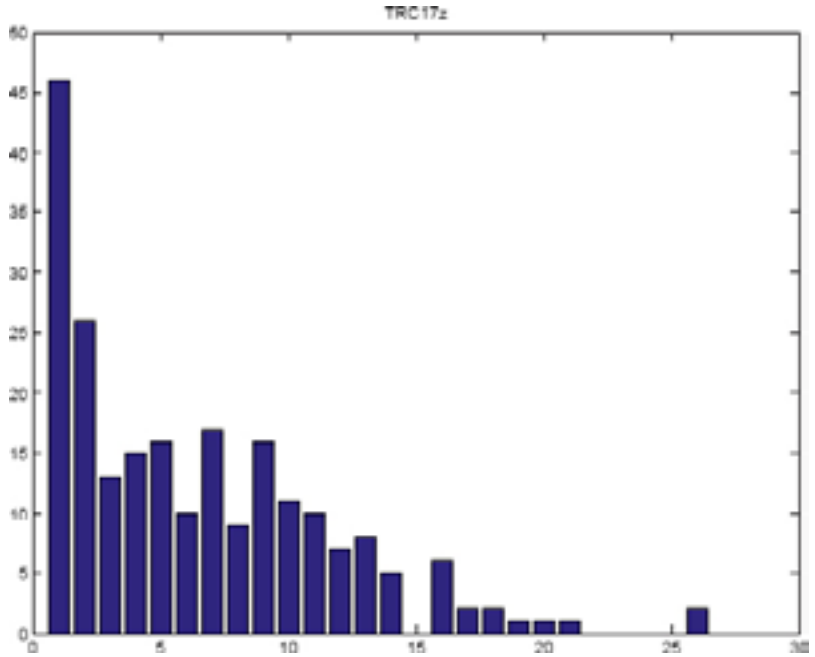

Figure B-22. *Histogram of TRC 17 in z-direction (x-axis in decimetres).*

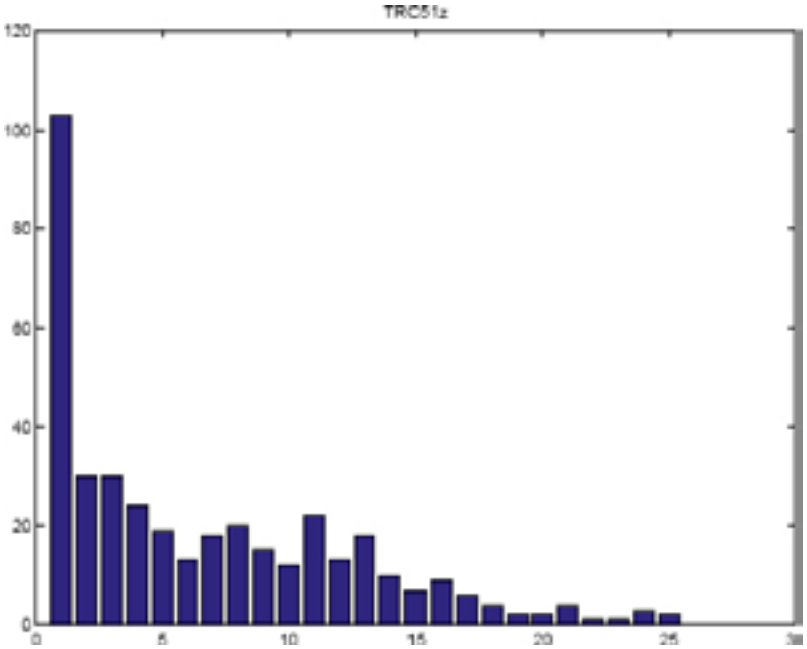

Figure B-23. *Histogram of TRC 51 in z-direction (x-axis in decimetres).*

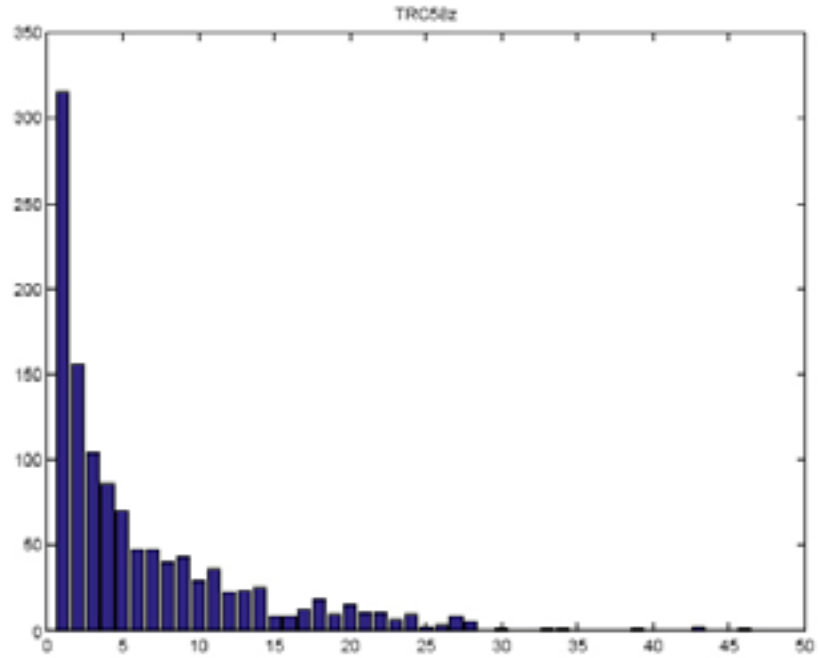

Figure B-24. *Histogram of TRC 58 in z-direction (x-axis in decimetres).*

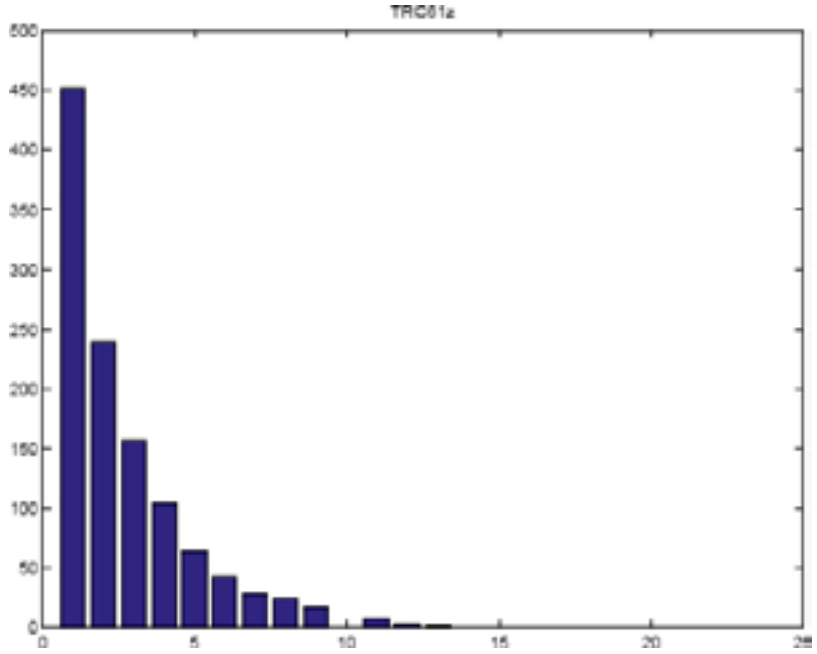

Figure B-25. *Histogram of TRC 57 in z-direction (x-axis in decimetres).*

Because of the large number of "borings" in the simulated volumes it is assumed that the histograms give a good representation of the simulated lengths of TRCs. A visual comparison of the histograms with lengths observed in the borehole data, see Figure B-26 indicates that T-PROGS is able to realistically represent TRC lengths registered in the borehole data.

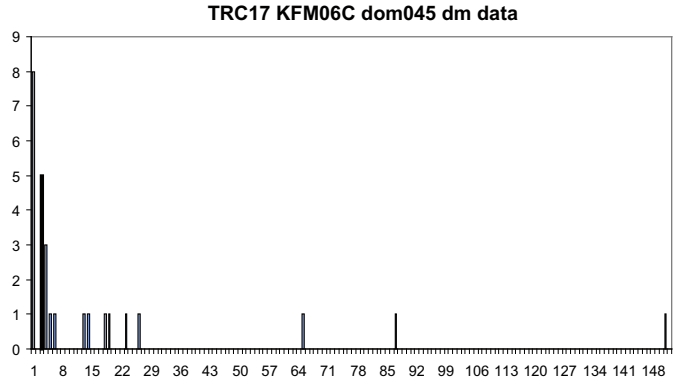

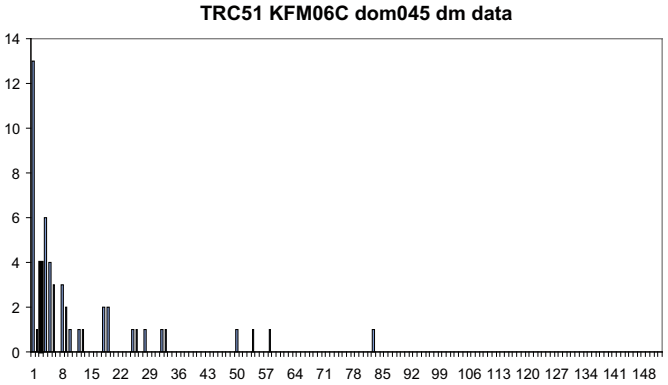

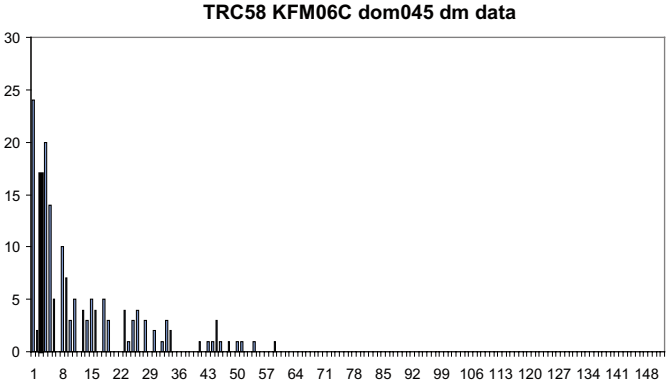

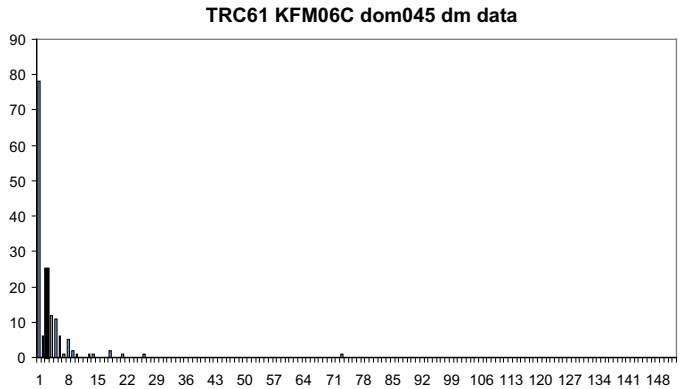

Figure B-26. *Histograms of TRC lengths in borehole KFM06C.*

Appendix C

Thermal distribution models

The following histograms are presented below.

- Histograms of thermal conductivity for the individual rock types based on TPS and SCA data.
- Histogram of thermal conductivity for each TRC based on combined data from the constituent rock types. The data for each rock type are weighted according to the relative proportions of each rock type in a rock domain, as well as the number of data values available for each rock type.
- Distribution models for each TRC based on smoothing of the weighted data histograms.

Tables summarising thermal conductivity statistics for each TRC and its constituent rock types based on TPS and SCA data are also presented.

TRC 57

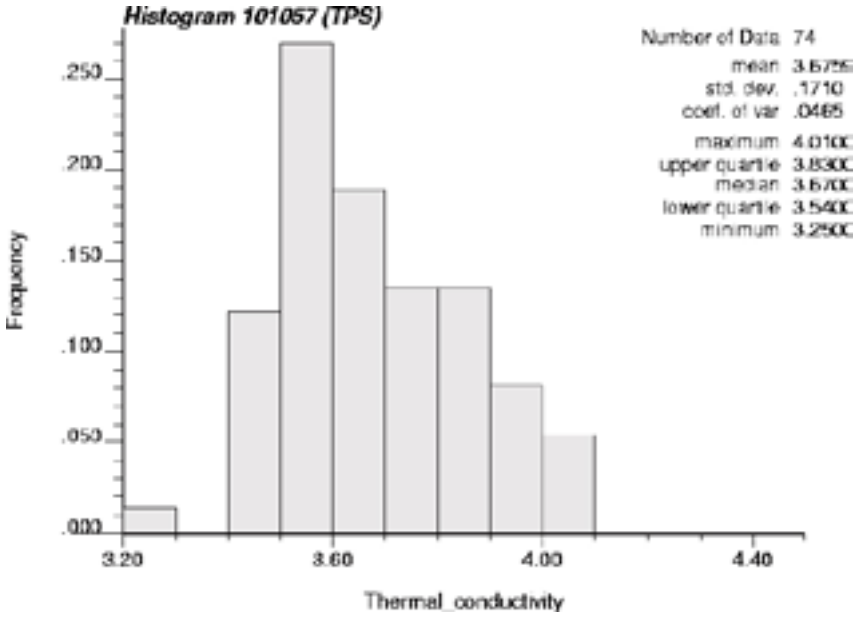

Figure C-1. *Histogram of thermal conductivity for granite to granodiorite (101057) based on TPS data.*

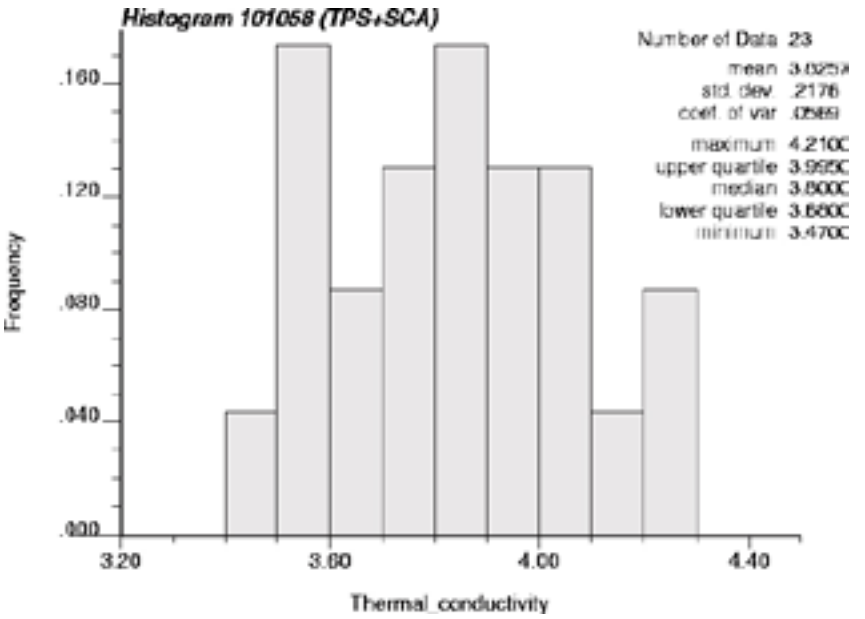

Figure C-2. *Histogram of thermal conductivity for granite, aplitic (101058) based on TPS and SCA data.*

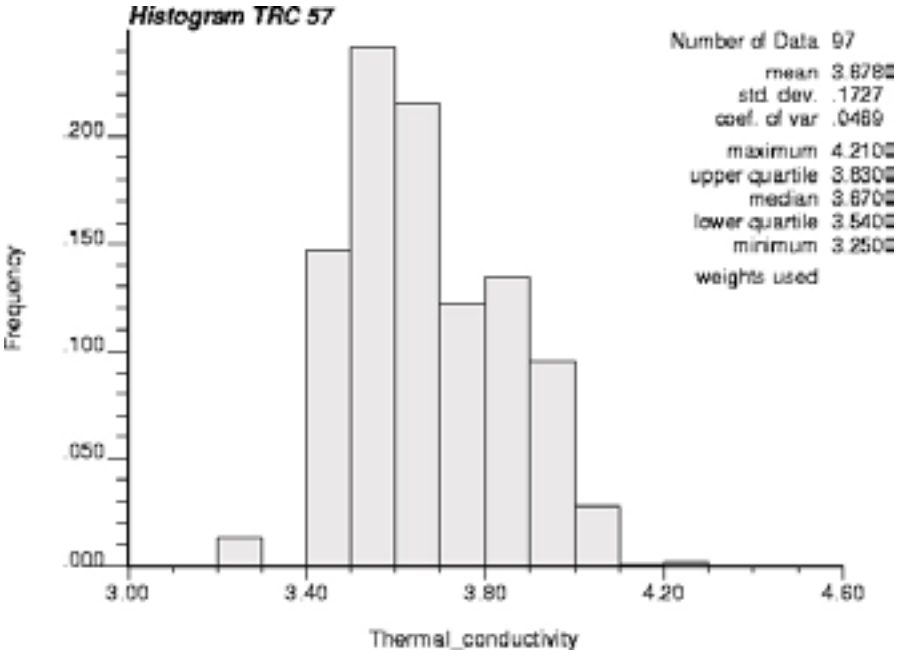

Figure C-3. *Histogram of thermal conductivity derived for TRC 57 based on combined data for two rock types: granite to granodiorite (101057) and granite, aplitic (101058).*

TRC 57

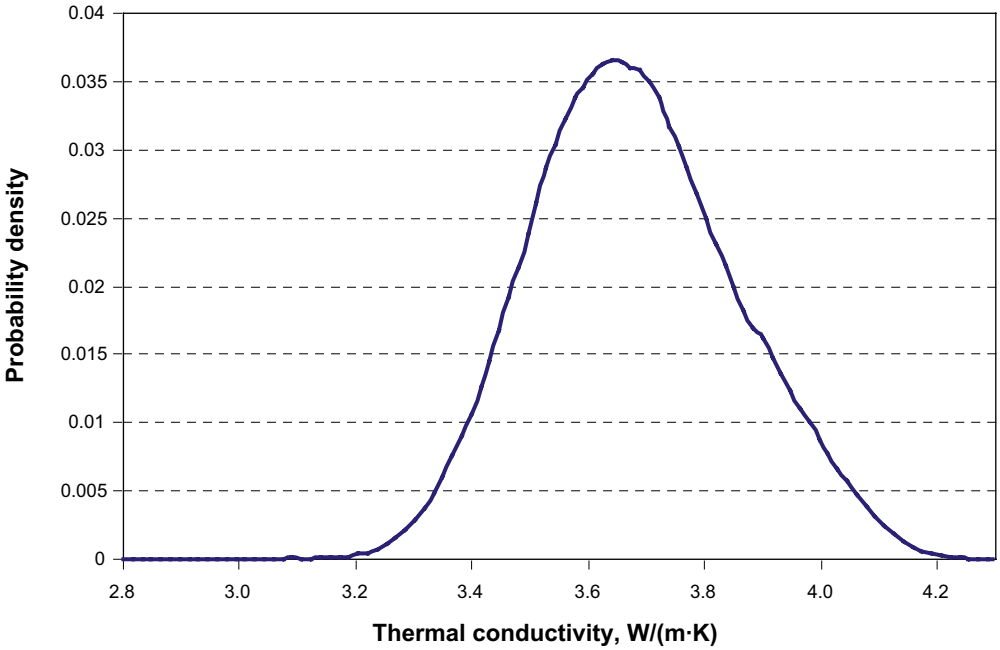

Figure C-4. *Distribution model of thermal conductivity for TRC 57 based on smoothing of the data histogram in Figure C-3.*

Thermal conductivity statistics for TRC 57 and its constituent rock types based on TPS and SCA data. Statistics for the TRC are based on data weighted according to the relative proportions of the each rock type as well as the number of data values available for each rock type.

Rock code/ TRC	Rock name	Mean	Standard deviation	n	Min	Max
101057	Granite to granodiorite	3.68	0.17	74	3.25	4.01
101058	Granite, aplitic	3.83	0.22	23	3.47	4.21
TRC 57		3.68	0.17	97		

TRC 58

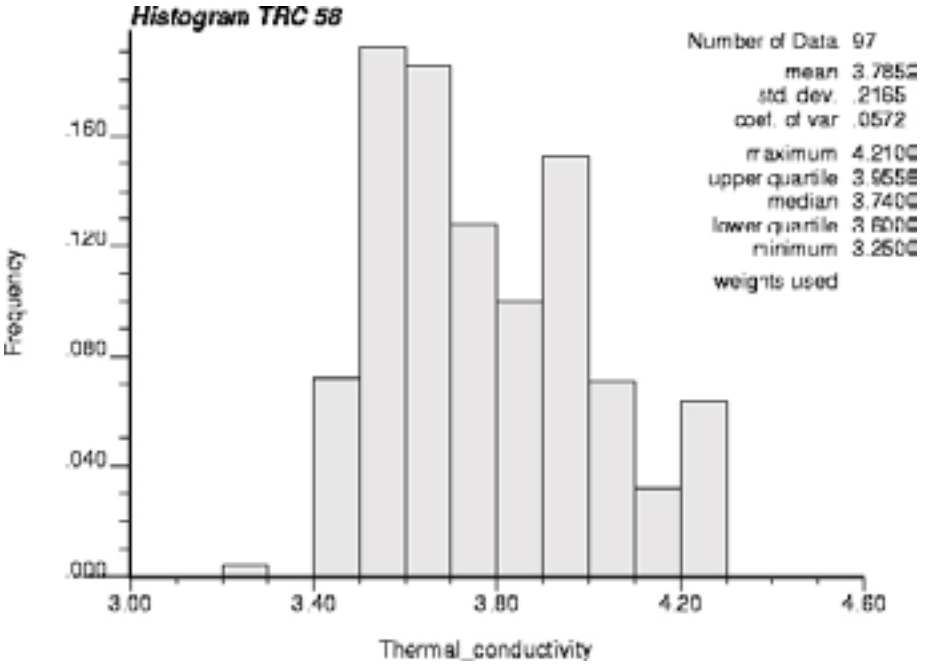

Figure C-5. *Histogram of thermal conductivity derived for TRC 58 based on combined data for two rock types: granite to granodiorite (101057) and granite, aplitic (101058).*

TRC 58

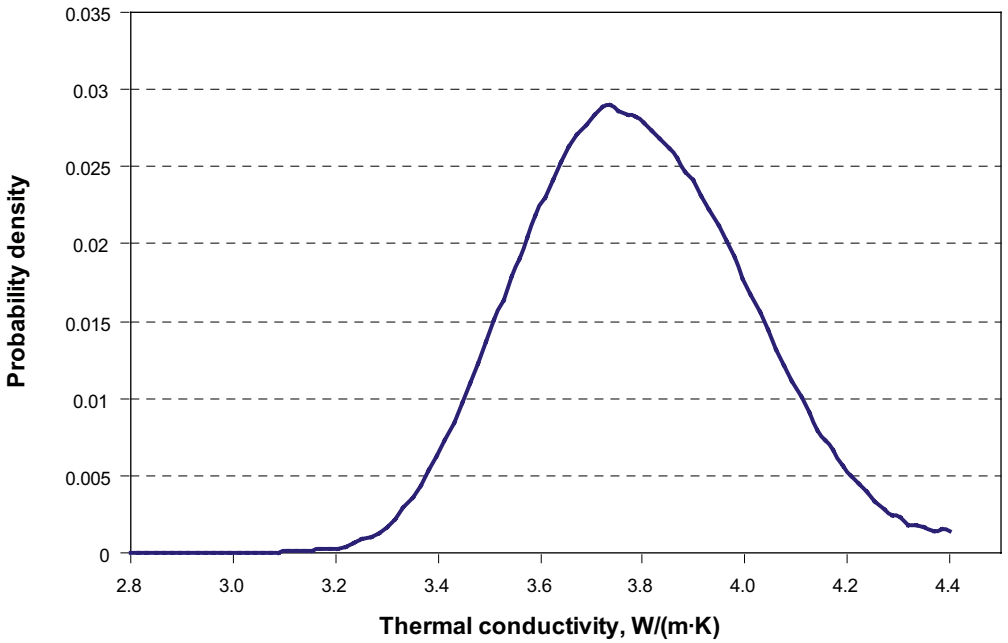

Figure C-6. *Distribution model of thermal conductivity for TRC 58 based on smoothing of the data histogram in Figure C-5.*

Thermal conductivity statistics for TRC 58 and its constituent rock types based on TPS and SCA data. Statistics for the TRC are based on data weighted according to the relative proportions of the each rock type as well as the number of data values available for each rock type.

Rock code/ TRC	Rock name	Mean	Standard deviation	n	Min	Max
101057	Granite to granodiorite	3.68	0.17	74	3.25	4.01
101058	Granite, aplitic	3.83	0.22	23	3.47	4.21
TRC 58		3.79	0.22	97		

TRC 61

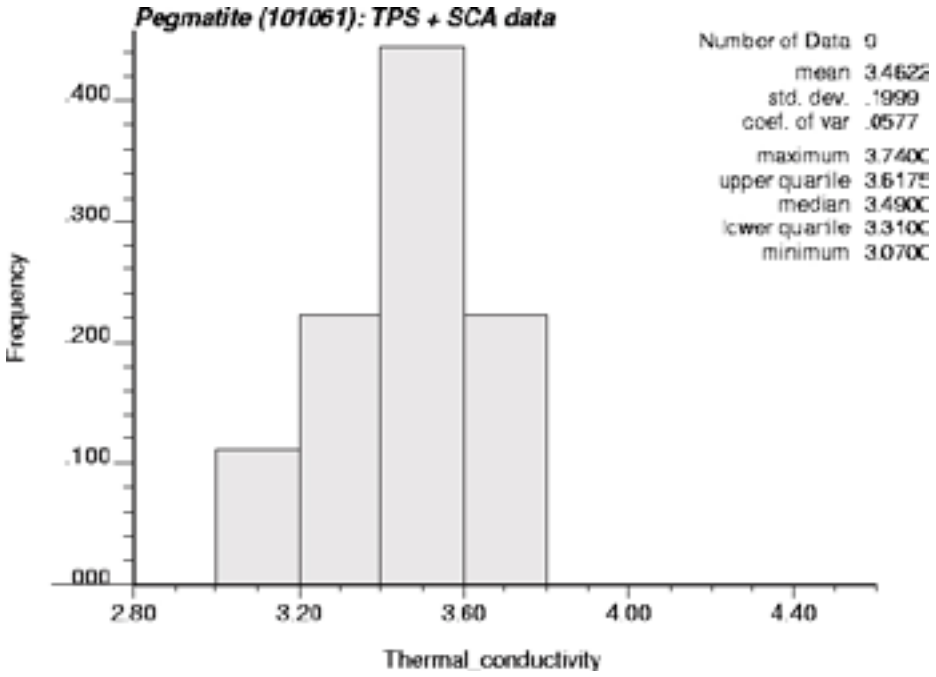

Figure C-7. *Histogram of thermal conductivity for pegmatite (101061) based on TPS and SCA data.*

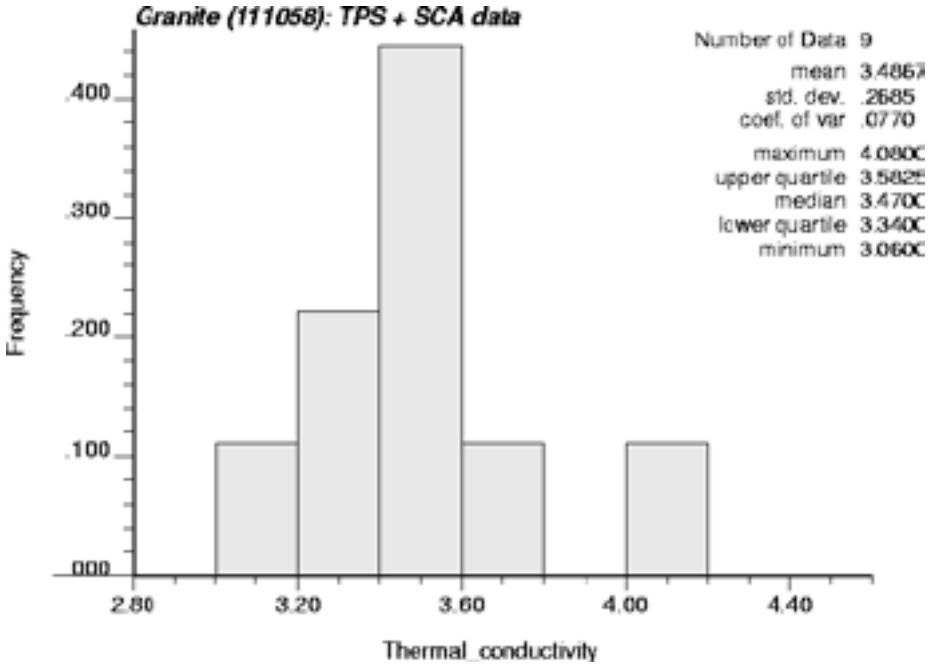

Figure C-8. *Histogram of thermal conductivity for granite (111058) based on TPS and SCA data.*

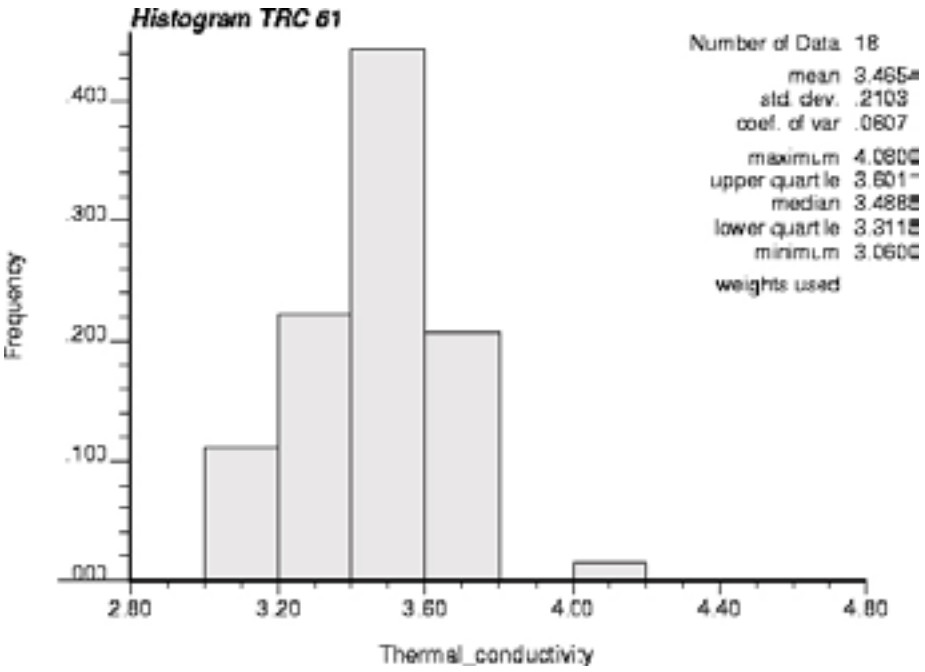

Figure C-9. *Histogram of thermal conductivity derived for TRC 61 based on combined data for two rock types: for pegmatite (101061) and granite (111058).*

TRC 61

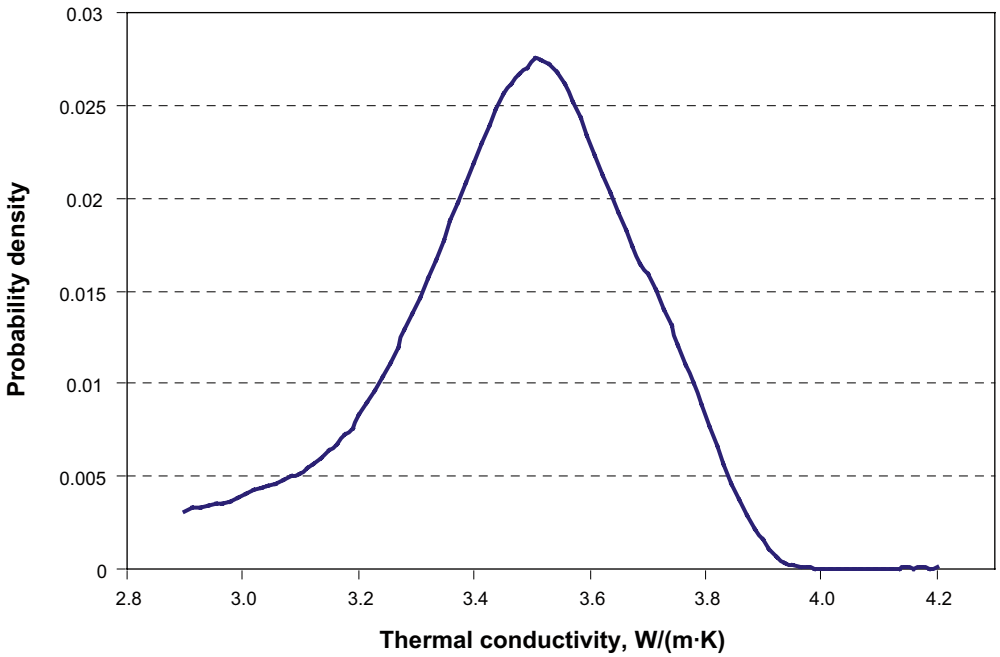

Figure C-10. *Distribution model of thermal conductivity for TRC 61 based on smoothing of the data histogram in Figure C-9.*

Thermal conductivity statistics for TRC 61 and its constituent rock types based on TPS and SCA data. Statistics for the TRC are based on data weighted according to the relative proportions of the each rock type as well as the number of data values available for each rock type.

Rock code/ TRC	Rock name	Mean	Standard deviation	n	Min	Max
101061	Pegmatite	3.46	0.21	9	3.07	3.74
111058	Granite	3.49	0.29	9	3.06	4.08
TRC 61		3.47	0.21	18		

TRC 17

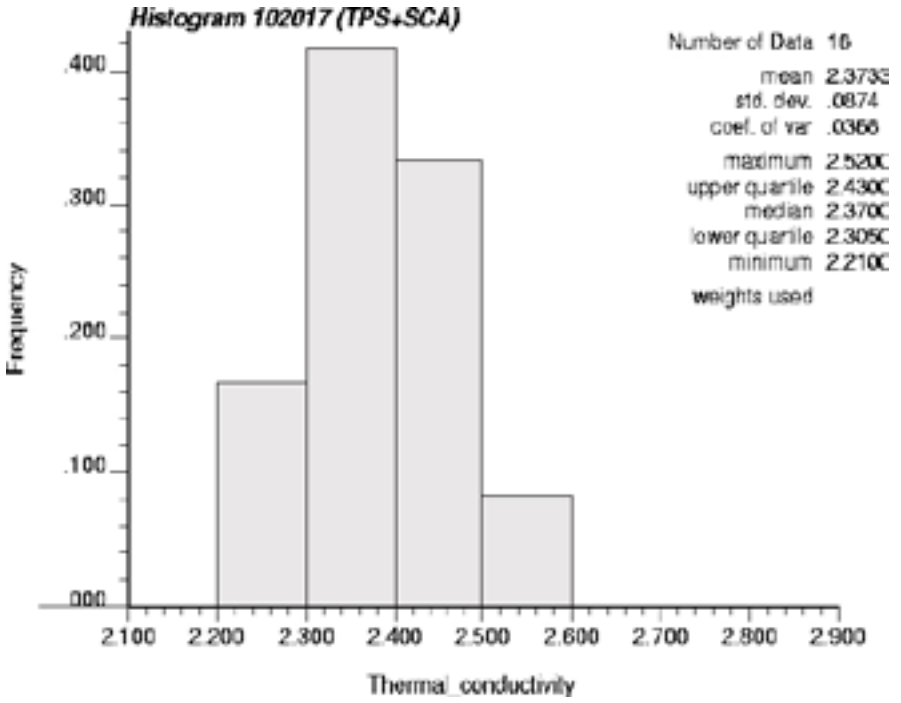

Figure C-11. *Histogram of thermal conductivity for amphibolite (102017) based on TPS and SCA data.*

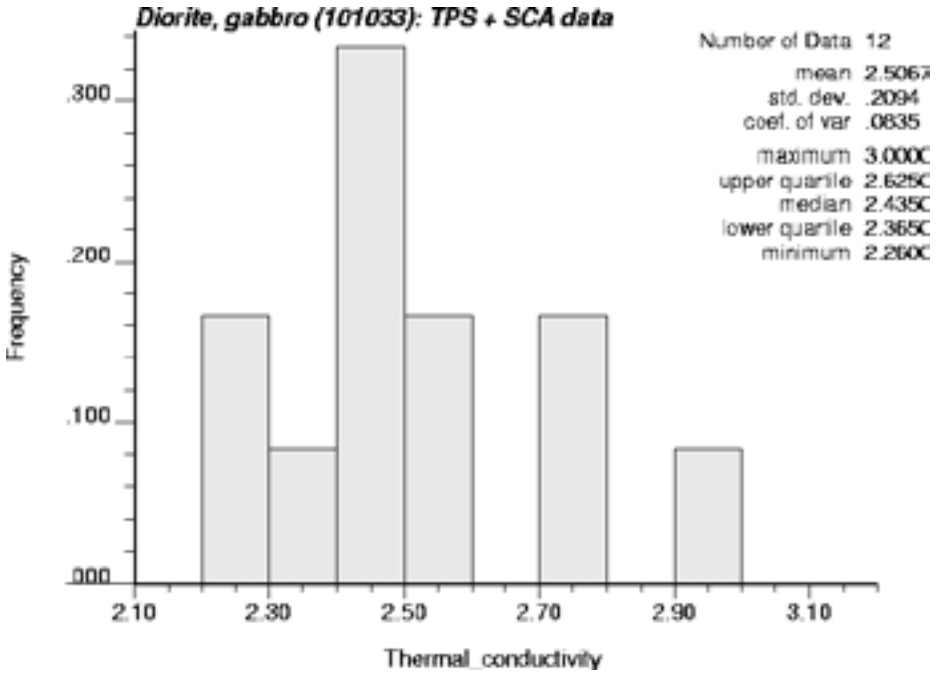

Figure C-12. *Histogram of thermal conductivity for diorite, quartz diorite and gabbro (101033) based on TPS and SCA data.*

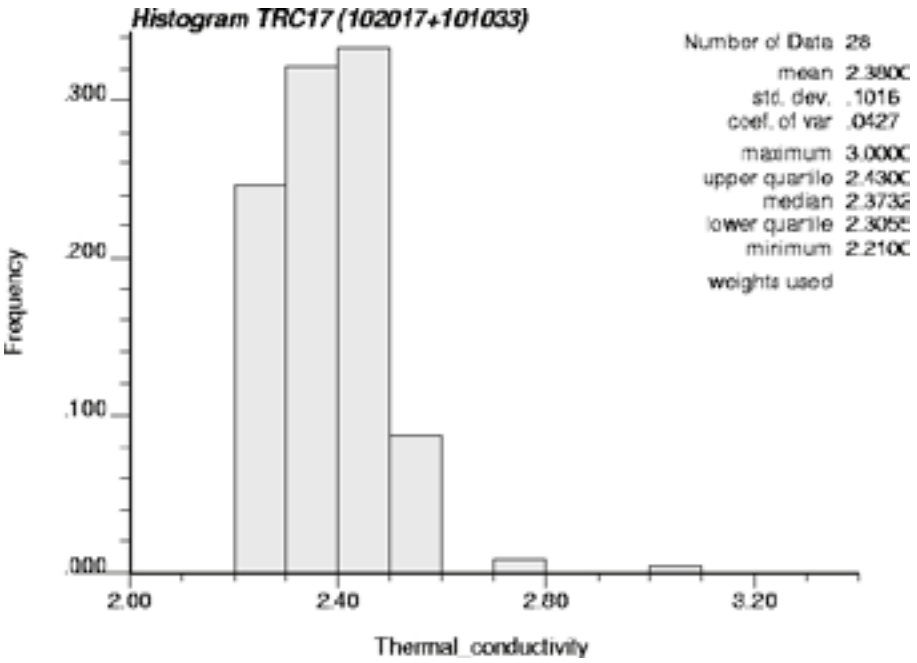

Figure C-13. *Histogram of thermal conductivity derived for TRC 17 based on combined data for two rock types: amphibolite (102017) and diorite, quartz diorite and gabbro (101033).*

TRC 17

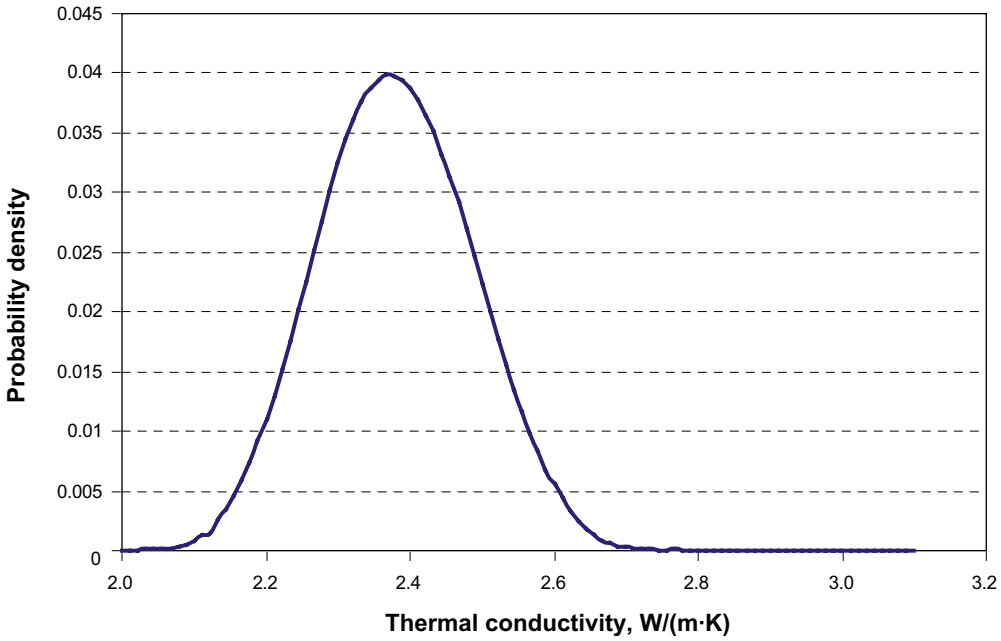

Figure C-14. *Distribution model of thermal conductivity for TRC 17 based on smoothing of the data histogram in Figure C-13.*

Thermal conductivity statistics for TRC 17 and its constituent rock types based on TPS and SCA data. Statistics for the TRC are based on data weighted according to the relative proportions of the each rock type as well as the number of data values available for each rock type.

Rock code/ TRC	Rock name	Mean	Standard deviation	n	Min	Max
102017	Amphibolite	2.37	0.09	16	2.21	2.52
101033	Diorite, quartz diorite and gabbro	2.51	0.22	12	2.26	3.00
TRC 17		2.38	0.10	28		

TRC 51

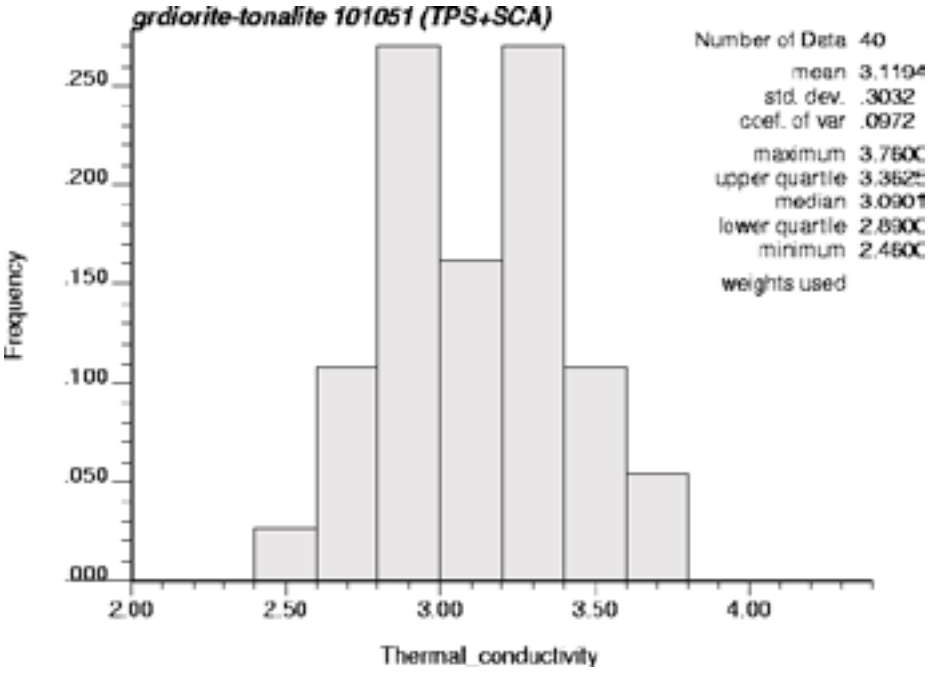

Figure C-15. *Histogram of thermal conductivity for granodiorite to tonalite (101051) based on TPS and SCA data.*

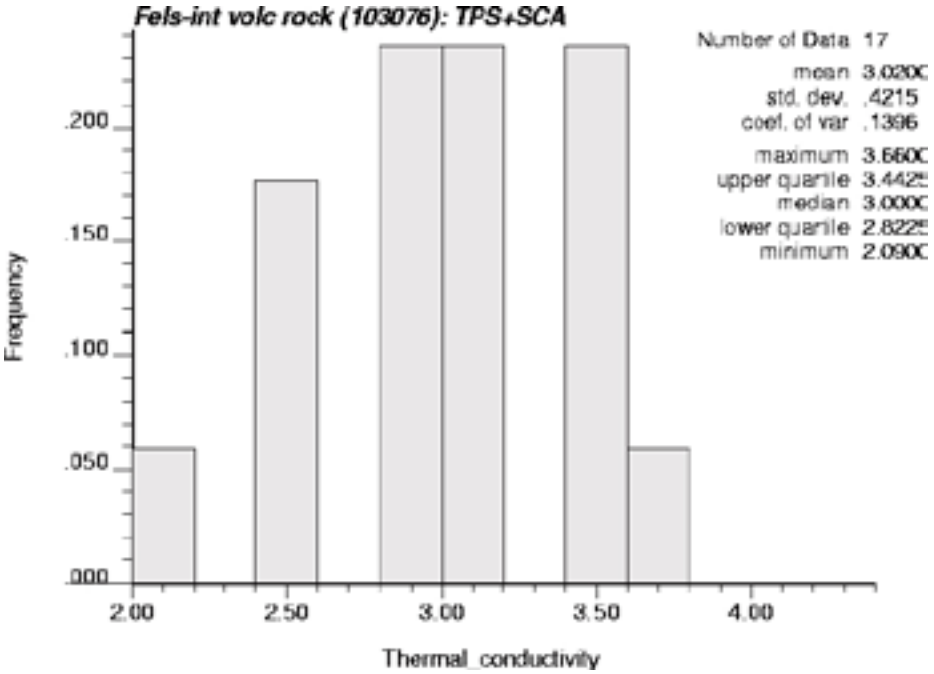

Figure C-16. *Histogram of thermal conductivity for felsic to intermediate volcanic rock (103076) based on TPS and SCA data.*

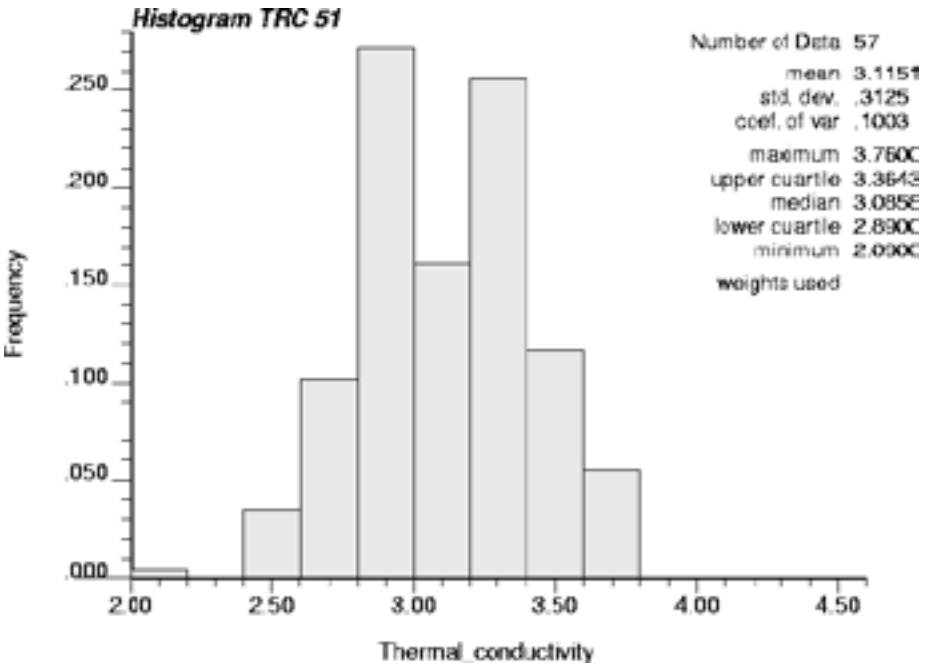

Figure C-17. *Histogram of thermal conductivity derived for TRC 51 based on combined data for two rock types: granodiorite to tonalite (101051) and felsic to intermediate volcanic rock (103076).*

Thermal conductivity statistics for the rock types constituting TRC 51 based on TPS and SCA data.

Rock code/ TRC	Rock name	Mean	Standard deviation	n	Min	Max
101051	Granodiorite to tonalite	3.12	0.30	40	2.46	3.76
103076	Felsic to intermediate volcanic rock	3.02	0.42	17	2.09	3.66

TRC 51A

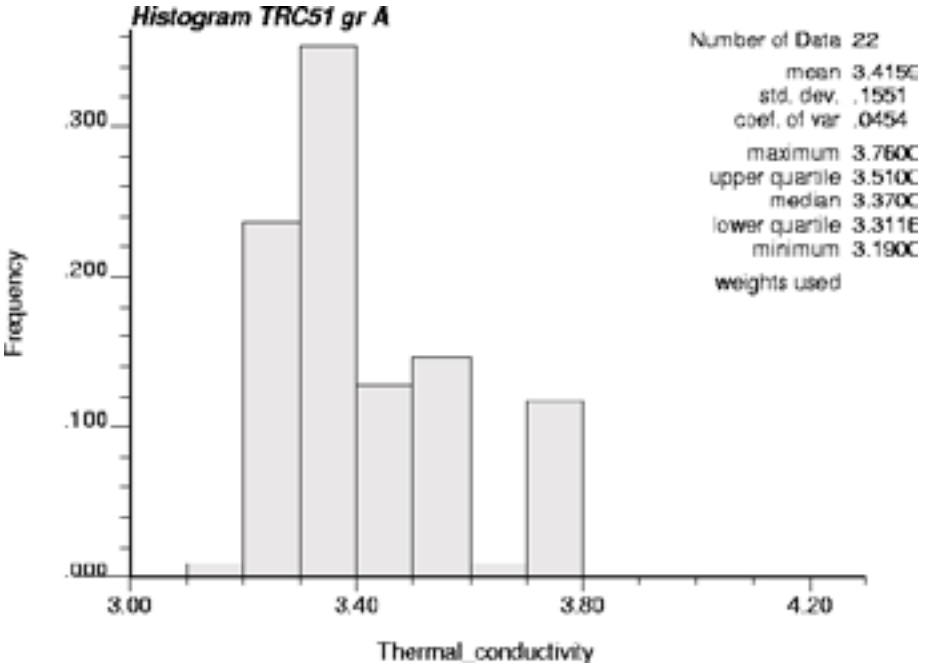

Figure C-18. *Histogram of thermal conductivity derived for TRC 51A based on combined data for two rock types: granodiorite to tonalite (101051) and felsic to intermediate volcanic rock (103076).*

TRC 51A

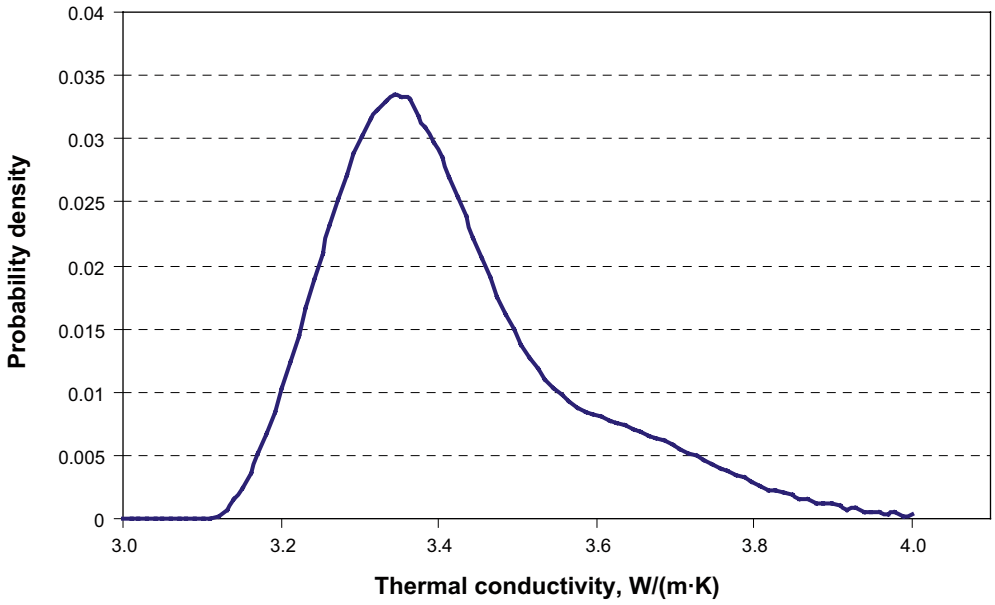

Figure C-19. *Distribution model of thermal conductivity for TRC 51A based on smoothing of the data histogram in Figure C-18.*

TRC 51B

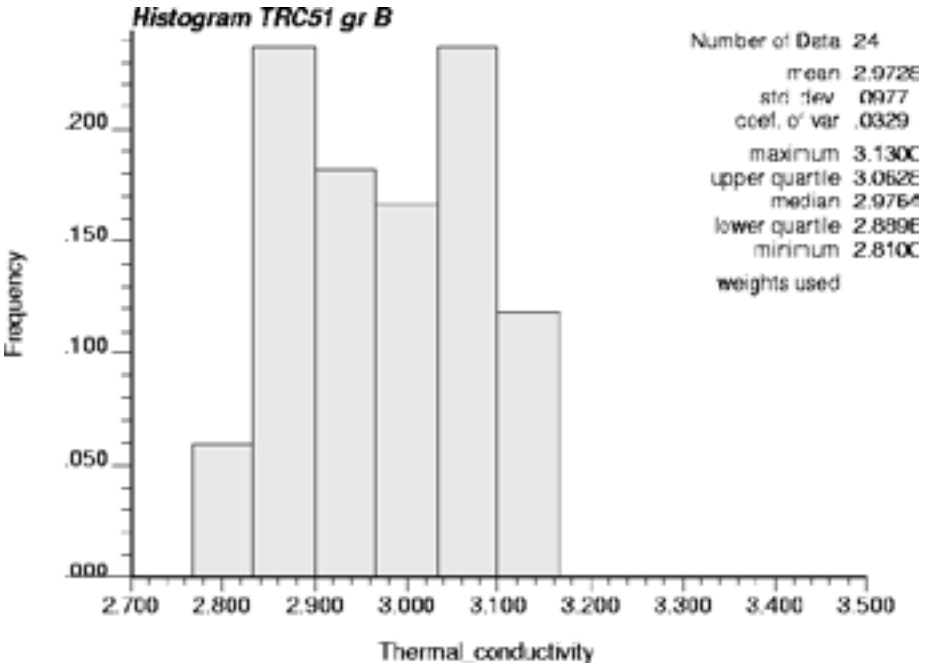

Figure C-20. *Histogram of thermal conductivity derived for TRC 51B based on combined data for two rock types: granodiorite to tonalite (101051) and felsic to intermediate volcanic rock (103076).*

TRC 51B

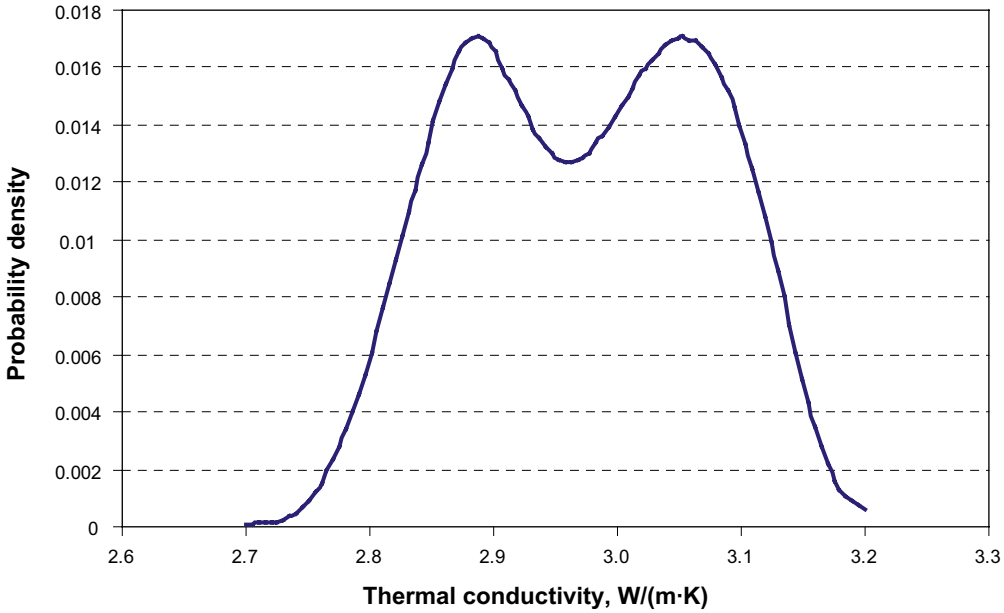

Figure C-21. *Distribution model of thermal conductivity for TRC 51B based on smoothing of the data histogram in Figure C-20.*

TRC 51C

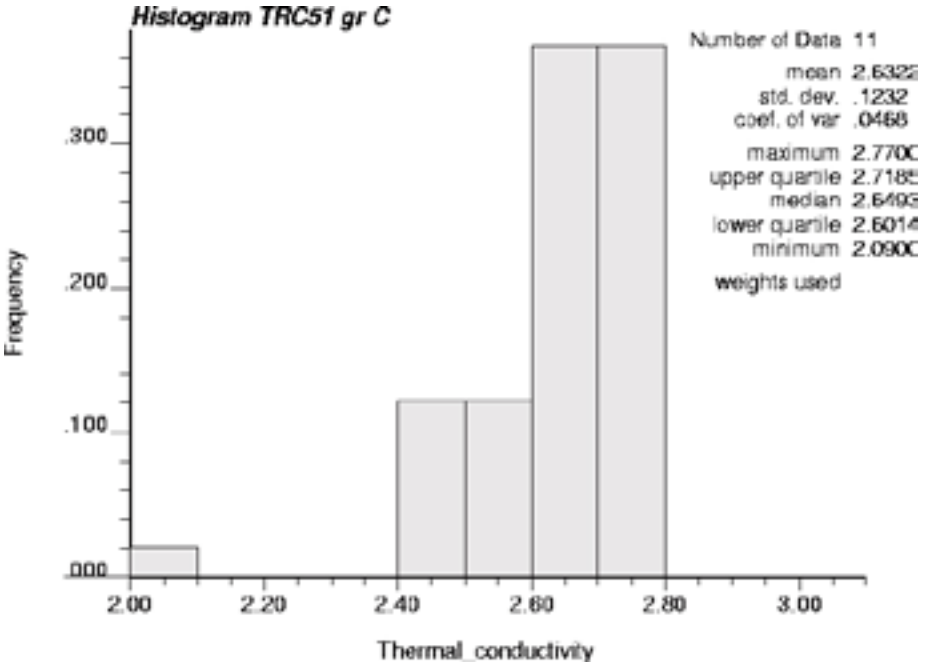

Figure C-22. *Histogram of thermal conductivity derived for TRC 51C based on combined data for two rock types: granodiorite to tonalite (101051) and felsic to intermediate volcanic rock (103076).*

TRC 51C

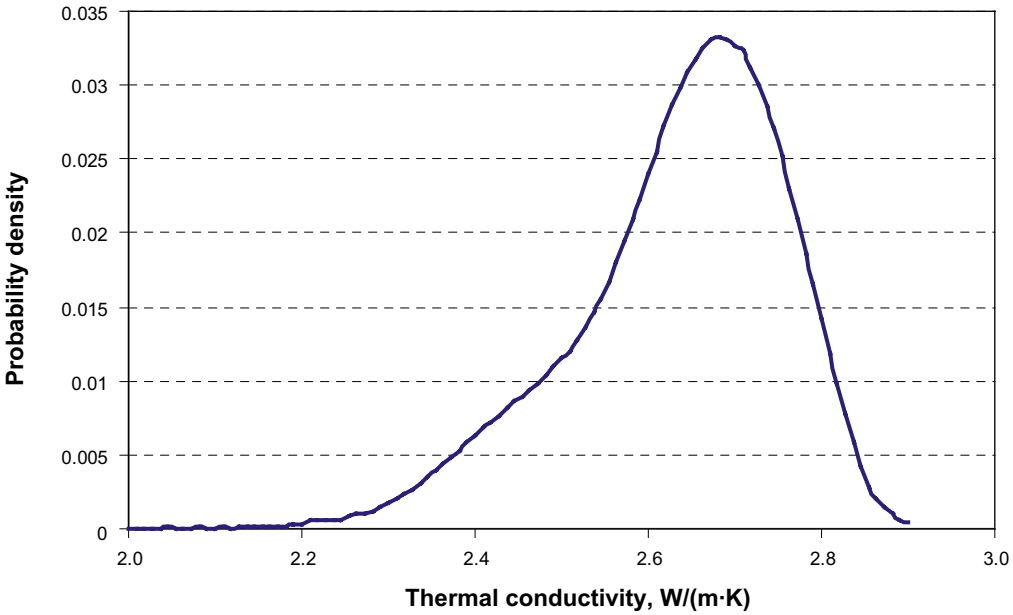

Figure C-23. *Distribution model of thermal conductivity for TRC 51C based on smoothing of the data histogram in Figure C-22.*

Thermal conductivity statistics for TRC 51A, TRC 51B and TRC 51C based on TPS and SCA data for rock types granodiorite to tonalite (101051) and felsic to intermediate volcanic rock (103076). Statistics for the TRC are based on data weighted according to the relative proportions of the each rock type as well as the number of data values available for each rock type.

TRC	Rock name	Mean	Standard deviation	n	Min	Max
TRC 51A		3.42	0.16	22		
TRC 51B		2.97	0.10	24		
TRC 51C		2.63	0.12	11		

Appendix D

Visualisations of thermal realisations TRC

Thermal histograms and visualisations of individual realisations

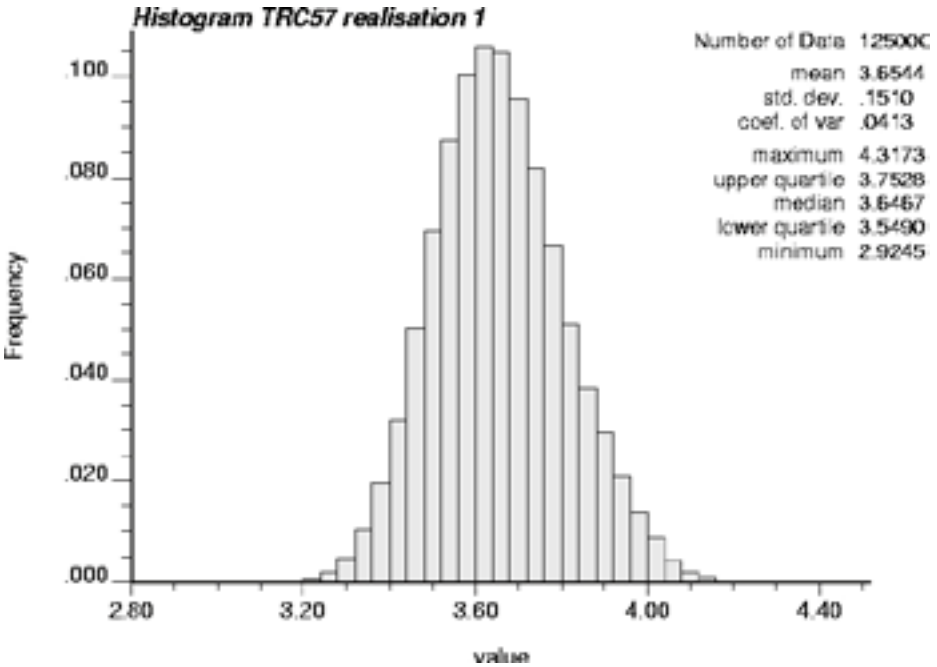

Figure D-1. *Histogram of 1 realisation at 0.1 m scale for TRC 57. Note the lower variance compared to the 150 combined realisations.*

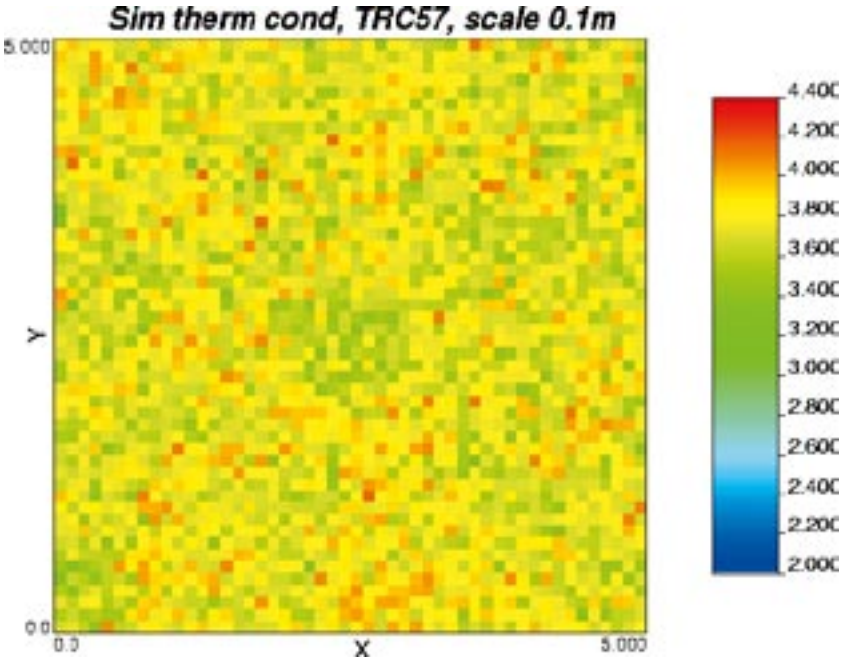

Figure D-2. *2D slice from one 3D realisation (0.1 m scale) illustrating the distribution of thermal conductivity values in TRC 57. R = 1, Slice = 25, xy-plane.*

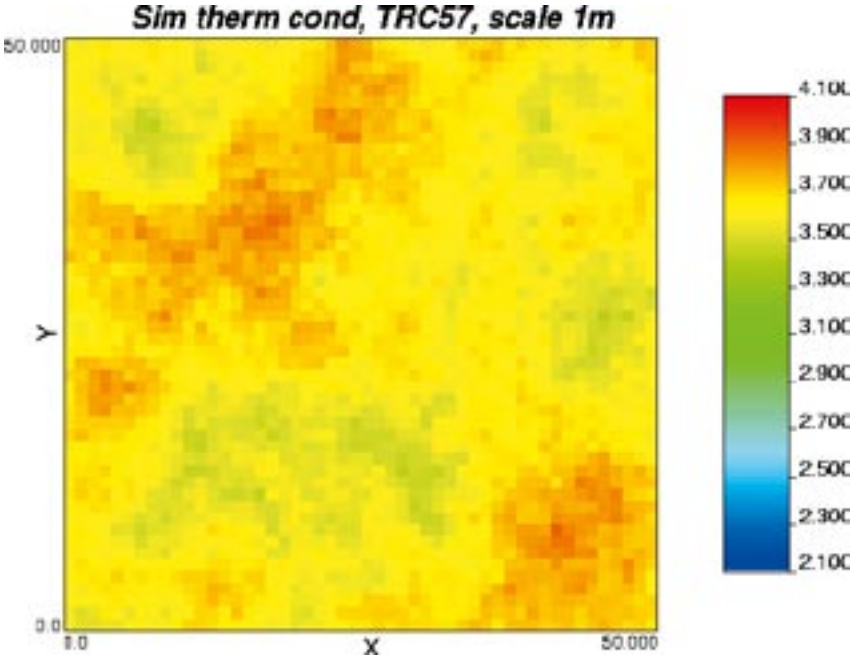

Figure D-3. *2D slice from one 3D realisation (simulation scale = 1 m) illustrating the distribution of thermal conductivity values in TRC 57. R = 1, Slice = 25, xy-plane.*

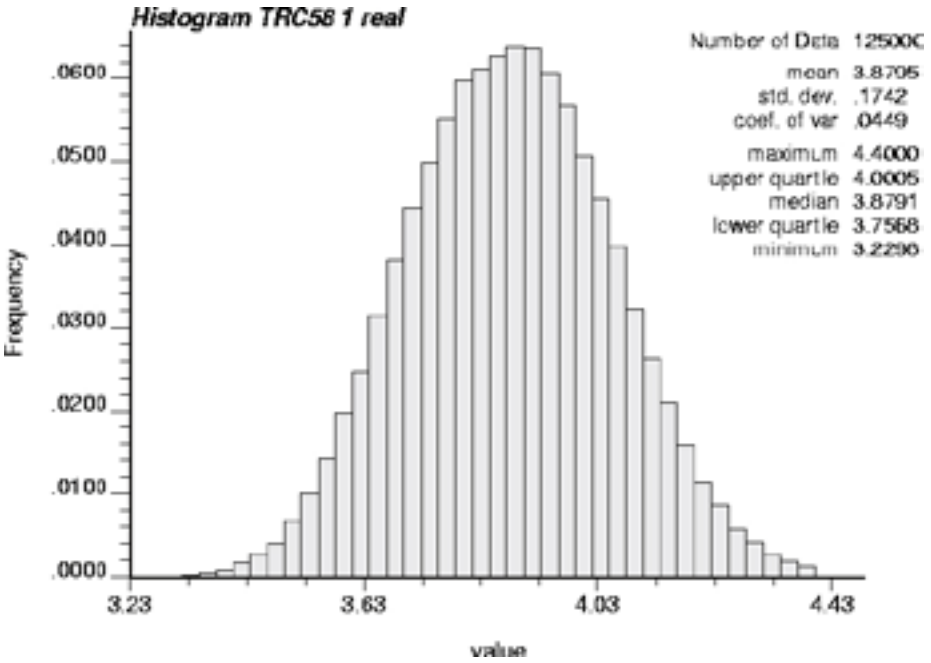

Figure D-4. *Histogram of 1 realisation at 0.1 m scale for TRC 58. Note the lower variance compared to the 150 combined realisations.*

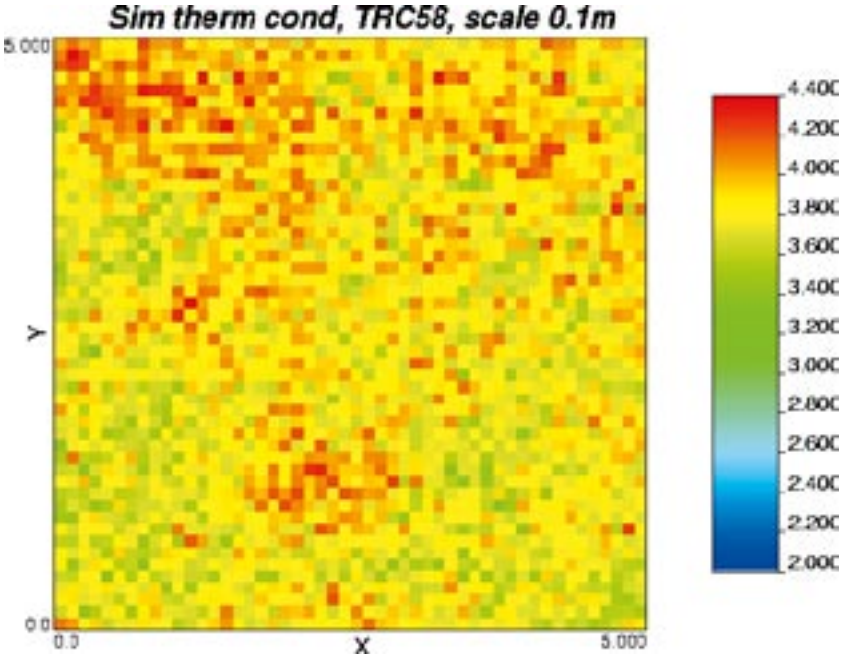

Figure D-5. *2D slice from one 3D realisation (0.1 m scale) illustrating the distribution of thermal conductivity values in TRC 58. R = 1, Slice = 25, xy-plane.*

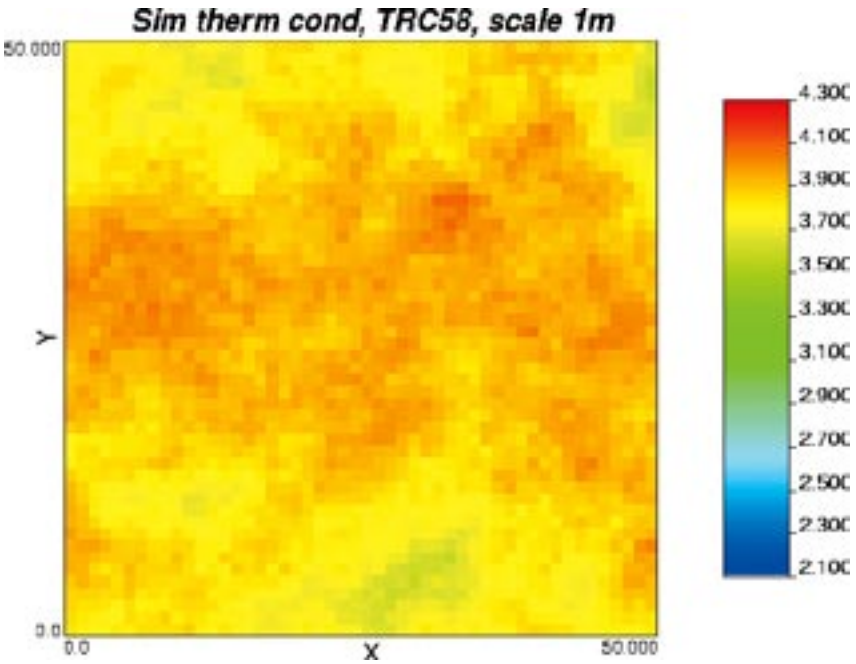

Figure D-6. *2D slice from one 3D realisation (simulation scale = 1 m) illustrating the distribution of thermal conductivity values in TRC 58. R = 1, Slice = 25, xy-plane. Note the spatial continuity apparent up to ca 30–40 m (range).*

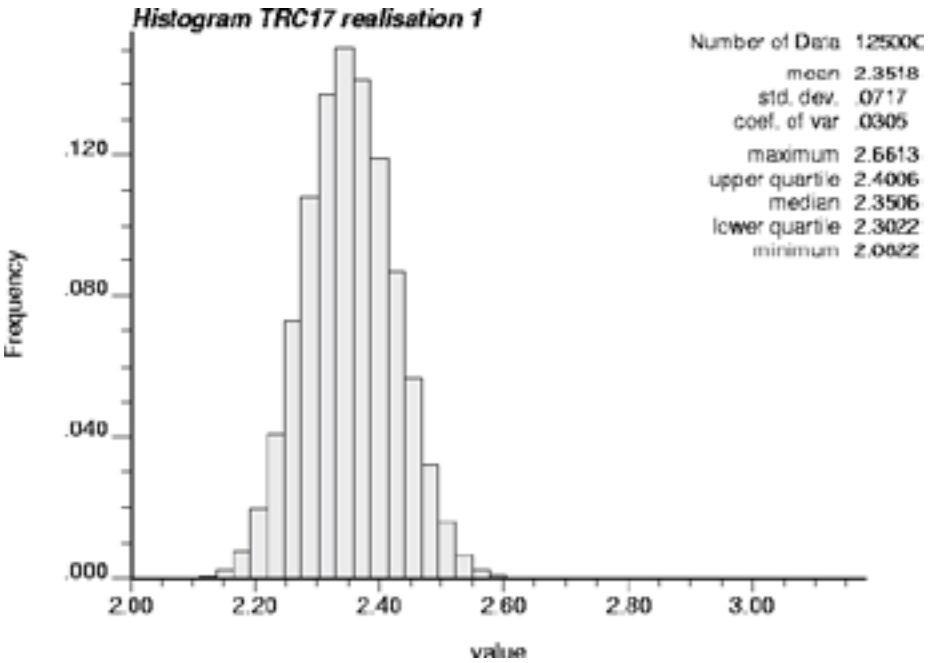

Figure D-7. *Histogram of 1 realisation at 0.1 m scale for TRC 17. Note the lower variance compared to the 150 combined realisations.*

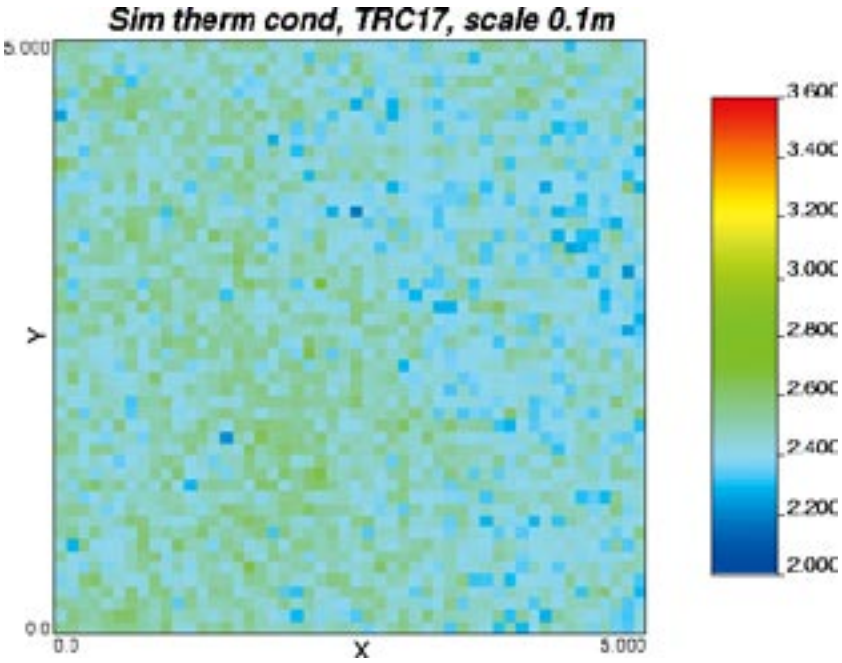

Figure D-8. *2D slice from one 3D realisation (0.1 m scale) illustrating the distribution of thermal conductivity values in TRC 17. R = 1, Slice = 25, xy-plane.*

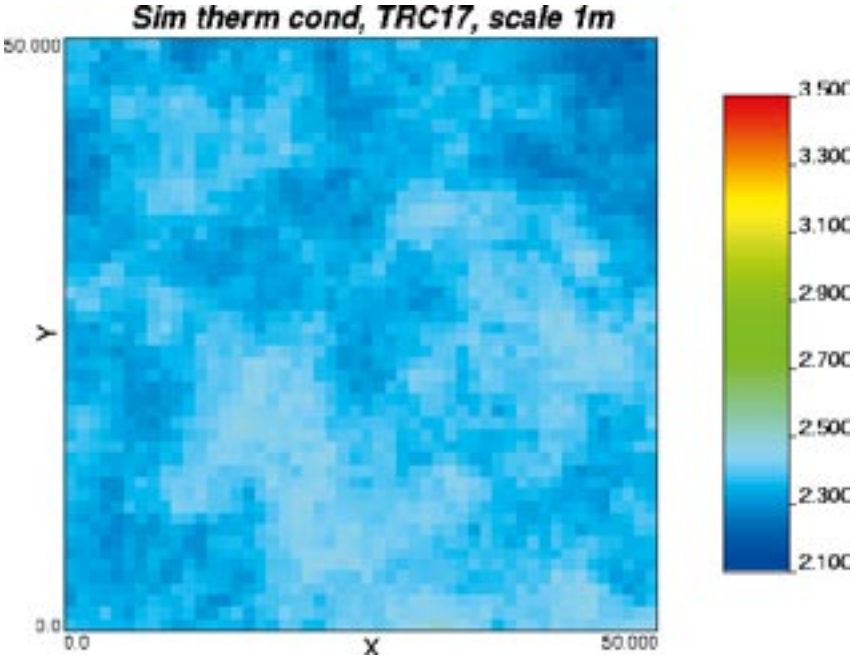

Figure D-9. *2D slice from one 3D realisation (simulation scale = 1 m) illustrating the distribution of thermal conductivity values in TRC 17. R = 1, Slice = 25, xy-plane.*

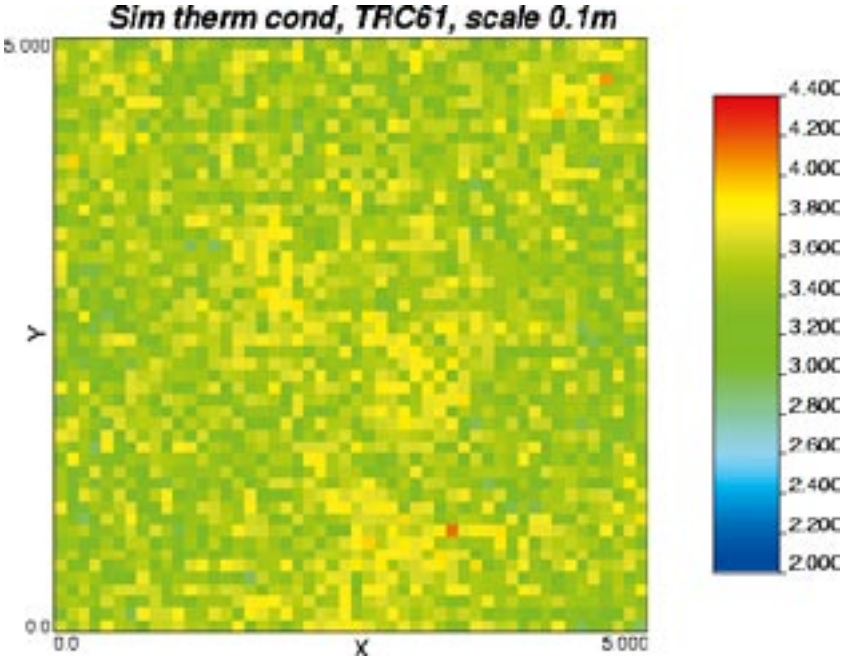

Figure D-10. *2D slice from one 3D realisation (0.1 m scale) illustrating the distribution of thermal conductivity values in TRC 61. R = 1, Slice = 25, xy-plane.*

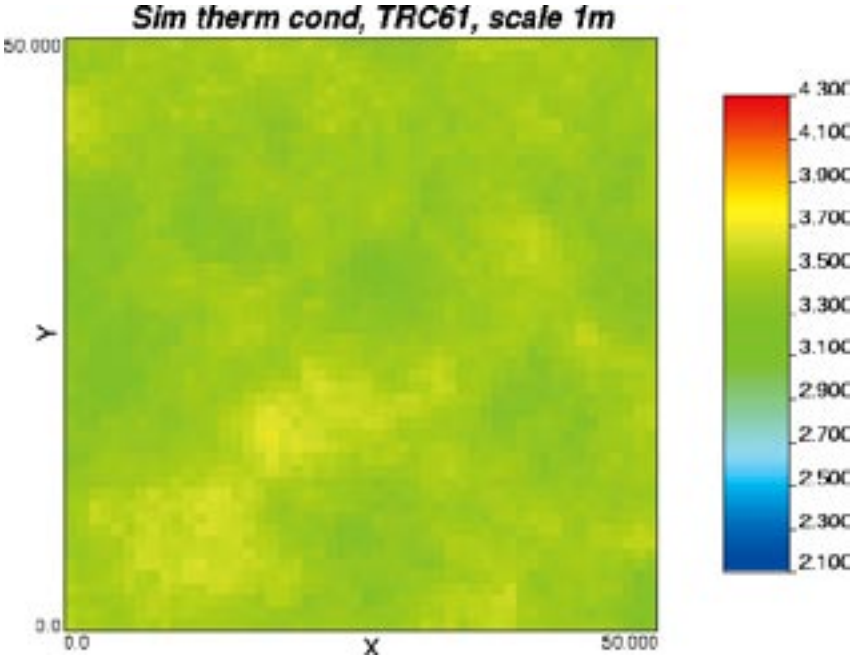

Figure D-11. *2D slice from one 3D realisation (simulation scale = 1 m) illustrating the distribution of thermal conductivity values in TRC 61. R = 1, Slice = 25, xy-plane.*

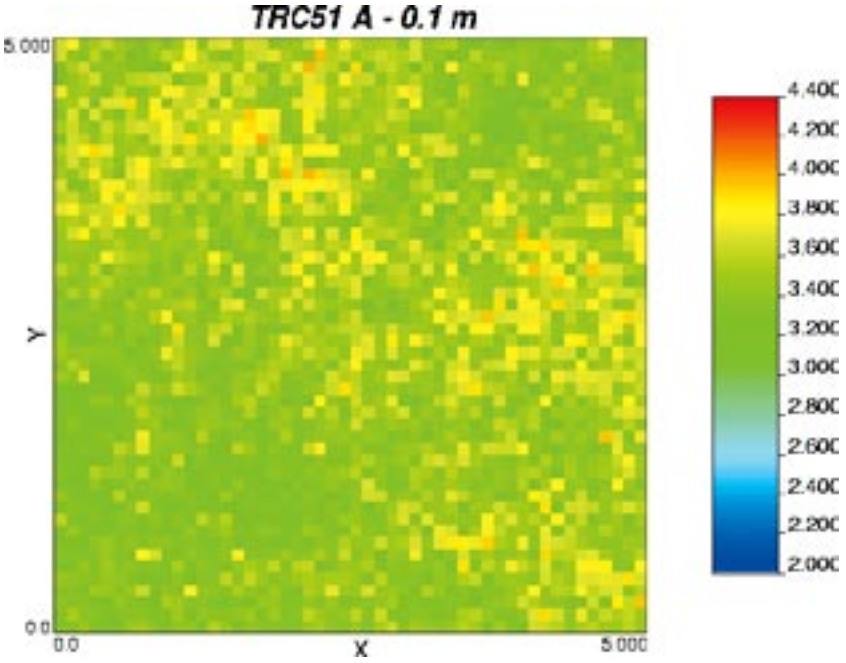

Figure D-12. *2D slice from one 3D realisation (simulation scale = 0.1 m) illustrating the distribution of thermal conductivity values in TRC 51, type A. R = 1, Slice = 25, xy-plane.*

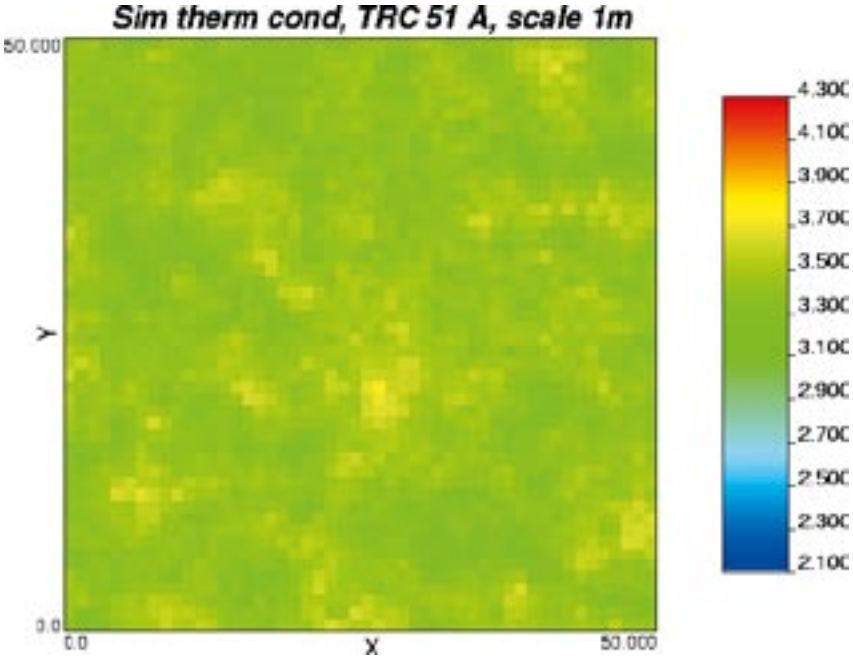

Figure D-13. *2D slice from one 3D realisation (simulation scale = 1 m) illustrating the distribution of thermal conductivity values in TRC 51, type A. R = 1, Slice = 25, xy-plane.*

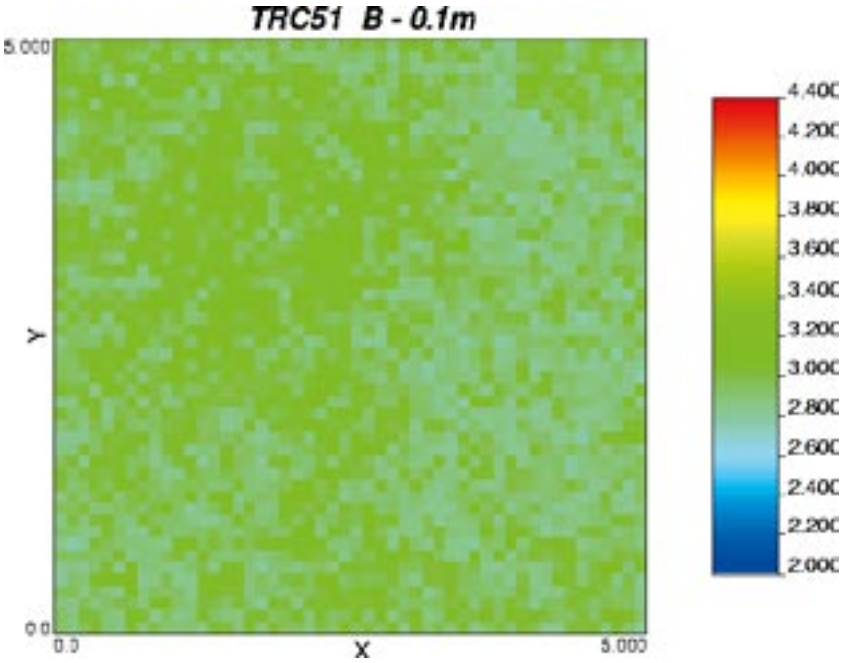

Figure D-14. *2D slice from one 3D realisation (simulation scale = 0.1 m) illustrating the distribution of thermal conductivity values in TRC 51, type B. R = 1, Slice = 25, xy-plane.*

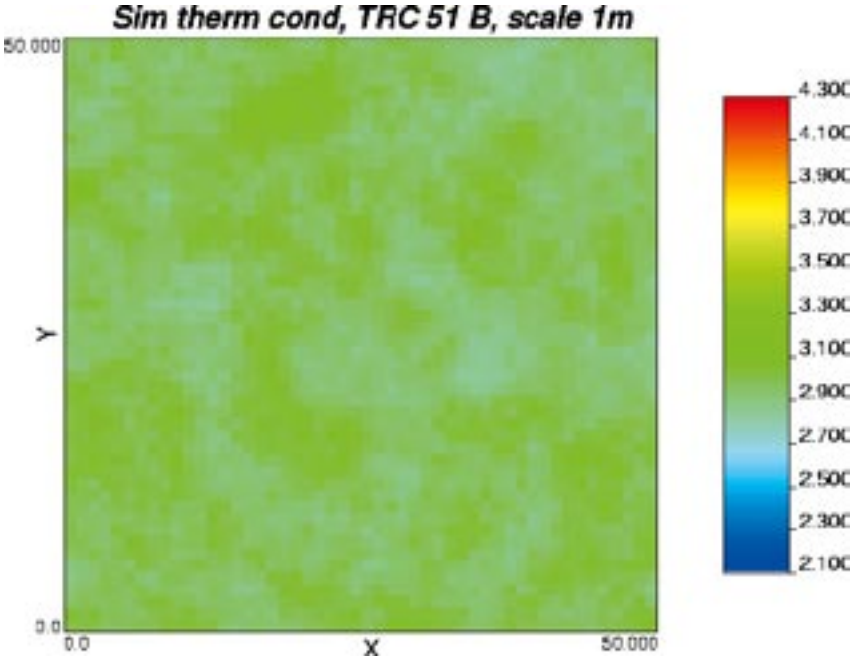

Figure D-15. *2D slice from one 3D realisation (simulation scale = 1 m) illustrating the distribution of thermal conductivity values in TRC 51, type B. R = 1, Slice = 25, xy-plane.*

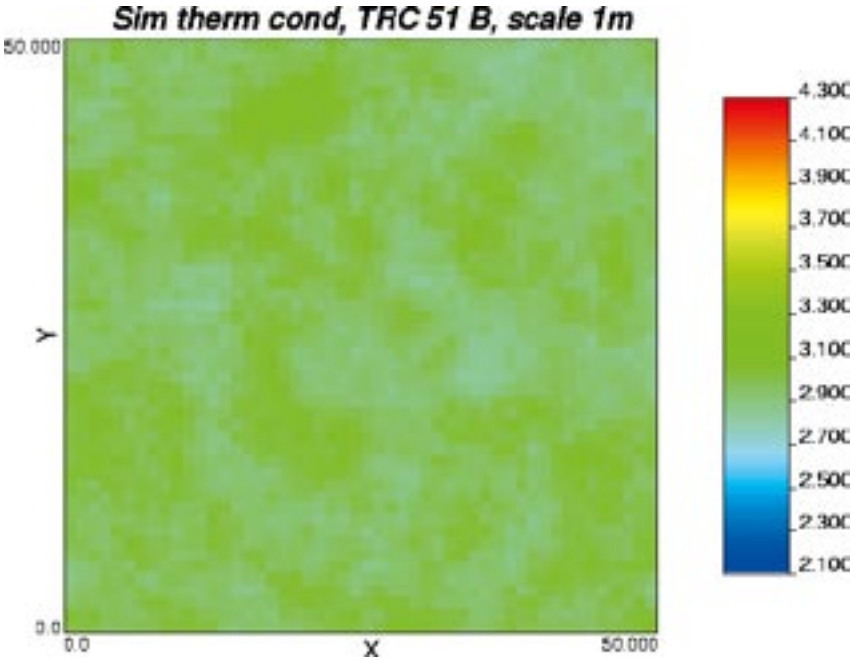

Figure D-16. *2D slice from one 3D realisation (simulation scale = 0.1 m) illustrating the distribution of thermal conductivity values in TRC 51, type C. R = 1, Slice = 25, xy-plane.*

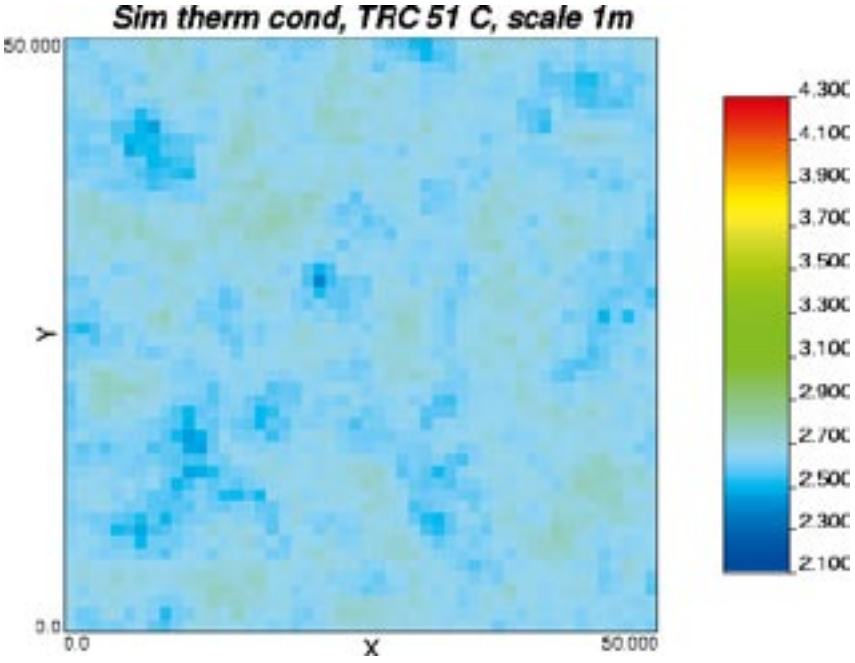

Figure D-17. *2D slice from one 3D realisation (simulation scale = 1 m) illustrating the distribution of thermal conductivity values in TRC 51, type C. R = 1, Slice = 25, xy-plane.*

Appendix E

Thermal distribution models from simulation

0.1 m simulations

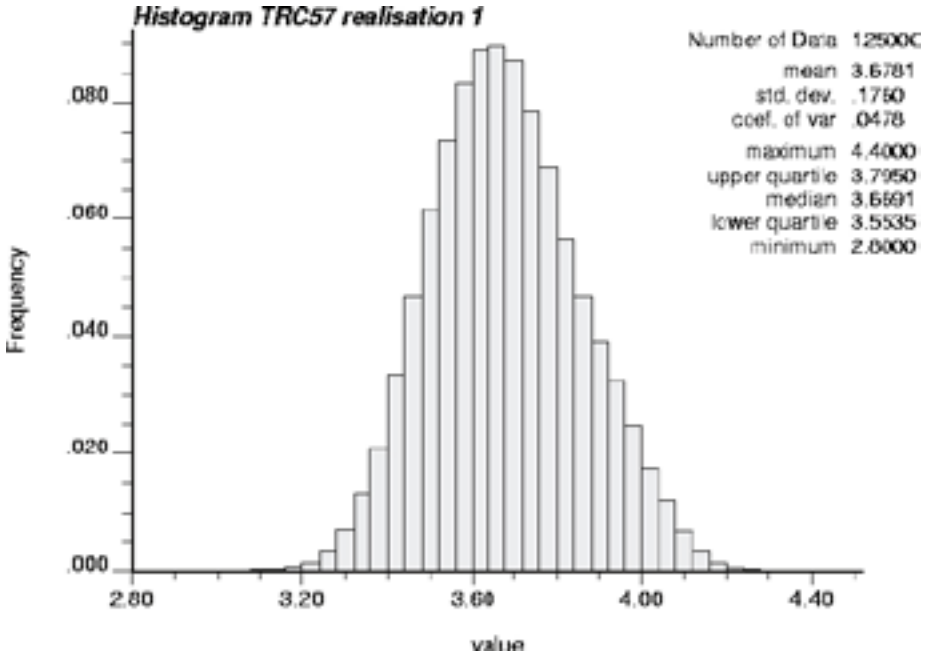

Figure E-1. *Statistics of the distribution model for TRC 57 for simulation at 0.1 m scale. The histogram is based on one realisation using a pure nugget, i.e. no spatial correlation.*

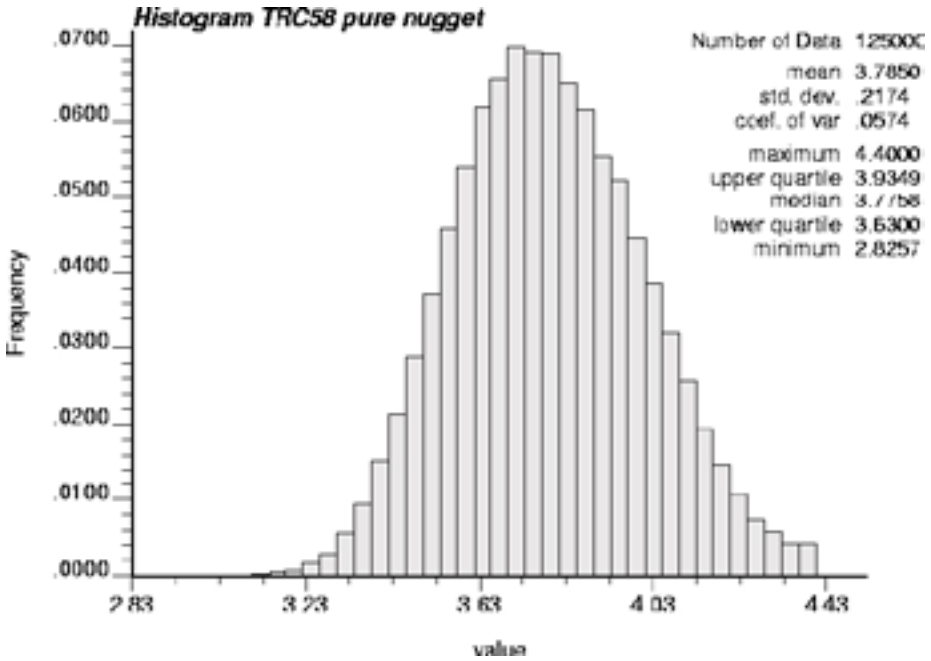

Figure E-2. *Statistics of the distribution model for TRC 58 for simulation at 0.1 m scale. The histogram is based on one realisation using a pure nugget, i.e. no spatial correlation.*

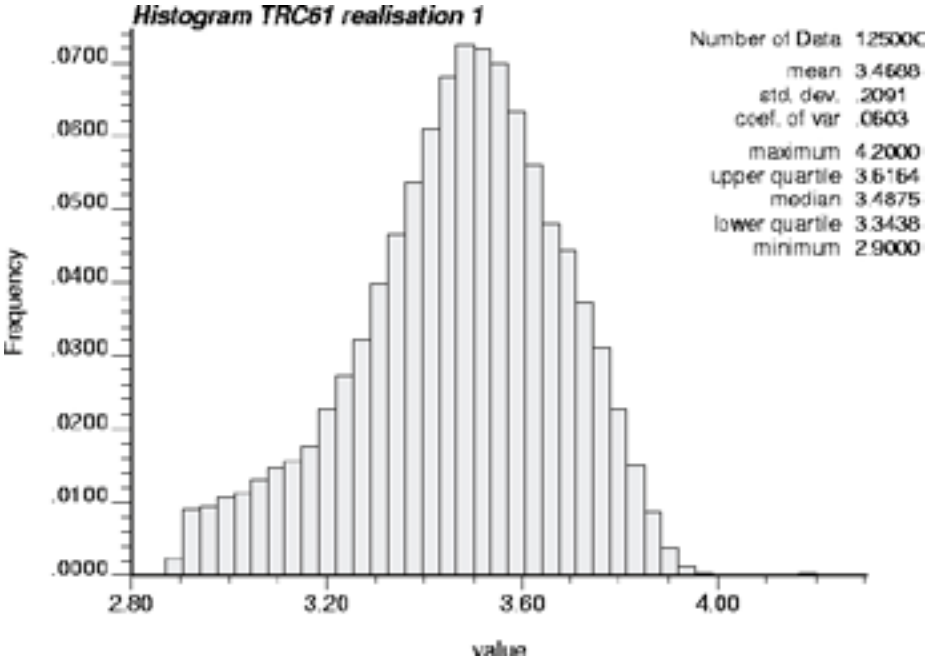

Figure E-3. *Statistics of the distribution model for TRC 61 for simulation at 0.1 m scale. The histogram is based on one realisation using a pure nugget, i.e. no spatial correlation.*

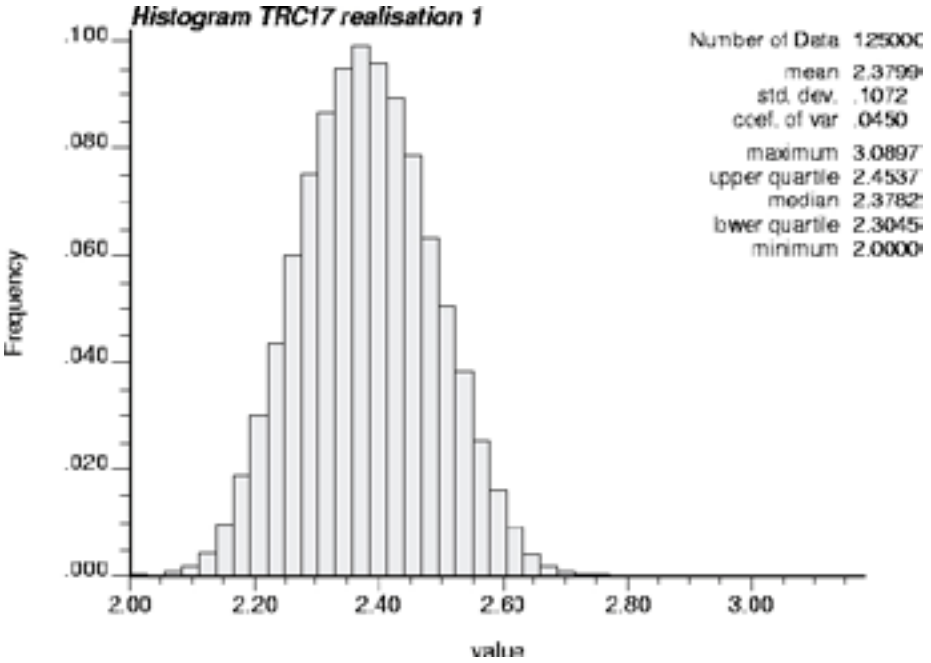

Figure E-4. *Statistics of the distribution model for TRC 17 for simulation at 0.1 m scale. The histogram is based on one realisation using a pure nugget, i.e. no spatial correlation.*

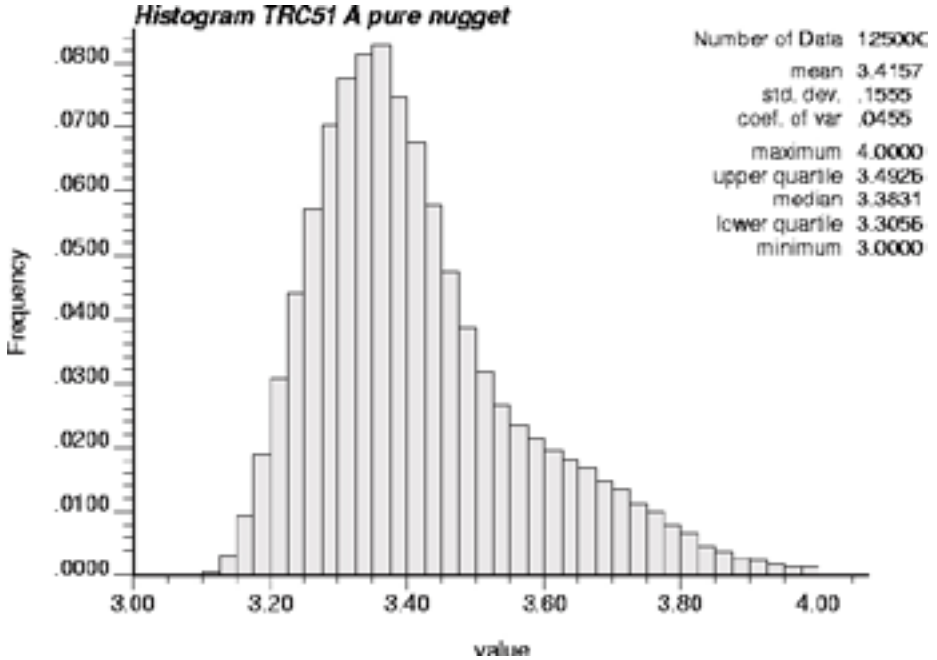

Figure E-5. *Statistics of the distribution model for TRC 51, type A for simulation at 0.1 m scale. The histogram is based on one realisation using a pure nugget, i.e. no spatial correlation.*

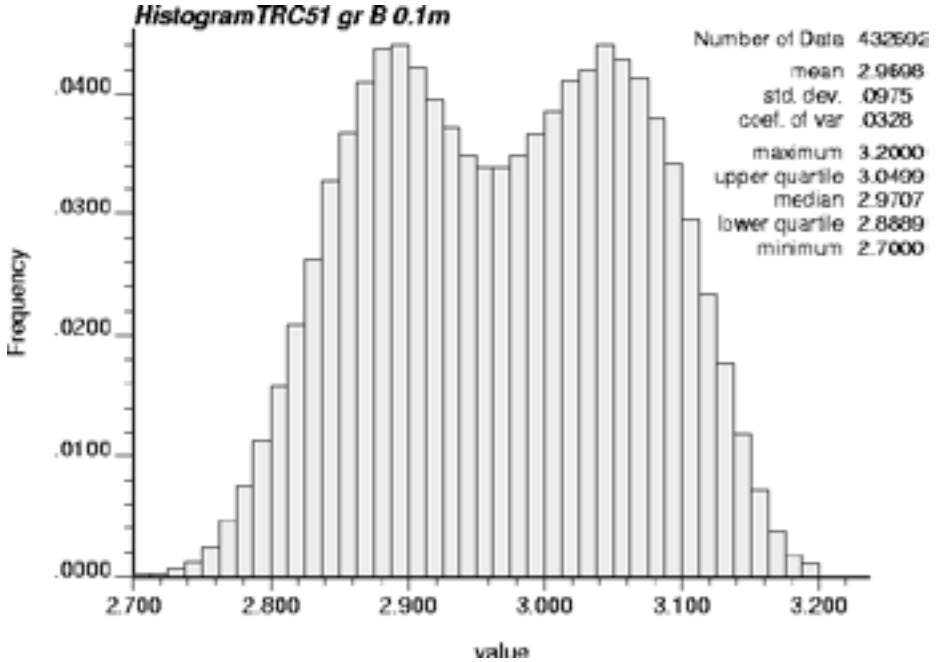

Figure E-6. *Statistics of the distribution model for TRC 51, type B for simulation at 0.1 m scale. The histogram is based on one realisation using a pure nugget, i.e. no spatial correlation.*

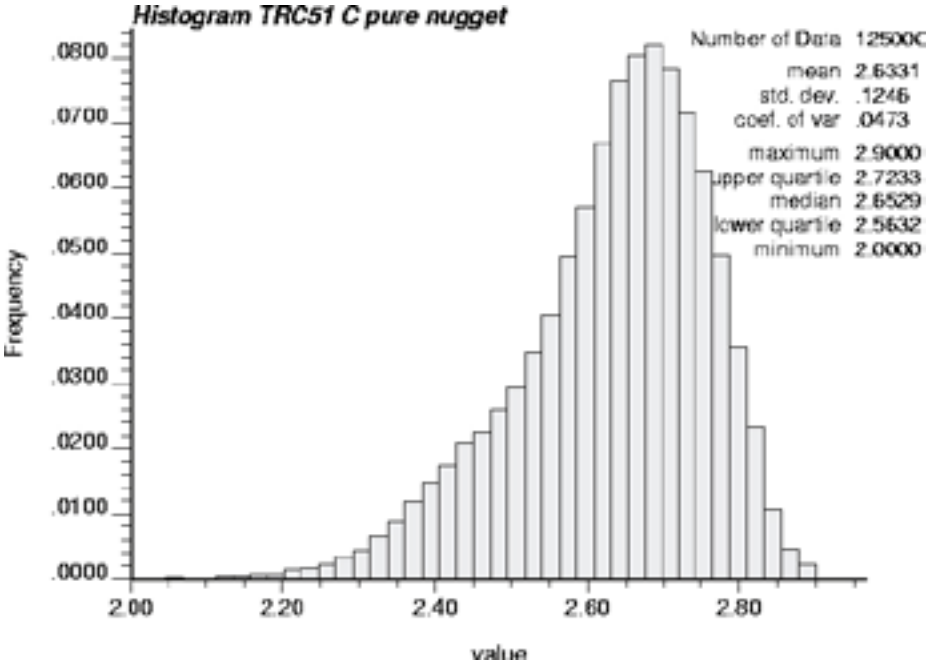

Figure E-7. *Statistics of the distribution model for TRC 51, type B for simulation at 0.1 m scale. The histogram is based on one realisation using a pure nugget, i.e. no spatial correlation.*

Appendix F

Variogram model reproduction

0.1 m simulations

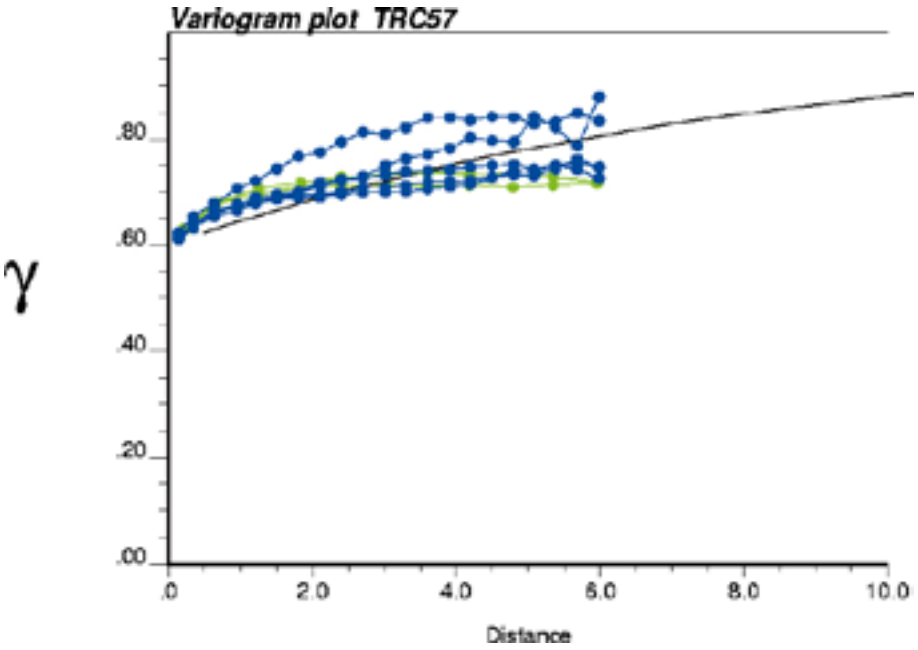

Figure F-1. *Comparison of the variogram model and variograms of 5 independent realisations for TRC 57. Search options used in simulating: search radii – 3.0 m; no. of simulated nodes – 48;, multiple grid search – yes; no of multiple grid refinements – 4. Lag distance (x-axis) in metres (m). Variogram is normalised to the variance of the simulated data.*

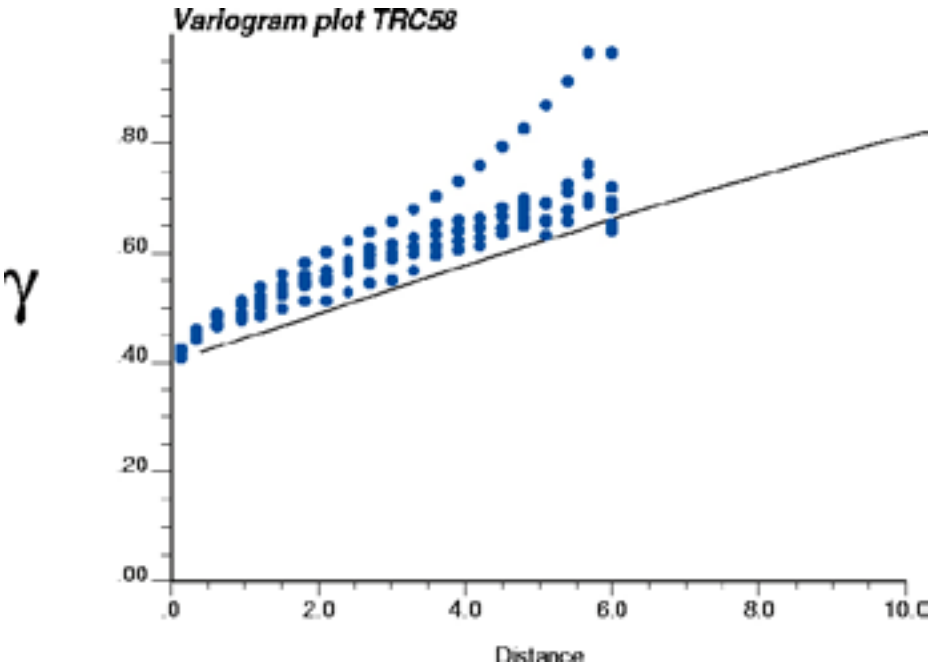

Figure F-2. *Comparison of the variogram model and variograms of 6 independent realisations for TRC 58. Search options used in simulating: search radii – 3.0 m; no. of simulated nodes – 32; multiple grid search – yes; no of multiple grid refinements – 3. Lag distance (x-axis) in metres (m). Variogram is normalised to the variance of the simulated data.*

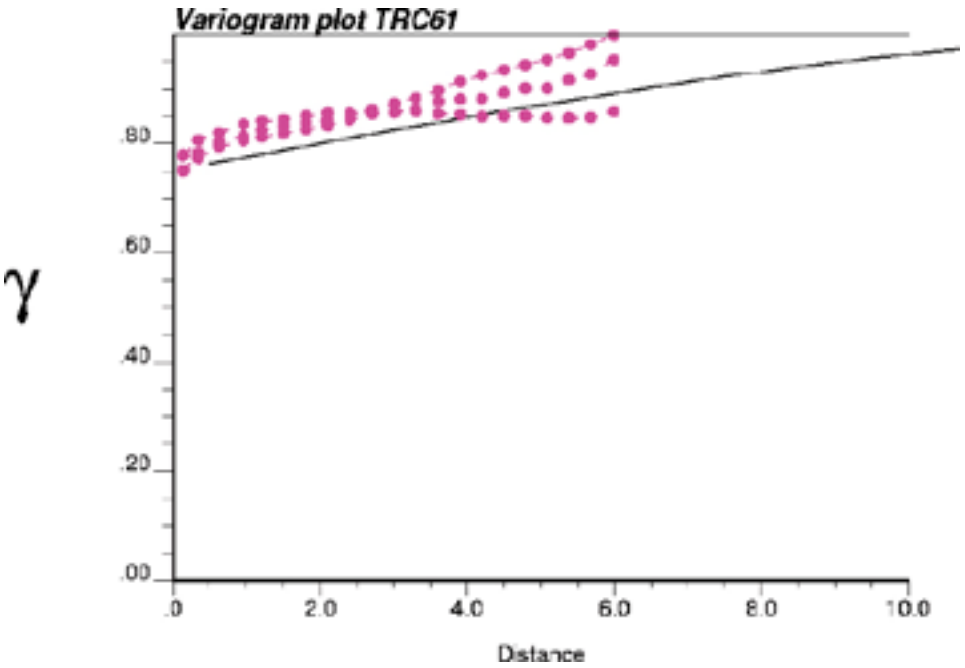

Figure F-3. *Comparison of the variogram model and variograms of 3 independent realisations for TRC 61. Search options used in simulating: search radii – 3.0 m; no. of simulated nodes – 48; multiple grid search – yes; no of multiple grid refinements – 3. Lag distance (x-axis) in metres (m). Variogram is normalised to the variance of the simulated data.*

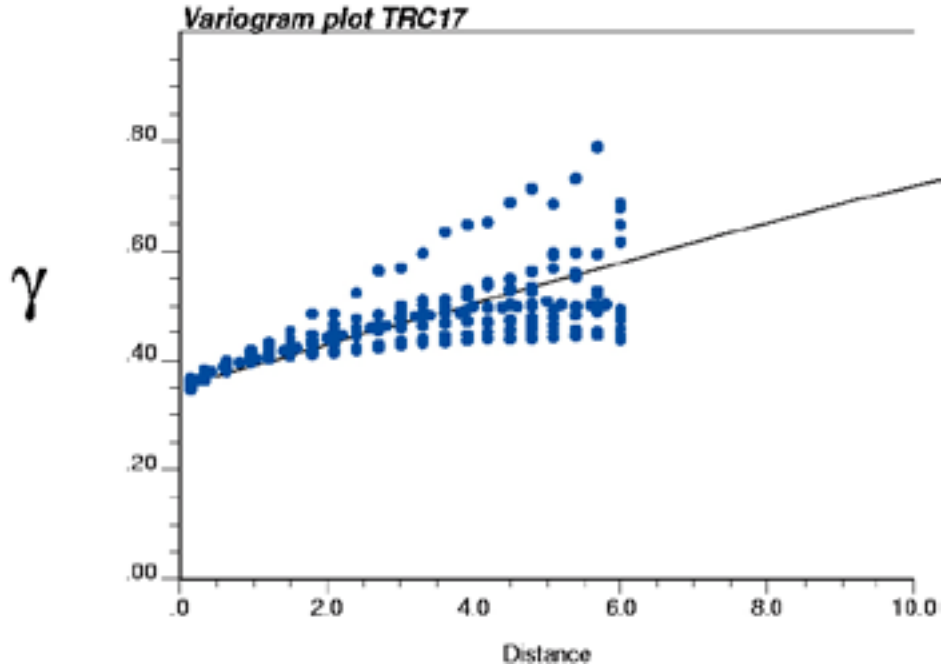

Figure F-4. *Comparison of the variogram model and variograms of 10 independent realisations for TRC 17. Search options used in simulating: search radii – 3.0 m; no. of simulated nodes – 48; multiple grid search – yes; no of multiple grid refinements – 3. Lag distance (x-axis) in metres (m). Variogram is normalised to the variance of the simulated data.*

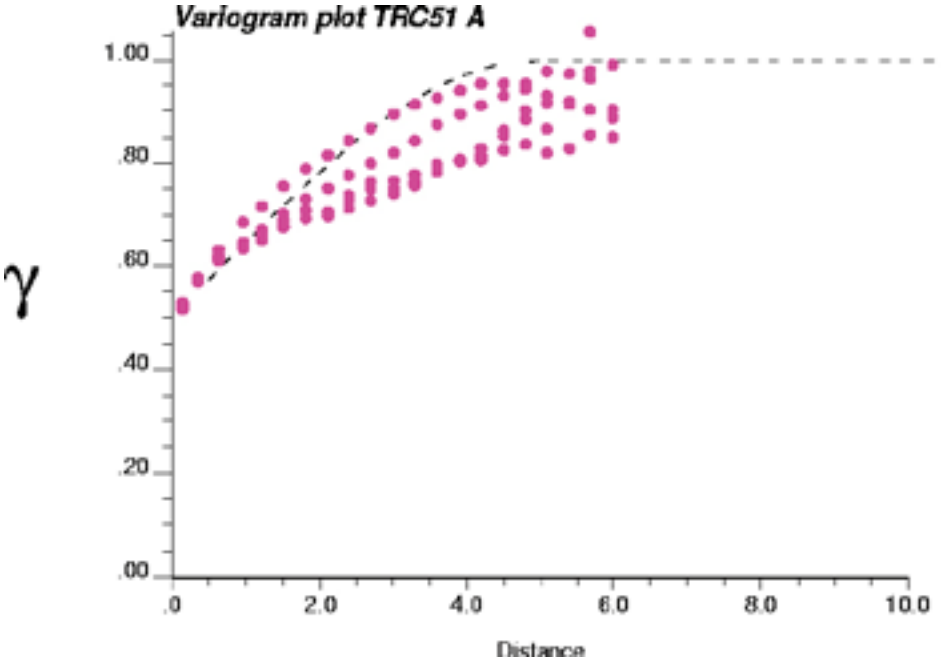

Figure F-5. *Comparison of the variogram model and variograms of 4 independent realisations for TRC 51, type A. Search options used in simulating: search radii – 2.0 m; no. of simulated nodes –24; multiple grid search – yes; no of multiple grid refinements – 3. Lag distance (x-axis) in metres (m). Variogram is normalised to the variance of the simulated data.*

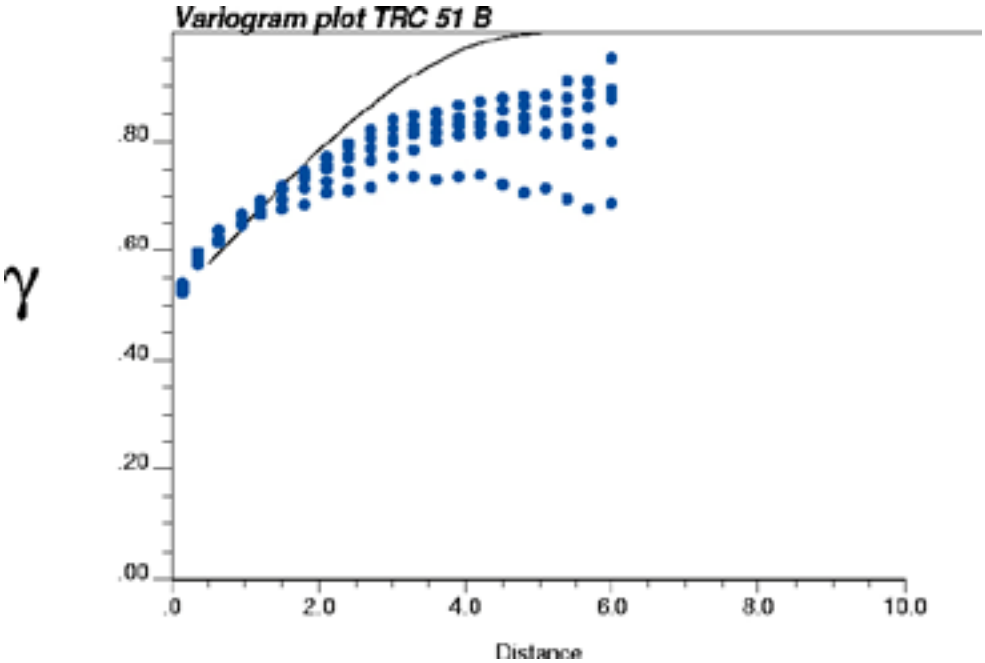

Figure F-6. *Comparison of the variogram model and variograms of 6 independent realisations for TRC 51, type B. Search options used in simulating: search radii – 2.0 m; no. of simulated nodes –24; multiple grid search – yes; no of multiple grid refinements – 3. Lag distance (x-axis) in metres (m). Variogram is normalised to the variance of the simulated data.*

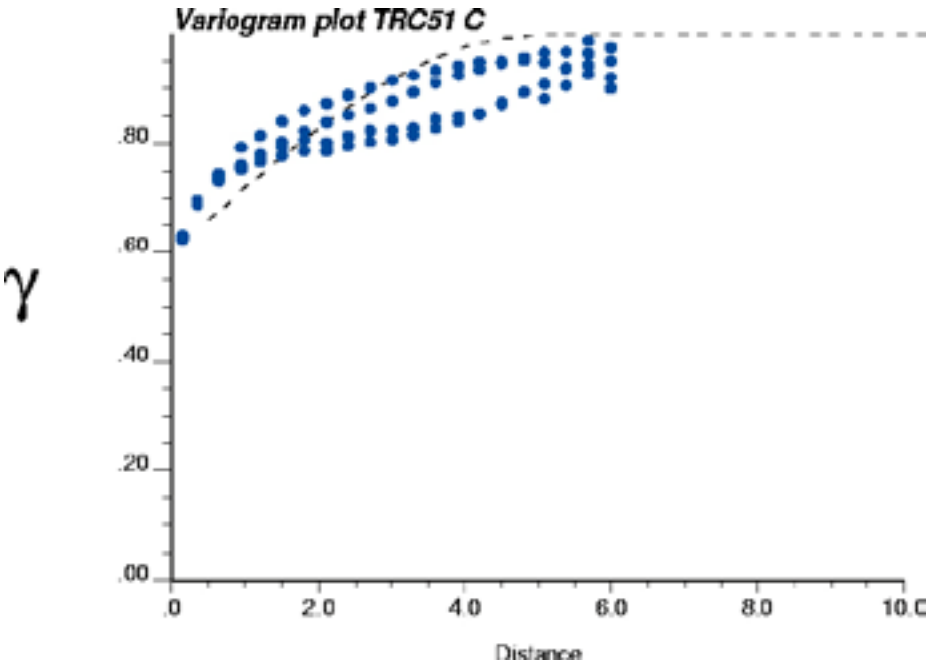

Figure F-7. *Comparison of the variogram model and variograms of 4 independent realisations for TRC 51, type C. Search options used in simulating: search radii – 2.0 m; no. of simulated nodes –24; multiple grid search – yes; no of multiple grid refinements – 3. Lag distance (x-axis) in metres (m). Variogram is normalised to the variance of the simulated data.*

1 m simulations

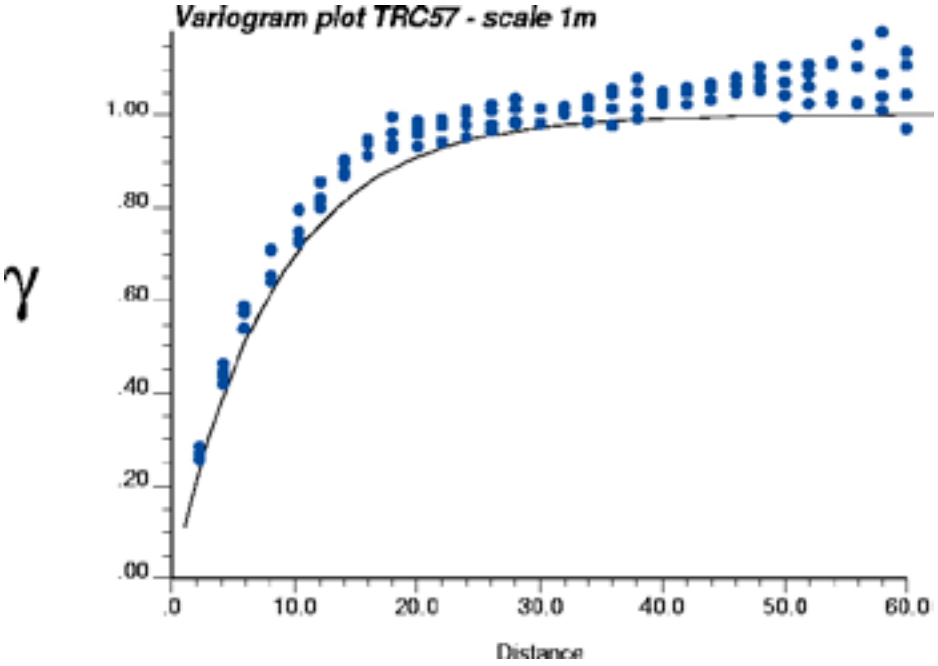

Figure F-8. *Comparison of the variogram model and variograms of 4 independent realisations for TRC 57. Search options used in simulating: search radii – 10 m; no. of simulated nodes – 32; multiple grid search – no. Lag distance (x-axis) in metres (m). Variogram is normalised to the variance of the simulated data.*

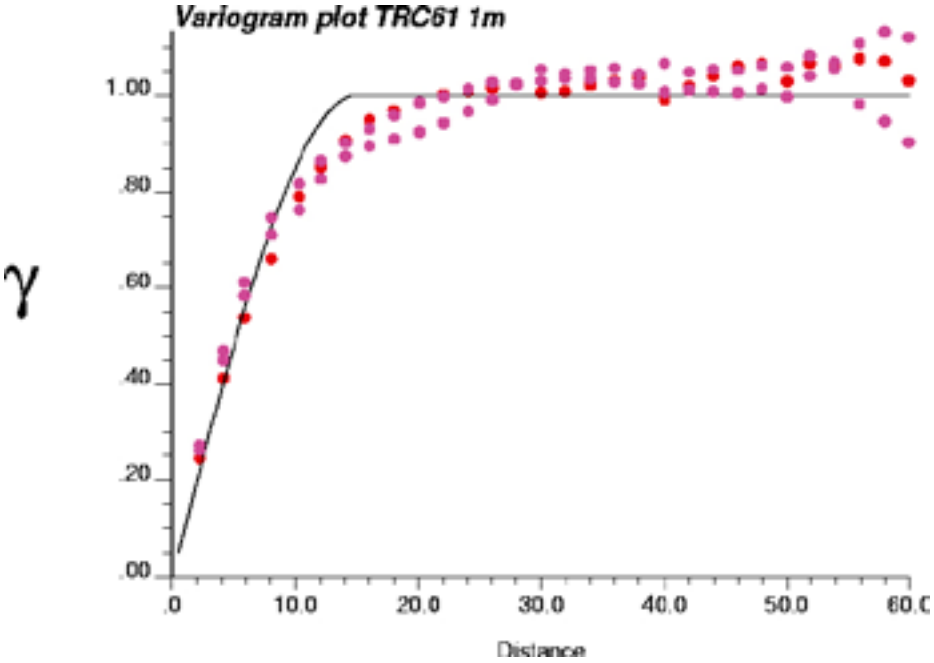

Figure F-9. *Comparison of the variogram model and variograms of 4 independent realisations for TRC 58. Search options used in simulating: search radii – 20 m; no. of simulated nodes – 32; multiple grid search – yes; no of multiple grid refinements – 3. Lag distance (x-axis) in metres (m). Variogram is normalised to the variance of the simulated data.*

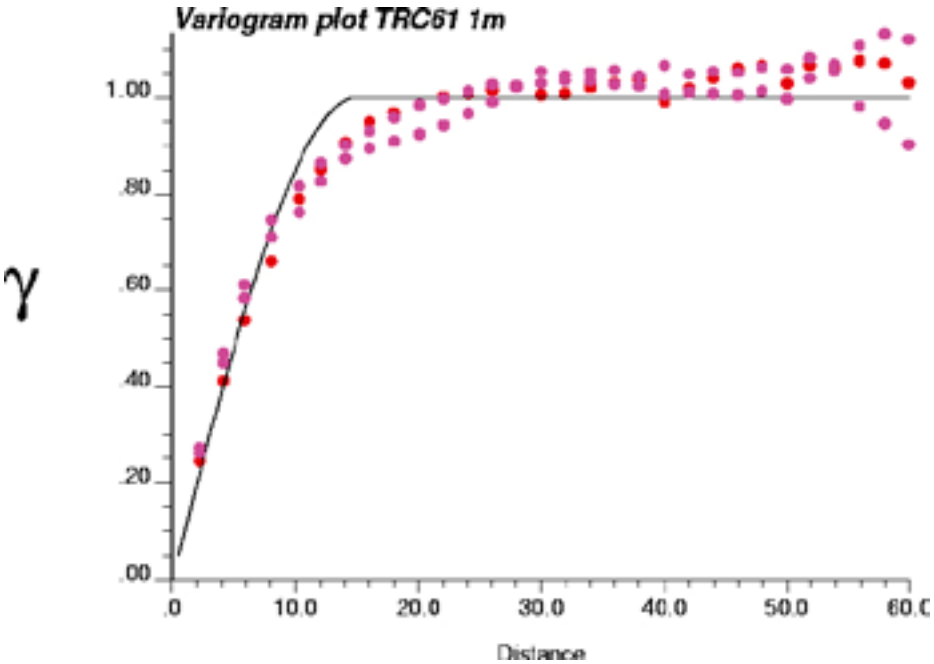

Figure F-10. *Comparison of the variogram model and variograms of 3 independent realisations for TRC 61. Search options used in simulating: search radii – 7.5 m; no. of simulated nodes – 32; multiple grid search – no. Lag distance (x-axis) in metres (m). Variogram is normalised to the variance of the simulated data.*

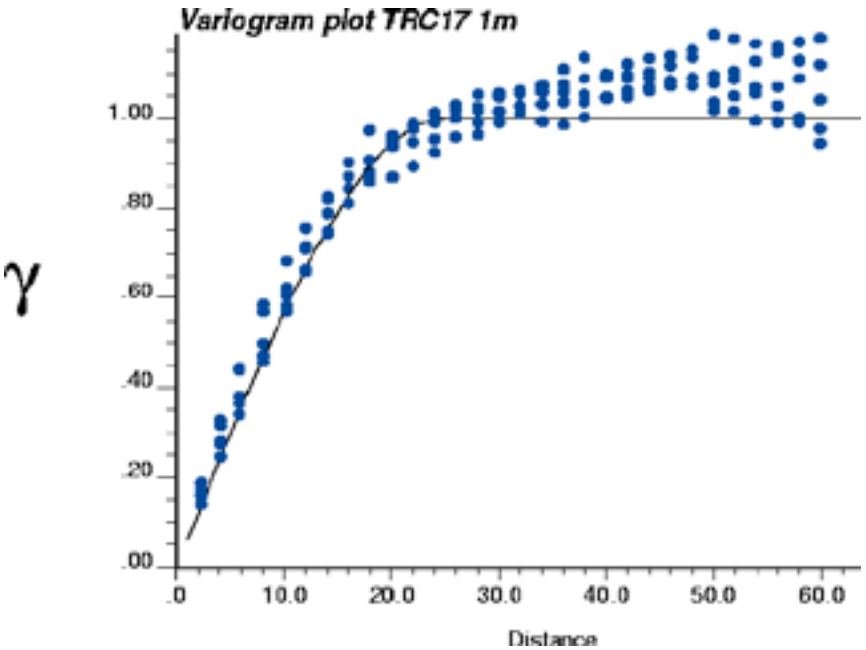

Figure F-11. *Comparison of the variogram model and variograms of 5 independent realisations for TRC 17. Search options used in simulating: search radii – 10 m; no. of simulated nodes – 32; multiple grid search – no. Lag distance (x-axis) in metres (m). Variogram is normalised to the variance of the simulated data.*

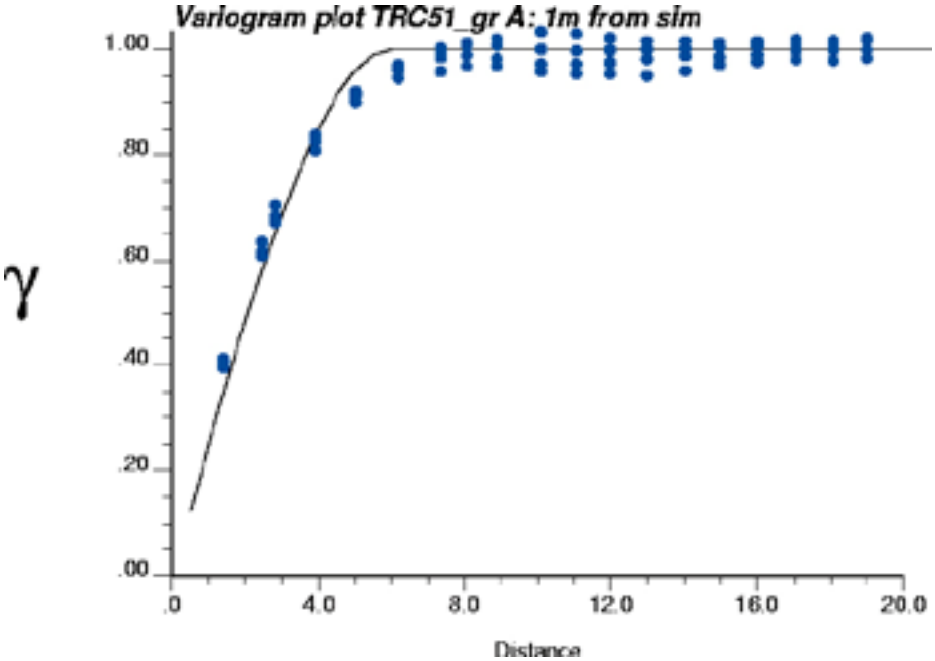

Figure F-12. *Comparison of the variogram model and variograms of 4 independent realisations for TRC 51, type A. Search options used in simulating: search radii – 3 m; no. of simulated nodes – 32; multiple grid search – no. Lag distance (x-axis) in metres (m). Variogram is normalised to the variance of the simulated data.*

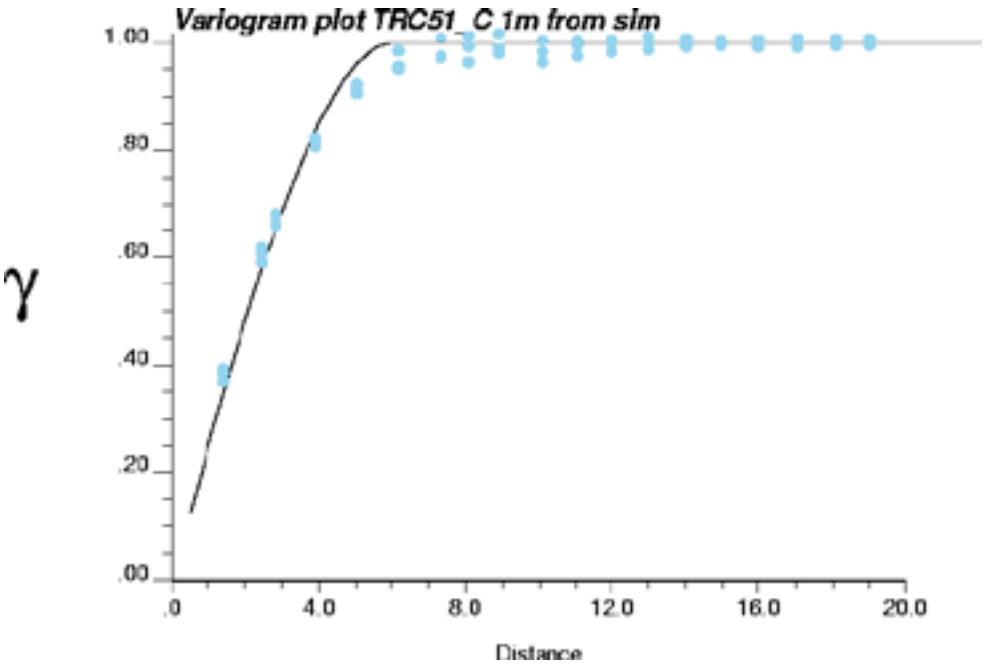

Figure F-13. *Comparison of the variogram model and variograms of 2 independent realisations for TRC 51, type C. Search options used in simulating: search radii – 3 m; no. of simulated nodes – 32; multiple grid search – no. Lag distance (x-axis) in metres (m). Variogram is normalised to the variance of the simulated data.*

Appendix G

TRC simulation results, histograms, scale 1 m

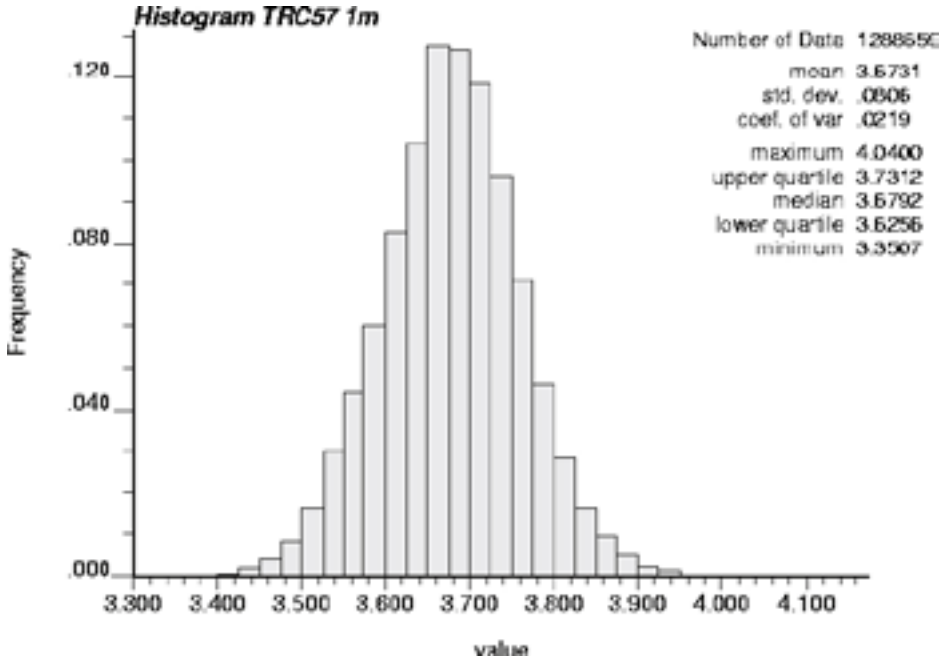

Figure G-1. *Histogram of simulation results of* ***TRC 57*** *at 1 m scale based on 1,000 realisations.*

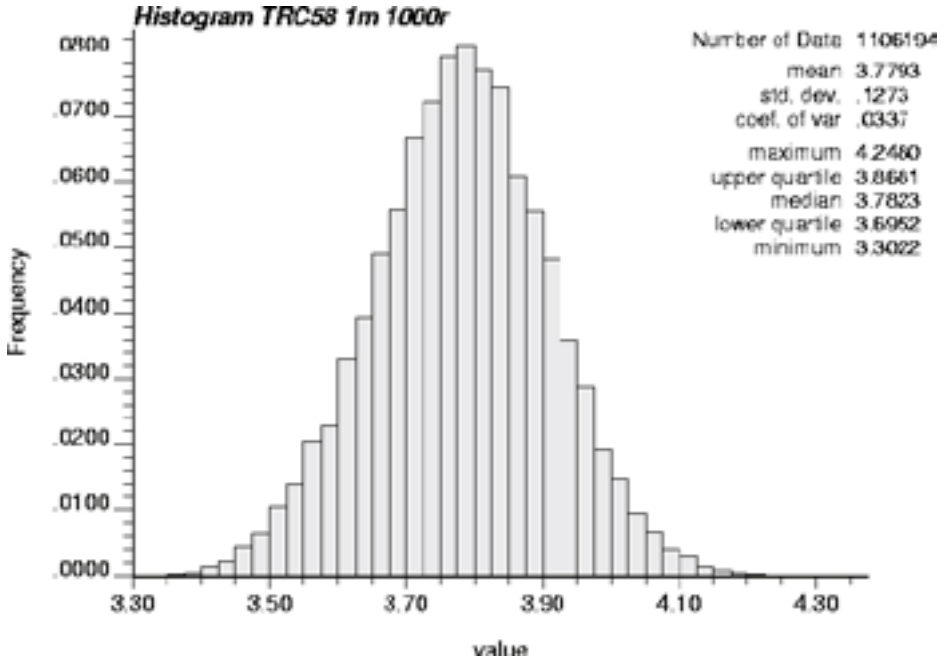

Figure G-2. *Histogram of simulation results of* ***TRC 58*** *at 1 m scale based on 1,000 realisations.*

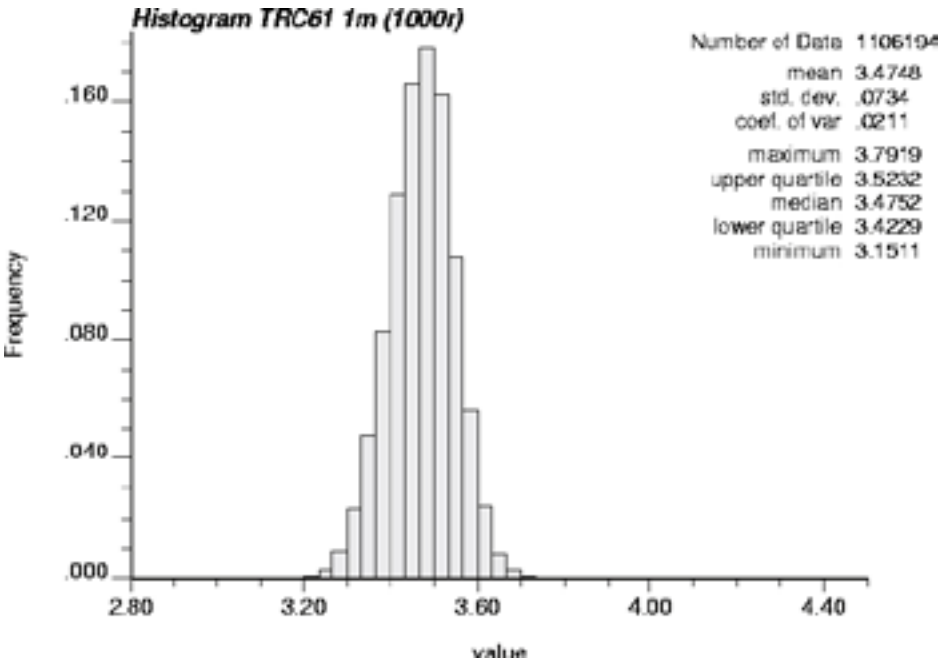

Figure G-3. *Histogram of simulation results of* ***TRC 61*** *at 1 m scale based on 1,000 realisations.*

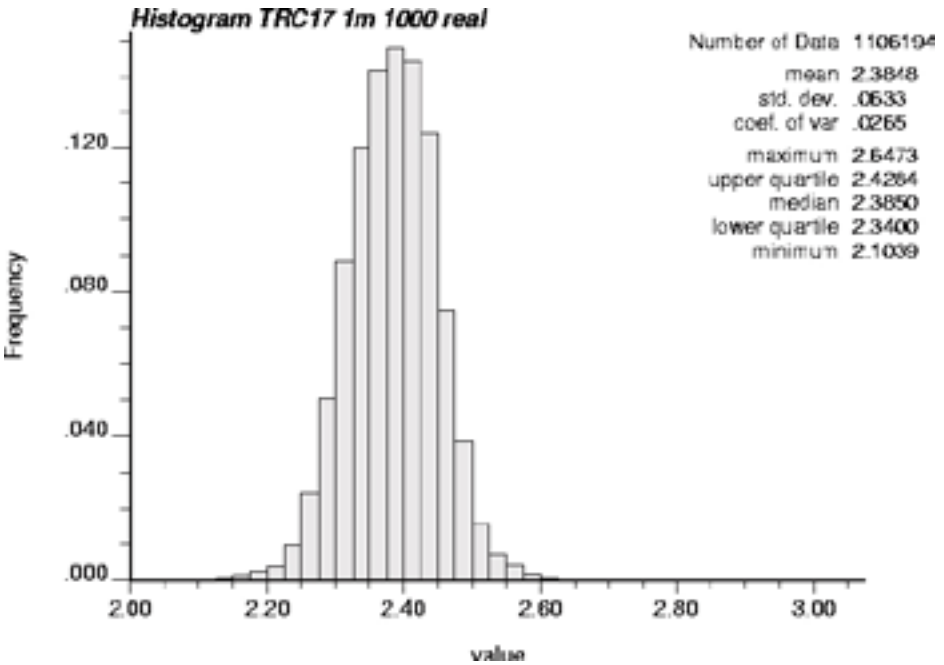

Figure G-4. *Histogram of simulation results of* ***TRC 17*** *at 1 m scale based on 1,000 realisations.*

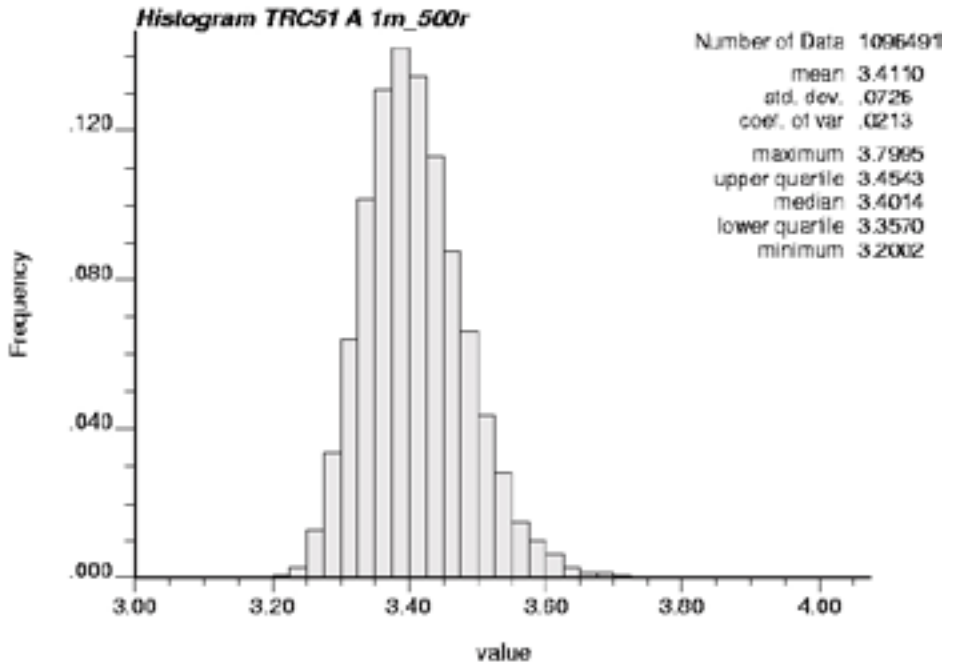

Figure G-5. *Histogram of simulation results of* ***TRC 51, type A****, at 1 m scale based on 500 realisations.*

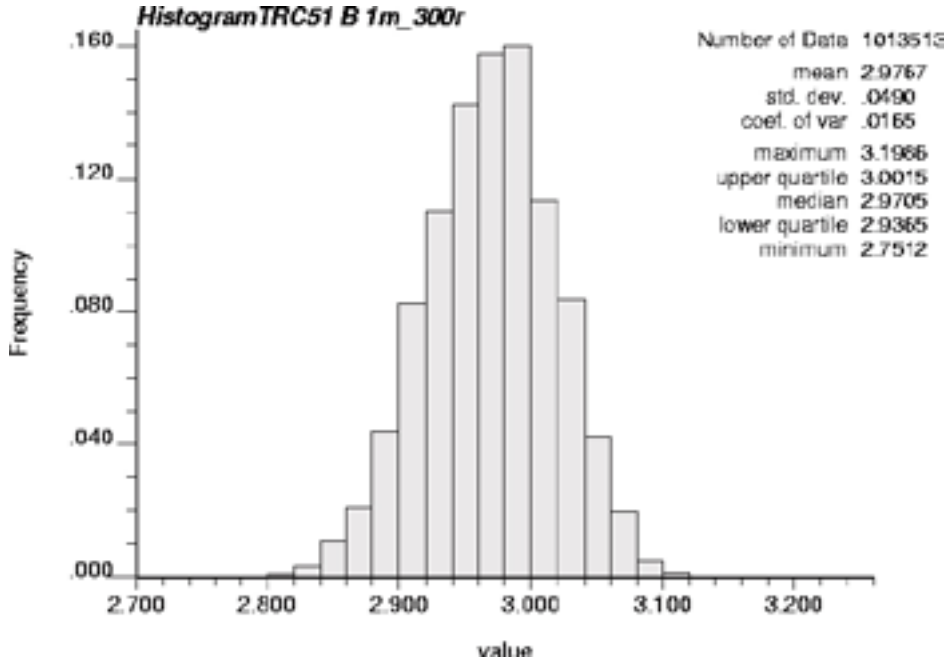

Figure G-6. *Histogram of simulation results of* ***TRC 51, type B****, at 1 m scale based on 300 realisations.*

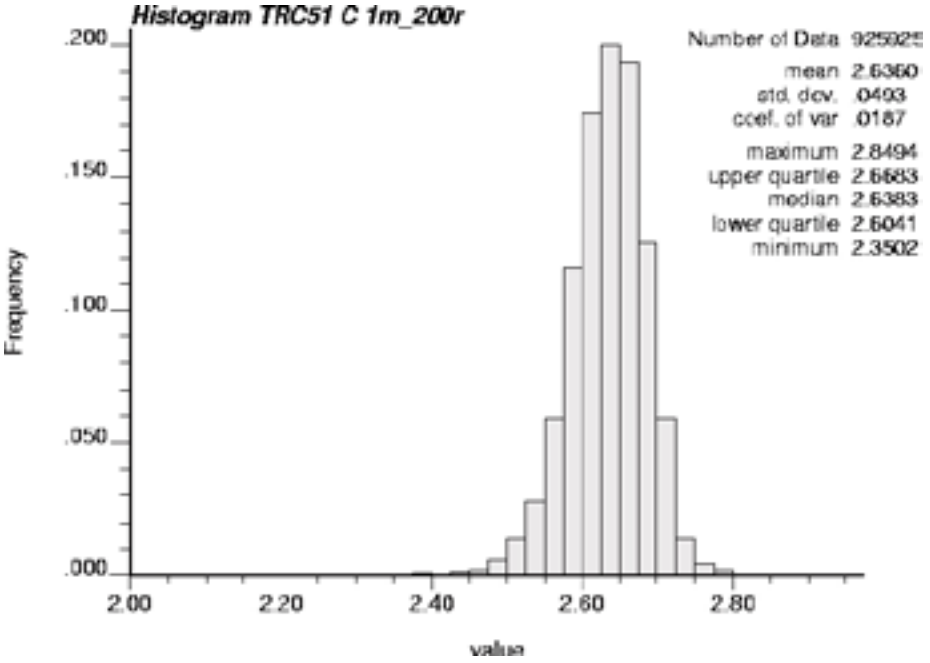

Figure G-7. *Histogram of simulation results of* ***TRC 51, type C****, at 1 m scale based on 200 realisations.*

Domain realisations – thermal properties

Domain RFM029, 0.1 m scale (Examples of realisations)

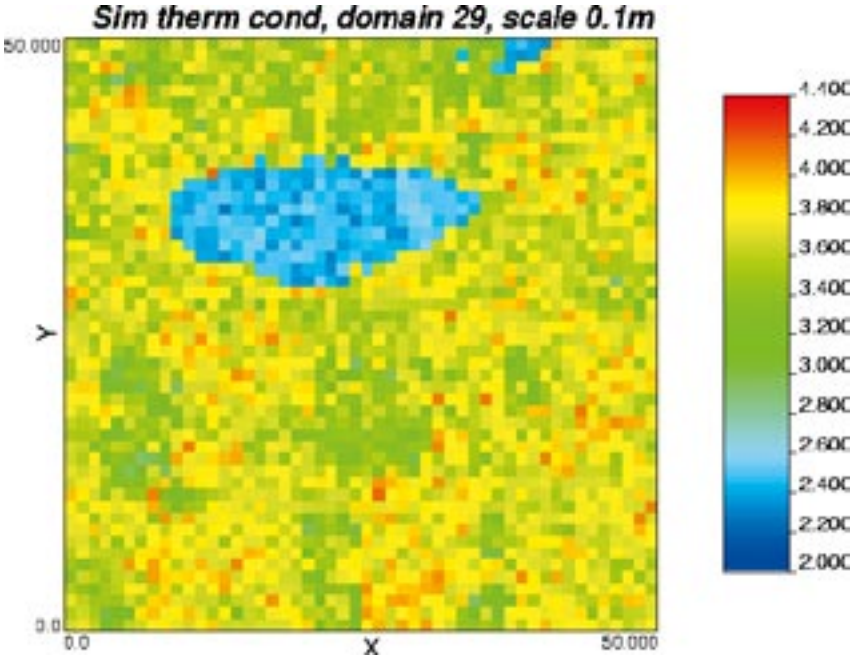

Domain RFM029: R = 1, Slice = 25, xy-plane

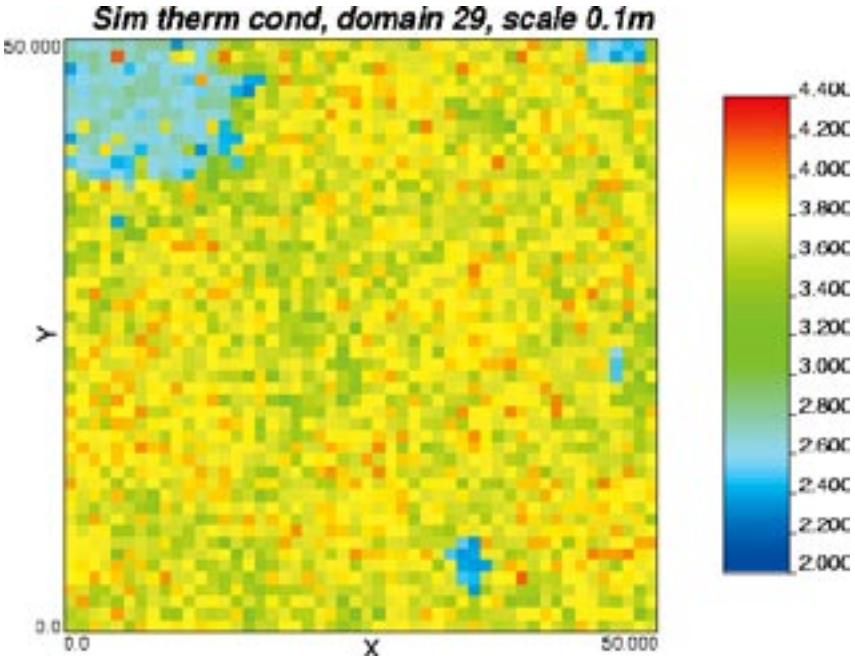

Domain RFM029: R = 150, Slice = 25, xy-plane

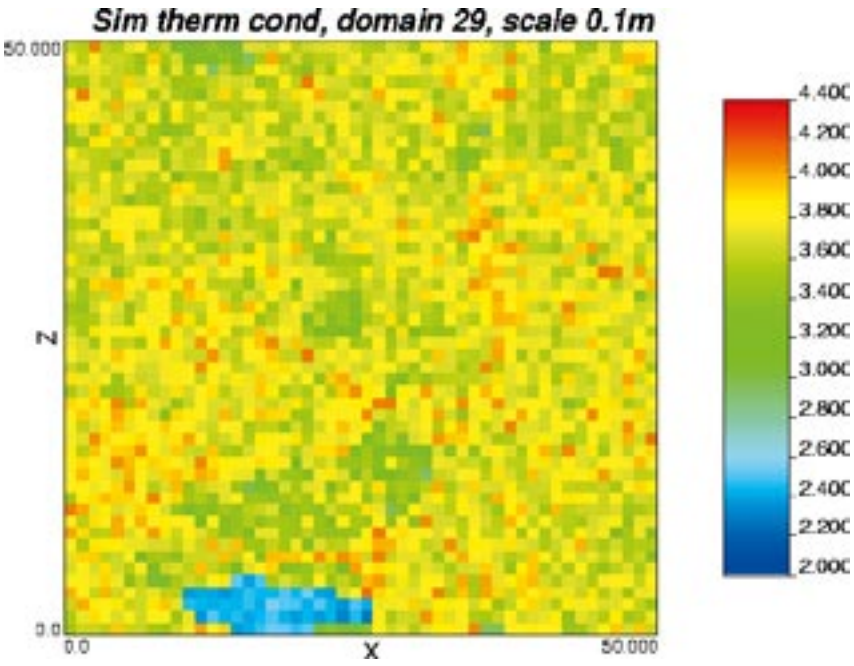

Domain RFM029: R = 1, Slice = 25, xz-plane

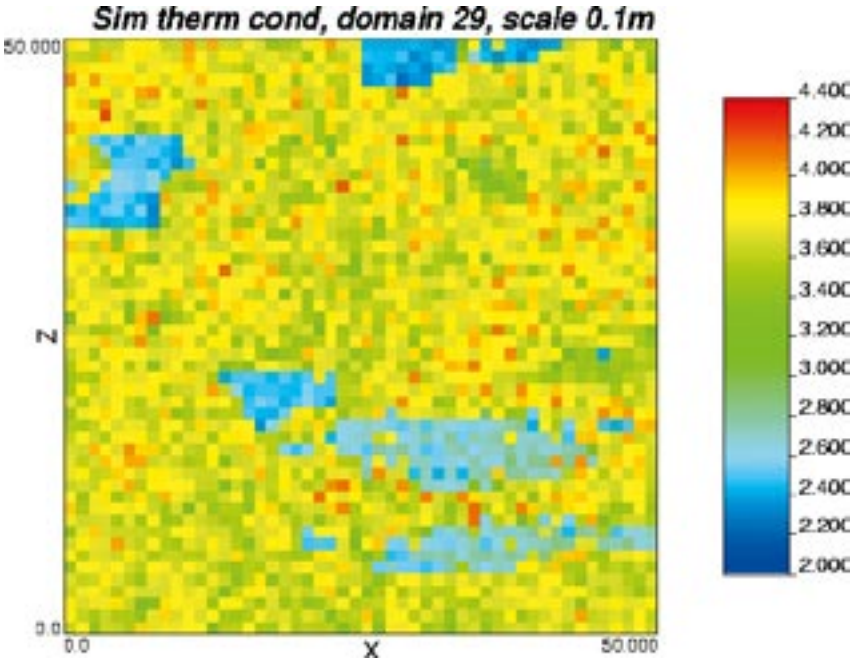

Domain RFM029: R = 150, Slice = 25, xz-plane

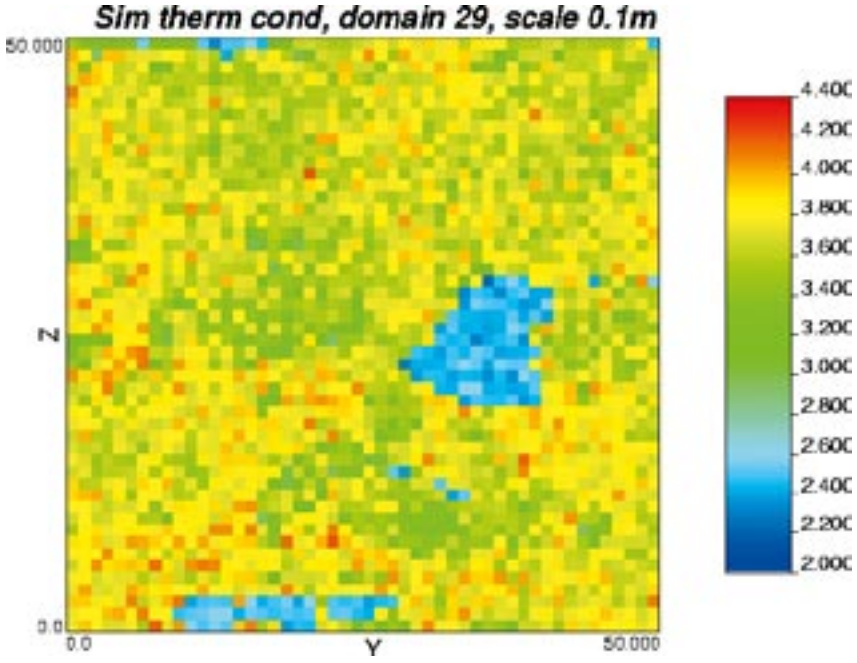

Domain RFM029: R = 1, Slice = 25, yz-plane

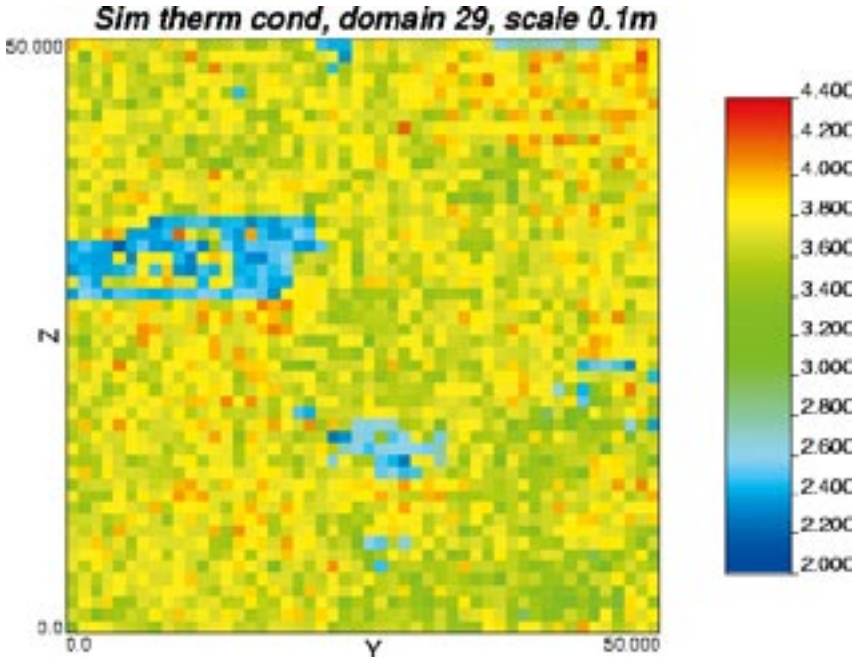

Domain RFM029: R = 150, Slice = 25, yz-plane

Domain RFM029, 1 m scale (Examples of realisations)

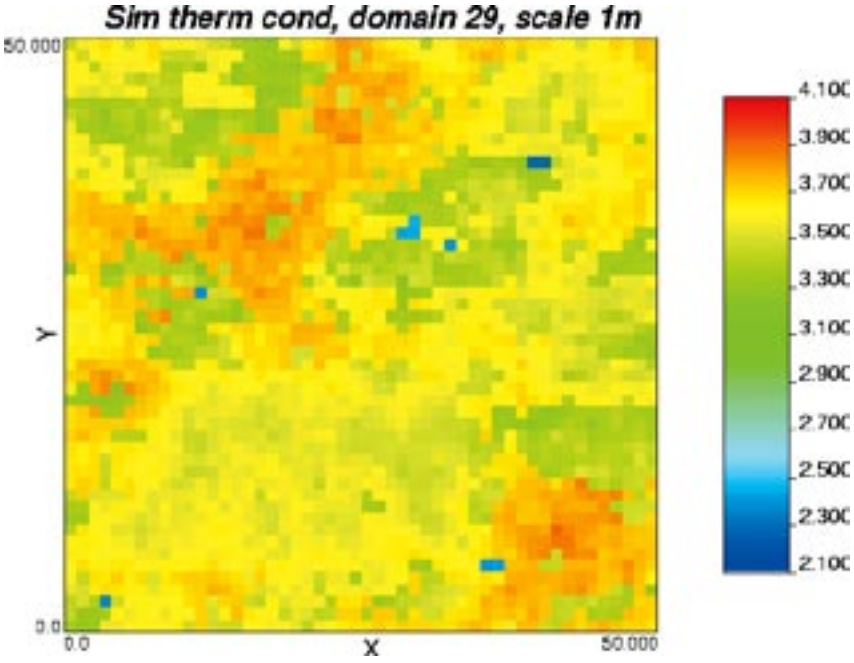

Domain RFM029: R = 1, Slice = 25, xy-plane

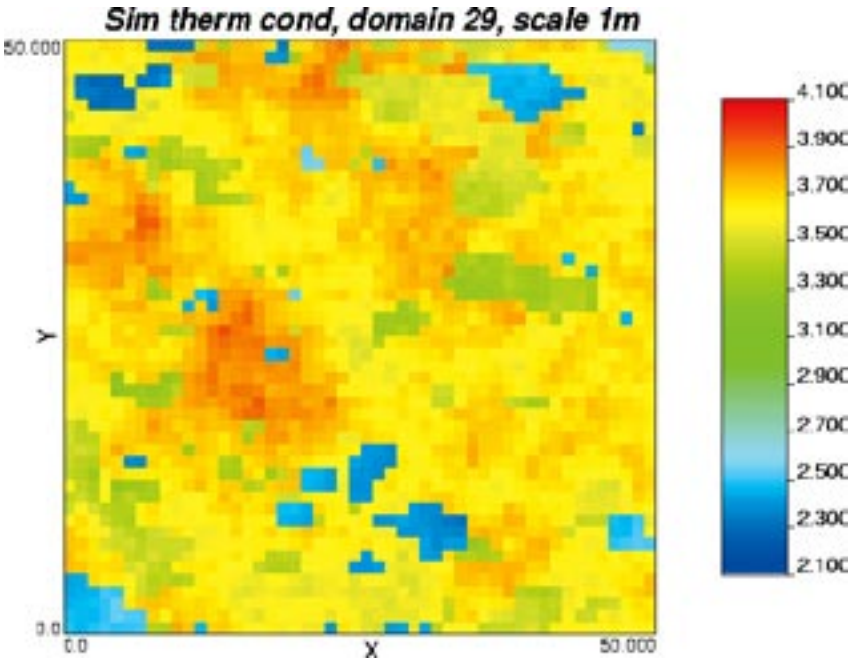

Domain RFM029: R = 1,000, Slice = 25, xy-plane

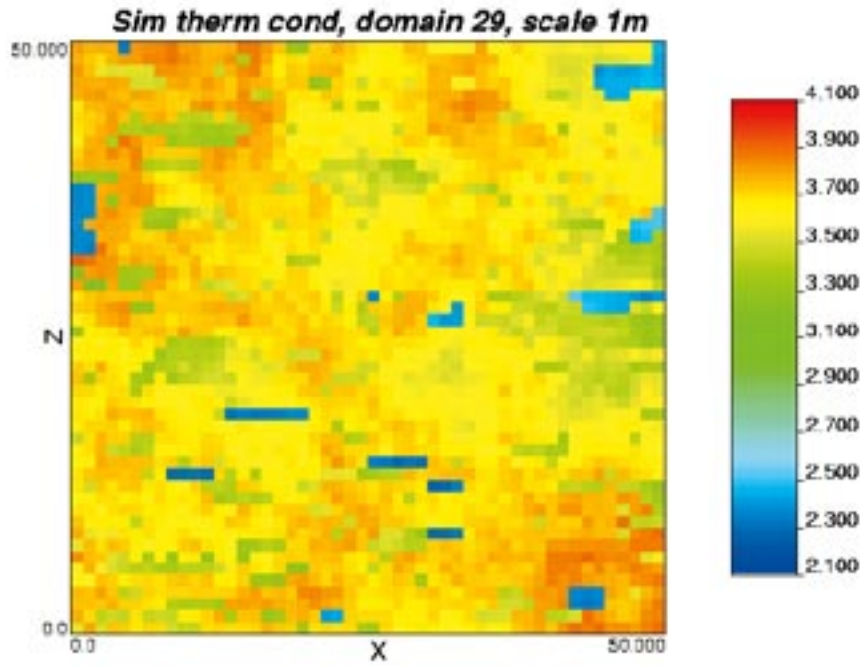

Domain RFM029: R = 1, Slice = 25, xz-plane

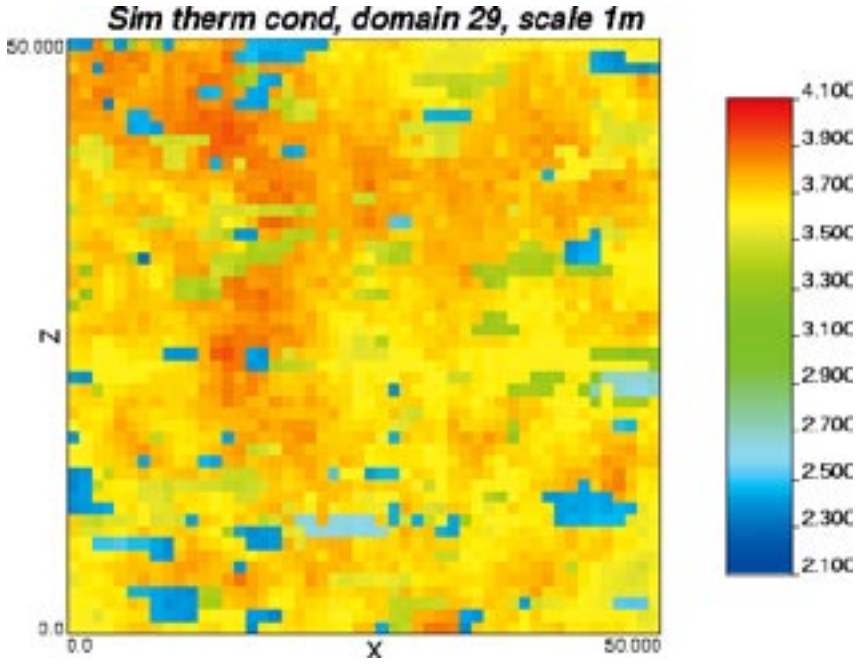

Domain RFM029: R = 1,000, Slice = 25, xz-plane

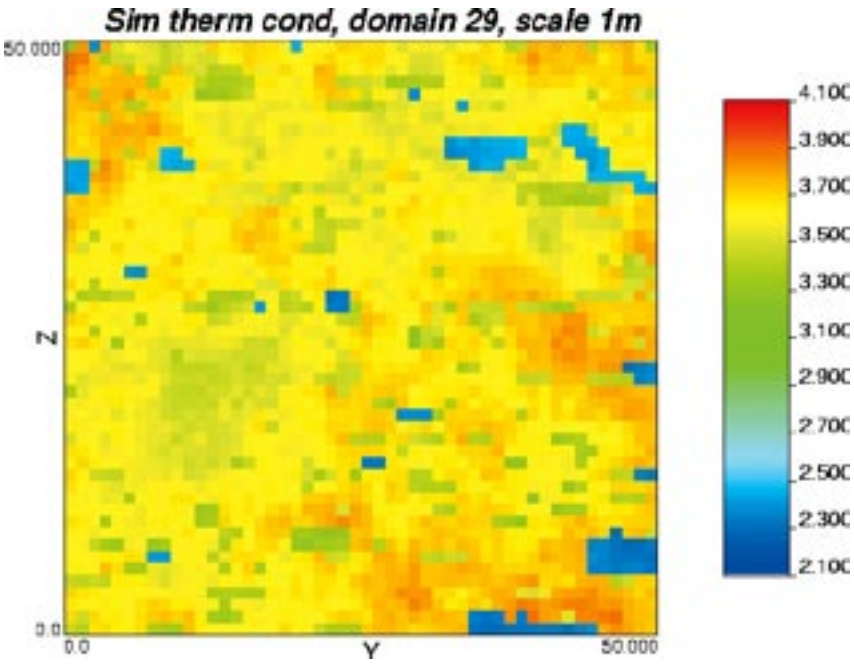

Domain RFM029: R = 1, Slice = 25, yz-plane

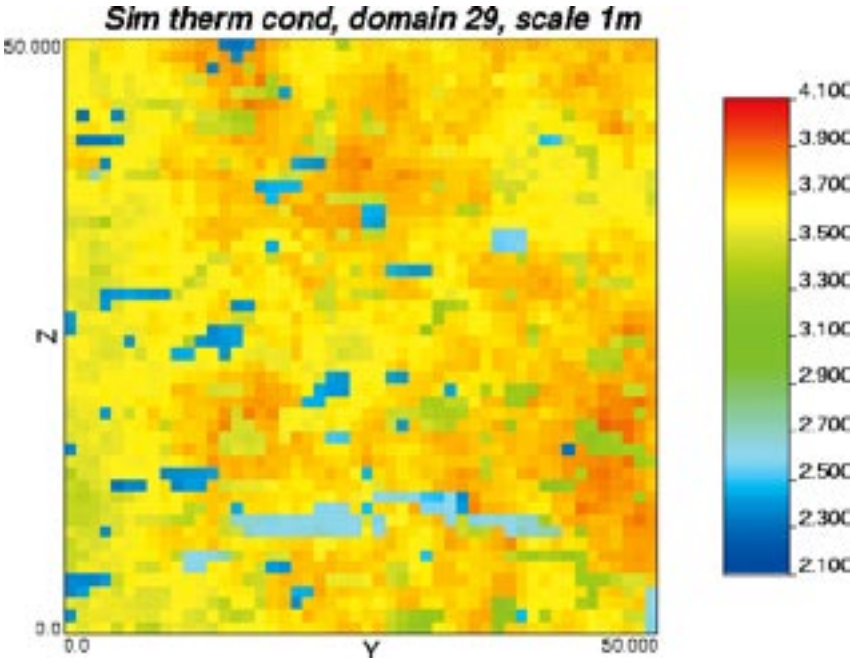

Domain RFM029: R = 1,000, Slice = 25, yz-plane

Domain RFM045, 0.1 m scale

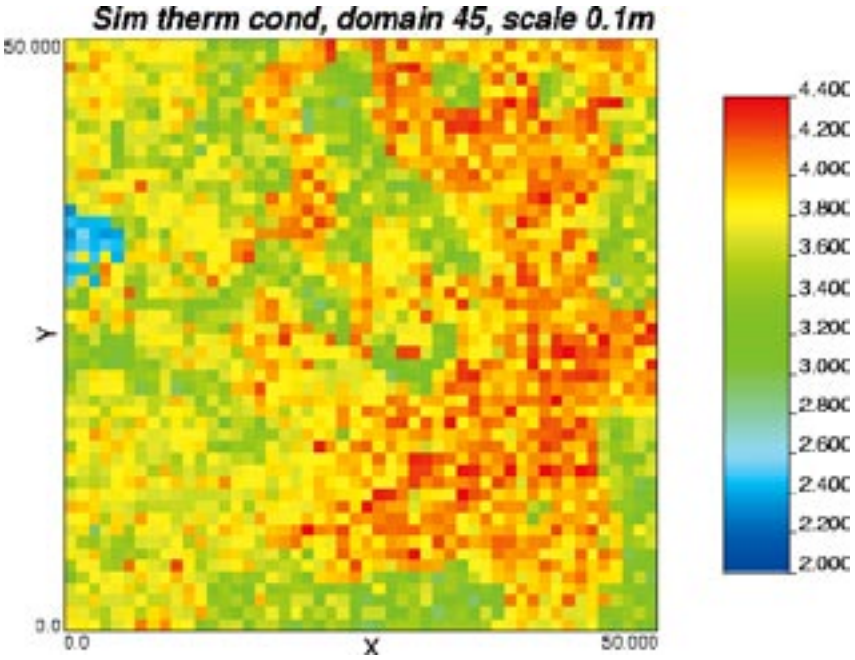

Domain RFM045: R = 1, Slice = 25, xy-plane

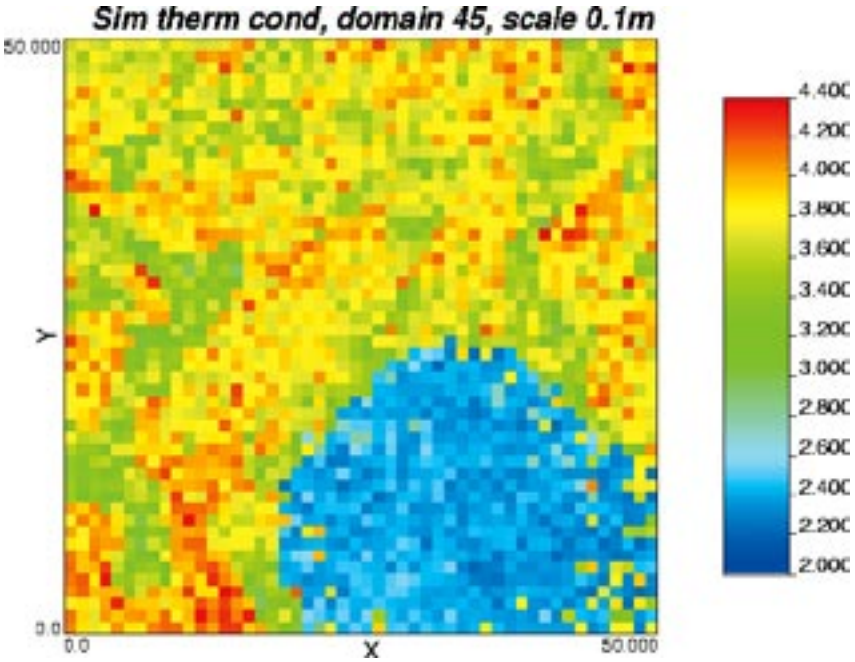

Domain RFM045: R = 100, Slice = 25, xy-plane

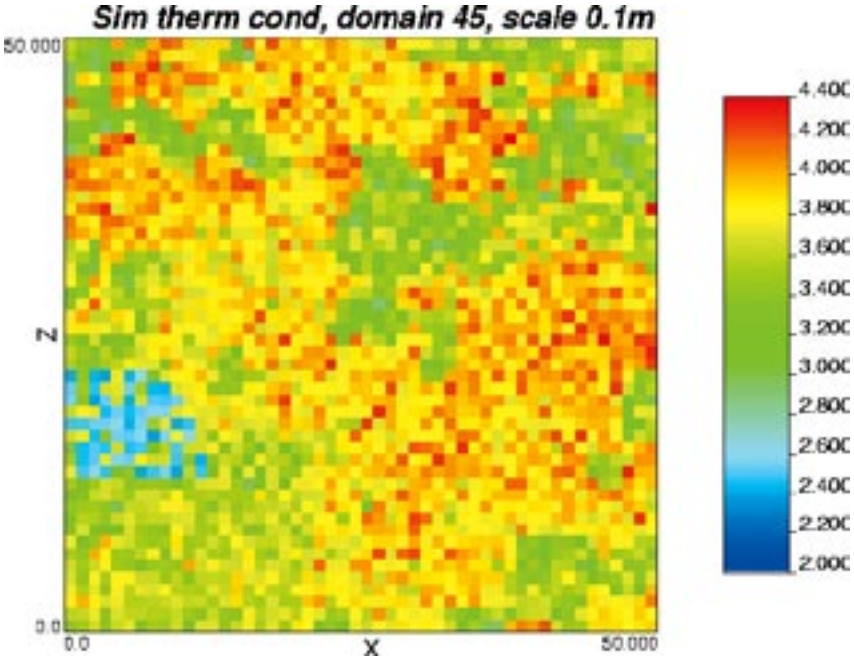

Domain RFM045: R = 1, Slice = 25, xz-plane

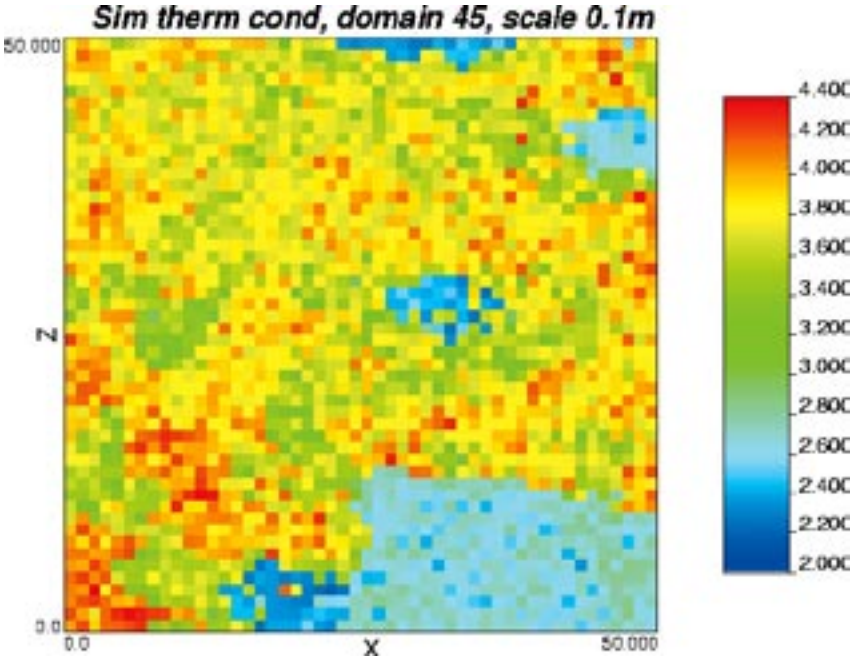

Domain RFM045: R = 100, Slice = 25, xz-plane

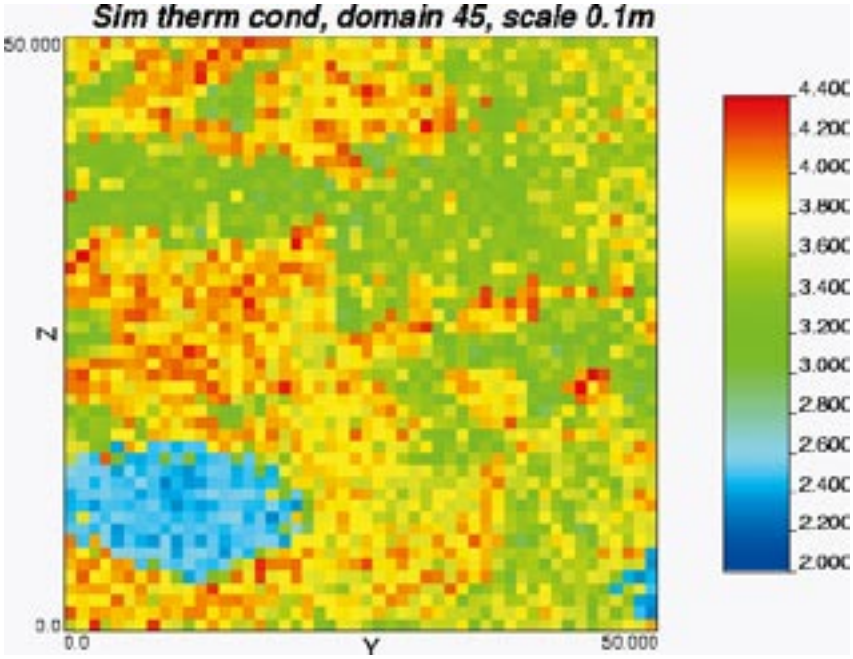

Domain RFM045: R = 1, Slice = 25, yz-plane

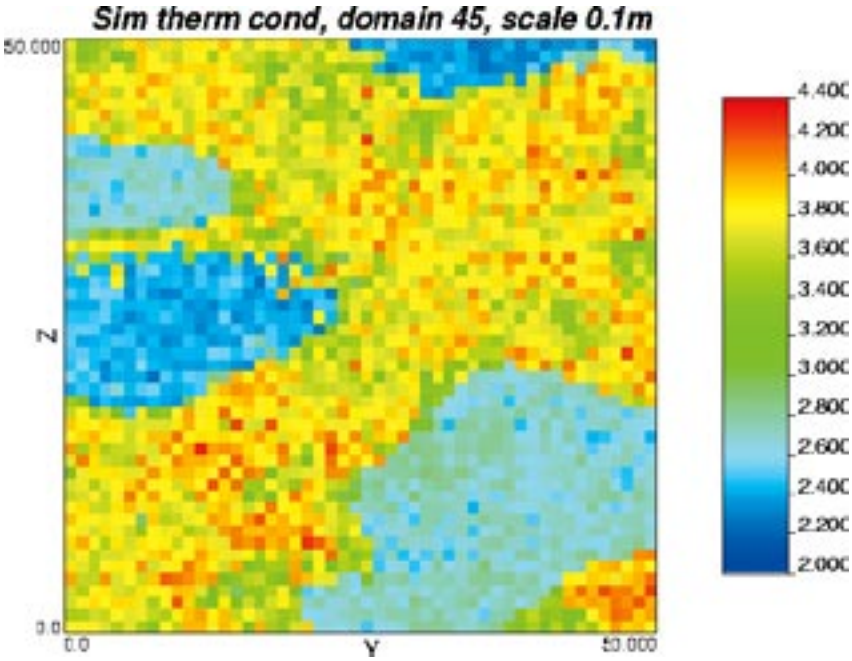

Domain RFM045: R = 100, Slice = 25, yz-plane

Domain RFM045, 1 m scale

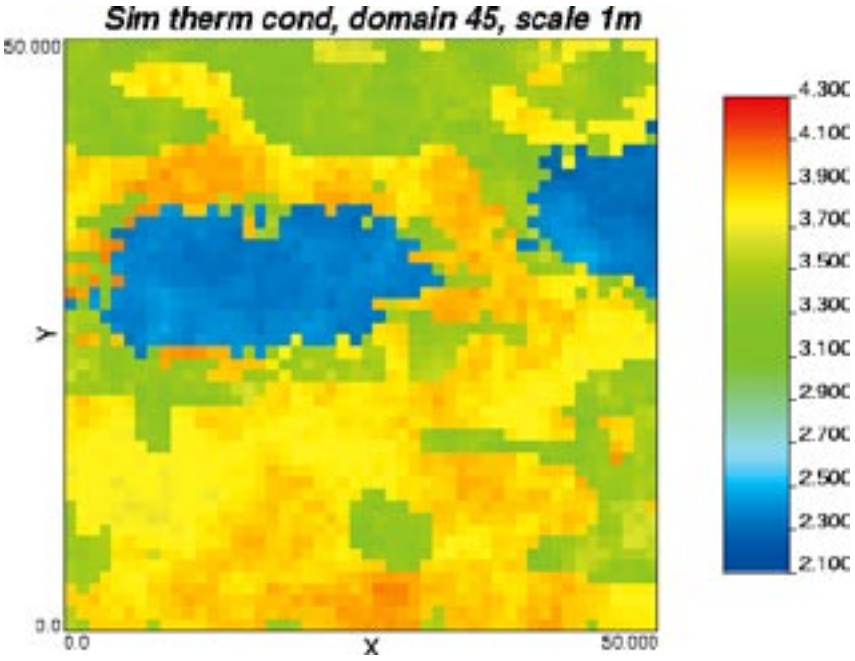

Domain RFM045: R = 1, Slice = 25, xy-plane

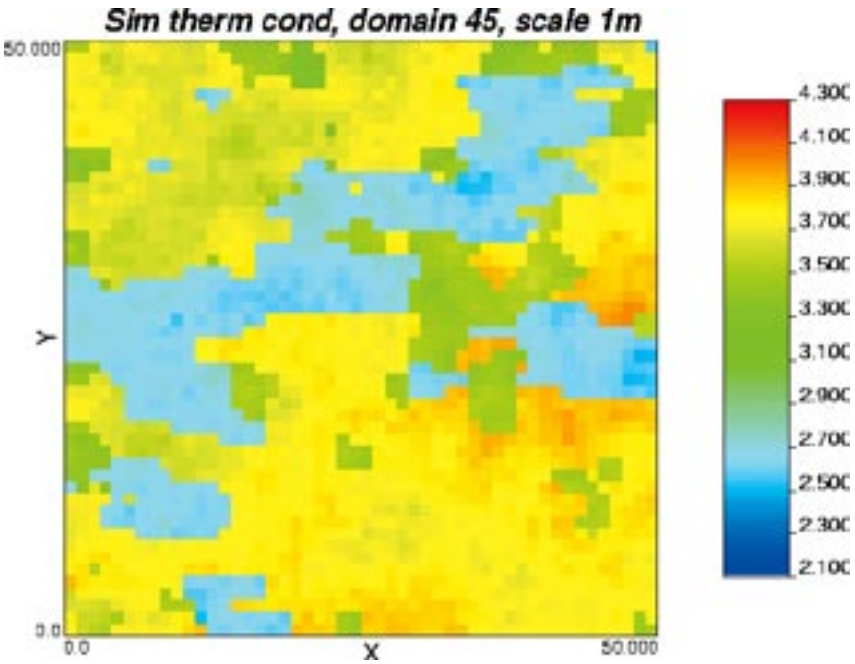

Domain RFM045: R = 400, Slice = 25, xy-plane

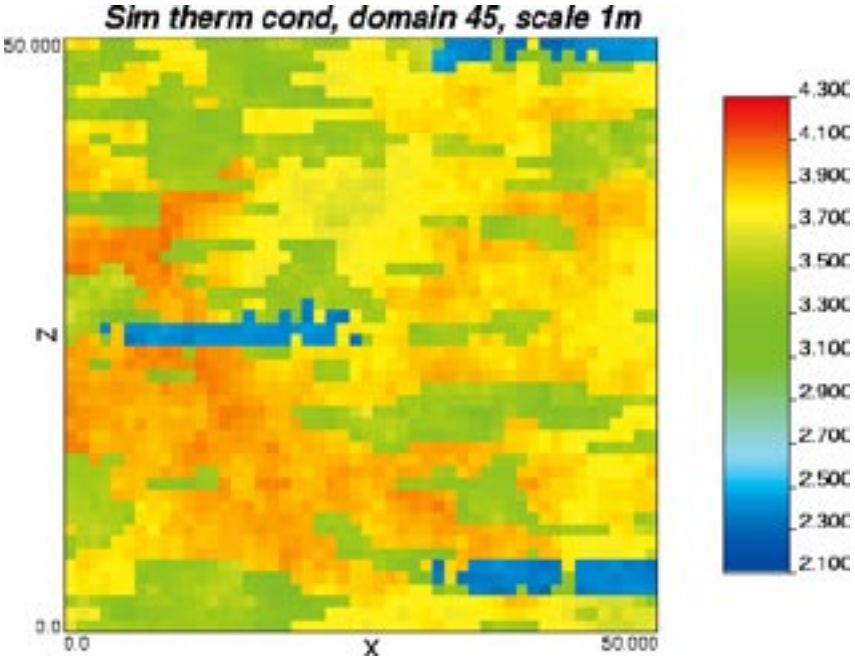

Domain RFM045: R = 1, Slice = 25, xz-plane

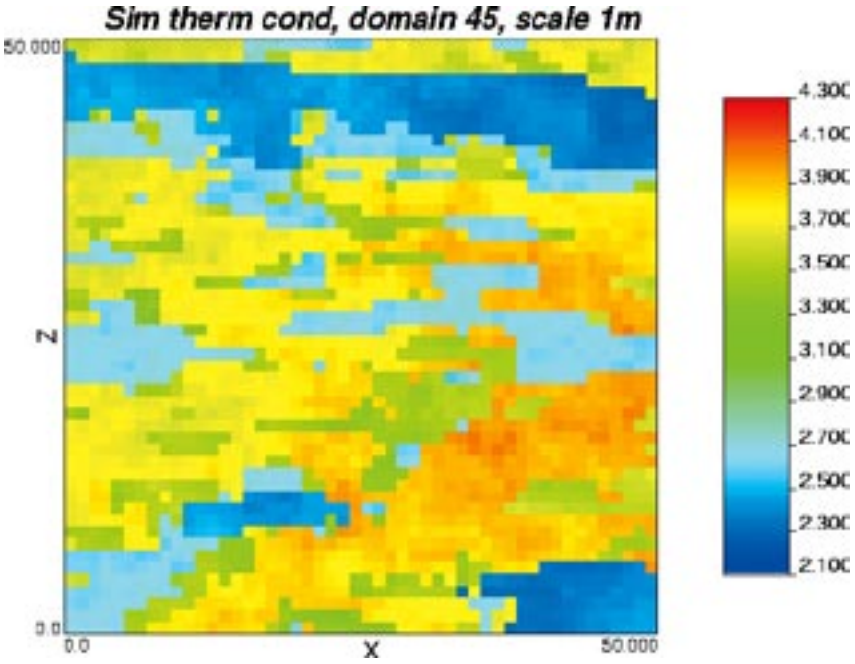

Domain RFM045: R = 400, Slice = 25, xz-plane

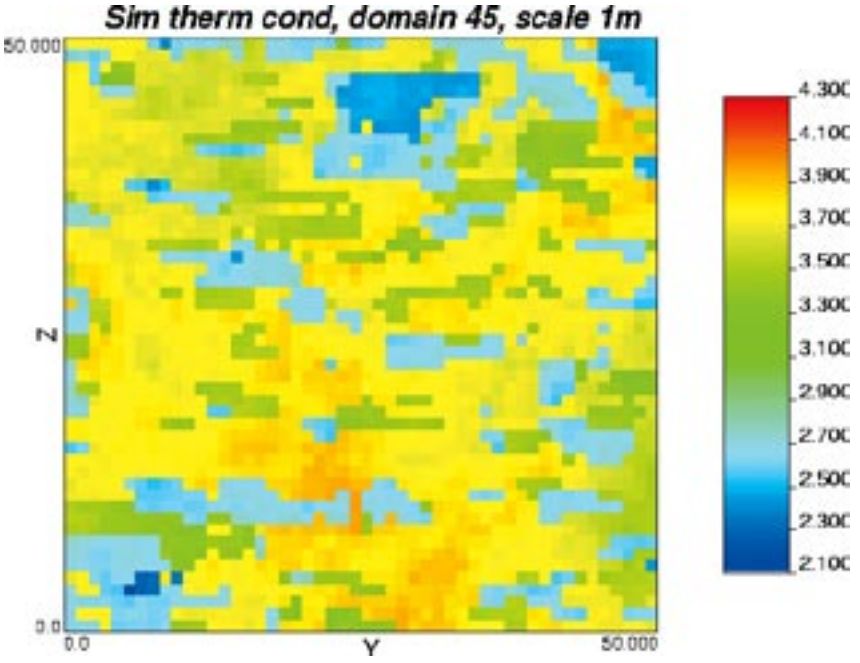

Domain RFM045: R = 1, Slice = 25, yz-plane

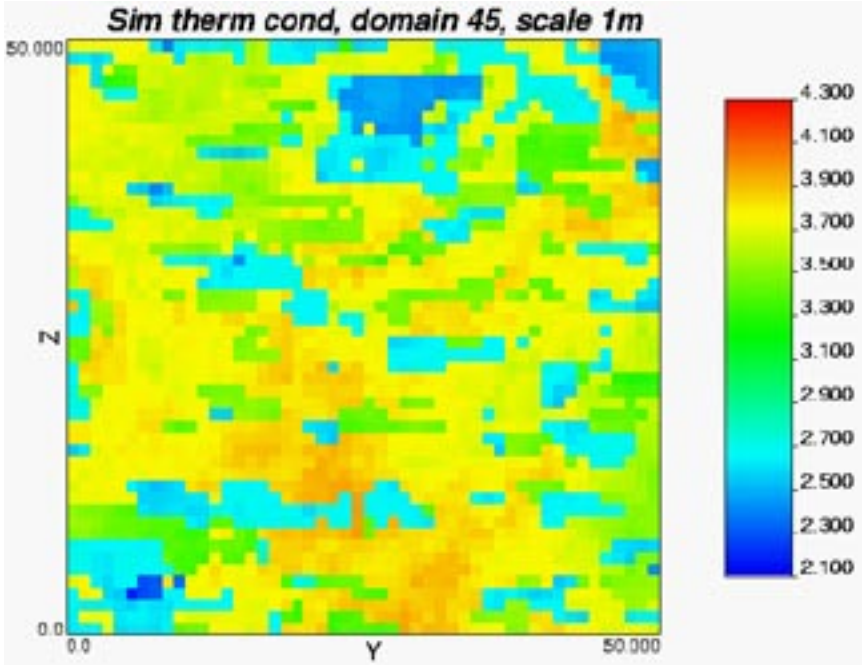

Domain RFM045: R = 400, Slice = 25, yz-plane

Appendix I

Coordinate transformations for geology simulations – Forsmark

Memorandum, June 14, 2007

Introduction

This memorandum describes the coordinate transformation procedure for setting up a model for the stochastic simulation of geology in T-PROGS. As input data, T-PROGS uses transition probabilities for the principal direction of anisotropy. To facilitate realistic modelling results the model volume therefore needs to be oriented in a transformed coordinate system, obtained through rotation of the main principal directions (Figure I-1) in three steps; (x, y, z) → (x', y', z') → (x'', y'', z'') → (x''', y''', z'''), Figures I-3 to I-5.

Geological information describing anisotropy is given as: (1) the trend and plunge of the mineral stretching orientation and (2) the strike and dip of the foliation. The orientation of rock units is a function of these. The theoretical description of the transformation to a coordinate system oriented in the principal direction of anisotropy as a function of the mineral stretching and foliation plane is given below.

Coordinate Transformation

The main principal directions are shown in Figure I-1.

Each domain has a local coordinate system (x''', y''', z''') governed by the principal direction of anisotropy and an origin defined by minimum easting, minimum northing, and maximum elevation from positions in borehole records supplied. The local coordinate system is obtained through rotations in three steps, as described below. This results in a transformed coordinate system with main axis (x''') parallel to the principal direction of anisotropy, see Figure I-2.

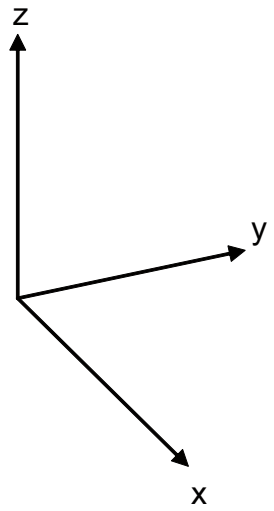

Figure I-1. *Main principal directions (x = easting direction, y = northing direction, z = elevation direction).*

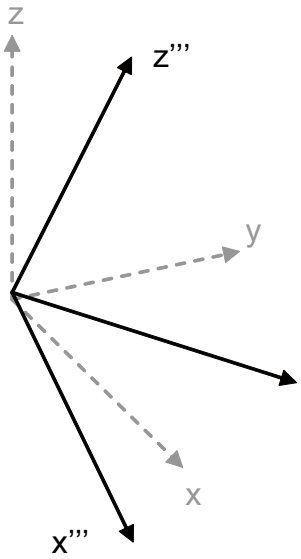

Figure I-2. *Principal directions of the local transformed coordinate system where x''' is parallel to the principal direction of anisotropy.*

For domain RFM045, the origin (x''' = y''' = z''' = x = y = z = 0) is located at:
Northing 6699927.79, Easting 1631300.33, Elevation –288.67

And for domain RFM029 at:
Northing 6698669.45, Easting 1630604.21, Elevation –2.70

The principal direction of anisotropy is parallel to the trend and plunge of the mineral stretching lineation (141°/39° for domain 045 and 157°/38° for domain 029). Two unit vectors (x_1,y_1,z_1) and (x_2,y_2,z_2) can be defined as:

$x_1 = \cos\ \alpha_1 \cos\ \beta_1$

$y_1 = -\sin \alpha_1\ \cos\ \beta_1$; (x_1,y_1,z_1) in principal direction of anisotropy

$z_1 = -\sin \beta_1$

and

$x_2 = \cos\ \alpha_2 \cos\ \beta_2$

$y_2 = -\sin \alpha_2\ \cos\ \beta_2$; (x_2,y_2,z_2) in direction of foliation and TRC contacts

$z_2 = -\sin \beta_2$

where

α_1 = trend–90° = 141°–90° = 51°, β_1 = plunge = 39°, α_2 = strike–90°+90° = 112.5 –90+90 = 112.5°, β_2 = dip = 60° ; for domain RFM045

and

α_1 = 157–90 = 67°, β_1 = 38°, α_2 = 150–90+90 = 150°, β_2 = 80° ; for domain RFM029.

The coordinate system is now rotated so that the x-axis points in the trend/plunge direction. The position (x_1,y_1,z_1) will then have the coordinates (1,0,0). The first rotation is thus the xy-plane α_1 degrees clockwise around the z-axis. The second rotation is the x'-z' plane β_1 degrees clockwise around the y'-axis. The final transformation is to rotate the y''-z'' plane γ_1 degrees around the x''-axis until $z_2 = 0$ for the position (x_2,y_2,z_2). The unit vectors (x_1,y_1,z_1) and (x_2,y_2,z_2) will then be in the new x'''-y''' plane and z''' is perpendicular to this plane. The three rotations are defined as follows:

First rotation

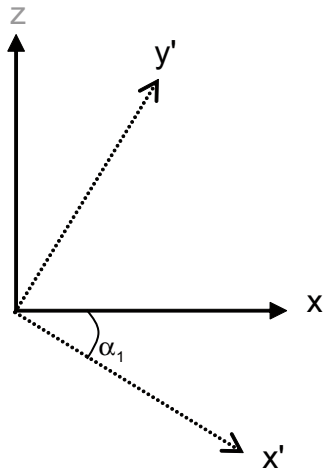

Figure I-3. *First rotation, α_1 degrees around the z-axis.*

$$\begin{bmatrix} x' \\ y' \\ z' \end{bmatrix} = \begin{bmatrix} \cos\ \alpha_1 & -\sin\ \alpha_1 & 0 \\ \sin\ \alpha_1 & \cos\ \alpha_1 & 0 \\ 0 & 0 & 1 \end{bmatrix} \begin{bmatrix} x \\ y \\ z \end{bmatrix}$$

Second rotation

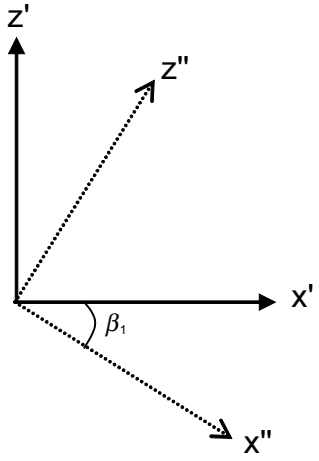

Figure I-4. *Second rotation, β_1 degrees around the y'-axis.*

$$\begin{bmatrix} x'' \\ y'' \\ z'' \end{bmatrix} = \begin{bmatrix} \cos\ \beta_1 & 0 & -\sin\ \beta_1 \\ 0 & 1 & 0 \\ \sin\ \beta_1 & 0 & \cos\ \beta_1 \end{bmatrix} \begin{bmatrix} x' \\ y' \\ z' \end{bmatrix}$$

Third rotation

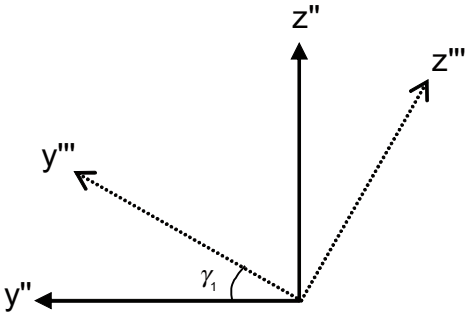

Figure I-5. *Third rotation, γ_1 degrees around the x''—axis.*

$$\begin{bmatrix} x''' \\ y''' \\ z''' \end{bmatrix} = \begin{bmatrix} 1 & 0 & 0 \\ 0 & \cos\ \gamma_1 & \sin\ \gamma_1 \\ 0 & -\sin\gamma_1 & \cos\ \gamma_1 \end{bmatrix} \times \begin{bmatrix} x'' \\ y'' \\ z'' \end{bmatrix}$$

where the angle γ_1 is defined by:

$$\tan\ \gamma_1 = \frac{z_2''}{y_2''} \Leftrightarrow y_2''\ \sin\ \gamma_1 = z_2''\ \cos\ \gamma_1 \Leftrightarrow -y_2''\ \sin\gamma_1 + z_2''\ \cos\ \gamma_1 = 0$$

Verification

To verify that the unit vectors (x_1,y_1,z_1) and (x_2,y_2,z_2) are within the new x'''-y''' plane and that (x_1,y_1,z_1) will have the new coordinates (1,0,0) the following can be set up:

$$\begin{bmatrix} x_1 \\ y_1 \\ z_1 \end{bmatrix} = \begin{bmatrix} \cos\ \alpha_1\ \cos\ \beta_1 \\ -\sin\alpha_1\ \cos\ \beta_1 \\ -\sin\beta_1 \end{bmatrix}$$

$$\begin{bmatrix} x_1' \\ y_1' \\ z_1' \end{bmatrix} = \begin{bmatrix} \cos\ \alpha_1 & -\sin\alpha_1 & 0 \\ \sin\alpha_1 & \cos\ \alpha_1 & 0 \\ 0 & 0 & 1 \end{bmatrix} \begin{bmatrix} \cos\ \alpha_1 \cos\ \beta_1 \\ -\sin\alpha_1 \cos\beta_1 \\ -\sin\beta_1 \end{bmatrix} = \begin{bmatrix} \cos^2\alpha_1\ \cos\ \beta_1 + \sin^2\alpha_1\ \cos\ \beta_1 \\ \sin\alpha_1 \cos\ \alpha_1 \cos\beta_1 - \cos\ \alpha_1\ \sin\ \alpha_1 \cos\beta_1 \\ -\ \sin\beta_1 \end{bmatrix} = \begin{bmatrix} \cos\beta_1 \\ 0 \\ -\sin\beta_1 \end{bmatrix}$$

$$\begin{bmatrix} x_1'' \\ y_1'' \\ z_1'' \end{bmatrix} = \begin{bmatrix} \cos\ \beta_1 & 0 & -\sin\beta_1 \\ 0 & 1 & 0 \\ \sin\beta_1 & 0 & \cos\ \beta_1 \end{bmatrix} \begin{bmatrix} \cos\ \beta_1 \\ 0 \\ -\sin\beta_1 \end{bmatrix} = \begin{bmatrix} 1 \\ 0 \\ 0 \end{bmatrix}$$

$$\begin{bmatrix} x_1''' \\ y_1''' \\ z_1''' \end{bmatrix} = \begin{bmatrix} 1 & 0 & 0 \\ 0 & \cos\ \gamma_1 & \sin\ \gamma_1 \\ 0 & -\sin\ \gamma_1 & \cos\ \gamma_1 \end{bmatrix} \begin{bmatrix} 1 \\ 0 \\ 0 \end{bmatrix} = \begin{bmatrix} 1 \\ 0 \\ 0 \end{bmatrix} \text{... Q.E.D.}$$

$$\begin{bmatrix} x_2 \\ y_2 \\ z_2 \end{bmatrix} = \begin{bmatrix} \cos\ \alpha_2 \cos\ \beta_2 \\ -\sin\alpha_2\ \cos\ \beta_2 \\ -\sin\beta_2 \end{bmatrix}$$

$$\begin{bmatrix} x_2' \\ y_2' \\ z_2' \end{bmatrix} = \begin{bmatrix} \cos\ \alpha_1 & -\sin\ \alpha_1 & 0 \\ \sin\ \alpha_1 & \cos\ \alpha_1 & 0 \\ 0 & 0 & 1 \end{bmatrix} \begin{bmatrix} \cos\ \alpha_2 \cos\ \beta_2 \\ -\sin\ \alpha_2 \cos\ \beta_2 \\ -\sin\ \beta_2 \end{bmatrix} = \begin{bmatrix} \cos\ \alpha_1 \cos\ \alpha_2 \cos\ \beta_2 + \sin\ \alpha_1\ \sin\ \alpha_2 \cos\ \beta_2 \\ \sin\ \alpha_1 \cos\ \alpha_2 \cos\ \beta_2 - \cos\ \alpha_1 \sin\ \alpha_2 \cos\ \beta_2 \\ -\sin\ \beta_2 \end{bmatrix}$$

$$\begin{bmatrix} x_2'' \\ y_2'' \\ z_2'' \end{bmatrix} = \begin{bmatrix} \cos\ \beta_1 & 0 & -\sin\ \beta_1 \\ 0 & 1 & 0 \\ \sin\ \beta_1 & 0 & \cos\ \beta_1 \end{bmatrix} \begin{bmatrix} \cos\ \alpha_1 \cos\ \alpha_2\ \cos\ \beta_2 + \sin\ \alpha_1 \sin\ \alpha_2 \cos\ \beta_2 \\ \sin\ \alpha_1\ \cos\ \alpha_2\ \cos\ \beta_2 - \cos\ \alpha_1 \sin \alpha_2 \cos\ \beta_2 \\ -\sin\ \beta_2 \end{bmatrix} =$$

$$\begin{bmatrix} \cos\ \beta_1 \cos\ \alpha_1 \cos\ \alpha_2 \cos\ \beta_2 + \cos\ \beta_1\ \sin\ \alpha_1 \sin \alpha_2 \cos\ \beta_2 + \sin \beta_1 \sin\ \beta_2 \\ \sin\ \alpha_1\ \cos\ \alpha_2\ \cos\ \beta_2 - \cos\ \alpha_1\ \sin\ \alpha_2\ \cos\ \beta_2 \\ \sin\ \beta_1 \cos\ \alpha_1 \cos\ \alpha_2 \cos\ \beta_2 + \sin \beta_1 \sin\ \alpha_1 \sin \alpha_2 \cos\ \beta_2 - \cos\ \beta_1\ \sin \beta_2 \end{bmatrix}$$

It can now be noted that:

$$\tan\ \gamma_1 = \frac{\sin\ \beta_1 \cos\ \alpha_1 \cos\ \alpha_2 \cos\ \beta_2 + \sin\ \beta_1 \sin\ \alpha_1 \sin\ \alpha_2 \cos\ \beta_2 - \cos\ \beta_1\ \sin\ \beta_2}{\sin\ \alpha_1\ \cos\ \alpha_2\ \cos\ \beta_2 - \cos\ \alpha_1\ \sin\ \alpha_2\ \cos\ \beta_2}$$

and that:

$$\begin{bmatrix} x_2''' \\ y_2''' \\ z_2''' \end{bmatrix} = \begin{bmatrix} 1 & 0 & 0 \\ 0 & \cos\ \gamma_1 & \sin\ \gamma_1 \\ 0 & -\sin\ \gamma_1 & \cos\ \gamma_1 \end{bmatrix} \begin{bmatrix} \cos\ \beta_1 \cos\ \alpha_1\ \cos\ \alpha_2\ \cos\ \beta_2 + \cos \beta_1 \sin\ \alpha_1 \sin\ \alpha_2\ \cos\ \beta_2 + \sin\ \beta_1 \sin \beta_2 \\ \sin\ \alpha_1\ \cos\ \alpha_2\ \cos\ \beta_2 - \cos\ \alpha_1 \sin\ \alpha_2\ \cos\ \beta_2 \\ \sin\ \beta_1\ \cos\ \alpha_1 \cos\ \alpha_2\ \cos\ \beta_2 + \sin\ \beta_1\ \sin\ \alpha_1 \sin\ \alpha_2\ \cos\ \beta_2 - \cos\ \beta_1 \sin \beta_2 \end{bmatrix}$$

$$= \begin{bmatrix} \cos\ \beta_1 \cos\ \alpha_1\ \cos\ \alpha_2 \cos\ \beta_2 + \cos\ \beta_1 \sin \alpha_1 \sin \alpha_2 \cos\ \beta_2 + \sin \beta_1 \sin \beta_2 \\ \begin{cases} \cos\ \gamma_1 \sin \alpha_1 \cos\ \alpha_2 \cos \beta_2 - \cos\ \gamma_1\ \cos\ \alpha_1 \sin \alpha_2 \cos\ \beta_2 + \sin\ \gamma_1\ \sin \beta_1 \cos\ \alpha_1\ \cos\ \alpha_2 \cos\ \beta_2 + \\ + \sin\ \gamma_1\ \sin \beta_1 \sin\ \alpha_1 \sin\ \alpha_2 \cos\ \beta_2 - \sin\ \gamma_1 \cos\ \beta_1 \sin\ \beta_2 \end{cases} \\ \begin{cases} -\sin\ \gamma_1 \sin \alpha_1 \cos\ \alpha_2 \cos \beta_2 + \sin\ \gamma_1\ \cos\ \alpha_1 \sin \alpha_2 \cos\ \beta_2 + \cos\ \gamma_1 \sin \beta_1 \cos\ \alpha_1\ \cos\ \alpha_2\ \cos\ \beta_2 + \\ + \cos\ \gamma_1\ \sin \beta_1 \sin\ \alpha_1 \sin\ \alpha_2\ \cos\ \beta_2 - \cos\ \gamma_1\ \cos \beta_1\ \sin \beta_2 \end{cases} \end{bmatrix}$$

$$z_2''' = -\sin\ \gamma_1 (\sin\ \alpha_1\ \cos\ \alpha_2\ \cos\ \beta_2 - \cos\ \alpha_1\ \sin\ \alpha_2 \cos\ \beta_2) + \cos\ \gamma_1 (\sin \beta_1 \cos\ \alpha_1 \cos\ \alpha_2 \cos\ \beta_2 +$$
$$+ \sin\ \beta_1\ \sin\ \alpha_1\ \sin\ \alpha_2 \cos\ \beta_2 - \cos\ \beta_1 \sin\ \beta_2) =$$
$$= -\sin\ \gamma_1 (\sin\ \alpha_1 \cos\ \alpha_2 \cos\ \beta_2 - \cos\ \alpha_1 \sin\ \alpha_2 \cos\ \beta_2) +$$
$$+ \cos\ \gamma_1\ \tan\ \gamma_1 (\sin\ \alpha_1 \cos\ \alpha_2 \cos \beta_2 - \cos\ \alpha_1 \sin\ \alpha_2 \cos\ \beta_2) = 0$$

Q.E.D.

From above it follows that both vectors (x_1,y_1,z_1) and (x_2,y_2,z_2) are within the new x'''-y''' plane.

Back transformation

When transforming back original coordinates, the procedure described above is performed in reverse order, α, β and γ angles represented with negative signs. The procedure is as described below:

Rotation 1:

$-\gamma_1$ degrees around the x’’’-axis transforms (x’’’,y’’’,z’’’) back to (x’’,y’’,z’’)

Rotation 2:

$-\beta_1$ degrees around the y’’-axis transforms (x’’,y’’,z’’) back to (x’,y’,z’)

Rotation 3:

$-\alpha_1$ degrees around the x’-axis transforms (x’,y’,z’) back to (x,y,z)

Nils Kellgren Tommy Norberg Lars Rosén